Oxygen chemoreception in larval zebrafish: From signal initiation to the hypoxic ventilatory response

Yihang Pan

Thesis submitted in partial fulfillment of the requirements for the
Doctorate in Philosophy degree in Biology.

Department of Biology
Faculty of Science
University of Ottawa

ABSTRACT

Multicellular organisms typically depend on O_2 for energy production to maintain normal cellular function, and even brief periods of O_2 deprivation may have fatal consequences. The aqueous environment is prone to changes in ambient water O_2 tension (PO_2) and thus the ability of fish to sense changes in water PO_2 and to elicit appropriate physiological responses is essential for their survival. Studies on fish O_2 chemoreception have identified neuroepithelial cells (NECs), which are characterized as having dense-cored vesicles containing serotonin (5-HT), as peripheral O_2 chemoreceptors. Upon exposure to hypoxia, isolated and cultured NECs *in vitro* depolarize, likely resulting in neurotransmitter release. However, to date there is no evidence that NECs are activated by hypoxia *in vivo* to initiate physiological responses such as the hypoxic ventilatory response (HVR), which is the focus of this thesis. Initial findings demonstrated that larval zebrafish fine-tune the HVR as early as 4 days post fertilization (dpf) and by 7 dpf, the HVR aids in O_2 uptake under hypoxic conditions. In addition, the HVR is multiphasic, with an initiation phase followed by a decline phase that gradually stabilizes above normoxic baseline values (Chapter 2). In the absence of tools to probe the hypoxia sensitivity of NECs *in vivo*, research focused on Merkel-like cells (MLCs), a newly proposed O_2 chemoreceptor in larval zebrafish. Using *in vivo* calcium imaging it was shown that MLCs are stimulated by hypoxia. Data suggest that MLCs are responsible for the initiation phase of the HVR, while peripheral sensory neurons (PSNs)/peripheral sensory ganglia (PSG) that innervate MLCs play a more important role in reducing ventilation during the decline phase of the HVR (Chapter 4). Attempts at identifying the putative neurotransmitter(s) involved in the O_2 signal transduction pathway revealed that adrenaline (AD), serotonin (5-HT), and dopamine (DA) are probable candidates (Chapter 4), though the presence of AD and DA within MLCs is yet to be

confirmed. In addition, 5-HT likely plays a role in the central nervous system (CNS), integrating peripheral signals resulting in the final HVR (Chapter 3). Taken together, this thesis provides the first evidence of putative O_2 chemoreceptors responding to hypoxia *in vivo* and thus significantly advances models for O_2 signal transduction in larval zebrafish.

RÉSUMÉ

Les organismes multicellulaires dépendent généralement de l'O_2 pour la production d'énergie afin de maintenir une fonction cellulaire normale, ainsi et même de brèves périodes de privation d'O_2 peuvent avoir des conséquences fatales. L'environnement aqueux étant sujet à des changements dans la pression partielle de l'O_2 de l'eau (PO_2). La capacité des poissons à détecter de tels changements et à susciter des réponses physiologiques appropriées est essentielle à leur survie. Des études sur la chimioréception de l'O_2 chez les poissons confirment la présence de cellules neuro - épithéliales (NEC). Celles-ci sont caractérisées par des vésicules à noyau dense contenant de la sérotonine (5-HT), en tant que chimiorécepteurs périphériques de l'O_2. Lors de l'exposition à l'hypoxie, les NECs isolées et cultivées *in vitro* se dépolarisent, entraînant probablement la libération de neurotransmetteurs. Cependant, jusqu'à présent, aucune preuve ne démontre que les chimiorécepteurs O_2 sont sensibles à l'hypoxie *in vivo*. Cette recherche de preuve constitue l'objet de cette thèse. Les premiers résultats ont prouvé que les larves de poissons zèbres affinent la réponse ventilatoire hypoxique (HVR) dès 4 jours après la fécondation (dpf) et par 7 dpf, la HVR aide à l'absorption d'O_2 dans des conditions hypoxiques. De plus, le HVR est multiphasique, avec une phase d'initiation suivie d'une phase de déclin qui se stabilise progressivement au-dessus de la ligne de référence de Normoxie (chapitre 2). En l'absence d'outils pour sonder la sensibilité à l'hypoxie des NEC *in vivo*, la recherche s'est concentrée sur les cellules de type Merkel (MLC), un chimiorécepteur O_2 nouvellement proposé chez les larves de poissons zèbres. En utilisant l'imagerie calcique *in vivo*, il a été montré que les MLC sont stimulées par l'hypoxie. Les données suggèrent que les MLC sont responsables de la phase d'initiation du HVR, tandis que les neurones sensoriels périphériques (PSN)/ganglions sensoriels périphériques (PSG) qui innervent les MLC jouent un rôle plus important dans la

réduction de la ventilation pendant la phase de déclin du HVR (chapitre 4). Les tentatives d'identification du ou des neurotransmetteurs putatifs impliqués dans la voie de transduction du signal O_2 ont révélé que l'adrénaline (AD), la sérotonine (5-HT) et la dopamine (DA) sont des candidats probables (chapitre 4), bien que la présence d'AD et de DA au sein des MLC reste à confirmer. De plus, la 5-HT joue probablement un rôle dans le système nerveux central (SNC), intégrant les signaux périphériques résultants dans le HVR final (chapitre 3). Dans l'ensemble, cette thèse fournit la première preuve de chimiorécepteurs putatifs O_2 répondant à l'hypoxie *in vivo* et fait ainsi considérablement progresser les modèles de transduction du signal O_2 chez les larves de poissons zèbres.

ACKNOWLEDGEMENTS

No PhD project can be completed without countless external support from colleagues, professors, and staff of the University of Ottawa. But first and foremost, I would like to thank my supervisor Dr. Steve Perry. Coming directly into the PhD program from an undergraduate degree, the transition was much smoother than anticipated due to Steve's guidance in the early days. His emphasis on the importance of pursuing both low-hanging and high-hanging fruit definitely helped shape how I think and design my experiments and made me the better scientist I am today. I would also like to express my gratitude for the academic freedom I was given. As long as it was within the realm of piscine chemoreception, I could pursue whatever caught my interest. This may be something that I will miss dearly down the road.

Although a supervisor plays a vital role in the PhD thesis, numerous other people are just as important. Dr. Andrew Esbaugh, thank you for bringing me into the interesting field of fish physiology and recommending me to Steve. Drs. Alex Zimmer and Milica Mandic, thank you for teaching me the ropes of the lab when I first arrived and the wonderful collaborations we had. Christine Archer, thank you for fish husbandry and the help with in acquiring various lines of zebrafish that were vital to my thesis. Andrew Ochalski, thank you for teaching me the tricks of microscopy. Last but not least, to all the past and present members of the Perry and Gilmour labs, thank you! Your support and friendship have contributed greatly to this thesis.

This thesis would also be impossible without the support of my family. I would especially like to thank my love, Bai, for her encouragement and support throughout this journey. Thank you!

Table of Contents

LIST OF FIGURES

LIST OF ABBREVIATIONS

5-HT	serotonin
ACh	acetylcholine
AD	adrenaline
ANOVA	analysis of variance
AR	acute response
ATP	adenosine triphosphate
BSA	bovine serum albumin
CBS	cystathionine β-synthase
CI	confidence interval
CNS	central nervous system
CO	carbon monoxide
CSE	cystathionine γ-lyase
DA	dopamine
DCVs	dense-cored vesicles
dpf	day/days post fertilization
dph	days post-hatch
f_v	ventilation frequency
GFP	green fluorescent protein
H_2S	hydrogen sulfide
HCVR	hypercapnic ventilatory response
HO	heme oxygenases
HPD	highest posterior density
HVR	hypoxic ventilatory response
iNOS	inducible nitric oxide synthase
MCMC	Markov chain Monte Carlo
MLCs	Merkel-like cells
$\dot{M}O_2$	O_2 consumption
MS-222	ethyl-3-aminobenzoate methanesulfonate salt
NA	noradrenaline

NECs	neuroepithelial cells
NMD	nonsense-mediated mRNA decay
nNOS	neuronal nitric oxide synthase
NO	nitric oxide
NOS	nitric oxide synthase
PBS	phosphate buffered saline
PBST	phosphate buffered saline containing 0.1% tween-20
pCPA	para-chlorophenylalanine
P_{crit}	critical O_2 tension
PFA	paraformaldehyde
PO_2	O_2 tension
PSGs	peripheral sensory ganglia
PSNs	peripheral sensory neurons
RMR	Routine metabolic rate
STD	short term depression
TH	tyrosine hydroxylase
TPH	tryptophan hydroxylase
WT	wild-type

CHAPTER 1. General Introduction

Notes on Chapter

Chapter 1 is partly adapted from a review published in Molecular and Cellular Endocrinology as per the following citation:

Pan, Y. K. and Perry, S. F. (2020). Neuroendocrine control of breathing in fish. Molecular and cellular endocrinology, 110800.

Author contributions: Y.K.P. prepared the manuscript; S.F.P. performed conceptualization, revision of the manuscript and supervision.

1.1 Introduction

Multicellular organisms typically depend on O_2 for energy production, which is a requirement for normal cellular function. Even brief periods of O_2 deprivation may have fatal consequences. Fish live in environments that are prone to changes (spatially or temporally) in ambient water O_2 tension [PO_2, (Mandic and Regan, 2018)]. Thus, the ability of fish to sense changes in water PO_2 and to elicit appropriate physiological responses is essential for their survival and requires the presence of O_2-sensing cells (O_2 chemoreceptors) able to monitor the external and/or internal environments. In fish, neuroepithelial cells (NECs), first reported in rainbow trout (*Oncorhynchus mykiss*) gills (Dunel-Erb et al., 1982), have been identified as O_2 chemoreceptors. The trout NECs are characterized by the presence of dense-cored vesicles (DCVs) containing serotonin (5-hydroxytryptamine; 5-HT), which degranulate (i.e. release 5-HT) when exposed to hypoxia (Dunel-Erb et al., 1982). The notion that piscine NECs are O_2 chemoreceptors has been extended to several species (Burleson et al., 2006; Jonz et al., 2004; Regan et al., 2011; Zaccone et al., 2017) and encompasses larval, juvenile and adult developmental stages (Cochrane et al., 2021; Jonz and Nurse, 2005). Based on *in vitro* experiments performed using zebrafish (*Danio rerio*) and *O. mykiss*, fish NECs are recognised as polymodal chemoreceptors, exhibiting responsiveness to hypoxia (Jonz et al., 2004), hypercapnia (Qin et al., 2010) and elevated ammonia levels (Porteus et al., 2021; Zhang et al., 2011). It is widely believed that gill NECs respond universally to these chemosensory stimuli by a reduction in plasma membrane K^+ conductance, membrane depolarization and activation of voltage-gated Ca^{2+} channels leading to an increase in intracellular Ca^{2+} levels and the secretion of neurotransmitters onto postsynaptic sensory neurons to elicit appropriate physiological responses (Perry et al., 2009). However, only some of these processes such as the inhibition of K^+ channels

(Burleson et al., 2006; Jonz et al., 2004) under hypoxic conditions or the rise in intracellular Ca^{2+} levels during hypoxia (Zachar et al., 2017), hypercapnia (Abdallah et al., 2015a) or high environmental ammonia (Zhang et al., 2011), have been shown in isolated NECs *in vitro*. There is but scant and indirect evidence that NECs exhibit any of these responses *in vivo*. Indeed, there are no *in vivo* data directly linking activation of NECs to physiological responses to environmental changes. In addition, the specific neurotransmitter(s) involved in the process remain(s) unidentified.

A fundamental response of fish to hypoxic conditions that is initiated by O_2 chemoreceptors is an increase in ventilation volume through a change in ventilation frequency (f_V) and/or amplitude in a process referred to as the hypoxic ventilatory response (HVR). The HVR helps to maintain arterial PO_2 in the face of decreasing water PO_2, delaying an inevitable decrease in O_2 uptake as the severity of hypoxia increases (Forgue et al., 1989; Glass et al., 1990; Itazawa and Takeda, 1978; Perry et al., 2009). Intriguingly, larval fish that rely predominantly on cutaneous gas exchange (Rombough, 2002; Rombough and Ure, 1991; Wells and Pinder, 1996) also hyperventilate in response to hypoxia (Burggren et al., 2016; Jonz and Nurse, 2005; Mandic et al., 2020), begging the question of the physiological significance of the HVR in larval fish.

The primary goal of this thesis is to elucidate further the O_2 chemoreception pathway in larval zebrafish and the associated downstream physiological responses, beginning with an investigation of the physiological benefit of the HVR in larvae with subsequent focus on identifying O_2 chemoreceptors *in vivo* and identifying processes that are involved in O_2 chemoreception *in vivo*. The three overarching hypotheses are:

1) The hypoxic ventilatory response aids in hypoxic survival in larval zebrafish.

2) Serotonin is involved in mediating the hypoxic ventilatory response.

3) Merkel-like cells, a newly proposed cell type, can serve as O_2 chemoreceptors in larval zebrafish.

It is hoped that this thesis will further advance our understanding of piscine O_2 chemoreception and its downstream pathways.

In the remainder of the introduction, I will review the three key points pertaining to my thesis: 1) the presumed O_2 chemoreceptors in fish, 2) neurotransmitters that have been implicated in the control of breathing, and 3) the time course and physiological significance of the hypoxic ventilatory response.

1.2 Piscine O_2 chemoreceptors

1.2.1 Gill NECs

The putative peripheral chemoreceptors in fish – neuroepithelial cells (NECs) – were first identified by Dunel-Erb et al. (1982) based on the morphology of the pulmonary NECs previously described in the walls of the respiratory tract of mammals. Using formaldehyde-induced fluorescence to reveal catecholamine- and indolamine-containing cells, they identified a population of cells on the gill filament epithelium facing the buccopharyngeal cavity and thus in contact with respiratory water. Based on indirect evidence, it was suggested that these NECs contain the monoamine 5-HT (Dunel-Erb et al., 1982), a finding that was later confirmed directly by immunocytochemistry using antibodies against 5-HT (Bailly et al., 1989; Bailly et al., 1992). Further examination of NECs in rainbow trout using electron microscopy revealed that these

cells are characterized by the presence of DCVs and are innervated by postsynaptic nerve profiles facing the DCVs (Bailly et al., 1992; Dunel-Erb et al., 1982). One population of the nerve endings are sensitive to 5,6-dihydroxytryptamine, a serotonergic neurotoxin, and another population of nerve endings is sensitive to 5- and 6-hydroxydopamines, a class of catecholaminergic neurotoxin (Bailly et al., 1992). Similarly, in zebrafish, NECs appear to receive innervation from a plexus of nerve fibres, with synaptic vesicles being polarized within the basal cytoplasm near the adjacent nerve fibres (Jonz and Nurse, 2003). Based on the morphology, location and innervation patterns of NECs, it was suggested that NECs act as chemoreceptors in fish, sensing changes in the levels of O_2 in the inhalant water and initiating the reflex cardiorespiratory responses potentially through the direct release of neuroactive agents including 5-HT (Bailly, 2009; Bailly et al., 1992; Dunel-Erb et al., 1982; Jonz and Nurse, 2003). Supporting this notion is the fact that the NECs in trout exposed to hypoxia exhibit DCVs that appear "degranulated" (Dunel-Erb et al., 1982). Changes in NEC morphology under hypoxic conditions also provided further indirect evidence of their potential involvement in chemoreception (Porteus et al., 2014b; Regan et al., 2011; Rossi et al., 2020; Shakarchi et al., 2013), under the assumption that peripheral chemoreceptors are "plastic" and would respond to changes in environmental O_2 levels.

The first compelling direct evidence that NECs are involved in O_2 chemoreception was obtained from whole-cell patch-clamp recordings obtained from NECs isolated from adult zebrafish gill filaments (Jonz et al., 2004). Under voltage-clamp, zebrafish NECs responded to hypoxia with a concentration-dependent decrease in K^+ current while under current-clamp, hypoxia produced membrane depolarization associated with a decrease in K^+ conductance. Both responses were quinidine-sensitive, suggesting that hypoxia sensing via NECs is mediated by

inhibition of a background K^+ conductance, closely resembling the O_2 sensitive background K^+ currents identified in the chemoreceptor type I cells of the carotid body in mammals, which generate a receptor potential necessary for neurosecretion and activation of sensory/response pathways (Gonzalez et al., 1994). Isolated zebrafish NECs also are responsive to CO_2; electrophysiological characterization of these cells using current or voltage clamp protocols revealed that with increasing CO_2 levels, a background K^+ channel was inhibited, resulting in a PCO_2-dependent depolarization of the NECs (Qin et al., 2010). Evidence obtained from Ca^{2+} imaging of isolated trout NECs suggested that NECs also are sensitive to increases in ammonia, with intracellular [Ca^{2+}] being elevated to a comparable extent by addition of 30 mmol l^{-1} KCl and 1 mmol l^{-1} NH_4Cl (Zhang et al., 2011). Evidence in support of NECs being neurosecretory in response to hypoxia was provided using isolated goldfish (*Carassius auratus*) NECs, where cells with an undisturbed cytosol responded to hypoxia with increased intracellular Ca^{2+} levels and synaptic vesicle activity (Zachar et al., 2017). Yet, despite evidence from *in vitro* studies suggesting that NECs function as tri-modal O_2, CO_2, and NH_3 chemoreceptors, there is a lack of direct evidence *in vivo* to support this view. The only *in vivo* evidence that might suggest a role of NECs in O_2 chemoreception comes from a recent study looking at Ca^{2+} events within the ganglia of cranial nerves IX and X from 5-6 days post fertilization (dpf) larval zebrafish. Upon hypoxia stimulus, these ganglia increase their activity (Yeh et al., 2019). This is interesting as cranial nerves IX and X appear to initiate most cardio-ventilatory responses to hypoxia such as the HVR [reviewed by Milsom (2012)], rhythmic stimulation of the ganglion of cranial nerve X can entrain the respiratory rhythm (De Graaf and Roberts, 1991), and both cranial nerves IX and X extend into the pharyngeal arch region and wrap around 5-HT positive cells, which the authors identified as NECs (Yeh et al., 2019). However, upon close inspection of their morphology and

position in the pharyngeal arch, these 5-HT positive cells actually are Merkel-like cells (MLCs). Merkel-like cells are serotonergic basal cells and together with the elongated taste receptor cells comprise the taste buds of fish and amphibians (Hansen et al., 2002; Wake and Schwenk, 1986). They differ from mammalian taste bud basal cells as there is no evidence of MLCs being proliferative (Kapsimali et al., 2011), whereas mammalian basal cells are proliferating cells that differentiate into taste support or receptor cells (Miura et al., 2001), suggesting that MLCs are unique to fish and amphibians. Merkel-like cells are termed "Merkel-like" as they share many ultrastructural features with the cutaneous Merkel cells first described by Merkel (1880), including small, spiny processes that project into the cytoplasm of surrounding cells and synaptic contacts with the innervating nerve fibers (Whitear, 1989). These features have led to speculation that MLCs may be involved in mechanoreception (Düring and Andres, 1976; Ogawa et al., 1997) and represent a homolog of the mammalian Merkel cell-neurite complex, which is important for sensory transduction (Lumpkin and Caterina, 2007; Ma, 2014; Maksimovic et al., 2013; Maricich et al., 2009). However despite these similarities, MLCs and Merkel cells differ in size, shape, the extent of cytoplasm, number of mitochondria, and number and form of vesicles, suggesting that these two are separate cell types and do not justify the assumption of comparable functions (Whitear, 1989). Considering that NECs are not fully innervated at 5-6 dpf (Jonz and Nurse, 2005), the data of Yeh et al. (2019) suggest that MLCs could serve as O_2 chemoreceptors in larval zebrafish prior to the innervation of NECs. Testing the hypothesis that MLCs are O_2 chemoreceptors is a central focus of this thesis.

1.2.2 Skin NECs

In addition to serotonergic NECs found on the gill filaments and lamellae, populations of cutaneous serotonergic NEC-like cells have been reported in zebrafish larvae (Coccimiglio and

Jonz, 2012; Jonz and Nurse, 2006), mangrove rivulus [*Kryptolebias marmoratus*, (Cochrane et al., 2021; Regan et al., 2011; Rossi et al., 2020)] and adult mudskipper [*Periophthalmodon schlosseri*, (Zaccone et al., 2017)]. Because these skin NECs morphologically resemble O_2-sensitive NECs of the gills, it was proposed that they act as extrabranchial O_2 chemoreceptors. In zebrafish, skin NECs exhibiting innervation are evident in embryos 1 dpf, before the onset of behavioral response to hypoxia (Coccimiglio and Jonz, 2012). A population of skin NECs also expresses synaptic vesicle protein, suggesting the capacity for secretion of neurotransmitters (Coccimiglio and Jonz, 2012). Under normoxic conditions, the total number of skin NECs in larval zebrafish gradually declined with age (3-7 dpf) and were rarely observed in adults. This decline in skin NEC numbers however, was prevented during hypoxia acclimation and was accelerated during acclimation to hyperoxia (Coccimiglio and Jonz, 2012). These results were the first to show that skin NECs in larval zebrafish are sensitive to changes in O_2. Skin NECs are present in larval mangrove rivulus at hatch but not innervated, even though the fish are able to mount a ventilatory response to hypoxia at this stage. In addition, skin NEC development in larval mangrove rivulus is largely unaffected by environmental O_2 levels during the embryonic stage, as neither skin NEC size nor density changed in response to hypoxia or hyperoxia acclimation (Cochrane et al., 2021). However, skin NEC morphology does change in response to environmental O_2 in adult mangrove rivulus, with an increase in cell surface area during hypoxia exposure (Regan et al., 2011) and decreasing in surface area after air exposure (Rossi et al., 2020).

Indirect evidence linking skin NECs and the HVR was provided from denervation experiments in 3-7 dpf larval zebrafish. Following partial chemical denervation of skin NECs using 6-hydroxydopamine, the hyperventilatory response to acute hypoxia was eliminated

(Coccimiglio and Jonz, 2012). The possibility of the drug directly impairing the ability of larvae to hyperventilate was ruled out as both treated or untreated larvae responded to NaCN, a potent ventilatory stimulant, with an increase in f_V (Coccimiglio and Jonz, 2012). Considering that functional gill NECs are also absent before 7 dpf, the authors attributed the HVR in developing zebrafish to be dependent upon innervation of skin NECs. Combined with the morphological changes of skin NECs under hypoxic condition (see above), these results suggest that skin NECs are sensitive to changes in O_2 and may play a role in initiating the responses to hypoxia in developing zebrafish.

1.2.3 Central O_2 chemoreceptors

The existence of a central O_2 chemoreceptor capable of stimulating breathing is not universally accepted, even within the mammalian literature (Funk and Gourine, 2018a; Funk and Gourine, 2018b; Gourine and Funk, 2017; SheikhBahaei, 2020; Teppema, 2018). In support of central O_2 chemoreceptors, there is experimental evidence that the HVR in a variety of mammalian species, although decreased initially, gradually recovers after peripheral chemoreceptor (carotid body) denervation (Gourine and Funk, 2017). In addition, the imposition of hypoxia within the central nervous system (CNS) alone, when carotid bodies were maintained normoxic by means of vascular isolation and separate perfusion, evoked significant increases in ventilation (Curran et al., 2000; Daristotle et al., 1991), suggesting the presence of central O_2 chemoreceptors. An opposing view however is that the partial or complete restoration of the HVR following carotid body denervation results from “upregulation” of aortic bodies, release from cortical inhibition, recruitment of accessory glomus tissue in the trunk, neuroplastic changes consisting of axon regeneration, building alternative circuitries and recruiting central O_2 sensors that may be normally silent (Teppema, 2018). Importantly, the central hypoxia-induced

rise in ventilation is either dependent upon peripheral chemoreceptor integrity (Curran et al., 2000) or does not lead to a progressive increase in ventilation as occurs when the peripheral chemoreceptors are stimulated (Daristotle et al., 1991), suggesting that there are no central O_2 chemoreceptors.

Few studies have examined central O_2 chemoreception in fish and the results of those few studies are inconclusive. Evidence for the presence of central O_2 chemoreceptors was the occurrence of hyperventilation with infusion of hypoxic blood into the dorsal aorta of otherwise normoxic sea raven [*Hemitripterus americanus*, (Saunders and Sutterlin, 1971)] whereas infusion of hypoxic blood into the ventral aorta also resulted in hyperventilation but only after a significant latency. It was thought that the delayed response reflected the time required for the hypoxic blood to travel to central chemoreceptors (Bamford, 1974). A more direct approach of exposing *in vitro* brain stem preparations of goldfish to hypoxia resulted in a 36% increase of rhythmic motor output (Côté et al., 2014). However, direct perfusion of the brain with hypoxic saline in both the tambaqui (*Colossoma macropomum*) and bowfin (*Amia calva*) failed to alter ventilation and reveal the presence of central chemoreceptors responsive to hypoxia (Hedrick et al., 1991; Milsom et al., 2002). Additionally, in the channel catfish (*Ictalurus punctatus*), ventilatory reflexes to hypoxia were abolished following branchial denervation (Burleson and Smatresk, 1990a), suggesting that that peripheral (branchial) sites are solely responsible for hypoxic chemoreception in this species. Although there is no direct evidence for the presence of piscine central O_2 chemoreceptors, the idea that central O_2 chemoreceptors may be present in fish is worthy of further investigation.

1.3 Neuromodulation of ventilation in fish

Despite the lack of direct evidence that NECs secrete neurotransmitters *in vivo* during hypoxia, hypercapnia or elevated ammonia, a wide array of neuroendocrine substances has been implicated in the control of breathing in fish. In addition to acting directly through neurosecretion from NECs onto afferent nerves, neuroendocrine substances could also act directly on central integrative sites or other central areas impinging on respiratory centers and/or on motor output pathways or effectors (muscles) directly (Burleson and Milsom, 1995a; Burleson and Milsom, 1995b). Previous studies have shown that neuroendocrine factors including serotonin, catecholamines, acetylcholine and gaseous neurotransmitters may play important roles in mediating the ventilatory responses (Burleson and Milsom, 1995a; Burleson and Milsom, 1995b; Jonz et al., 2015; Perry et al., 2016; Rahbar et al., 2016; Randall and Taylor, 1991; Shakarchi et al., 2013). In mammals, there is a growing consensus that the purines ATP and adenosine are the principal signaling molecules released by peripheral chemoreceptors, which ultimately activate cardiorespiratory centers in the brainstem leading to appropriate changes in ventilation (Leonard et al., 2018). In contrast, there is less certainty concerning the principal neuroendocrine factors that mediate the ventilatory responses in fish.

1.3.1 Serotonin (5-HT)

5-HT has received much attention as a neuroendocrine regulator of breathing owing to its presence within NECs – the putative O_2 chemoreceptors. Early evidence of 5-HT playing a role in the control of breathing arose from electrophysiological studies where application of 5-HT to the external gill surfaces of spiny dogfish (*Squalus acanthias*) initiated discharge of afferent nerve fibers of the gill filaments (Poole and Satchell, 1979). Later, it was shown that single nerve

fibres in the gills of rainbow trout were excited during perfusion with 5-HT, albeit with a modest and transient activity. Notably, these were the same nerve fibers that responded to either internal or external hypoxia (Burleson and Milsom, 1995a). Burleson and Milsom (1995b) further showed that intra-arterial injection of 5-HT resulted in a significant increase in gill ventilation rate, consistent with previous findings (Fritsche et al., 1992; Thomas et al., 1979). Ventilatory responses to exogenous 5-HT have now been reported in several additional species including European eel [*Anguilla anguilla*, (Janvier et al., 1996)], Gulf toadfish [*Opsanus beta*, (McDonald et al., 2010; Panlilio et al., 2016)], and zebrafish (Abdallah et al., 2015b; Shakarchi et al., 2013). Based on pharmacological studies, it would appear that 5-HT_2 and 5-HT_3 receptors are responsible for the modulation of breathing through 5-HT. In Gulf toadfish, ventilation amplitude was stimulated by 5-HT_2 receptor agonists and this response was blocked by ketanserin, a 5-HT_2 receptor antagonist (McDonald et al., 2010). Similarly, in zebrafish, ketanserin inhibited the hyperventilatory response initiated by acute hypoxia (Shakarchi et al., 2013). In European eel (Janvier et al., 1996) and zebrafish (Jonz et al., 2015), 5-HT_3 receptor agonists alone can elicit a hyperventilatory response, while 5-HT_3 receptor blockade reduces the hyperventilation in response to external 5-HT or acute hypoxia.

Knowledge concerning the specific site of action *in vivo* is scarce owing, in part, to the technical challenge of blocking/activating site-specific 5-HT receptors. In the few studies using rainbow trout, exogenously administered 5-HT in the brain caused a potent stimulatory effect on ventilation, which was mimicked by α-methyl-5-HT, a 5-HT_2 receptor agonist, leading the authors to conclude that 5-HT mediates ventilation centrally, potentially through 5-HT_2 receptors (Kermorgant et al., 2014a). In addition, fluoxetine, a selective 5-HT reuptake inhibitor, administrated into the brain also increased ventilation amplitude, further supporting 5-HT's role

in mediating ventilation through central pathways (Kermorgant et al., 2014b). Alternatively, 5-HT could be playing an indirect role in the control of ventilation, because it is known to provoke large increases in circulating catecholamine levels (Fritsche et al., 1993; Fritsche et al., 1992), which themselves are implicated in the neuroendocrine control of breathing (see below).

1.3.2 Catecholamines

Catecholamines [adrenaline (AD), noradrenaline (NA), and dopamine (DA)] are another class of neuroendocrine factors that have been extensively studied as possible modulators of breathing in fishes. The idea that circulating catecholamines may contribute to ventilatory responses in fish originated with the studies of Peyraud-Waitzenegger and colleagues (Peyraud-Waitzenegger, 1979; Peyraud-Waitzenegger et al., 1980) using the European eel (*Anguilla anguilla*). In those studies, intravenously administered adrenaline or noradrenaline caused a hyperventilatory response in summer months owing to stimulation of β-adrenoreceptors, whereas adrenaline or noradrenaline caused a hypoventilatory response in winter months owing to the stimulation of α-adrenoreceptors (Peyraud-Waitzenegger, 1979; Peyraud-Waitzenegger et al., 1980). Subsequent studies extending to other species and utilizing a variety of protocols demonstrated that the effects of circulating catecholamines on ventilation are highly variable regardless of season with responses ranging from hypoventilation to hyperventilation and in some cases, no effect [see Table 1 in Pan and Perry (2020)]. Ultimately, two opposing views on the role of circulating catecholamines on the control of breathing emerged. In one (Randall and Taylor, 1991), circulating catecholamines are thought to play a critical role in eliciting hyperventilatory responses, while in the other (Perry et al., 1992), circulating catecholamines do not play a significant role in the control of ventilation, but rather that breathing is controlled primarily by both external and internal respiratory/acid-base status. It is now generally accepted

that circulating catecholamines although frequently elevated during periods of hyperventilation, do not contribute significantly to the initiation of increased ventilation but may play a secondary modulatory role. Certainly, there is no doubt that fish can mobilize catecholamines to the blood plasma at times when ventilation is stimulated such as when exposed to acute hypoxia (Boutilier et al., 1988; Butler et al., 1978; Kinkead et al., 1991; Perry and Gilmour, 1996; Perry et al., 1991; Perry and Reid, 1992; Perry et al., 2004; Perry and Wood, 1989; Reid and Perry, 2003). However, some species such as spiny dogfish (*Squalus acanthias*) may not exhibit an increase in catecholamine levels despite elevated ventilation (Perry and Gilmour, 1996), and in other species, the release of catecholamines into the circulation is delayed until the stressor becomes severe, by which time the fish is already hyperventilating (Perry and Reid, 1992; Perry et al., 2004). Additionally, intra-arterial/intravenous administration of catecholamines to fish with elevated breathing does not increase ventilation further and in some cases, ventilation may actually decrease (Kinkead and Perry, 1991; Milsom et al., 2002; Perry and Thomas, 1991).

While circulating catecholamines are unlikely to initiate hyperventilation, it is possible that catecholamines acting as neurotransmitters might influence breathing, potentially via sympathetic stimulation of gill O_2 chemoreceptors or activation of central respiratory neurons. Currently, there are no data in fish to support the sympathetic stimulation of gill O_2 chemoreceptors hypothesis. Even though the β-adrenoreceptor antagonist propranolol inhibited O_2 receptor discharge from perfused *O. mykiss* first gill arch preparation (Burleson and Milsom, 1990), β-adrenergic stimulation of the same preparation using adrenaline, noradrenaline or isoproterenol had little effect on neural activity from chemoreceptor afferent neurons (Burleson and Milsom, 1995a). However, there is some evidence in mammals that intravenous catecholamine infusion can stimulate carotid body chemoreceptors (Joels and White, 1968). The

activation of central respiratory neurons hypothesis is more probable because noradrenaline can cross the blood-brain barrier in some fish species including rainbow trout (Nekvasil and Olson, 1986), possibly explaining the effects of catecholamines on breathing. Moreover, direct injection of catecholamines in the vicinity of the central pattern generator or the respiratory motor neurons caused a marked change in the pattern of central respiratory drive measured as bursting activity in branchial nerves, suggesting that catecholamines can alter breathing patterns in the central nervous system (Randall and Taylor, 1991).

Recent studies examining the role of catecholamines in regulating ventilation is scarce, but a previous study showed that exogenous dopamine depressed ventilation frequency in zebrafish at 7 – 21 dpf (Shakarchi et al., 2013). Data from our own lab also suggests that 4 dpf larval zebrafish hyperventilate when exposed to adrenaline (Pan and Perry, 2020). Given the ease of genetic manipulation, zebrafish may emerge as a good model to further assess the roles of circulating versus neuronal catecholamines in the control of breathing in fish.

1.3.3 Acetylcholine (ACh)

In mammals, there is compelling evidence that acetylcholine is one of the primary excitatory neurotransmitters within the peripheral chemoreceptor – the carotid body glomus cells (Nurse, 2010). However, the role of acetylcholine in the control of breathing in fish has received little attention. There is evidence of presumptive cholinergic NECs localized to the gills in fish. In zebrafish and mangrove rivulus, non-serotonergic NEC-like cells express the vesicular acetylcholine transporter (Regan et al., 2011; Shakarchi et al., 2013), a protein that mediates loading of acetylcholine into secretory vesicles, which may be used as a marker for cholinergic cells (Prado et al., 2002). In the absence of further investigation, it is unclear whether these cholinergic cells function as chemoreceptors.

As for acetylcholine itself, there is evidence both for and against its role in the control of breathing in fish. Early evidence for cholinergic influence of ventilation was demonstrated in African lungfish (*Protopterus aethiopicus*), where intravenous administration of nicotine elicited an increase in both pulmonary and branchial breathing (Johansen and Lenfant, 1968). Later, afferent nerve activity from rainbow trout perfused first gill arch preparations was stimulated markedly by acetylcholine or nicotine, while muscarine elicited only a moderate stimulation. However, the muscarinic receptor antagonist atropine prevented the stimulation caused by acetylcholine, nicotine, muscarine as well as hypoxia in the gill arch preparations (Burleson and Milsom, 1995a). Intra-arterial injection of acetylcholine, nicotine or muscarine into rainbow trout also caused an increase in ventilation through increases in both f_V and opercular pressure, yet atropine had no effect on these ventilation variables (Burleson and Milsom, 1995b). Similarly, atropine also did not abolish the ventilatory responses to hypoxia and NaCN in channel catfish (Burleson and Smatresk, 1990b). Moreover, intra-arterial injection of atropine did not attenuate the increase in f_V or opercular pressure in the Adriatic sturgeon (*Acipenser naccarii*) in response to hypoxia or NaCN (McKenzie et al., 1995). More recently, the cholinergic control of breathing was examined in zebrafish. Exogenous application of acetylcholine increased ventilation frequency in late stage (14 – 21 dpf) larvae (Rahbar et al., 2016; Shakarchi et al., 2013) but not in younger (10 – 12 dpf) larvae (Shakarchi et al., 2013), yet nicotine was able to irreversibly increase f_V in both stages (Jonz et al., 2015). The increase in ventilation caused by acetylcholine was blocked by the nicotinic acetylcholine receptor antagonist hexamethonium (Shakarchi et al., 2013) or high doses of atropine (Rahbar et al., 2016). Overall, the results of these studies suggest that there may be a cholinergic control of breathing in fish, which possibly is mediated by the nicotinic rather than the muscarinic acetylcholine receptors.

1.3.4 Adenosine triphosphate (ATP)

ATP is a primary excitatory neurotransmitter within the carotid body in mammals (Nurse, 2010) that has received little attention in fish with respect to its role in the control of breathing. In the few studies that examined the purinergic control of ventilation, it was shown that the hyperventilatory response to hypoxia is inhibited by exogenous application of P2X3 purinoceptor antagonists and adenosine antagonists (Coe et al., 2017; Rahbar et al., 2016; Stecyk and Farrell, 2006). Importantly, the exogenous administration of ATP-γ-S, a broad-spectrum purinoceptor agonist, elicited hyperventilation in zebrafish (Coe et al., 2017). Immunohistochemical studies showed that P2X3 receptors are present in 5-HT-positive NECs of zebrafish gill filaments, as well as in adjacent non-serotonergic cells, suggesting a paracrine role for NEC P2X3 receptors in modulating neurotransmitter release in the gill (Rahbar et al., 2016).

More definitive evidence for the purinergic control of ventilation at the central level was demonstrated using isolated brainstem preparations of the lamprey (*Petromyzon marinus*). ATP caused a biphasic respiratory response that was related to ATP metabolism, because increases in fictive respiratory frequency were evoked by the non-hydrolysable purinoceptor agonist ATP-γ-S, while observed decreases in fictive respiratory frequency were mimicked by the ATP metabolite adenosine. These results suggest that in the brainstem, the determination of fictive breathing is related, in part, by the balance between ATP- and adenosine-induced effects (Cinelli et al., 2017).

1.3.5 Gaseous neurotransmitters (gasotransmitters)

Gasotransmitters including nitric oxide (NO), carbon monoxide (CO) and hydrogen sulfide (H_2S), are small membrane permeable biologically active gases produced endogenously that can

act as potent intracellular signaling molecules to influence an array of diverse physiological functions via autocrine, paracrine or neuroendocrine routes (Olson et al., 2012). The role of gasotransmitters in the control of breathing was reviewed in detail by Perry *et al.* (2016), and thus only a brief summary is provided here.

The formation of NO is catalyzed by nitric oxide synthase (NOS), of which two isoforms are found in fish – neuronal NOS (nNOS) and inducible NOS [iNOS, (Perry et al., 2016). Of the two isoforms, nNOS was localized to NECs of both Indian catfish [*Heteropneustes fossilis*, (Mauceri et al., 1999)] and zebrafish (Porteus et al., 2015). In zebrafish larvae, NO produced via nNOS contributes to the hyperventilatory response to hypoxia while in adult zebrafish, NO is inhibitory and may contribute to hypoventilatory responses to hyperoxia (Porteus et al., 2015). Centrally, nNOS is present in the brain regions involved in respiratory integration and rhythm generation of zebrafish as early as 5 dpf (Holmqvist et al., 2000; Holmqvist et al., 2004), but its function in the central control of breathing has not yet been investigated.

Endogenous CO is produced largely by heme oxygenases (HO). Of the three heme oxygenase isoforms (HO-1, HO-2 and HO-3) that are known to exist in mammals, only two have been identified in fish; the inducible HO-1 and the constitutively expressed HO-2 (Perry et al., 2016). Of the two isoforms, HO-1 was localized to a sub-population of NECs in larval zebrafish (Tzaneva and Perry, 2016) and NECs of cold- but not warm- acclimated goldfish [*Carassius auratus*, (Tzaneva and Perry, 2014)]. Similar to mammals where CO is an inhibitory gaseous messenger in the carotid body (Prabhakar, 2012), inhibition of HO-1 in cold-acclimated goldfish increased the ventilatory response to hypoxia (Tzaneva and Perry, 2014), and knockdown of HO-1 in larval zebrafish significantly elevated f_V under normoxic conditions, which was reduced by the addition of exogenous CO (Tzaneva and Perry, 2016). These results suggest that the

endogenous production of CO via HO-1 plays an inhibitory role in the control of ventilation in fish.

The most recently discovered gasotransmitter, H_2S (Wang, 2002), may play the most important role in the sensing of O_2 and the control of breathing. Biosynthesis of H_2S is predominantly mediated by the enzymes cystathionine β-synthase (CBS) and cystathionine γ-lyase (CSE), both of which are expressed within the gills of rainbow trout. Homogenized trout gills are able to produce H_2S enzymatically, a reaction which is inhibited by O_2. More importantly, intrabuccal injection of H_2S in unanesthetized trout increased f_V and amplitude similar to that of the hypoxic response (Olson et al., 2008). In zebrafish, CSE, but interestingly not CBS, is co-localized in skin NECs of 4 dpf larvae, indicating that H_2S is likely produced endogenously (Porteus et al., 2014a). At this stage, larvae responded to exogenous H_2S by increasing ventilation; inhibiting the production of endogenous H_2S either pharmacologically or by knocking down CBS or CSE blunted or abolished the acute hypoxic ventilatory response (Porteus et al., 2014a). Adult zebrafish also hyperventilated in response to exogenous H_2S and as in larvae, pharmacological inhibition of H_2S production reduced the hypoxic hyperventilatory response (Porteus et al., 2014a). In zebrafish NECs isolated from adult gill filaments, hypoxia or H_2S application produced a similar ~10-mV depolarization (Olson et al., 2008), These results are consistent with findings in mammals where hypoxia evoked H_2S production in the carotid body glomus cells leads to increased cytosolic Ca^{2+} and the secretion of catecholamines (Makarenko et al., 2012; Peng et al., 2010).

1.4 The hypoxic ventilatory response (HVR)

To date, all fish species studied exhibit a HVR when exposed to hypoxia (Perry et al., 2009). This simple statement however does not do justice to the complexity of this response, as the HVR is not just a simple increase of ventilation under the challenge of hypoxia. Depending on the pattern, intensity and duration of the hypoxic stimuli, the patterns of the HVR may differ greatly (Porteus et al., 2011; Powell et al., 1998). In fish, the temporal profiles of the HVR have not been extensively studied, but in mammals exposed to a single, continuous hypoxia (ranging from minutes to hours), the HVR appears as a biphasic response consisting of a short initial rise in ventilation (augmentation phase) rapidly followed by a secondary roll-off or depression phase (Bissonnette, 2000; Moss, 2000; Teppema and Dahan, 2010). The pattern of HVR also differs slightly between neonatal and adult animals, with neonates exhibiting a small augmentation phase compared to the depression phase, resulting in a lower baseline ventilation compared to normoxia, while adults have a much greater augmentation phase and a smaller depression phase, resulting in a new steady state of ventilation that is ~25–40% above the normoxic baseline when under hypoxic conditions (Bissonnette, 2000; Moss, 2000; Teppema and Dahan, 2010). The augmentation phase in mammals is mediated by peripheral chemoreceptors, as carotid body denervation abolishes or greatly attenuates this response. However, the mechanisms mediating the depression phase is much more controversial, with a time-dependent decrease in peripheral chemoreceptor activity or sensitivity, impaired central integration of peripheral chemoreceptor input, decreased metabolism, and active inhibition of central regions involved in ventilation by inhibitory neurotransmitters all as possible mechanism (Bissonnette, 2000; Powell et al., 1998; Teppema and Dahan, 2010). For a more comprehensive review of the mechanisms underlying

both the augmentation and depression phase, the reader is referred to these reviews by Bissonnette (2000) and Teppema and Dahan (2010).

The majority of studies examining the HVR in fish have focused on a single time point or a few time points during hypoxia exposure and lacked the sensitivity to observe temporal patterns of the HVR, particularly during the acute phase. Regardless, in general most species increase total gill ventilation by increasing ventilation amplitude with small increases in f_V when exposed to hypoxia (Perry et al., 2009). Studies of prolonged hypoxia exposure (> 2 h) suggest that the HVR of fish also may be biphasic, although the depression phase that occurs within 5–30 min of hypoxic exposure in mammals may take several hours to develop in bowfin[*Amia calva*, (Porteus et al., 2011)]. Recently, studies from our lab have shown that the HVR in larval zebrafish is biphasic under short term continuous hypoxia exposure (Mandic et al., 2019; Zimmer et al., 2020). This interesting finding suggests that a complex network controlling ventilation is likely well-developed at this stage, even though larval zebrafish (< 14 dpf) do not possess developed gills and rely predominantly on cutaneous respiration (Rombough, 2002).

In adult fish, the HVR serves to minimise the negative consequences of hypoxia on respiratory gas transfer. Under increased ventilation, the residence time of water flowing over the gill lamellae is decreased, in turn decreasing the difference in PO_2 between inspired and expired water and serving to increase the water-to-blood PO_2 gradient and raising O_2 diffusive conductance (Perry et al., 2009; Perry and Gilmour, 2002). An important outcome of the HVR is delaying the transition from aerobic to anaerobic metabolism during progressively severe hypoxia. Interestingly, some larval fish species also exhibit a HVR (Burggren et al., 2016; Holeton, 1971; Jonz and Nurse, 2005; McDonald and McMahon, 1977; Peterson, 1975). The HVR in larvae is intriguing because at this stage of development, these fish possess undeveloped

gills that contribute little to gas and ion exchange, in comparison to skin (Fu et al., 2010; Rombough, 2002; Rombough and Ure, 1991; Wells and Pinder, 1996; Zimmer et al., 2014). Thus, the physiological significance of the HVR and its temporal patterns in larval fish that rely predominately on cutaneous gas transfer are areas deserving of further research; each is addressed in Chapter 2.

1.5 Rationale and outline of the thesis

There is a general consensus that gill and skin NECs are the peripheral O_2 chemoreceptors in fish. Surprisingly, however, there is no evidence that either gill or skill NECs are O_2 sensitive ***in vivo***, nor has a link been established between NEC activation and the HVR. Research in piscine O_2 chemoreception also has focused on identifying the neurotransmitters involved in O_2 sensing and signal transduction, with most studies using pharmalogical activation/inhibition of various neurotransmitter receptors. An inherent downside of this approach is that when measuring ventilation as an end-point, interpretation of the data is confounded by the multiple possible sites of action of these drugs. With the recent advances in genetic manipulation, especially Tol2 based transgenesis techniques and CRISPR/Cas9 based knockout techniques (Zimmer et al., 2019), zebrafish is emerging as an important model species to further examine piscine O_2 chemoreception through gene editing. The main goal of my thesis is to use genetically manipulated zebrafish larvae to demonstrate O_2 sensitivity of peripheral O_2 chemoreceptors *in vivo*, identify potential neurotransmitters involved in O_2 chemoreception by examining cellular responses within a signaling network believed to contribute to the control of breathing, and to establish a link between peripheral O_2 chemoreceptors and the HVR. However, before proceeding, I needed to address questions regarding the physiological significance of O_2

chemoreception and the HVR in zebrafish larvae. Because the larvae rely predominately on cutaneous gas transfer, the benefit of increasing water flow over the undeveloped gill is of questionable value. Thus, my thesis is composed of three data chapters; Chapter 2 focuses on the physiological significance of the HVR in larval zebrafish, Chapter 3 addresses the role of 5-HT in O_2 chemoreception/HVR, and Chapter 4 present *in vivo* evidence of O_2 chemoreception in Merkel-like cells (MLCs), a newly proposed piscine peripheral O_2 chemoreceptor. Chapter 5 attempts to synthesize the principles gained from these studies and proposes a model for piscine O_2 chemoreception, beginning with peripheral O_2 chemoreception and culminating in the HVR. Where possible, I have tried to avoid repetition, but some duplication is unavoidable because this thesis is composed partly of published manuscripts. This thesis provides valuable and novel insights into piscine O_2 chemoreception and offers additional directions for future research.

CHAPTER 2. Evaluating the physiological significance of hypoxic hyperventilation in larval zebrafish *(Danio rerio)*

Notes on Chapter

The present chapter is published in Journal of Experimental Biology as per the following citation:

Pan, Y. K.*, Mandic, M.*, Zimmer, A. M. and Perry, S. F. (2019). Evaluating the physiological significance of hypoxic hyperventilation in larval zebrafish (*Danio rerio*). J. Exp. Biol 222, jeb204800. (* equal contribution)

Author contributions: Y.K.P., M.M., and S.F.P. performed conceptualization of the experiments; Y.K.P. and M.M. performed and analyzed data from the ventilation and respirometry experiments; A.M.Z. performed and analyzed data from the SMOT experiment; all authors participated in data interpretation; Y.K.P. prepared the manuscript, all authors contributed to the revision of the manuscript; S.F.P. provided supervision.

Abstract

In water-breathing fishes, the hypoxic ventilatory response (HVR) represents an increase in water flow over the gills during exposure to lowered ambient O_2 levels. The HVR is a critical defense mechanism that serves to delay the negative consequences of hypoxia on aerobic respiration. However, the physiological significance of the HVR in larval fishes is unclear as they do not have a fully developed gill and rely primarily on cutaneous gas transfer. Using larval zebrafish (4, 7, 10 and 15 days post fertilization; dpf), we examined their HVR under three levels of hypoxia (25, 45 and 60 mmHg). The larvae exhibited widely different HVRs as a function of developmental age and level of the hypoxia. Yet, critical O_2 tensions (P_{crit}) remained constant (30 - 34 mmHg) over the same period of development. Micro-optrode O_2 sensors were used to measure a significant decrease in buccal cavity water O_2 tensions in 4 and 7 dpf larvae compared to the water they inspired, demonstrating significant extraction of O_2 from the buccal cavity. To assess the physiological significance of the HVR, ventilatory water flow was prevented in larvae at 4 and 7 dpf by embedding their heads in agar. An increase in P_{crit} was observed in 7 but not 4 dpf larvae, suggesting that buccal ventilation is important for O_2 extraction by 7 dpf. Combined, these data indicate that branchial/buccal gas transfer plays a significant role in O_2 uptake during hypoxia, and supports a physiological benefit of the HVR in early life stages of zebrafish.

2.1 Introduction

The hypoxic ventilatory response (HVR) is a widely conserved physiological phenomenon in fish exposed to lowered ambient water O_2 tension (PO_2). By increasing ventilation frequency (f_V) and/or ventilation amplitude, the vast majority of water-breathing fishes studied to date exhibit an increase in the volume of water flowing over the gills when exposed to hypoxia (Perry et al., 2009). By decreasing the residence time of water flowing over the gill lamellae, an increase in ventilation volume serves to decrease the PO_2 difference between inspired and expired water, hence raising the average PO_2 of the ventilatory water and increasing the water-to-blood PO_2 gradient (ΔPO_2). In addition to raising O_2 diffusive conductance (O_2 uptake/ΔPO_2), the increased average ventilatory water PO_2 minimizes the decline in arterial PO_2 during hypoxia (Perry et al., 2009; Perry and Gilmour, 2002). Thus, hyperventilation during hypoxia ultimately delays the transition from aerobic to anaerobic metabolism. A drawback of the HVR is an increase in energy expenditure for ventilation, which is believed to be relatively high even under normoxic conditions (Jones and Schwarzfeld, 1974; Steffensen, 1985). As water PO_2 first begins to drop, ventilation rises to a maximal rate, and then decreases during the most severe levels of hypoxia (Cerezo and García García, 2004; Scott et al., 2008) presumably at the point where the cost of increasing ventilation exceeds the benefits to O_2 transfer (Perry et al., 2009).

Similar to adults, some larval fish species also hyperventilate in response to hypoxia (Burggren et al., 2016; Holeton, 1971; Jonz and Nurse, 2005; McDonald and McMahon, 1977; Peterson, 1975). The hyperventilatory response of larvae is intriguing because at this stage of development, these fish possess undeveloped gills that contribute little to gas and ion exchange,

in comparison to skin (Fu et al., 2010; Rombough, 2002; Rombough and Ure, 1991; Wells and Pinder, 1996; Zimmer et al., 2014).

At the time of hatch, the gill of the rainbow trout (*Oncorhynchus mykiss*) larva possesses filaments, with rudimentary lamellae developing soon after (Gonzalez et al., 1996; Morgan, 1974; Rombough, 1999). However, the gill of post-hatch trout larvae is not the primary site for gas or ion transfer. Indeed, at hatch, the gill does not contribute to ammonia excretion (Zimmer et al., 2014) and accounts for merely 10% of Na^+ uptake and approximately 20% of total O_2 uptake (Fu et al., 2010; Zimmer et al., 2014). The gill does not become the primary site of O_2 uptake until 27 days post-hatch [dph, (Fu et al., 2010; Zimmer et al., 2014)]. Nonetheless, it is clear that larval trout exhibit a HVR as early as 1 dph (Holeton, 1971). Similarly, in zebrafish (*Danio rerio*), gill development does not occur until just after hatching [at 3 days post fertilization (dpf) at 28 ºC], beginning with the appearance of gill filament primordia on the pharyngeal arches, followed by the appearance of lamellae at 7 dpf (Jonz and Nurse, 2005; Kimmel et al., 1995). Like trout, early larval zebrafish also do not utilize gills as a primary site for O_2 uptake (Rombough, 2002). Based on the empirical relationship between skin surface area per unit O_2 uptake and body mass (Rombough, 2004) as well as the results of experiments that prevented buccal water flow (Rombough, 2002), it was determined that gills are not required for O_2 uptake until 10 - 14 dpf. Yet, despite the gills not being the primary O_2 uptake site in early development, larval zebrafish initiate the HVR as early as 3 dpf (Jonz and Nurse, 2005).

Given the limited role of the larval gill in O_2 uptake, the physiological significance of a hyperventilatory response to hypoxia in larval fishes is unclear. It has been suggested, however, that the development of the HVR before complete formation of the gill may act to ensure that O_2-sensing pathways are functional by the time the larvae become dependent on branchial

respiration (Jonz and Nurse, 2005). Because small larvae reside in a viscous environment (i.e. low Reynolds number), fluid accelerated by ventilation rapidly decelerates between cycles, potentially incurring a higher ventilation energy expenditure than in adult fish (Rombough, 1988). Thus, it is conceivable that increasing ventilation might decrease survival time in hypoxia if the hyperventilatory response is of no physiological benefit. We therefore hypothesize that zebrafish larvae can regulate the HVR depending on PO_2 levels, and that the HVR plays a physiological role in maintaining O_2 uptake in larval zebrafish. A first objective was to examine the HVR at several development stages (4, 7, 10 and 15 dpf) and to determine whether the dynamic characteristics of the HVR are related to critical O_2 tension (P_{crit}), the PO_2 below which the fish can no longer maintain a stable rate of O_2 consumption [$\dot{M}O_2$, (Ultsch et al., 1978)]. A second objective was to measure PO_2 within the buccal cavity of 4 and 7 dpf larvae to determine whether O_2 is extracted from water in the buccal cavity. Lastly, we prevented larvae from ventilating and observed whether the fish exhibited a reduced capacity for O_2 uptake.

2.2 Materials and Methods

2.2.1 Experimental animals

Zebrafish were obtained from in-house stock at the University of Ottawa aquatic care facility. Fish were maintained at 28°C under a 14 h:10 h light:dark cycle in dechloraminated city of Ottawa tap water and fed to satiation twice daily. Adults were bred using breeding traps as per standard methods (Westerfield, 2000) to obtain embryos. Briefly, one male and two females were separated the night before breeding using a divider in 2 L breeding traps. Once lights turned on the next day, water in the tank was changed and the dividers were removed allowing the zebrafish to breed. Embryos were collected and reared initially in an incubator (28.5°C) in 50 ml

Petri dishes containing dechloraminated city of Ottawa tap water and 0.05% Methylene Blue. At 5 days post fertilization (dpf), larvae were transferred to static 1 l tanks and fed once daily except on the day of the experiment when food was withheld. Water was changed daily in the Petri dishes and every other day in the static tanks. The larvae were raised in static tanks until 7, 10 or 15 dpf. All procedures for animal use and experimentation were carried out in compliance with the University of Ottawa Animal Care and Veterinary Service guidelines under protocol BL-226 and adhered to the recommendations for animal use provided by the Canadian Council for Animal Care.

2.2.2 Ventilation in developing larvae

The hypoxic ventilatory response, specifically ventilation frequency (f_V), was measured at 4, 7, 10 and 15 dpf during acute exposure to hypoxia (60, 45 or 25 mmHg). These developmental stages were chosen based on the timing of the physical development of the gills, as well as the development of O_2-sensing pathways within the gills of zebrafish larvae. At 4 dpf, gill filament primordia are present on the pharyngeal arches yet the putative O_2 chemoreceptors – neuroepithelial cells (NECs) of the gill filaments – do not appear until 5 dpf (Jonz and Nurse, 2005). By 7 dpf, lamellae begin to form, and all NECs receive innervation (Jonz and Nurse, 2005) yet regular buccal movements are not observed until 8 dpf (Jonz and Nurse, 2005). Lastly, the 15 dpf point was chosen as it is believed that gills become the dominant site of gas transfer at 14 dpf (Rombough, 2002). An individual larva was placed in a glass micro-capillary tube with an inner diameter of 1 mm. Water containing 0.05 mg ml^{-1} Tris-buffered (pH 7.6) MS-222 (ethyl-3-aminobenzoate methanesulfonate salt, Syndel Laboratories, Nanaimo, Canada) maintained at 28.5 ºC was gravity-fed through the microcapillary tube at a rate of 1.6 – 1.8 ml min^{-1}. Tris-buffered MS-222 was used to minimize the movement in larval zebrafish to facilitate f_V analysis

(Jonz and Nurse, 2005). Each larva was allowed to recover from handling in the chamber for 10 min in normoxic water (PO_2 = 153 mmHg) prior to the start of the trial. During each trial, f_V was recorded by video for 5 min under normoxic conditions (baseline), followed by 15 min under hypoxia and an additional 5 min after returning to normoxia. Videos were recorded using an iPhone SE mounted onto a dissecting microscope (stereo trinocular microscope, AmScope, Irvine, USA). Average f_V was determined for each minute by counting either buccal or opercular movements depending on the fish orientation in the chamber and the visibility of the mouth and/or operculae. Each larval zebrafish was exposed to only one single level of hypoxia; different animals were used for different levels of hypoxia.

2.2.3 Respirometry in developing larvae

Routine metabolic rate (RMR) and P_{crit} were measured using closed system respirometry. Larvae of the same developmental age were placed into individual respirometry wells (80 µl for 4 and 7 dpf; 500 µl for 10 and 15 dpf) using a 24-well glass microplate (Loligo Systems, Viborg, Denmark) fitted with O_2 sensor spots. The microplate was sealed with adhesive plate seals (AB0580, ThermoFisher Scientific, Mississauga, Canada) and maintained at 29 ºC using a water bath. The sealed microplate and water bath were attached to an O_2 fluorescence sensor (SDR SensorDish Reader, PreSens, Regensburg, Germany), and PO_2 levels were measured until they plateaued, at which point the experiment was ended. Larval fish weights were obtained by raising separate batches of fish to the same developmental age. Fish (n = 11-18) were pooled into a single mini 5 µm cell strainer (pluriSelect, San Diego, USA) and excess water was removed by centrifugation (100 × *g*). Weights were measured using an analytical balance, and at least six pooled weights were obtained for each developmental age and used in the following calculation of $\dot{M}O_2$ (µmol g^{-1} h^{-1}):

$$\dot{\mathrm{M}}O_2 = \frac{\Delta \mathrm{P}O_2 \times \alpha O_2 \times V}{M}$$

Where ΔPO_2 is the slope of PO_2 over time (mmHg h^{-1}), αO_2 is the solubility coefficient of O_2 (µmol l^{-1} $mmHg^{-1}$) in freshwater at 28°C (Boutilier et al., 1984), V is the respirometer volume (l) and M is the body mass of fish (g). The volume of the fish accounted for less than 0.4% of the respirometer volume and thus was not considered to displace a significant volume in the respirometer. Data were binned in 5 mmHg intervals. Metabolic rate was calculated as the average $\dot{M}O_2$ before PO_2 levels dropped below 90 mmHg. This cut-off was chosen because both 7 dpf larvae and adults do not hyperventilate when PO_2 is above 90 mmHg (unpublished observations; Vulesevic and Perry, 2006). P_{crit} was calculated by the "broken-stick" regression approach, adopted from Yeager and Ultsch (1989). This approach estimates P_{crit} as the intersection of the two linear regression lines that best fit the PO_2 versus $\dot{M}O_2$ plot and was carried out using the REGRESS software (www.wfu.edu/~mudayja/software/o2.exe). PO_2 versus $\dot{M}O_2$ plots and P_{crit} regression lines were inspected “blindly” by two researchers independently for quality control, and only those that both researchers deemed to be valid traces were retained. Traces that were excluded either did not have a stable oxy-regulatory phase in the PO_2 versus $\dot{M}O_2$ curve to fit a tightly fitted line or used less than 4 data points to fit the oxy-conforming phase of the curve, indicating that the fit was likely driven by an outlier.

Respirometry was also conducted on 4 and 7 dpf larvae whose heads were embedded in agar (applying an “agar helmet”) to prevent gill ventilation (Rombough, 2002). To apply the agar, larvae were lightly anesthetised in 0.05 mg ml^{-1} Tris-buffered MS-222. A larva was transferred onto a glass slide and excess water around the larva was removed using a pipette. 1 – 2 µl of 2.5% low melting point agarose (ThermoFisher Scientific, Mississauga, Canada) was applied to the head and was allowed to set before excess agar was trimmed off using a micro

scalpel. Control fish were subjected to the same treatment excluding the application of agar. The treated larvae were allowed to recover from anaesthesia and handling for 1 h before RMR and P_{crit} were measured as described above. To determine whether the agar might also be impeding O_2 diffusion (in addition to preventing ventilatory water flow), a "proof of principle" experiment was conducted in which RMR and P_{crit} were compared in larvae with agar applied to the head only and in larvae experiencing encasement of the whole body in agar. The results (data not shown) demonstrated that RMR ($P = 0.75$, Mann-Whitney rank sum test) and P_{crit} ($P = 0.13$, Student's t-test) did not differ in the two treatment groups suggesting that applying agar to the head is a viable method of preventing ventilation without affecting cutaneous O_2 uptake.

2.2.4 Visualization of buccal cavity water flow

Water flow through the buccal cavity of a ventilating 4 dpf larval zebrafish was visualized by injecting 0.5% phenol red (Sigma-Aldrich, Oakville, Canada) solution in front of the mouth. Video was recorded using an iPhone SE mounted onto a Nikon SMZ 1500 stereo dissecting microscope (Nikon Instruments, Melville, USA).

2.2.5 Local O_2 consumption within the buccal cavity

To test whether O_2 is extracted from water upon passage through the buccal cavity of 4 and 7 dpf larval zebrafish, an O_2 micro-optrode technique was used. This system (Hughes et al., 2019) consists of an O_2-sensing fibre-optic micro-optrode (tip diameter = 20 µm) attached to a detector system (Applicable Electronics, New Haven, USA), which was operated by custom software (ASET-LV4; Science Wares, Falmouth, USA). Optrodes were calibrated with a "zero-solution" containing 40 mg ml^{-1} anyhydrous sodium sulfite dissolved in water in which measurements were made and a well-aerated sample of water.

Larvae were anaesthetized with 0.3 mg ml^{-1} of Tris-buffered MS-222 to the point at which ventilation ceased but heartbeat continued, and placed in a Petri dish containing water

with the same anaesthetic level. Using a dissecting microscope (SMZ 1500; Nikon Instruments, Melville, USA) the micro-optrodes were placed either directly in front of the mouth to obtain PO_2 of the inspired water or into the mouth to obtain buccal cavity PO_2. In both cases, optrodes were left in place until a stable signal was achieved (usually within 3-5 min), after which PO_2 was measured every 10 s over 5 replicate measurements.

A separate experiment was designed to measure the PO_2 of the water leaving the buccal cavity in a ventilating 7 dpf zebrafish. Larvae were exposed to a light anaesthetic dose (0.05 mg ml^{-1} Tris-buffered MS-222) and to 10 µmol l^{-1} L-Adrenaline (+)-bitartrate salt (Sigma-Aldrich, Oakville, Canada) in the surrounding water (to stimulate ventilation) because the fish needed to be ventilating in order to assess the ability of oxygen extraction through the buccal cavity. In the absence of adrenaline, ventilation rates were too low (1-2 breaths min^{-1}) under normoxic conditions. Upon exposure to adrenaline, ventilation rates initially were high (~ 60 breaths min^{-1}), but these rates eventually slowed (5-10 breaths min^{-1}) at which point measurements were made. Given that the cutaneous surfaces surrounding the opercula of larval zebrafish likely contribute to O_2 uptake (Hughes et al., 2019), absolute expired PO_2 could not be assessed. Rather, the change in local PO_2 behind the operculum that occurred following a breath was assessed as a measure of O_2 extraction capacity in ventilating 7 dpf larvae.

2.2.6 Statistical Analysis

Breathing frequencies of zebrafish expsosed to hypoxia were analyzed using Markov chain Monte Carlo (MCMC) sampler for multivariate generalized linear models using MCMCglmm package (Hadfield, 2010) in R (https://www.R-project.org/). In two of the models, all f_V measurements were fitted as dependent varaibles and either developmental age or PO_2 was fitted as a fixed effect (fitted separately for each trait). In a separate model, f_V measurements in

hypoxia were fitted as dependent variables and the last minute of the 5 min normoxia treatment was fitted as a fixed effect. The model included an unstructured (co)variance matrix at the residual level, using weakly informative inverse-Wishart priors with the scale parameter defined as a diagonal matrix containing values of one and distribution parameters set to 0.001 for the degrees of freedom. Posterior distributions were estimated from 13,000 MCMC iterations sampled at 10 iteration intervals following an initial burn-in period of 3000 iterations. This yielded effective samples sizes of 1000 for the parameters of interest. We inspected the 95% highest posterior density (HPD) associated with each fixed effect estimate to check whether they overlapped with zero. A 95% HPD interval contains most of the posterior distribution and is analogous to a confidence interval (CI) in the frequentist approach; a 95% HPD that overlaps 0 indicates that the effect does not differ significantly from zero. Thus, for each estimate associated with the fixed effect we determined whether the 95% HPDs included or excluded zero. For similar analysis see Mandic et al. (2019).

All other statistical analyses were carried out in Sigmaplot (Systat Software, USA). Respirometry data were analyzed using one-way analysis of variance (ANOVA). Routine metabolic rate data did not pass a normality test (Shapiro–Wilk test), thus the Kruskal-Wallis ANOVA on ranks was used followed by Dunn's *post hoc* test. Critical PO_2 data passed both normality and equal variance tests (Levene's test), thus ANOVA was performed on these data. The difference between inspired and buccal cavity PO_2 in fish of the same developmental age was compared using a paired t-test. For 4 dpf larvae, the data did not pass the normality test, and thus a Wilcoxon signed rank test was used. Difference in ΔPO_2 between 4 and 7 dpf larvae was compared using a Student's t-test. Respirometry data for fish with and without agar were analyzed by comparing only the difference in RMR or P_{crit} between these two groups at the same

developmental age. RMR data for 4 dpf larvae was analyzed using a Student's t-test. RMR data for 7 dpf larvae, and P_{crit} data for 4 and 7 dpf larvae either failed the normality or equal variance test, and thus Mann-Whitney rank sum test was performed. Slopes of $\dot{M}O_2$ versus PO_2 before P_{crit} for each group in the agar experiment were tested against 0 for significance using a linear regression. For all tests, significance was set at $P < 0.05$.

2.3 Results

2.3.1 Ventilation frequency, resting metabolic rate and critical O_2 tension across developmental age groups

For larvae at all developmental ages, exposure to hypoxia resulted in an increase in f_V, which returned to baseline levels within minutes when larvae were switched back to normoxic conditions (Fig. 2.1; Fig. S2.1). However, the duration and intensity of hyperventilation were determined by both developmental age and severity of the hypoxia. In 4 dpf larvae (Fig. 2.1A), f_V increased and remained significantly elevated during exposure to 25 mmHg hypoxia (Fig. S2.1A), while the significant increase in f_V was transient (5 – 10 min) when larvae were exposed to either 45 or 60 mmHg hypoxia (Fig. S2.1B, C). By 7 dpf (Fig. 2.1B), f_V increased and was maintained elevated in larvae exposed to both 25 and 45 mmHg hypoxia (Fig. S2.1D, E), with hyperventilation being transient for the first 10 min when exposed to 60 mmHg hypoxia only (Fig. S2.1F). In both 10 (Fig. 2.1C) and 15 dpf larvae (Fig. 2.1D), f_V increased and remained elevated at all three hypoxia levels tested (Fig. S2.1G-L). Interestingly, f_V decreased to below baseline levels in 15 dpf larvae when returned back to normoxia (Fig. S2.1J-L). Comparing larvae of the same developmental age, exposure to 25 mmHg resulted in a significantly higher f_V than in the 45 or 60 mmHg exposures at all developmental ages (Fig. S2.2A, C-D, F-G, I-J, L).

At 4 and 7 dpf, 45 and 60 mmHg exposure resulted in the same extent of increase in f_V (Fig. S2.2B, E), but by 10 and 15 dpf, 45 mmHg exposure resulted in a significantly greater increase of f_V compared to 60 mmHg exposure (Fig. S2.2H, K). For larvae at different development ages exposed to the same level of hypoxia, there was a general trend for the maximum f_V to increase as the larvae developed (Fig. S2.3).

Oxygen consumption was measured at developmental ages matching those of larvae in the ventilation experiment (Fig. 2.2A). Routine metabolic rate was significantly lower in 7 dpf larvae compared to the other developmental ages (Fig. 2.2B), but P_{crit} was the same across all developmental ages (30 - 34 mmHg, Fig. 2.2C).

2.3.2 Buccal cavity PO_2

At 4 dpf, larvae were able to inspire water through the mouth and expire water from their operculae (Fig. 2.3). Larvae at 4 and 7 dpf were able to extract O_2 in the buccal cavity (Fig. 2.4). Buccal cavity PO_2 was significantly lower than inspired PO_2 in both 4 and 7 dpf larvae, however the younger larvae showed a significantly greater difference between inspired and buccal cavity PO_2 (Fig. 2.4B). True expired water PO_2 could not be assessed, thus the local changes in PO_2 behind the operculum that occurred following a breath were assessed in ventilating 7 dpf larvae, showing a decrease after each breath when f_V was between 5-10 breaths min^{-1} (see representative trace, Fig. 2.4C).

2.3.3 The effects of blocking ventilation on resting metabolic rate and critical O_2 tension

$\dot{M}O_2$ was measured in 4 and 7 dpf larvae that were prevented from ventilating by applying an agar helmet to the head (Fig. 2.5). At 4 dpf, larvae showed a significantly lower RMR (Fig. 2.5C) when ventilation was blocked compared to larvae that were able to ventilate, yet P_{crit} (Fig. 2.5D) was not different between the two treatment groups. On the other hand, RMR

(Fig. 2.5C) was not different in 7 dpf larvae between the ventilating and non-ventilating larvae, but P_{crit} (Fig. 2.5D) was significantly higher for larvae that were unable to hyperventilate. $\dot{M}O_2$ increased as water PO_2 levels gradually decreased to P_{crit} for ventilating larvae of both developmental ages; the slopes (4 dpf: -0.12, 7 dpf: -0.13) were significantly lower than zero ($P < 0.0001$ for both 4 and 7 dpf). However, $\dot{M}O_2$ remained constant until P_{crit} for larvae that were unable to ventilate; the slopes (4 dpf: -0.03, 7 dpf: 0.01) were not significantly different from zero (4 dpf: $P = 0.15$, 7 dpf: $P = 0.58$, Fig. 2.5A, B).

2.4 Tables and Figures

Figure 2.1. The interactive effects of hypoxia and developmental age on ventilation frequency (f_V) in larval zebrafish. Larvae [n = 9 for 7 days post fertilization (dpf) exposed to 60 mmHg; n = 17 for 4 dpf exposed to 45 mmHg; n = 10 for all other groups] at (A) 4 dpf, (B) 7 dpf, (C) 10 dpf and (D) 15 dpf exposed to 5 min normoxia (153 mmHg) followed by 15 min of hypoxia at either 60 mmHg (black triangles), 45 mmHg (grey squares), or 25 mmHg (unfilled circles) and subsequently returned to normoxia for 5 min. Vertical dashed lines represent delineations between normoxia, hypoxia and normoxic recovery. Data are presented as means ± s.e.m. Traces were analyzed using Markov chain Monte Carlo sampler for multivariate generalized linear models, and the statistical analysis can be found in Figs. S1-S5.

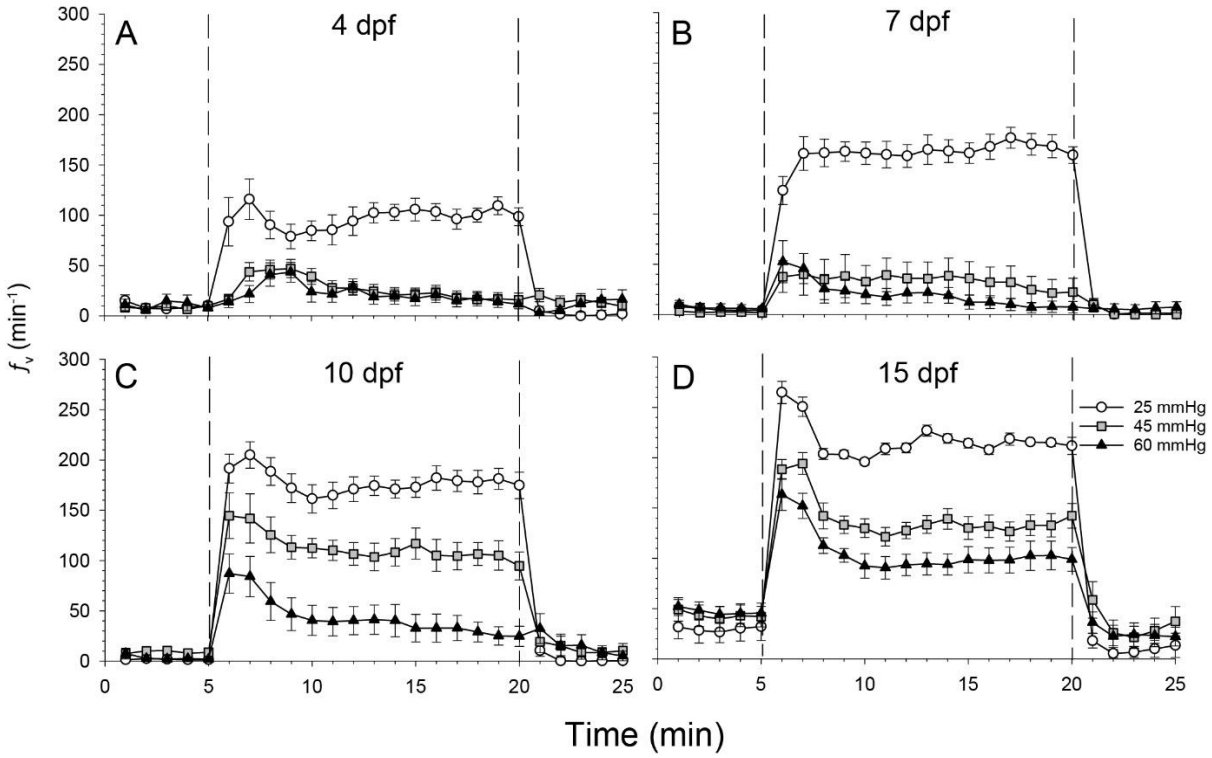
A
4 dpf
B
7 dpf
C
10 dpf
D
15 dpf
25 mmHg
45 mmHg
60 mmHg
f_v (min^{-1})
Time (min)

Fig. 2.1

Figure 2.2. Respirometry data for 4, 7, 10 and 15 days post fertilization (dpf) larvae. (A) Water oxygen tension (PO_2) versus oxygen consumption rate ($\dot{M}O_2$) for 4 dpf (black diamonds, n = 14), 7 dpf (grey squares, n = 12), 10 dpf (grey triangles, n = 10), and 15 dpf (unfilled circles, n = 12) larvae. (B) Routine metabolic rate (RMR) and (C) critical oxygen tension (P_{crit}) data were calculated from the PO_2 versus $\dot{M}O_2$ plot. Data are presented as means ± s.e.m. Values with different letters are significantly different ($P < 0.05$).

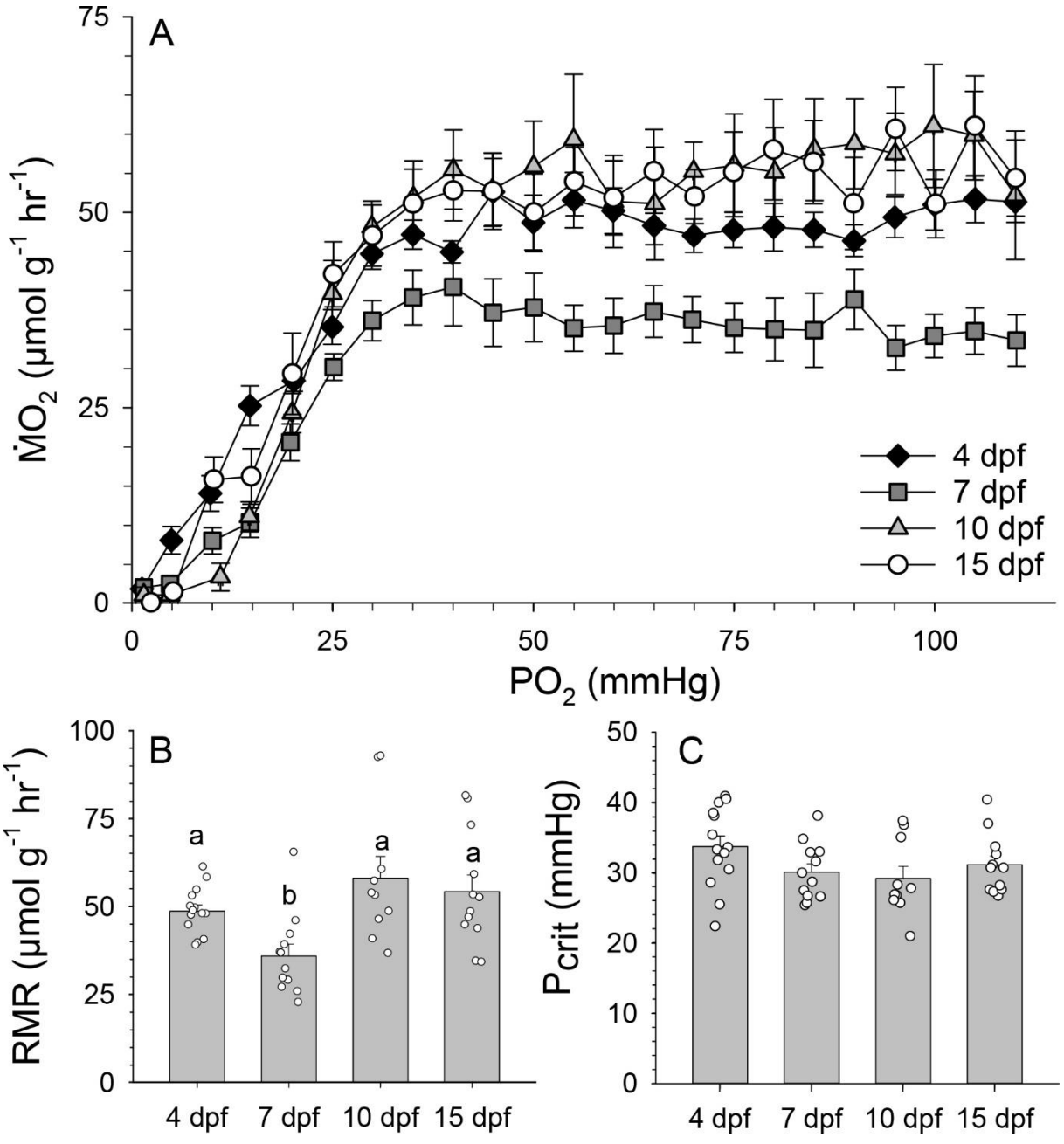
A
$\dot{M}O_2$ (µmol g^{-1} hr^{-1})
PO_2 (mmHg)
4 dpf
7 dpf
10 dpf
15 dpf
B
RMR (µmol g^{-1} hr^{-1})
a
b
a
a
C
P_{crit} (mmHg)

Fig. 2.2

Figure 2.3. Image sequence of 4 days post fertilization (dpf) zebrafish larva inspiring water from the mouth and expiring water out of the operculae. Concentrated phenol red solution was injected at the mouth (A), and was inspired by the ventilating larva (B, C). The phenol red solution was ejected during "coughing" (D) and reabsorbed into the buccal cavity (E), prior to exiting the operculae (F). The white line represents the front of the phenol red solution.

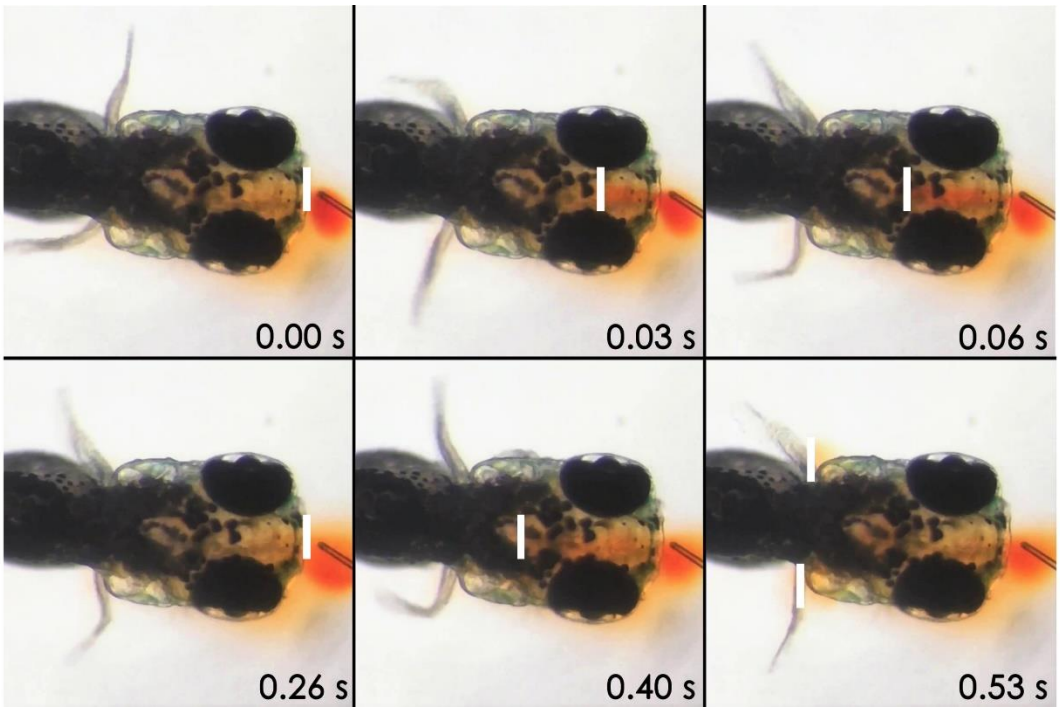

Fig. 2.3

Figure 2.4. Water O2 tensions (PO2) levels measured at the head region of larval zebrafish using micro-optrodes. (A) Inspired PO_2 was measured at position 1, buccal cavity PO_2 was measured just above the gill basket shown in position 2, and expired PO_2 was measured at position 3. (B) Inspired (grey) and buccal cavity (white) PO_2 levels measured in 4 days post fertilization [dpf, (n = 9)] and 7 dpf (n= 8) larvae, as well as the ΔPO_2 between the two groups. Data are presented as means ± s.e.m. Asterisks represent the level of significance. (* $P < 0.05$, ** $P < 0.01$, *** $P < 0.001$). (C) Representative trace of expired PO_2 levels measured at position 3 in a 7 dpf larva. Arrows represent distinct breaths.

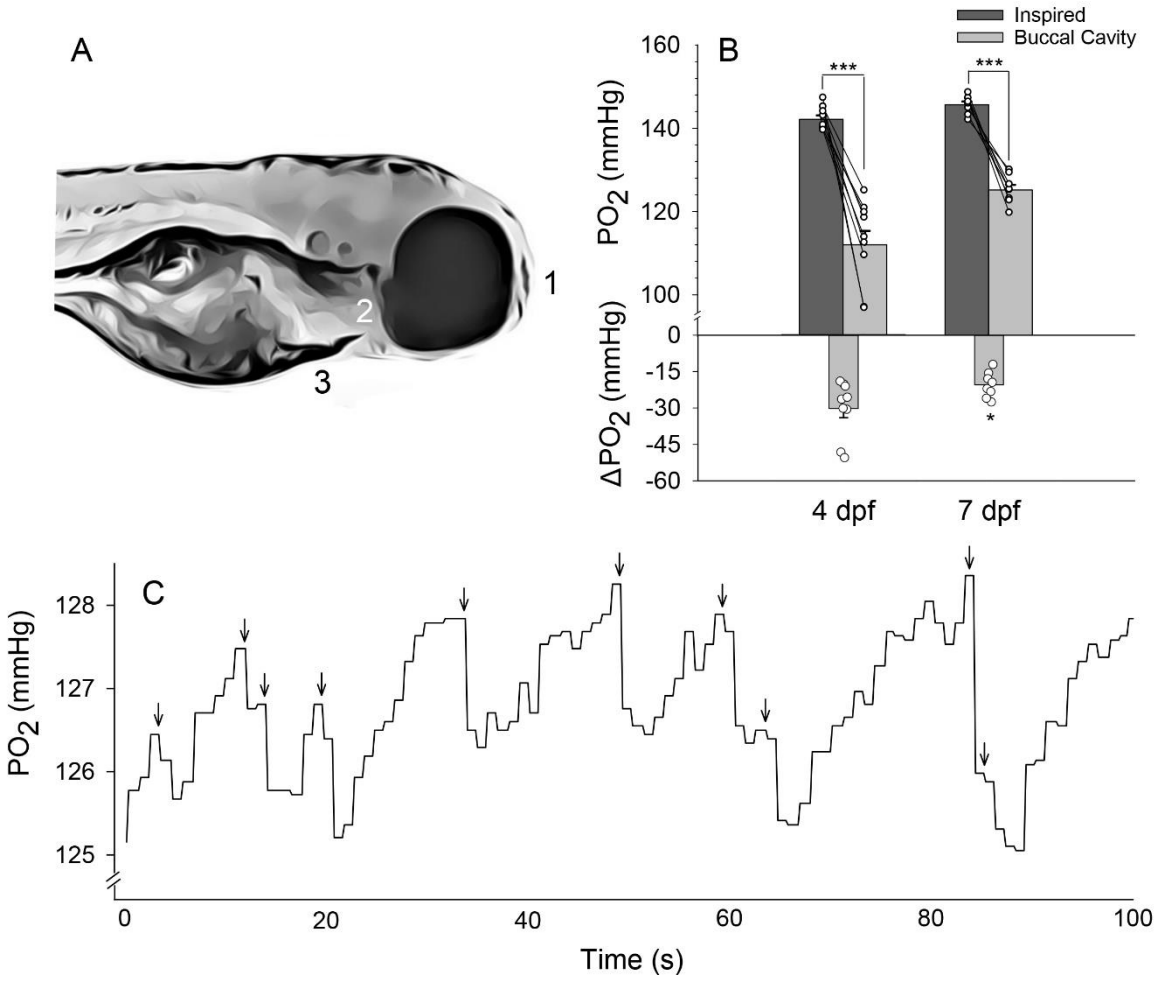
A
1
2
3
B
Inspired
Buccal Cavity
160
140
120
100
0
-15
-30
-45
-60
PO2 (mmHg)
ΔPO2 (mmHg)
***
***
*
4 dpf
7 dpf
C
128
127
126
125
PO2 (mmHg)
0
20
40
60
80
100
Time (s)

Fig. 2.4

Figure 2.5. Respirometry data for agar helmet versus non-agar helmet treated larvae.

Water O_2 tension (PO_2) versus O_2 consumption ($\dot{M}O_2$) for agar helmet treated larvae (unfilled symbols) and non-agar helmet treated larvae (filled symbols) in (A) 4 days post fertilization [dpf, (n = 13 for no agar larvae, n = 11 for agar helmet larvae)] and (B) 7 dpf (n = 17 for no agar larvae, n = 11 for agar helmet larvae) zebrafish. Arrows indicate the critical O_2 tension (P_{crit}) for each treatment. (C) Routine metabolic rate (RMR) and (D) P_{crit} data were calculated from the PO_2 versus $\dot{M}O_2$ plots. Data are presented as means ± s.e.m. Asterisks represent the level of significance. (* $P < 0.05$, ** $P < 0.01$, *** $P < 0.001$).

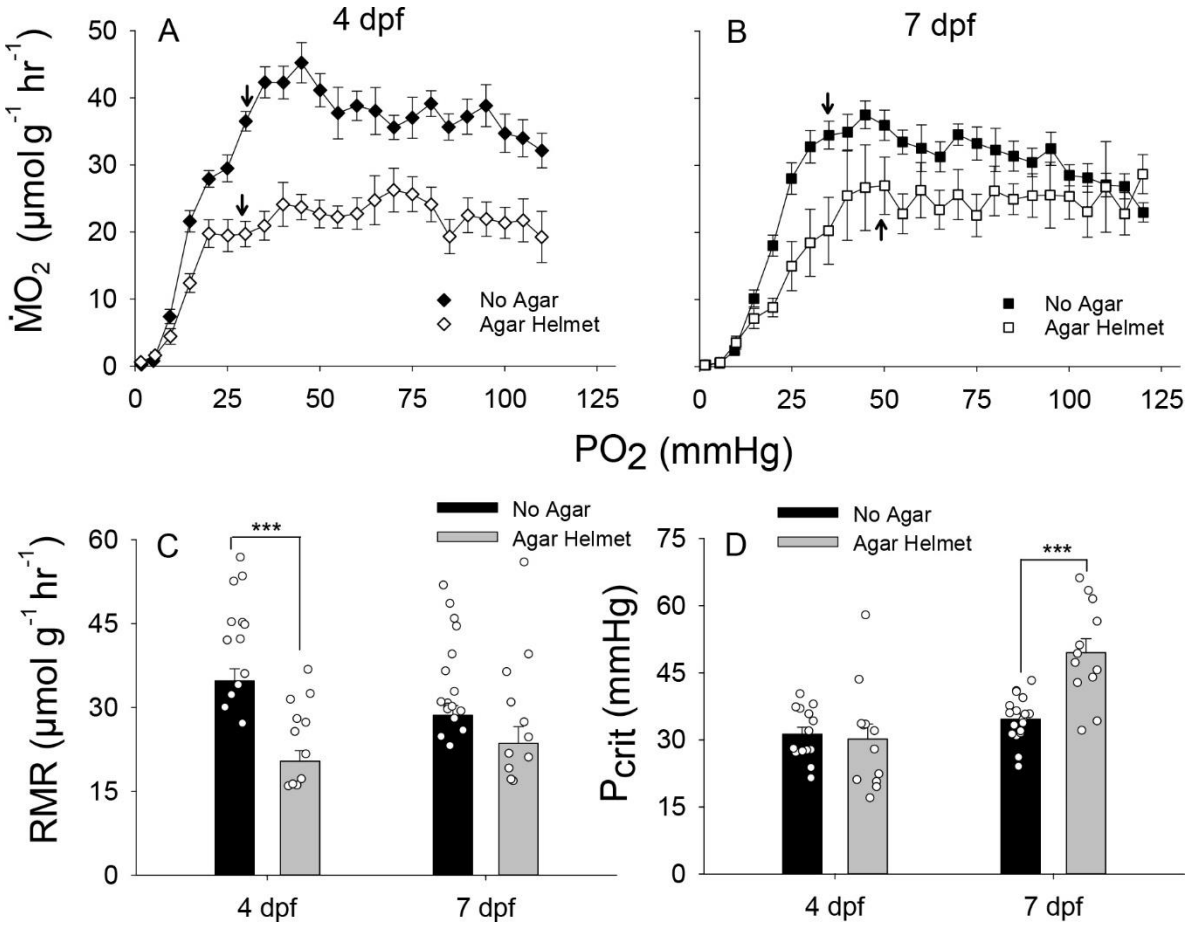
A
4 dpf
B
7 dpf
$\dot{M}O_2$ (µmol g^{-1} hr^{-1})
No Agar
Agar Helmet
PO_2 (mmHg)
C
D
RMR (µmol g^{-1} hr^{-1})
P_{crit} (mmHg)
***
4 dpf
7 dpf

Fig. 2.5

2.5 Discussion

The goals of this study were to determine whether larval zebrafish can regulate their HVR and whether this physiological response is beneficial. Based on previous studies, it is known that the gills are not the primary site of O_2 uptake in early larval stages of fishes (Fu et al., 2010; Rombough, 2002; Rombough and Ure, 1991; Wells and Pinder, 1996; Zimmer et al., 2014), leading to the question of why larval fishes hyperventilate in response to hypoxia. The results of this study clearly show that larval zebrafish are not only able to regulate their HVR, but also rely on it to maintain O_2 uptake under hypoxic conditions as early as 7 dpf.

Depending on species, the HVR consists of an increase in f_V or ventilation amplitude, or both, to increase the volume of water flowing over the gills (Perry et al., 2009). In this study, we focused on f_V because adult zebrafish increase f_V, but not ventilation amplitude, during hypoxia (Vulesevic et al., 2006) and there is currently no reliable method for measuring ventilation amplitude in larval zebrafish. The results of the present study demonstrate that larval zebrafish are not only able to hyperventilate during hypoxia as early as 4 dpf, as has been previously reported (Jonz and Nurse, 2005; Mandic et al., 2019), but that they are also able to modify the magnitude and the duration of the HVR based on the level of hypoxia imposed and the developmental age. In 4 and 7 dpf larvae exposed to mild hypoxia (60 mmHg), the increase in fv was transient, decreasing back to baseline levels after 5-10 min. It is possible that up to 7 dpf, cutaneous respiration is sufficient to meet metabolic demands, even in mild hypoxic conditions, and thus sustained hyperventilation is avoided as ventilation itself is an energetically costly response (Jones and Schwarzfeld, 1974; Steffensen, 1985). Alternatively, the return of f_V to baseline levels could reflect a gradual desensitization of the oxygen chemoreceptors – NECs. In zebrafish larvae, NECs are located on the skin (Coccimiglio and Jonz, 2012) and gill filament

primordia (Jonz and Nurse, 2005), but NECs on the gill filament primordia are not innervated until 7 dpf (Jonz and Nurse, 2005). It is possible that gill NECs are able to sense internal and external PO_2 levels owing to their location within a permeable epithelium between the respiratory water flow and the arterial blood supply, whereas NECs on the skin are more likely to sense external PO_2 levels only (Jonz et al., 2004). Thus, it is possible that the increase in f_V arises from the skin NECs sensing a change in ambient PO_2 and that under mild hypoxia the fall in blood PO_2 is not severe enough to provide additional sensory input required to sustain the HVR. Therefore, NECs are speculated to gradually desensitize and f_V returns to baseline levels.

Although *f*v was significantly elevated throughout the duration of hypoxia in 10 and 15 dpf larvae, the greatest increase in *f*v occurred in the first 5 min of exposure. When returned to normoxia, f_V of 15 dpf larvae dropped to below baseline levels. This post-hypoxic hypoventilation is characteristic of short term depression within the hypoxic ventilatory time domain, whereby a transient overshoot in f_V is observed at the onset of hypoxic stimulation, or a transient undershoot in f_V at the termination of hypoxic stimulation, that lasts seconds to minutes (Powell et al., 1998), and has been observed in adult fish species (Maxime et al., 1995) though the specific mechanism is unclear. In mouse however, the short term depression is likely associated with an inhibition of f_V rather than a decrease in responsiveness to the hypoxic stimulus (Hayashi et al., 1993). Thus we suggest that larval zebrafish also exhibit a high level of ventilatory control, being able to initiate a hyperventilatory response of variable magnitude and duration with the possibility of inhibitory and excitatory inputs simultaneously regulating the overall ventilatory response.

Although larvae at different development ages initiate slightly different hyperventilatory responses, their RMR and P_{crit} are the same, with the exception of a lower RMR in 7 dpf larvae.

Rombough and Drader (2009) reported a similar phenomenon in zebrafish in which RMR was lower in 7 dpf larvae compared to 5 and 14 dpf larvae. Similarly, it was observed that RMR decreased between 5 and 7 dpf in zebrafish (Grillitsch et al., 2005). Complete yolk sac absorption occurs at 5 dpf in zebrafish (Kimmel et al., 1995), while respiratory lamellae do not appear until 7 dpf (Jonz and Nurse, 2005). The yolk sac epithelium can serve as a respiratory tissue, contributing up to 33% of O_2 uptake (Rombough, 1998; Wells and Pinder, 1996). Thus, a drop in RMR at 7 dpf could reflect a decreased ability for cutaneous O_2 uptake, at a time when branchial O_2 transfer is not yet fully functional.

Critical PO_2 was constant across the four developmental ages, indicating that differences in the temporal dynamics of the HVR were not correlated with P_{crit}. In larvae at 4 dpf, the HVR was sustained for the duration of exposure only at the most severe level of hypoxia (25 mm Hg) or below P_{crit}. With increasing age, the larval HVR was sustained for the duration of exposure at higher and higher PO_2 values compared to P_{crit}. This finding suggests that at 4 dpf, the hyperventilatory response is not necessary and that cutaneous respiration, alone, is likely sufficient to meet O_2 demand. It is interesting that the HVR is not sustained in 4 and 7 dpf until external PO_2 levels fall near to P_{crit}, because at this point $\dot{M}O_2$ is already under decline, questioning the physiological benefit of hyperventilation as it no longer delays the transition from aerobic to anaerobic metabolism. However, from 10 to 15 dpf, the hyperventilatory response begins to play a greater role at external PO_2 levels well above P_{crit}, arguably contributing more to total O_2 uptake. The fact that the HVR was sustained at higher PO_2s with increasing developmental age (10 -15 dpf) presumably reflects the inability of cutaneous O_2 uptake to meet metabolic demands in the older larvae.

We presented direct evidence that larvae as young as 4 dpf were able to inspire water into the buccal cavity and extract O_2 prior to the expired water exiting the operculae. The decrease in buccal cavity PO_2 compared to inspired water, as well as a fall in PO_2 at the operculae where water is expired following each breath clearly demonstrated that O_2 was being removed from the ventilatory water. The effect of water residence time within the buccal cavity was assessed by examining the relationship between inter-breath duration and the relative change in local PO_2 at the operculum following a breath. The decrease in PO_2 was positively correlated with the water residence time within the buccal cavity, with water residence time contributing to 13% of the observed variation (data not shown). It should be noted that with the experimental design, it was not possible to determine whether the decline in buccal cavity PO_2 was caused by localized O_2 consumption or by the movement of O_2 into the blood to be transported throughout the body.

In addition to showing that O_2 can be extracted in the buccal cavity of 4 and 7 dpf larvae, we also examined the physiological importance of buccal cavity O_2 extraction by preventing ventilation. In 4 dpf larvae, blocking ventilation by applying an agar helmet resulted in a decrease in RMR yet P_{crit} remained the same. This decrease in RMR was unlikely caused by the agar impeding cutaneous gas exchange, as agar itself is highly porous to water and there was no difference in RMR in fish fully encased in agar and fish with agar covering the head only (data not shown). As larvae with agar helmets were still able to move their fins, it is also unlikely that this decrease in RMR can be attributed to less water being ventilated across their cutaneous respiratory surfaces. This decrease in RMR may have resulted from reduced movement, as fish with agar helmets swam less. However, given that the P_{crit} is the same between 4 dpf larvae that can and cannot ventilate, it is likely that cutaneous respiration alone is able to satisfy their metabolic demands. These data suggest that the HVR does not have a physiological benefit in

zebrafish larvae at 4 dpf. Thus, as previously hypothesized, the HVR may be an innate response in 4 dpf larvae, acting to ensure that O_2-sensing pathways are functional by the time the larvae become dependent on branchial respiration (Jonz and Nurse, 2005). However, this is clearly not the case in 7 dpf larvae, because P_{crit} was significantly higher in fish that were unable to hyperventilate, suggesting that hyperventilation is aiding O_2 uptake during hypoxia. This result is surprising, considering that 4 dpf have a lower PO_2 within their buccal cavity compared to 7 dpf larvae. However, it should be noted that for the micro-optrode experiment design, it was not possible to determine whether the decline in buccal cavity PO_2 was caused by localized O_2 consumption or by the movement of O_2 into the blood to be transported throughout the body. Thus, a possible explanation is that protein turnover (related to gill development) is higher in the 4 dpf larvae, resulting in a greater proportion of regional O_2 consumption, as gills have been shown to be a sink for O_2 in larval trout immediately after hatch (Rombough, 1992). Alternatively, the gills or buccal cavity of 7 dpf larvae may be more highly vascularized than in 4 dpf larvae, resulting in more blood containing O_2 that was extracted from cutaneous sites of gas exchange supplying the buccal/branchial vasculature of 7 dpf larvae. This would potentially reduce O_2 extraction from the water in 7 dpf compared to 4 dpf larvae. This lower PO_2 within the buccal cavity of 4 dpf larvae also does not contradict the idea that hyperventilation is beneficial at 7 dpf but not necessarily at 4 dpf, because all O_2 measurements were conducted under normoxic conditions owing to limitations of the experimental set up. Potentially in normoxia, cutaneous O_2 uptake alone is able to satisfy O_2 demands in 7 dpf larvae as well. But under hypoxic conditions, O_2 uptake through the buccal cavity plays a more important role.

In conclusion, the current study demonstrated that larval zebrafish are able to regulate their HVR and that by 7 dpf, this response significantly contributes to overall O_2 uptake under

hypoxic conditions. This finding suggests that hyperventilation and branchial respiration are of physiological benefit in larvae as early as 7 dpf and thus is in contrast with previous conclusions that cutaneous respiration, alone, provides sufficient O_2 to meet respiratory demands of early stage larvae (Rombough, 2002; Rombough, 2007). These previous studies, however, examined the partitioning of cutaneous versus branchial O_2 uptake under normoxia. Similar to the finding of Rombough and Drader (2009) that hemoglobin enhances O_2 uptake in larval zebrafish only in hypoxia, it is possible that branchial respiration and hyperventilation play a significant role in zebrafish larvae but only in hypoxia.

2.6 Supplementary Figures

Figure S2.1. The average differences in f_V (delta f_V) between normoxia and hypoxia, and normoxia and recovery in larval zebrafish (data based on Figure 1). Larvae at 4 days post fertilization [dpf, (A-C)], 7 dpf (D-F), 10 dpf (G-I) and 15 dpf (J-L) were exposed to 25 mmHg (A,D,G,J), 45 mmHg (B,E,H,K) and 60 mmHg (C,F,I,L). Estimates are presented with 95% credible interval based on Bayesian analysis. Each point represents the mode and the 95% CI of the posterior distribution associated with the difference in f_V of hypoxia and recovery relative to normoxia. Shown are mode (filled squares) and 95% CI (black lines) of the posterior distribution. Data are significant if the 95% CI do not intersect zero (dotted horizontal line).

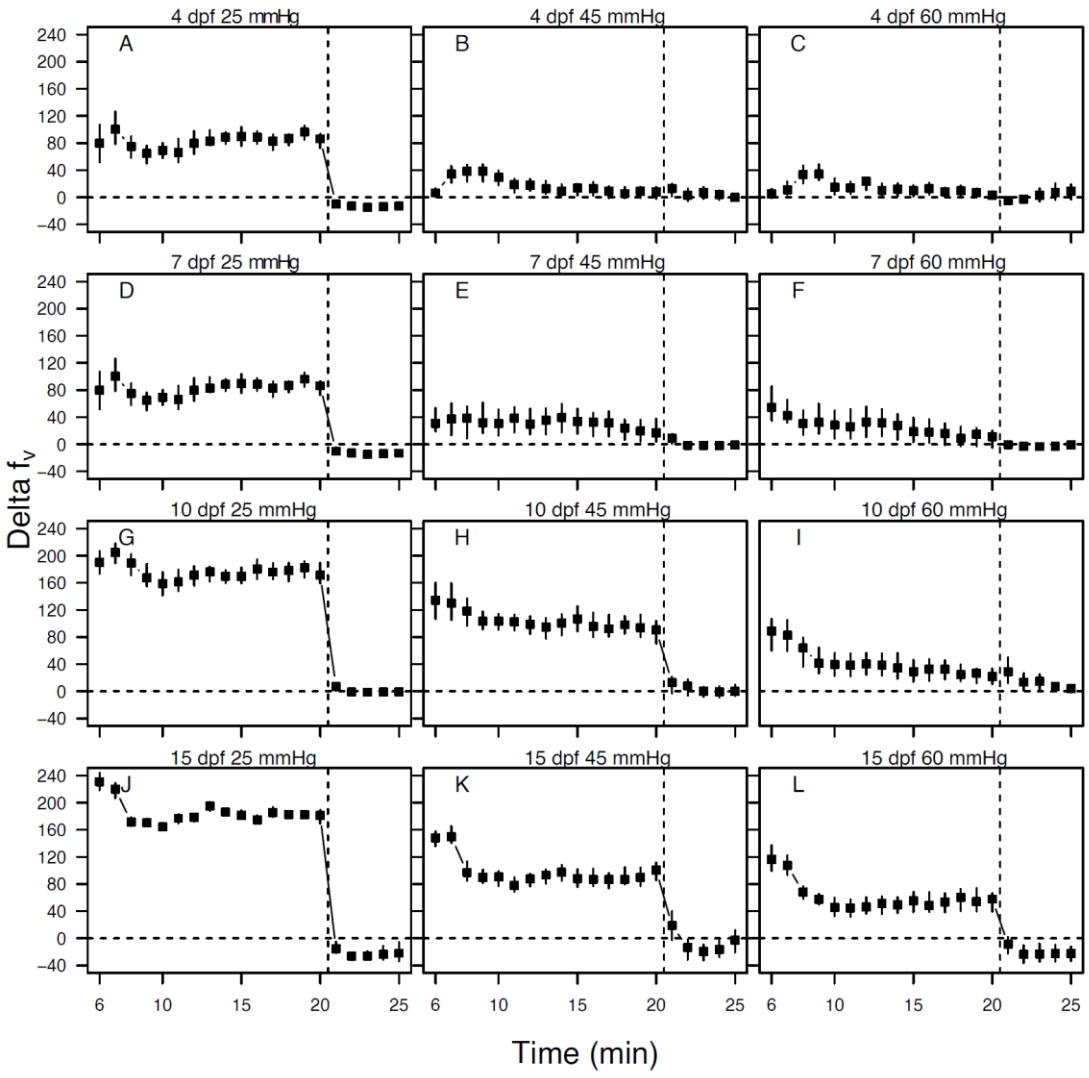
4 dpf 25 mmHg
4 dpf 45 mmHg
4 dpf 60 mmHg
7 dpf 25 mmHg
7 dpf 45 mmHg
7 dpf 60 mmHg
10 dpf 25 mmHg
10 dpf 45 mmHg
10 dpf 60 mmHg
15 dpf 25 mmHg
15 dpf 45 mmHg
15 dpf 60 mmHg
A
B
C
D
E
F
G
H
I
J
K
L
Delta f_v
Time (min)

Fig. S2.1

Figure S2.2. The average difference in f_V (delta f_V) in larvae at 25 and 45 mmHg relative to 60 mmHg and at 25 mmHg relative to 45 mmHg (data based on Figure 1). The larvae are compared at normoxia (5 min), hypoxia (15 min) and recovery (5 min) at 4 days post fertilization [dpf, (A,B,C)], 7 dpf (D,E,F), 10 dpf (G,H,I) and 15 dpf (J,K,L). Estimates are presented with 95% credible interval based on Bayesian analysis. Each point represents the mode and the 95% CI of the posterior distribution associated with the difference in f_V of larvae either at 25 mmHg or 45 mmHg relative to 60 mmHg, or 25 mmHg relative to 45 mmHg larvae. Shown are mode (filled squares) and 95% CI (black lines) of the posterior distribution. Data are significant if the 95% CI do not intersect zero (dotted horizontal line).

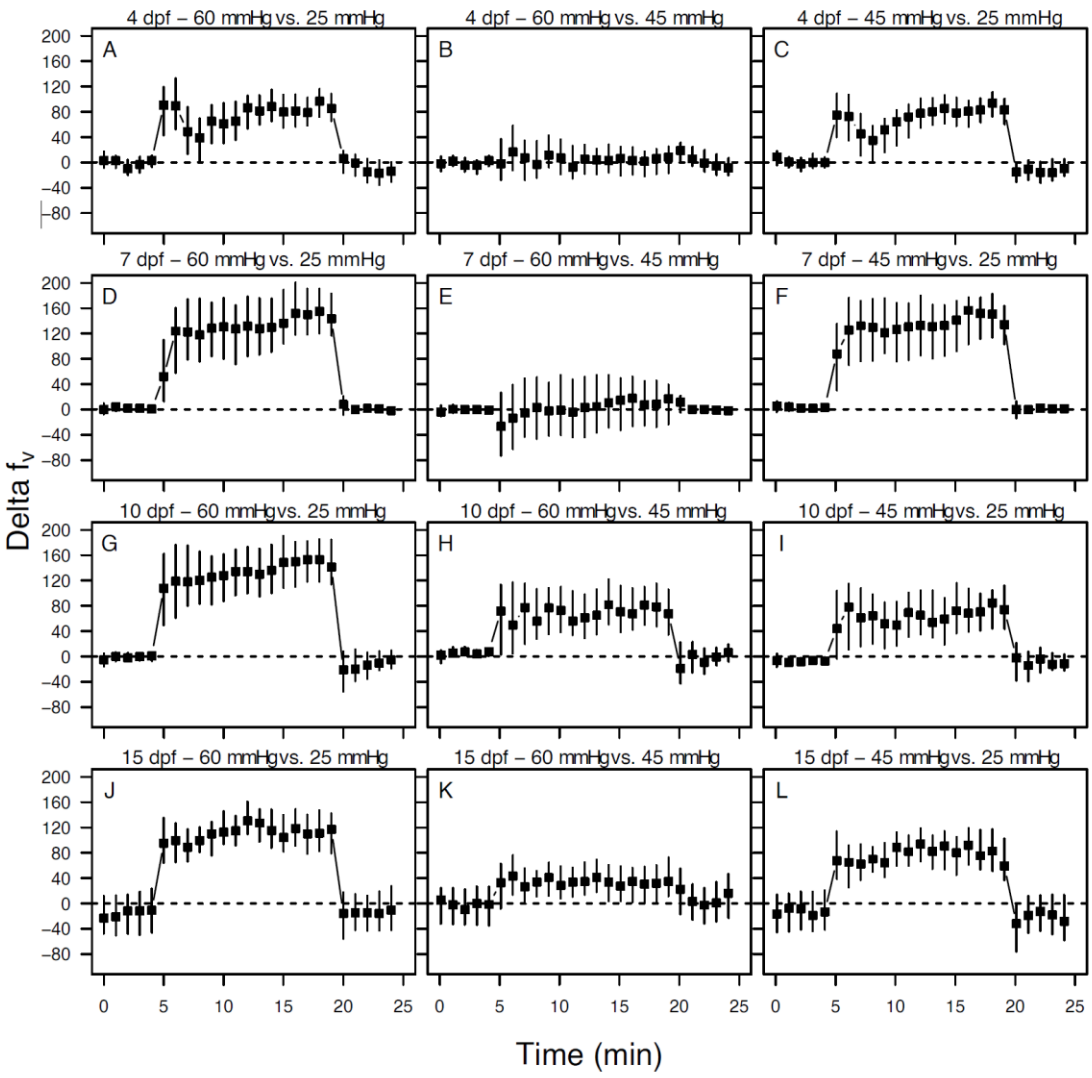
4 dpf – 60 mmHg vs. 25 mmHg
4 dpf – 60 mmHg vs. 45 mmHg
4 dpf – 45 mmHg vs. 25 mmHg
7 dpf – 60 mmHg vs. 25 mmHg
7 dpf – 60 mmHg vs. 45 mmHg
7 dpf – 45 mmHg vs. 25 mmHg
10 dpf – 60 mmHg vs. 25 mmHg
10 dpf – 60 mmHg vs. 45 mmHg
10 dpf – 45 mmHg vs. 25 mmHg
15 dpf – 60 mmHg vs. 25 mmHg
15 dpf – 60 mmHg vs. 45 mmHg
15 dpf – 45 mmHg vs. 25 mmHg
A
B
C
D
E
F
G
H
I
J
K
L
Delta f_v
Time (min)

Fig. S2.2

Figure S2.3. The average difference in f_V (delta f_V) in larvae at 7, 10 and 15 days post fertilization (dpf) relative to 4 dpf, at 10 and 15 dpf relative to 7 dpf, and at 10 dpf relative to 15 dpf (data based on Figure 1). The larvae are compared at normoxia (5 min), hypoxia (15 min) and recovery (5 min) at 25 mmHg (A-C,J-L), 45 mmHg (D-F, M-O) and 60 mmHg (G-I,P-R). Estimates are presented with 95% credible interval based on Bayesian analysis. Each point represents the mode and the 95% CI of the posterior distribution associated with the difference in f_V of larvae at different developmental stages relative to 4, 7 or 10 dpf larvae. Shown are mode (filled squares) and 95% CI (black lines) of the posterior distribution. Data are significant if the 95% CI do not intersect zero (dotted horizontal line).

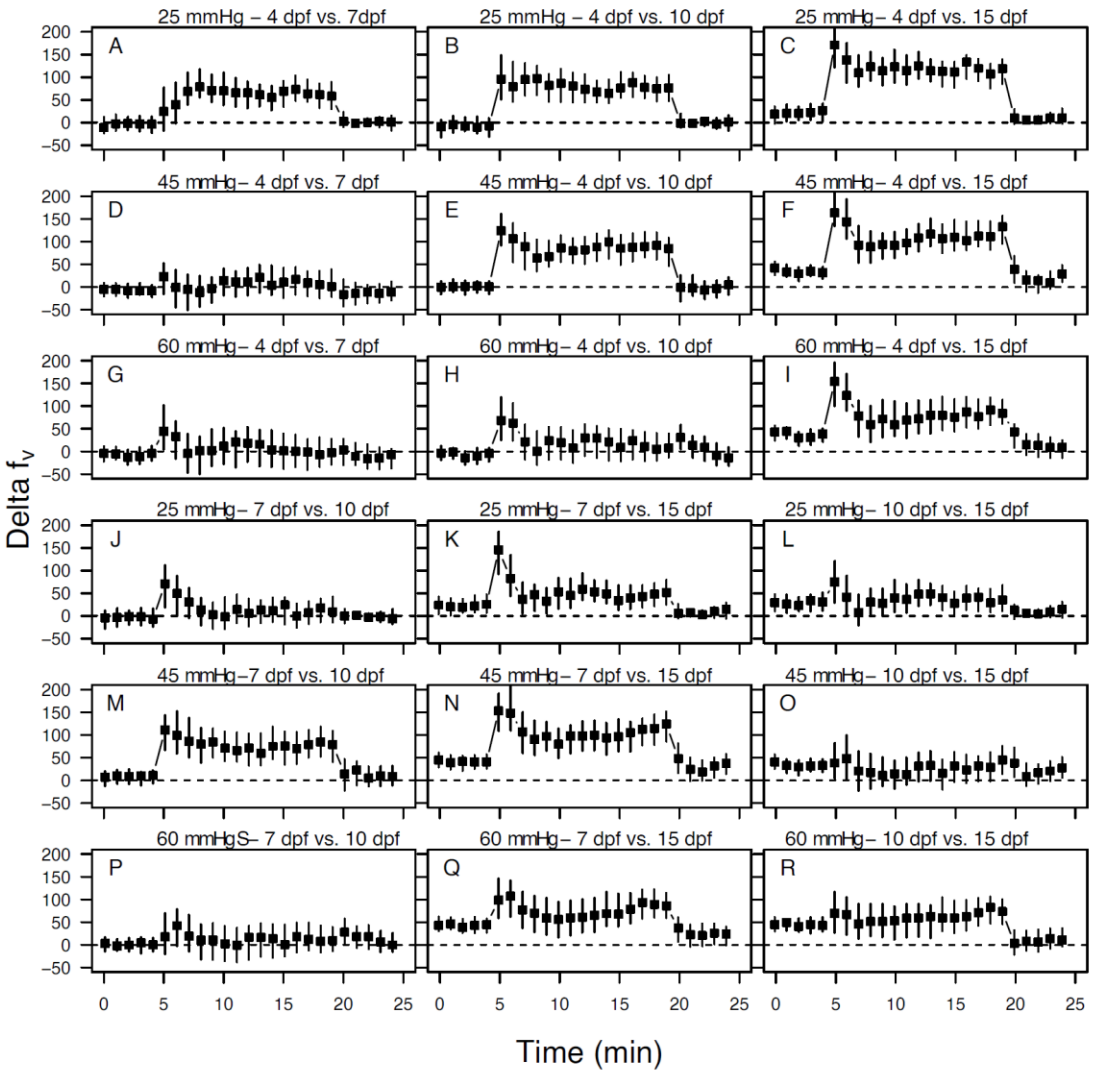
25 mmHg – 4 dpf vs. 7dpf
25 mmHg – 4 dpf vs. 10 dpf
25 mmHg – 4 dpf vs. 15 dpf
45 mmHg – 4 dpf vs. 7 dpf
45 mmHg – 4 dpf vs. 10 dpf
45 mmHg – 4 dpf vs. 15 dpf
60 mmHg – 4 dpf vs. 7 dpf
60 mmHg – 4 dpf vs. 10 dpf
60 mmHg – 4 dpf vs. 15 dpf
25 mmHg – 7 dpf vs. 10 dpf
25 mmHg – 7 dpf vs. 15 dpf
25 mmHg – 10 dpf vs. 15 dpf
45 mmHg –7 dpf vs. 10 dpf
45 mmHg – 7 dpf vs. 15 dpf
45 mmHg – 10 dpf vs. 15 dpf
60 mmHgS– 7 dpf vs. 10 dpf
60 mmHg – 7 dpf vs. 15 dpf
60 mmHg – 10 dpf vs. 15 dpf
A
B
C
D
E
F
G
H
I
J
K
L
M
N
O
P
Q
R
Delta f_v
Time (min)

Fig. S2.3

CHAPTER 3. Disruption of *tph1* genes demonstrates the importance of serotonin in regulating ventilation in larval zebrafish (*Danio rerio*)

Notes on Chapter

The present chapter is published in Respiratory Physiology & Neurobiology as per the following citation:

Pan, Y. K., Jensen, G., & Perry, S. F. (2021). Disruption of *tph1* genes demonstrates the importance of serotonin in regulating ventilation in larval zebrafish (*Danio rerio*). Respiratory Physiology & Neurobiology, 285, 103594.

Author contributions: All authors performed conceptualization of the experiments; Y.K.P. performed and analyzed data from the experiments; all authors participated in data interpretation; Y.K.P. prepared the manuscript; all authors contributed to the revision of the manuscript; S.F.P. provided supervision.

Abstract

Serotonergic neuroepithelial cells (NECs) in larval zebrafish are believed to be O_2 chemoreceptors. Serotonin (5-HT) within these NECs has been implicated as a neurotransmitter mediating the hypoxic ventilatory response (HVR). Here, we use knockout approaches to discern the role of 5-HT in regulating the HVR by targeting the rate limiting enzyme for 5-HT synthesis, tryptophan hydroxylase (Tph). Using transgenic lines, we determined that Tph1a is expressed in skin and pharyngeal arch NECs, as well as in pharyngeal arch Merkel-like cells (MLCs), whereas Tph1b is expressed predominately in MLCs. Knocking out the two *tph1* paralogs resulted in similar changes in detectable serotonergic cell density between the two mutants, yet their responses to hypoxia (35 mmHg) were different. Larvae lacking Tph1a (*tph1a*$^{-/-}$ mutants) displayed a higher ventilation rate when exposed to hypoxia compared to wild-types, whereas *tph1b*$^{-/-}$ mutants exhibited a lower ventilation rate suggesting that 5-HT located in locations other than NECs, may play a dominant role in regulating the HVR.

3.1 Introduction

The ability to sense O_2 levels in the environment to initiate physiological responses (e.g. ventilatory adjustments) aimed at maintaining O_2 homeostasis is a fundamental requirement for the survival of multicellular organisms. In adult mammals, O_2 chemoreception is mediated by peripheral chemoreceptor cells (type I or glomus cells) residing in the carotid body (Nurse, 2010). Upon exposure to hypoxia, K^+ channels are inhibited in type I cells leading to, or facilitating, membrane depolarization, Ca^{2+} entry through voltage-gated channels and neurosecretion to initiate downstream responses including hyperventilation (Nurse, 2010).

In teleost fish, the functional analogs of the peripheral respiratory chemoreceptors of mammals are termed neuroepithelial cells [NECs, (Jonz and Nurse, 2009; Milsom and Burleson, 2007)]. The NECs of the adult gill are characterized by an abundance of dense-cored vesicles containing serotonin [5-HT, (Dunel-Erb et al., 1982; Jonz et al., 2004)]. Serotonergic NECs also are found on the skin of larval fish, where they are thought to play an important role in O_2 chemoreception before the maturation of gill NECs (Coccimiglio and Jonz, 2012). Similar to carotid body type I cells, isolated gill NECs respond to acute hypoxia with K^+ channel inhibition, membrane depolarization, a rise in intracellular Ca^{2+} levels and increased synaptic vesicle activity (Burleson et al., 2006; Jonz et al., 2004; Qin et al., 2010; Zachar et al., 2017). However, unlike type I cells that contain multiple putative neurotransmitters within the same cell, including 5-HT, catecholamines and acetylcholine, most NECs contain predominantly 5-HT (Porteus et al., 2013). Thus in fish, 5-HT is speculated to be an important neurochemical in O_2 chemoreception and for mediating the hypoxic ventilatory response (HVR) initiated by O_2 chemoreceptors.

The earliest studies examining the role of 5-HT in O_2 chemoreception and the regulation of ventilation demonstrated that in both the spiny dogfish [*Squalus acanthias*, (Poole and Satchell, 1979)] and rainbow trout [*Oncorhynchus mykiss*, (Burleson and Milsom, 1995a)], addition of 5-HT to the perfusion media activated afferent nerve fibers of the gill filaments. Subsequent studies reported that application of 5-HT via intra-arterial injections or bathing in 5-HT solutions caused increases in ventilation or aquatic surface respiration in several species including rainbow trout (Burleson and Milsom, 1995b; Fritsche et al., 1992), European eel [*Anguilla Anguilla*, (Janvier et al., 1996)], toadfish [*Opsanus beta*, (McDonald et al., 2010)], and zebrafish [*Danio rerio*, (Abdallah et al., 2015b; Shakarchi et al., 2013)]. Although these studies demonstrated a potential overall role for 5-HT in O_2 chemoreception and the control of breathing, they could not distinguish the effects mediated by 5-HT released from peripheral NECs versus 5-HT acting at one or more upstream or downstream locations. To address this issue directly, Kermorgant et al. (2014a) injected 5-HT into the brain of rainbow trout and observed a potent stimulatory effect on ventilation. Similar increases in ventilation were observed when fluoxetine, a selective 5-HT reuptake inhibitor, was injected into the brain (Kermorgant et al., 2014b). Despite these previous studies, the exact sites at which 5-HT acts to stimulate ventilation remain unknown. To date, all evidence is indirect, either showing 5-HT containing cells in gills and skin of fish, or demonstrating ventilatory responses to exogenous 5-HT. The absence of definitive data, in part, reflects the technical challenges associated with blocking/activating site-specific 5-HT receptors. However, with the recent advances in genetic manipulation techniques such as CRISPR knockout (Chang et al., 2013; Hwang et al., 2013; Zimmer et al., 2019), new approaches are available to address these questions in zebrafish, an amenable model species.

The first and rate-limiting step in the biosynthesis of 5-HT is catalyzed by tryptophan hydroxylase (Tph), and thus Tph is often used as a marker for 5-HT synthesis and serotoninergic activity. In zebrafish, three paralogs of *tph* genes are present; *tph1a*, *tph1b* and *tph2*. All three paralogs are expressed in the central nervous system [CNS, (Lillesaar, 2011)], while data on the peripheral expression of the three paralogs is scarce, with some data suggesting that *tph1b* is expressed in Merkel-like cells (MLCs) at the base of taste bud cells (Kapsimali et al., 2011; Soulika et al., 2016). In mammals, *tph2* is the neuronal-specific enzyme that controls brain 5-HT synthesis whereas *tph1* is responsible for peripheral, non-neuronal 5-HT synthesis (Côté et al., 2003; Zhang et al., 2006). In this study we chose to examine the peripheral expression of *tph1a* and *tph1b* to determine whether either gene is responsible for 5-HT presence in NECs. In addition, we generated/obtained *tph1a* and *tph1b* knockout zebrafish to examine the effects of 5-HT originating from the different paralogs, on ventilation.

3.2 Materials and Methods

3.2.1 Experimental Animals

Adult zebrafish, *Danio rerio* (F. Hamilton 1822), were housed in 10 l polycarbonate tanks in a recirculating aquatic system (Aquatic Habitats, Apopka, FL, USA). Fish were maintained at 28°C under a 14 h:10 h light:dark cycle in dechloraminated city of Ottawa tap water and fed to satiation twice a day. Wild-type (WT) zebrafish were obtained from in-house stock at the University of Ottawa aquatic care facility. The *Tg(tph1a:mCherry)* transgenic line and *tph1a*$^{-/-}$ mutant line were generated in house as described below. The *Tg(tph1b:mCherry)* line was obtained courtesy of Dr. Marika Kapsimali of IBENS, France (Soulika et al., 2016), and the

tph1b$^{-/-}$ mutant line was obtained courtesy of Dr. Joanna Yeh of Harvard University. The *tph1a*$^{-/-}$ *b*$^{-/-}$ line (knock out of both *tph1a* and *tph1b* genes) was generated by cross breeding the *tph1a*$^{-/-}$ and *tph1b*$^{-/-}$ fish followed by inbreeding the F1 generation. Embryos from all genotypes were obtained using standard protocols (Westerfield, 2000). Embryos were collected and reared in 50 ml Petri dishes containing E3 medium (in mM: 5 NaCl, 0.17 KCl, 0.33 $MgSO_4$, 0.33 $CaCl_2$, and 0.1% methylene blue) in an incubator maintained at 28.5°C. For larvae that were raised beyond 5 dpf, they were transferred to static 1 l tanks on day 5 and fed daily. Water was changed daily in the Petri dishes and every alternate day in the static tanks. All procedures for animal use and experimentation were carried out in compliance with the University of Ottawa Animal Care and Veterinary Service guidelines under protocol BL-226 and adhered to the recommendations for animal use provided by the Canadian Council for Animal Care.

3.2.2 Generation of *Tg(tph1a:mCherry)* zebrafish

A 5 kb element immediately upstream of the *tph1a* gene was PCR amplified using Q5 high-fidelity DNA polymerase (NEB, Cat#: M0491S) (Fwd: 5'-CTCAGGCTGCAATTGGGAGA-3', Rev: 5'-GAGACTCTGCGCTTGGCTAT-3') and cloned into a Tol2-mCherry expression vector containing the *myl7:egfp* heart-specific transgenesis marker in the reverse orientation using restriction cloning. Transposase mRNA was synthesized from linearized transposase plasmid courtesy of Dr. Marc Ekker (University of Ottawa) using mMESSAGE mMACHINE SP6 kit (Invitrogen, Cat#: AM1340). To generate founder transgenic fish, one-cell-stage WT embryos were injected with ~1 nl of 100 ng/µl *tol2-tph1a* promoter plasmid and 200 ng/µl transposase mRNA and screened for cardiac GFP expression at 2 dpf. Founders with cardiac GFP expression were raised to adults and crossed with WTs to screen for embryos expressing mCherry to establish the line.

3.2.3 Generation of *tph1a*$^{-/-}$ mutant zebrafish

Expression of *tph1a* was knocked out using CRISPR/Cas9. The guide sequence of the sgRNA was designed using CHOPCHOP (https://chopchop.cbu.uib.no/) and was specific to a region of exon 2 of *tph1a* (GGCTGCGGTTGTGTTTTCCC). The sgRNA was synthesized using a cloning-free method described previously (Talbot and Amacher, 2014). Cas9 mRNA was synthesized from zebrafish codon-optimized Cas9 (Jao et al., 2013) using mMESSAGE mMACHINE SP6 kit (Invitrogen, Cat#: AM1340). One-cell-stage WT embryos were injected with ~1 nl of injection solution containing 150 pg Cas9 mRNA, 50 pg of sgRNA, and 0.01% phenol red suspended in Danieau buffer (in mM: 58 NaCl, 0.7 KCl, 0.4 $MgSO_4$, 0.6 $Ca(NO_3)_2$, and 5.0 Hepes; pH 7.6). Embryos were reared to sexual maturity (60-90 dpf) and mutants in this adult F0 population were identified through DNA extraction of fin clips and Sanger Sequencing (Genome Quebec, McGill University, Montreal, Canada). Two mutant lines were established using founders carrying a 7-bp or 38-bp deletion.

3.2.4 Real-time PCR

Real-time PCR was performed to assess the expression of *tph* genes in 4 dpf WT, *tph1a*$^{-/-}$, *tph1b*$^{-/-}$ and *tph1a*$^{-/-}$*b*$^{-/-}$ zebrafish. Larvae were killed by chilling in an ice bath and 20 individuals were homogenized via sonication in 0.5 ml Trizol (Invitrogen, Cat#: 15596018). RNA was extracted from these homogenates following the manufacturer's protocol. RNA concentration was determined using NanoDrop™ 2000 spectrophotometer (Thermo Scientific) and RNA quality was verified using gel electrophoresis and qualitative assessment of the relative intensities of the 28 and 18s ribosomal RNA bands. RNA was treated with DNaseI (Invitrogen, Cat#: 18068015) prior to cDNA synthesis from 0.5 µg total RNA using iScript cDNA synthesis kit (Bio-Rad, Cat#: 1708890). Real-time PCR was performed in 10 µl reactions containing 5 µl

SsoFast EvaGreen supermix (Bio-Rad, Cat#: 1725201), 500 nmol/l forward and reverse primers (Table S3.1) and 4 µl cDNA template. Controls (no template added) were run in every assay and non-reverse transcribed samples were run for every primer pair. Reaction efficiency for all primer pairs was between 90% and 110%. Final data were normalized to total RNA input rather than reference genes, because reference gene expression levels may be unstable in developing larvae of the different genotypes (Hu et al., 2016).

3.2.5 5-HT Elisa

Whole body 5-HT levels were determined using serotonin research ELISA kits (ALPCO, Cat#: 17-SERHU-E01-RES). 4 dpf WT, *tph1a*$^{-/-}$, *tph1b*$^{-/-}$ and *tph1a*$^{-/-}$*b*$^{-/-}$ zebrafish were euthanized in ice cold system water and severed just anterior to the yolk sac to separate the larvae into a head and a body region. Samples were prepared by homogenizing 10 heads or bodies in 20 µl of homogenizing solution (0.01 M HCl, 1 mM EDTA, 4 mM sodium metabisulfite supplemented with 1% stabilizing agent from Elisa kit). The homogenate was centrifuged at 10,000 x g for 10 min at 4ºC and 10 µl supernatant was collected and diluted in 490 µl of diluent from the Elisa kit. Each sample was stored at -80 ºC until performance of the assays following the user's manual.

3.2.6 Antisense morpholino injection

Zebrafish embryos were injected at the border of the cell and yolk at the one cell stage with an antisense oligonucleotide (Gene Tools, LLC) designed to bind to the translation start site of *tph1a* (5'-TCGAGTACATGCTGATGTTTGCTGA-3'), *tph1b* (5'-GCATGGATGGATGCTCTTGTTTTAT-3'), and *tph2* (5'-CAATGGGTTCAGCACTCACCATGGA-3'). Morpholino stock was diluted in Danieau buffer

and 0.05% phenol red to 4 ng/ul and 1 nl was injected into each embryo. A control morpholino (5'-CCTCTTACCTCAGTTACAATTTATA-3') that has no known target sequence in zebrafish also was injected at 4 ng/embryo in a separate batch of embryos during each round of injection. A dose of 4 ng was chosen because it was the highest dose we could use that did not cause morphological deformation to the larvae and for which results were reproducible between batches. After injection, embryos were placed in a Petri dish containing E3 medium and maintained in an incubator at 28°C.

3.2.7 Immunohistochemistry

Larvae were fixed overnight at 4°C in 4% paraformaldehyde (PFA) prepared in phosphate buffered saline (PBS). The following day, larvae were rinsed 5X in PBS containing 0.1% tween-20 (PBST) and dehydrated through a series of 5-min washes in increasing concentrations of methanol in PBST (25, 50%, 75% and 100% MeOH). Dehydrated embryos were held at -20°C for 2 h before rehydrating them using the same methanol/PBST series in reverse order. Further antigen retrieval was performed by placing larvae in a 150 mM tris-HCl solution (pH 9.0) for 10 min at room temperature, followed by 15 min at 65°C. Larvae were placed in a blocking solution containing 0.8% Triton-X 100, 3% bovine serum albumin (BSA), and 2% normal goat serum (Sigma Aldrich Inc., Cat#: NS02L-1ML) dissolved in PBST for 1 h at room temperature. Primary antibodies (rabbit anti-5-HT (Sigma Aldrich Inc., Cat#: S5545) 1:250 dilution, mouse anti-mCherry (Sigma Aldrich Inc., Cat#:SAB2702291) 1:500 dilution) were added in blocking solution and specimens were placed on a shaker overnight at 4°C in darkness. After 5 x 5 min washes in PBST, secondary antibodies [goat anti-rabbit Alexa Fluor 568, goat anti-mouse Alexa Fluor 594, donkey anti-rabbit Alex Fluor 647 (Thermo Fisher Cat#: A-11011, A-11005, and A-31573)] were added at a dilution of 1:500 in 0.8% Triton-X 100 dissolved in PBST. Larvae were incubated with

the secondary antibody in the dark at room temperature for 1 h, washed 5 X 5 min in PBST and mounted using Vectasheild^{TM} antifade mounting medium (Vector Laboratories, Cat#: H-1000-10) in a concave depression glass slide for imaging. Larval zebrafish were imaged using an A1R MP^{+} confocal microscope (Nikon Instruments Inc.) with 25X/1.10 W, 20X/0.75 MImm or 10X/0.50 W objectives.

3.2.8 Serotonergic cell density analysis

For analyzing serotonergic cell density on the tail, larval zebrafish were imaged in lateral view. The entire tail was imaged, and serotonergic cells were counted using ImageJ (https://imagej.nih.gov/ij/). Briefly, the image was first converted to 8 bits and threshold set just above background. The "analyze particles" plugin was used to count cells greater than 20 μm^2 in area with a circularity of at least 0.3. Density was obtained by dividing the cell count with the area of the tail in the image. For analyzing serotonergic cell density in the pharyngeal arch region, larval zebrafish were imaged with the dorsal plane facing up. The area of the head was then obtained using ImageJ, and three rectangles with a length-to-width ratio of 1:3, each corresponding to 1.25% of the total head area, were placed "randomly" in the pharyngeal arch region. The number of serotonergic cells in each rectangle was counted using ImageJ as described above and cell density was obtained by dividing the number of cells by the total area of the three rectangles. For all cell density analyses, images were relabelled and analyzed "blindly" without knowing the genotypes of the fish in the image. It is important to point out that this method enables quantification of the numbers of *detectable* NECs (i.e. NECS with levels of 5-HT above background). It is highly likely that NECs lacking 5-HT are still present in the knockout fish but remain undetectable.

3.2.9 Measurements of ventilation

The hypoxic ventilatory response was assessed by monitoring ventilation frequency (f_V) in WT, *tph1a*$^{-/-}$, *tph1b*$^{-/-}$ and *tph1a*$^{-/-}$*b*$^{-/-}$ larvae during exposure to hypoxia (35 mmHg) at 4, 7 and 15 dpf as described previously (Pan et al., 2019). Briefly, after light anesthesia (0.05 mg ml^{-1} Tris-buffered MS-222 (ethyl-3-aminobenzoate methanesulfonate salt, Sigma Aldrich Inc.), an individual larva was placed in a microcapillary tube with an inner diameter of 1 mm. Zebrafish water containing MS222 (as above) at 28.5ºC was delivered to the microcapillary tube by gravity at a rate of 1.6 – 1.8 ml min^{-1}. A previous study demonstrated that at the anesthesia concentration used, the response of larvae to hypoxia was not significantly reduced (Jonz and Nurse, 2005). Each larva was allowed to adjust to the chamber for 10 min in normoxic water (PO_2 = 153 mmHg) prior to the start of the trial. During each trial, f_V was recorded for 5 min under normoxic conditions (baseline), followed by 15 min of hypoxia (treatment) and an additional 5 min after returning to normoxia (recovery) using an iPhone mounted onto a dissecting microscope (stereo trinocular microscope (AmScope). Breathing frequency was then determined for each minute by counting either buccal or opercular movements depending on the orientation of the fish in the chamber and the visibility of the mouth and/or operculum.

3.2.10 Statistical analysis

Ventilation frequency of zebrafish larvae from hypoxia exposure was analyzed using Markov chain Monte Carlo sampler for multivariate generalized linear models using MCMCglmm package (Hadfield, 2010) in R (https://www.R-project.org/). In one type of model, all f_V measurements were fitted as dependent variables and either genotype or pCPA treatment was fitted as a fixed effect (fitted separately for each trait). In a separate type of model, f_V measurements in hypoxia or 5-HT or both hypoxia and 5-HT were fitted as dependent variables and the last minute of the 5 min normoxia treatment was fitted as a fixed effect. The model included an unstructured

(co)variance matrix at the residual level, using weakly informative inverse-Wishart priors with the scale parameter defined as a diagonal matrix containing values of one and distribution parameters set to 0.001 for the degrees of freedom. Posterior distributions were estimated from 13,000 MCMC iterations sampled at 10 iteration intervals following an initial burn-in period of 3000 iterations. This yielded effective samples sizes of 1000 for the parameters of interest. We inspected the 95% highest posterior density (HPD) associated with each fixed effect estimate to check whether they overlapped with zero. A 95% HPD interval contains most of the posterior distribution and is analogous to a confidence interval (CI) in the frequentist approach; a 95% HPD that overlaps 0 indicates that the effect does not differ significantly from zero. Thus, for each estimate associated with the fixed effect we determined whether the 95% HPDs included or excluded zero.

All other statistical analyses were carried out in Sigmaplot (Systat Software). Single facror comparisons among multiple means were conducted using a one-way ANOVA, while two-factor comparisons among multiple means were conducted using a two-way ANOVA. When data did not pass normality test (Shapiro–Wilk test), data were either log transformed or the Kruskal-Wallis ANOVA on ranks was used. Holm–Šidák *post hoc* test was used if a significant interaction was detected. Significance was set at $P<0.05$.

3.3 Results

3.3.1 Tph1a and Tph1b expression profiles in zebrafish larvae

The expression profiles of Tph1a and Tph1b were observed using *Tg(tph1a:mCherry)* and *Tg(tph1b:mCherry)* lines, respectively (Figs. 3.1-3.2). Peripherally, Tph1a was expressed both in the pharyngeal arch region (Fig. 3.1B-C) and on the skin (Fig. 3.1D-E) of the larva.

Within the pharyngeal arch region, Tph1a was expressed in both Merkel-like cells (MLCs) and pharyngeal arch NECs (see Fig. S3.1 for differentiation between MLCs and pharyngeal arch NECs). Skin NECs are identified as 5-HT positive cells anywhere on the skin of the larva; i.e. 5-HT positive cells on the skin of the head, trunk or tail region are all treated as the same population of skin NECs. In addition, Tph1a was observed in the heart (Fig. 3.1B). Centrally, Tph1a expression was observed in the pineal gland (Fig. 3.1E), consistent with *tph1a* expression profiles obtained using in-situ hybridization (Lillesaar, 2011).

Peripheral Tph1b expression was consistently observed in MLCs (Fig. 3.2B) and web like cell projections on the fin of the larva (Fig. 3.2C) that are not skin NECs. Tph1b expression was also occasionally observed in skin NECs (Fig. 3.2D), though expression was inconsistent unlike for Tph1a. Within the CNS, Tph1b was expressed in the brainstem region (Fig. 3.2E) and the hypothalamus (Fig. 3.2E), consistent with *tph1b* expression profiles obtained using in-situ hybridization (Lillesaar, 2011). Interestingly, 5-HT colocalization with Tph1b was observed only in the hypothalamus (Fig. 3.2E) and not the brainstem region (Fig. 3.2D).

3.3.2 Gene expression and 5-HT levels in *tph* knockouts

Whole-body expression of the *tph* paralogs was measured in *tph* knockouts (Fig. 3.3). In both *tph1a*$^{-/-}$ and *tph1a*$^{-/-}$*b*$^{-/-}$ fish, *tph1a* expression level was lower compared to either WT or *tph1b*$^{-/-}$. On the other hand, *tph1b* expression levels were higher in both *tph1b*$^{-/-}$ and *tph1a*$^{-/-}$*b*$^{-/-}$ larvae compared to WT or *tph1a*$^{-/-}$ fish. *Tph2* expression levels were constant in all four genotypes. 5-HT levels were measured in both the head and body regions of the four genotypes (Fig. 3.4). In the head region, 5-HT levels were not different between the genotypes, while in the body region, 5-HT levels were significantly higher in WTs compared to the *tph* knockouts,

resulting in higher total 5-HT levels in the whole larva when comparing WTs to the *tph* knockouts.

3.3.3 Detectable serotonergic cell density in *tph* knockout and knockdown larvae

Knocking out or knocking down *tph* genes resulted in age- and paralog-specific effects on detectable serotonergic cell densities on the skin and pharyngeal arch regions (Figs. 3.5-3.6). In general, *tph1a*$^{-/-}$, *tph1b*$^{-/-}$ and *tph1a*$^{-/-}$*b*$^{-/-}$ mutants exhibited lower detectable serotonergic cell densities on the skin at 4 dpf compared to WTs. This difference was absent at 7 or 15 dpf, with the exception of *tph1b*$^{-/-}$ at 15 dpf (Fig. 3.5E). At the pharyngeal arch region however, only *tph1a*$^{-/-}$ mutants showed lower detectable serotonergic cell density when compared to the WTs (Fig. 3.5F). In larvae experiencing *tph* gene knockdown, only *tph1b* morpholino resulted in a reduction of detectable serotonergic cells on the skin when compared to the control morpholino (Fig. 3.6A). In addition, when injecting the *tph1b* morpholino into *tph1a*$^{-/-}$ or *tph1b*$^{-/-}$ mutants, only *tph1a*$^{-/-}$ mutants showed a further reduction in detectable skin serotonergic cell density (Fig. 3.6B).

3.3.4 Ventilation experiments

Ventilation experiments were first performed using 4, 7 and 15 dpf *tph* knockout mutants as well as 4 dpf *tph1b* knockdown morphants (Fig. 3.7). When exposed to hypoxia, mutants of all genotypes and WTs at all three developmental stages exhibited an increase in f_V (Figs. 3.7A-C, S3.2). However, when compared to WTs during hypoxia exposure, *tph1a*$^{-/-}$ mutants tended to have higher f_V at 4 and 7 dpf; f_V was similar to WTs by 15 dpf (Fig. S3.3A, D, G). *tph1b*$^{-/-}$ mutants consistently showed a lower f_V during hypoxia at all three developmental stages when compared to WTs (Fig. S3.3B, E, H). Double mutants (*tph1a*$^{-/-}$*b*$^{-/-}$) exhibited complex breathing

patterns during hypoxia when compared to WTs. At 4 dpf, *tph1a*$^{-/-}$*b*$^{-/-}$ had similar f_V to the WTs in hypoxia (Fig. S3.3C). However, at 7 and 15 dpf when exposed to hypoxia, *tph1a*$^{-/-}$*b*$^{-/-}$ increased f_V markedly in the first 5 min to levels even higher than in WTs. f_V then gradually decreased and was sustained at levels slightly lower than that of WTs (Fig. S3.3F, I). Despite *tph1b*$^{-/-}$ mutants having lower f_V in hypoxia compared to WTs, the ventilatory response to hypoxia of *tph1b* morphants was identical to control morpholino injected larvae at 4 dpf (Fig. 3.7D, S4).

3.4 Tables and Figures

Figure 3.1. Colocalization of Tph1a (red) and 5-HT (magenta) in *Tg(tph1a:mCherry)* zebrafish larvae at 4 days post fertilization (dpf). (A) Lateral view of whole mount 4 dpf larval zebrafish co-stained for Tph1a and 5-HT. (B) Colocalization of Tph1a and 5-HT in the head region of the larva. Arrow points to Tph1a expression within the heart of the larva. Endogenous eGFP (green) expression in the heart is present due to the insertion of *myl7:eGFP* as a screening marker in the transgenic line. Arrowheads point to Tph1a expression in an unidentified structure within the midbrain region. (C) Colocalization of Tph1a and 5-HT in the pharyngeal arch region of the larva. Arrows show colocalization of Tph1a and 5-HT in Merkel-like cells (MLCs) in the pharyngeal arch region, while arrowheads show colocalization of Tph1a and 5-HT in pharyngeal arch neuroepithelial cells (NECs). See Fig. S3.1 for differentiation of MLCs and NECs in the pharyngeal arch region. (D) Colocalization of Tph1a and 5-HT on the skin of the larva in the tail region. Arrowheads show colocalization of Tph1a and 5-HT in skin NECs. (E) Dorsal view of whole mount 4 dpf larval zebrafish co-stained for Tph1a and 5-HT. Larva in (E) is a separate larva than the one in (A-D). Arrows show colocalization of Tph1a and 5-HT in the pineal gland, while arrowheads show colocalization of Tph1a and 5-HT in the skin NECs.

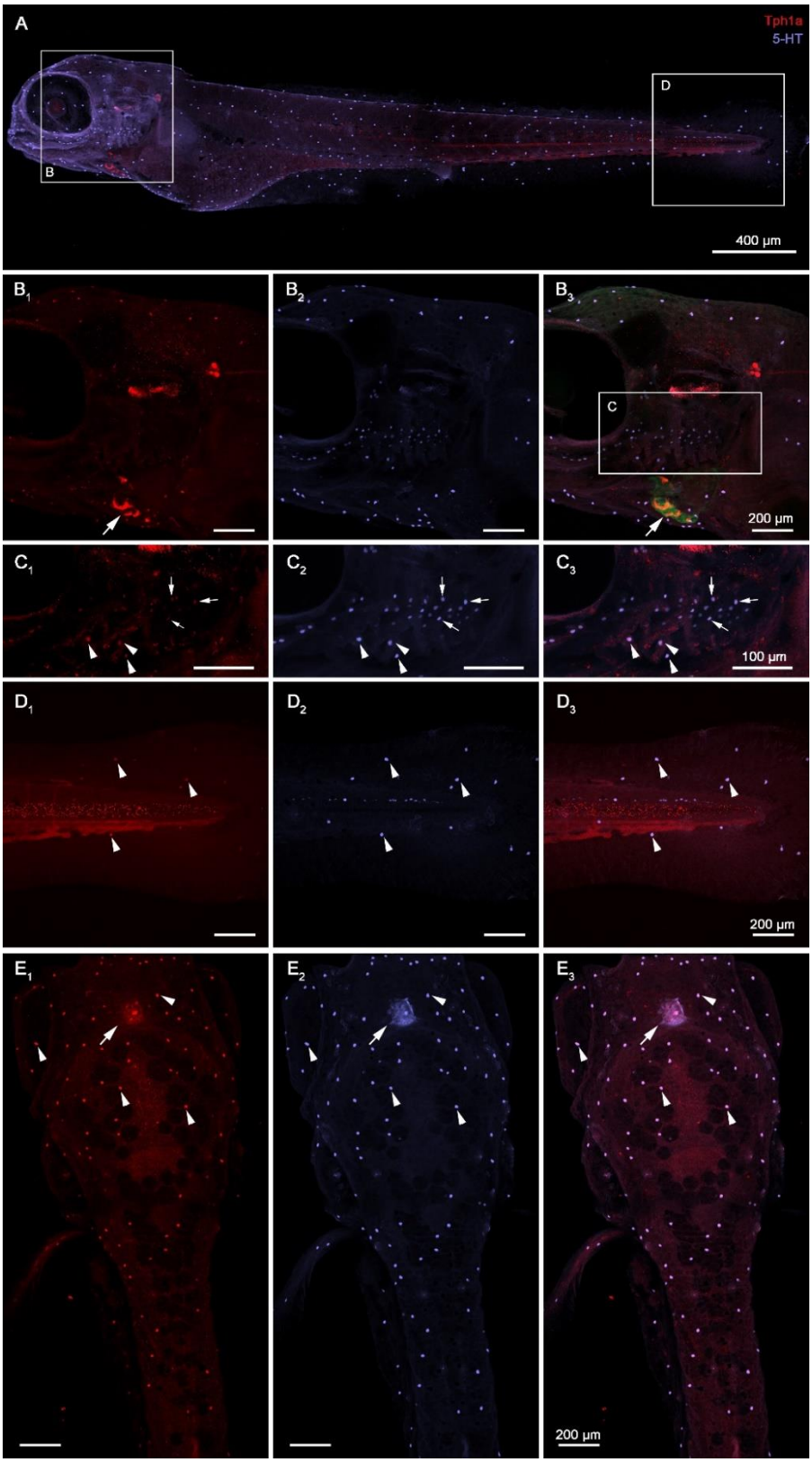
A
Tph1a
5-HT
B
D
400 µm
B1
B2
B3
C
200 µm
C1
C2
C3
100 µm
D1
D2
D3
200 µm
E1
E2
E3
200 µm

Fig. 3.1

Figure 3.2. Colocalization of Tph1b (red) and 5-HT (magenta) in *Tg(tph1b:mCherry)* line. (A) Lateral view of whole mount 4 days post fertilization (dpf) larval zebrafish co-stained for Tph1b and 5-HT. (B) Colocalization of Tph1b and 5-HT in the head region of the larva. Arrowheads show colocalization of Tph1b and 5-HT in MLCs in the pharyngeal arch region. (C) Colocalization of Tph1b and 5-HT on the skin of the larva in the tail region. No colocalization of Tph1b and 5-HT was observed in the tail region of this larva. Arrows point to web like cells on the fin of the larva expressing Tph1b only. (D) Dorsal view of whole mount 4 dpf larval zebrafish co-stained for Tph1b and 5-HT. Larva in (D) is a separate larva than the one in (A-C). Arrowheads show colocalization of Tph1b and 5-HT in skin NECs of this specific larva. Inset panels show a zoomed in skin NEC with colocalization of Tph1b and 5-HT. Brightness of the inset panel was modified to more clearly illustrate Tph1b staining in the skin NECs. Arrows point to Tph1b expressed in the brainstem region (outlined by dashed white lines). (E) High magnification image of the hypothalamus obtained by staining for Tph1b and 5-HT on 30 µm thick cryo-sections. The region identified in (D) shows the region where (E) is imaged, though (D) and (E) were obtained from separate larvae. Colocalization of Tph1b and 5-HT is observed in the hypothalamus. RHyp, rostral hypothalamus; CHyp, caudal hypothalamus.

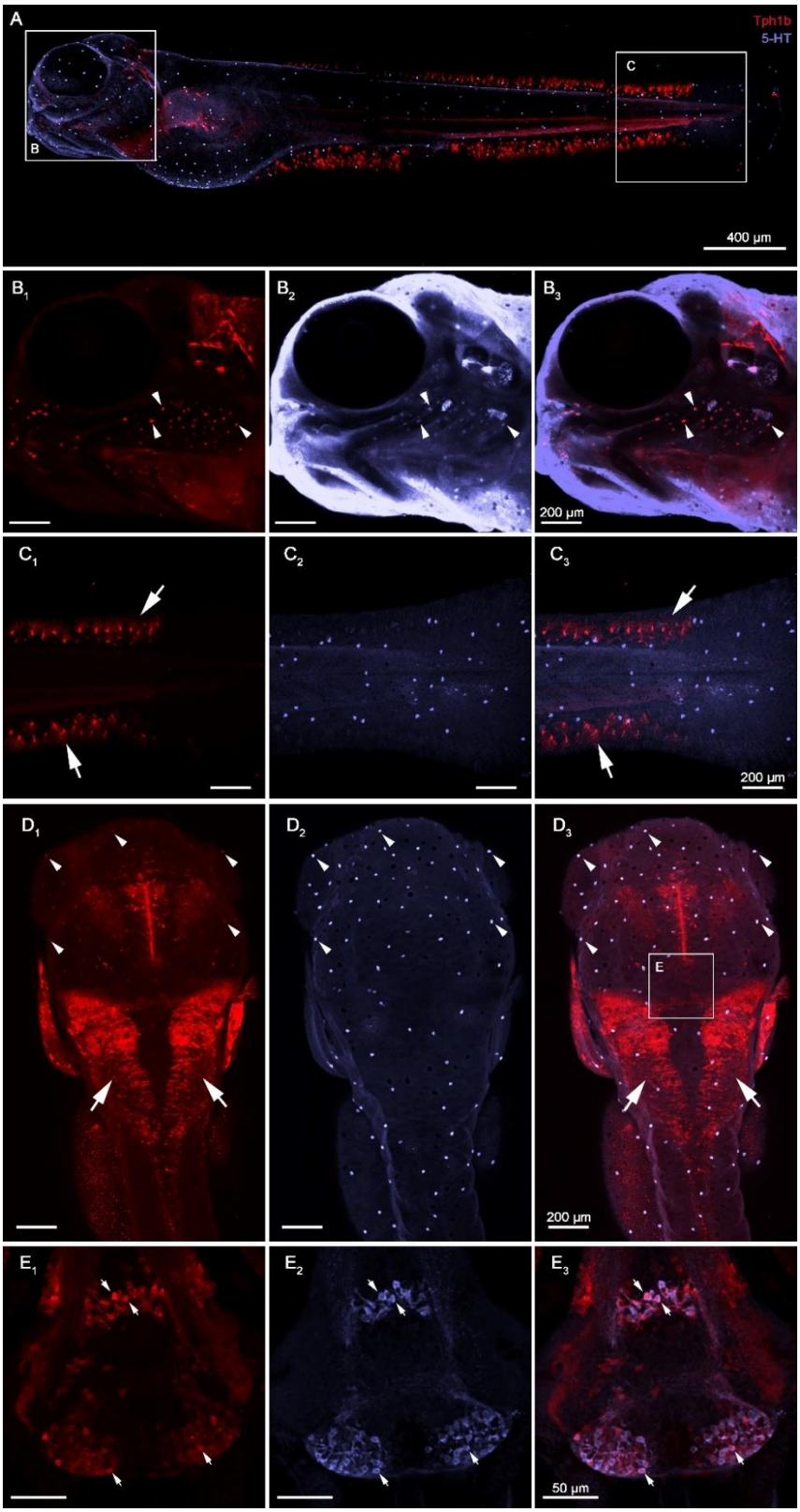
A
Tph1b
5-HT
B
C
400 µm
B1
B2
B3
200 µm
C1
C2
C3
200 µm
D1
D2
D3
E
200 µm
E1
E2
E3
50 µm

Fig. 3.2

Figure 3.3. Real-time PCR data of *tph* genes in the *tph1* knockouts. mRNA levels of *tph1a*, *tph1b* and *tph2* gene in 4 days post fertilization WT, *tph1a*$^{-/-}$, *tph1b*$^{-/-}$ and *tph1a*$^{-/-}$*b*$^{-/-}$ larvae. Data were normalized to total input RNA. N=6 for each group. Data are presented as means ± s.e.m. Statistical analysis was conducted using two-way ANOVA (Holm–Šidák post-hoc multiple comparison test at $P < 0.05$). Asterisks represent significance ($P < 0.05$) within each target gene.

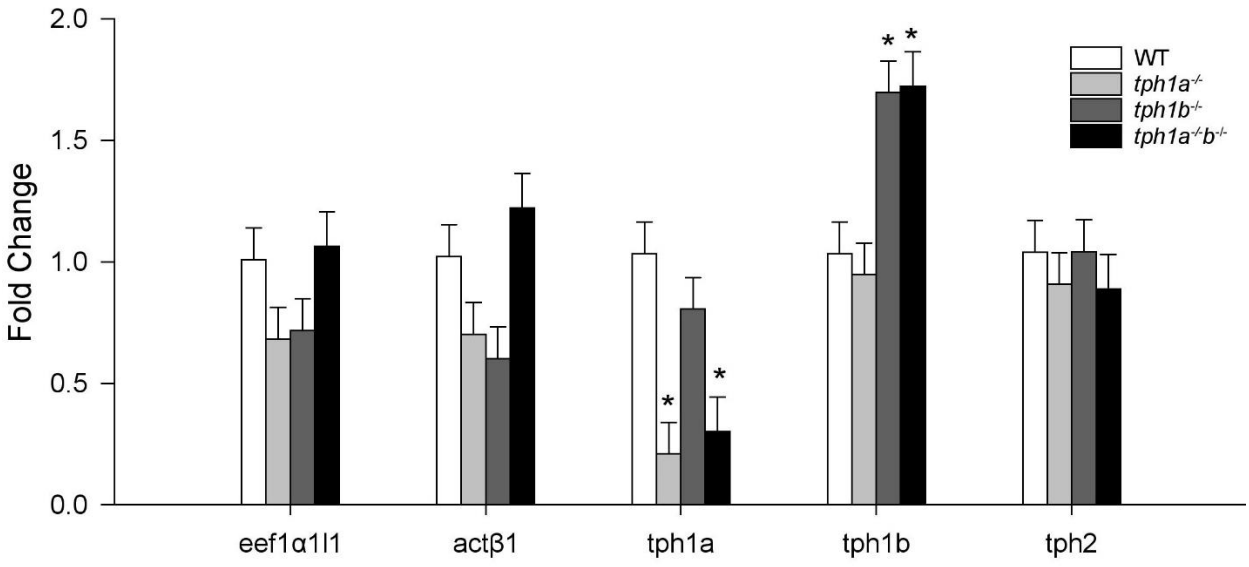
2.0
1.5
1.0
0.5
0.0
Fold Change
WT
tph1a-/-
tph1b-/-
tph1a-/-b-/-
*
*
*
*
eef1α1l1
actβ1
tph1a
tph1b
tph2

Fig. 3.3

Figure 3.4. Serotonin (5-HT) concentration in *tph1* knockouts. 5-HT in the head and body region of 4 days post fertilization WT, *tph1a*$^{-/-}$, *tph1b*$^{-/-}$ and *tph1a*$^{-/-}$*b*$^{-/-}$ larvae zebrafish; N=12 for each genotype. Data are presented as means ± s.e.m. Statistical analysis was conducted using two-way ANOVA (Holm–Šidák post-hoc multiple comparison test at $P < 0.05$). Uppercase letters represent significance in the body region. Lower case letters represent significance in the whole larvae obtained by summing the 5-HT in the head and body regions. Asterisks represent significance ($P < 0.05$) between the head and body region within the same genotype.

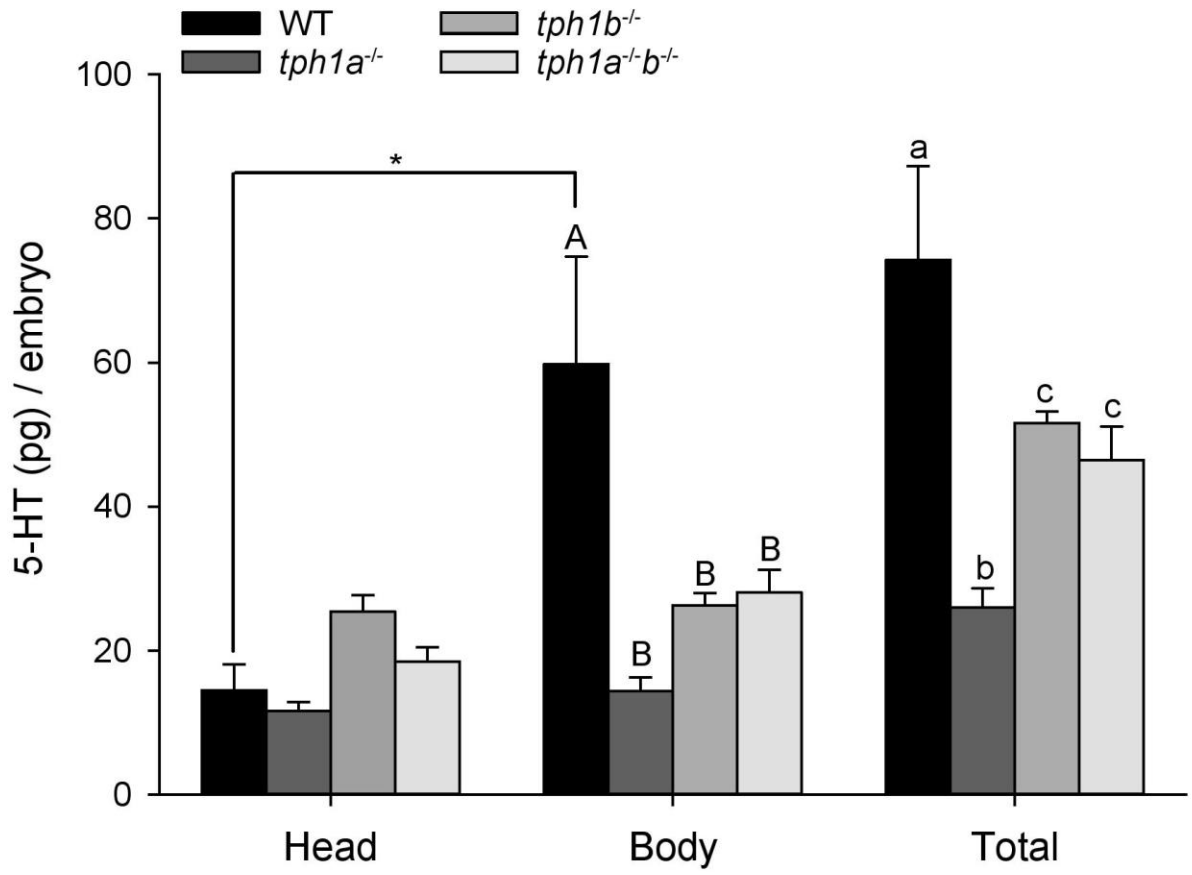
WT
tph1a-/-
tph1b-/-
tph1a-/-b-/-
5-HT (pg) / embryo
100
80
60
40
20
0
*
A
B
B
a
b
c
c
Head
Body
Total

Fig. 3.4

Figure 3.5. Detectable 5-HT positive cell density on the skin and pharyngeal arch of *tph1* mutant larvae. (A) Representative image of 5-HT positive cells on the skin of 4 days post fertilization (dpf) WT larvae. Scale bar equals 200 μm. (B) Representative image of tail region in larvae used for skin 5-HT positive cell density analysis. Scale bar equals 50 μm. (C, D) Representative image of the head region of a 4 dpf WT larva used for pharyngeal arch 5-HT positive cell density analysis. Scale bars equal 200 μm in (C) and 100 μm in (D). (E, F) Detectable 5-HT positive cell density on the skin and pharyngeal arch of WT, *tph1a*$^{-/-}$, *tph1b*$^{-/-}$ and *tph1a*$^{-/-}$*b*$^{-/-}$ larvae at different developmental stages. N=8-12 for each group. Data are presented as means ± s.e.m. Statistical analysis was conducted using two-way ANOVA (Holm–Šidák post-hoc multiple comparison test at $P < 0.05$). Asterisks represent significance ($P < 0.05$) between genotypes when compared within the same developmental stage.

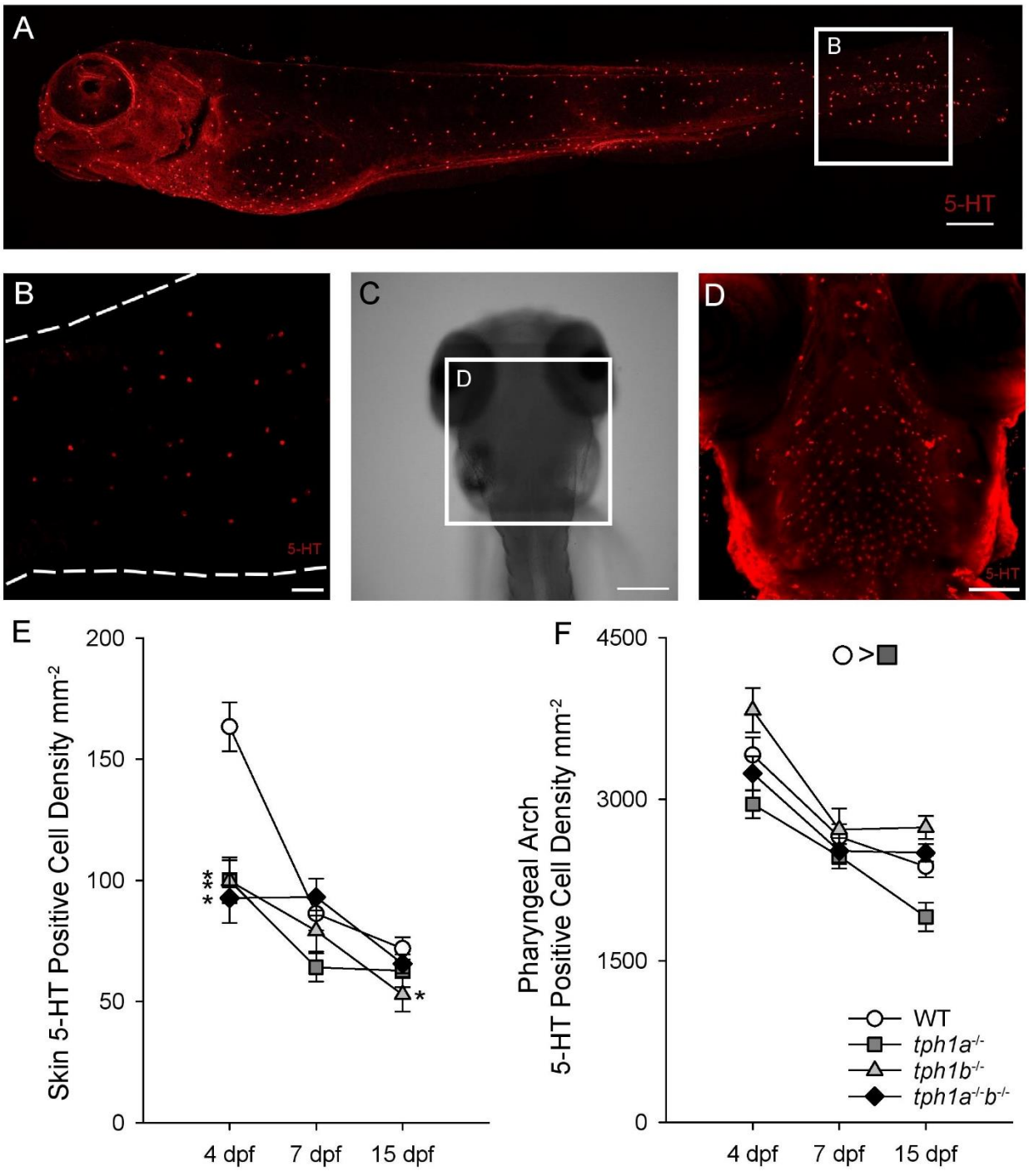
A
B
5-HT
B
5-HT
C
D
D
5-HT
E
Skin 5-HT Positive Cell Density mm-2
200
150
100
50
0
***
*
4 dpf
7 dpf
15 dpf
F
Pharyngeal Arch
5-HT Positive Cell Density mm-2
4500
3000
1500
0
O>■
WT
tph1a-/-
tph1b-/-
tph1a-/-b-/-
4 dpf
7 dpf
15 dpf

Fig. 3.5

Figure 3.6. Detectable 5-HT positive cell density in 4 days post fertilization *tph* morpholino knockdown larvae. (A) Detectable 5-HT positive cell density on the skin of *tph1a*, *tph1b*, *tph2* morpholino injected WT larvae. N=20 for each group. Data are presented as means ± s.e.m. Statistical analysis was conducted using one-way ANOVA (Holm–Šidák post-hoc multiple comparison test at $P < 0.05$). Asterisks represent significance ($P < 0.05$). (B) Detectable 5-HT positive cell density on the skin of WT, *tph1a*$^{-/-}$, and *tph1b*$^{-/-}$ larvae injected with *tph1b* morpholino. N=20 for each group. Data are presented as means ± s.e.m. Statistical analysis was conducted using two-way ANOVA (Holm–Šidák post-hoc multiple comparison test at $P < 0.05$). Asterisks represent significance ($P < 0.05$) within each genotype. Different letters indicate significance between genotypes.

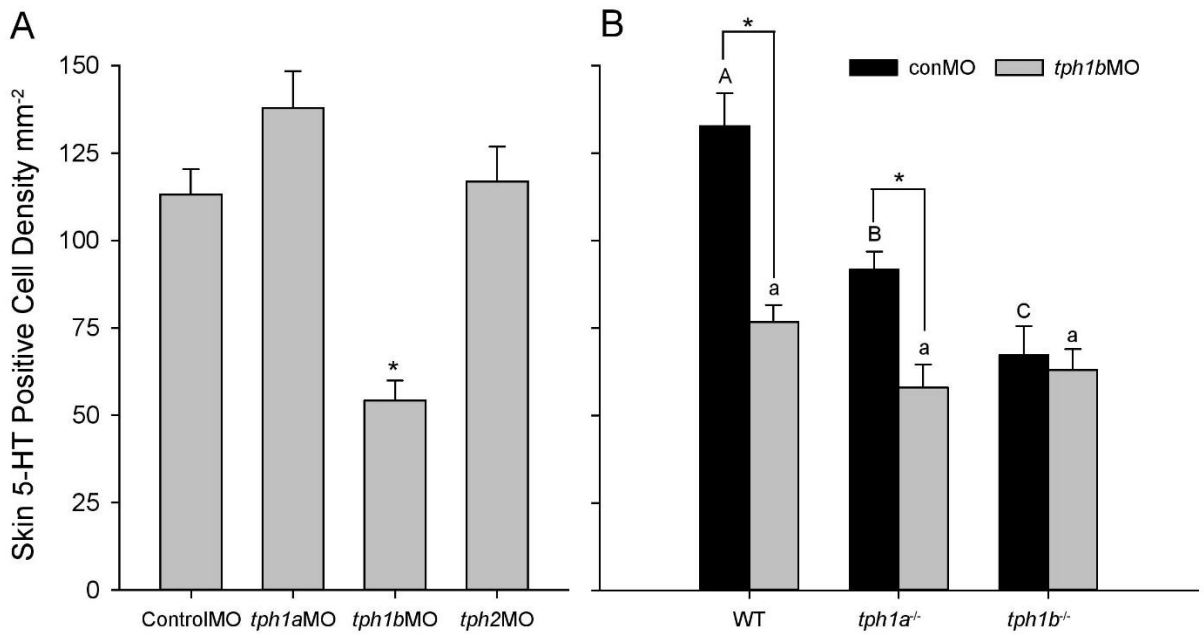
A
B
Skin 5-HT Positive Cell Density mm-2
150
125
100
75
50
25
0
*
ControlMO
tph1aMO
tph1bMO
tph2MO
conMO
tph1bMO
A
a
B
a
C
a
*
*
WT
tph1a-/-
tph1b-/-

Fig. 3.6

Figure 3.7. The interactive effects of hypoxia and developmental age on ventilation frequency (f_V) in larval zebrafish. WT, *tph1a*$^{-/-}$, *tph1b*$^{-/-}$ and *tph1a*$^{-/-}$*b*$^{-/-}$ (N=12 for each group at each developmental age) larvae at 4 days post fertilization [dpf, (A)], 7 dpf (B), 15 dpf (C) were exposed to hypoxia (35 mmHg) and subsequently returned to normoxia (153 mmHg). WT 4 dpf larvae injected with control morpholino (N=10) or *tph1b* morpholino (N=9) were subjected to the same conditions (D). Vertical dashed lines represent delineations among normoxia, hypoxia and recovery. Data are presented as means ± s.e.m. See Figs. S3.2-S3.4 for statistical analysis.

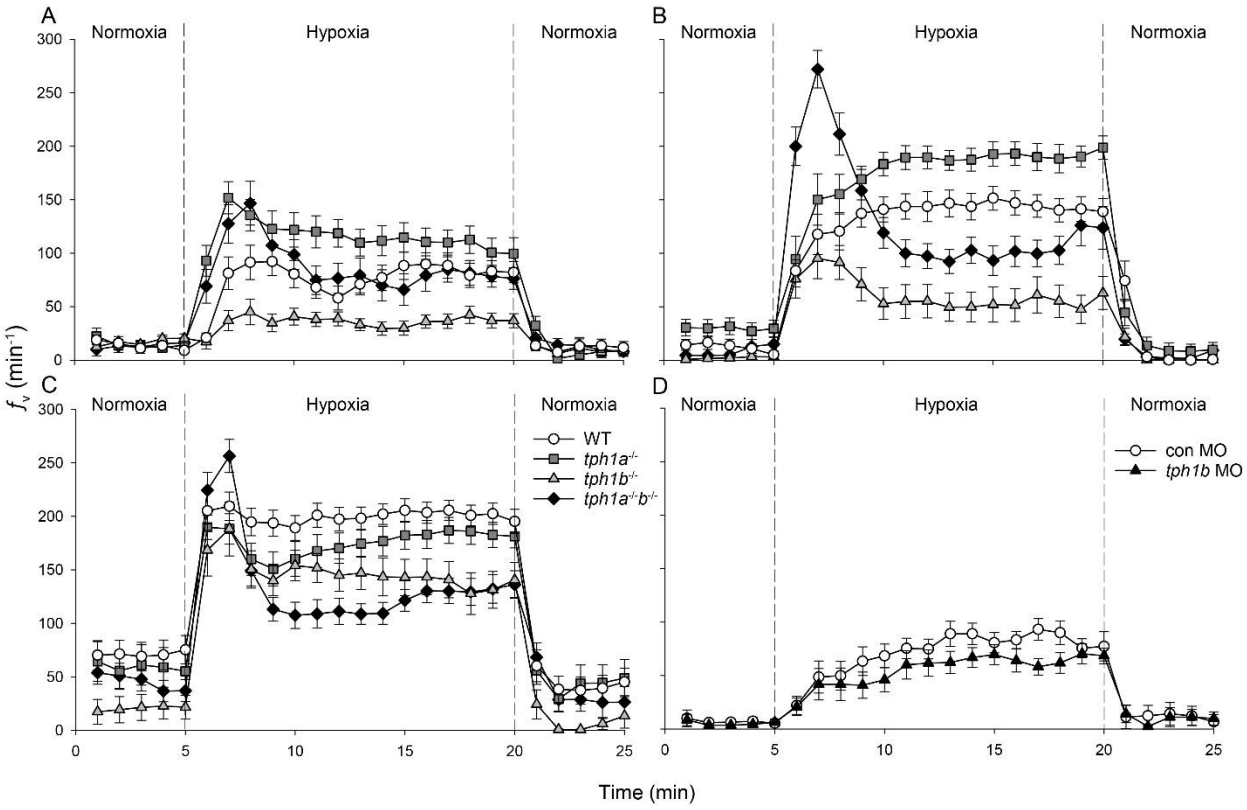
A
B
C
D
Normoxia
Hypoxia
Normoxia
f_v (min^{-1})
Time (min)
WT
tph1a-/-
tph1b-/-
tph1a-/-b-/-
con MO
tph1b MO

Fig. 3.7

3.5 Discussion

The purpose of this study was to discern the specific paralog(s) of *tph* responsible for 5-HT synthesis in NECs of larval zebrafish thereby enabling an examination of the role of NEC 5-HT in regulating ventilation during acute hypoxia. The planned approach was to compare ventilatory responses to hypoxia in wild-type larvae with responses in *tph* knockout lines, at least one of which was expected to lack the capacity to synthesize 5-HT in NECs. In an attempt to generate *tph2* knockouts, we observed that even though *tph2*$^{-/-}$ mutants obtained from heterozygote crosses were able to survive to adulthood, they were unable to produce viable offspring and thus this study focused exclusively on the two *tph1* paralogs.

Transgenic lines expressing mCherry demonstrated that both pharyngeal arch and skin NECs express Tph1 paralogs and thus are likely able to synthesize 5-HT. However, even complete knockout of *tph1* (*tph1a*$^{-/-}$*b*$^{-/-}$) failed to eliminate 5-HT expression in NECs although transient effects were observed. Regardless, the results obtained using *tph1* knockouts demonstrated that 5-HT plays a role in regulating ventilation, although its effect is not necessarily attributable to the 5-HT localized in NECs.

3.5.1 Tph1 expression in NECs

Previous studies describing the location of the zebrafish *tph* paralogs in larval zebrafish focused primarily on their presence in the brain and spinal cord (Lillesaar, 2011), with little peripheral expression data reported. An important focus of the current study was to assess the distribution of Tph paralogs in the NECs of larval zebrafish to determine which paralogs are responsible for 5-HT production in these presumptive O_2 chemosensory cells. Although 5-HT is the standard marker used to identify NECs in larval and adult zebrafish, the source of 5-HT was

previously unknown. Using *Tg(tph1a:mCherry)* and *Tg(tph1b:mCherry)* lines respectively, it was determined that NECs in the pharyngeal arch express Tph1a (Fig. 3.1), and NECs on the skin of larval zebrafish express both Tph1a and Tph1b (Figs. 3.1D-E, 3.2D) although, unlike for Tph1a, Tph1b expression was not observed consistently. A possible explanation is that Tph1b is transiently expressed at a low level within skin NECs during early development, and it was difficult to routinely obtain larvae for imaging when Tph1b expression was at its highest. In addition, the *tph1b* promoter could be susceptible to positional effects, as was observed previously for the *tph2* promoter (Yokogawa et al., 2012), which could lead to only a population of the larvae expressing Tph1b within the skin NECs. A third population of neurosecretory serotonergic cells found in the oropharyngeal cavity – Merkel-like cells (MLCs) – that are associated with taste buds (Zachar and Jonz, 2012a) also expressed both Tph1a and Tph1b paralogs (Figs. 3.1-3.2). Because Tph is the rate-limiting enzyme in the biosynthesis of 5-HT, the expression of Tph1 paralogs in NECs and MLCs suggest that 5-HT is synthesized directly within these cells. In addition, Tph1b is also peripherally expressed in web like cells on the fin of the larvae (Fig. 3.2A, C). These cells could be *tph1b* positive fibroblasts previously described in adult zebrafish fin joints that plays a role in the regeneration of fin rays (Tornini et al., 2016).

3.5.2 Knockout or knockdown of *tph1* alters hypoxic ventilatory responses that appear unrelated to changes in detectable serotonergic NECs

5-HT has been implicated in regulating ventilation in several fish species (Burleson and Milsom, 1995b; Fritsche et al., 1992; Janvier et al., 1996; McDonald et al., 2010; Panlilio et al., 2016). More specifically in zebrafish, exogenous 5-HT administered *in vivo* revealed its potential for stimulating ventilation in larvae after 7 dpf (Shakarchi et al., 2013) or aquatic surface respiration in adults (Abdallah et al., 2015b). Moreover, the ventilatory response to hypoxia was

abolished by the 5-HT_2 receptor antagonist ketanserin in larvae older than 7 dpf (Shakarchi et al., 2013). However, these previous experiments employing pharmacological approaches were unable to distinguish between the potential central effects of 5-HT from those specifically mediated by 5-HT within NECs.

In an attempt to address this question, t*ph1* knockout lines were generated/obtained to further examine if 5-HT in NECs play a role in regulating ventilatory responses. Due to a lack of reliable Tph1a or Tph1b antibody (six different homologous custom antibodies were generated and tested without success), knockout of *tph1a* and *tph1b* were verified indirectly by measuring *tph* paralog gene expression and tissue 5-HT levels. Decreased expression of *tph1a* in both *tph1a*$^{-/-}$ and *tph1a*$^{-/-}$*b*$^{-/-}$ mutants compared to WTs suggests that mRNA was undergoing nonsense-mediated mRNA decay (NMD), a cellular mechanism that degrades transcripts not encoding a functional protein, which can indicate successful knockout (Anderson et al., 2017; Chang et al., 2007). Interestingly, *tph1b* expression on the other hand was increased in both *tph1b*$^{-/-}$ and *tph1a*$^{-/-}$*b*$^{-/-}$ mutants. Such an increase in knockout gene mRNA was reported previously in *rhcgb* mutant zebrafish (Zimmer and Perry, 2020), suggesting that not all mutant mRNA is subject to NMD (Anderson et al., 2017). Indeed, the increased mRNA expression may reflect a futile attempt to increase expression of the targeted protein owing to the production of truncated protein. Gene expression data also reveled that compensatory expression of other *tph* paralogs did not occur in the mutants. Importantly, 5-HT levels were lower in the body region of the *tph1a*$^{-/-}$, *tph1b*$^{-/-}$ and *tph1a*$^{-/-}$*b*$^{-/-}$ mutants, although 5-HT levels in the head region were similar across the four genotypes. This finding suggests that similar to mammals, *tph1* paralogs plays a predominant role in peripheral rather than central 5-HT synthesis (Côté et al., 2003; McKinney et al., 2005; Walther and Bader, 2003).

Because skin NECs express both Tph1a and Tph1b, a decrease in detectable serotonergic skin NEC density in *tph1a*$^{-/-}$, *tph1b*$^{-/-}$, *tph1a*$^{-/-}$*b*$^{-/-}$ mutants and *tph1b* morphants at 4 dpf was expected (Fig. 3.5E, 6A) when using 5-HT as a NEC marker. It is important to note that even though 5-HT is depleted within NECs, it is likely that NECs are still present but less detectable due to the lack of 5-HT. A further decrease of serotonergic skin NEC density in *tph1a*$^{-/-}$ but not *tph1b*$^{-/-}$ mutants (Fig. 3.6B) in *tph1b* morphants supports the specificity and effectiveness of the *tph1b* morpholino injected. This difference in detectable serotonergic skin NEC density among the genotypes disappeared by 7 dpf due to a much higher rate of decrease in detectable serotonergic skin NECs in the WTs. In the pharyngeal arch region, both NECs and MLCs express 5-HT and were difficult to differentiate based on 5-HT staining alone in a dorsal view where all serotonergic cells can be imaged, and thus total detectable serotonergic cell density was examined. Interestingly, only *tph1a*$^{-/-}$ mutants exhibited a lower detectable 5-HT positive cell density than the WTs. The lack of difference between *tph1a*$^{-/-}$*b*$^{-/-}$ mutants and WTs suggests that similar to other 5-HT synthesizing cells, these 5-HT positive cells likely absorb 5-HT from the extracellular space via the serotonin (5-HT) reuptake transporter (SERT). However, whether or not SERT is expressed in pharyngeal arch NECs or MLCs is unknown and requires further study. Alternatively, there is also the possibility that 5-HT is not biosynthesized *de novo* from tryptophan; instead, it could be produced by aromatic L-aromatic amino acid decarboxylase - mediated conversion of 5-hydroxy-L-tryptophan absorbed from the plasma and/or nerve fibers as previously reported for 5-HT present in mammalian taste bud cells (Pan et al., 2018). Because *tph1a*$^{-/-}$, *tph1b*$^{-/-}$ and *tph1a*$^{-/-}$*b*$^{-/-}$ mutants still displayed detectable serotonergic skin NECs or 5-HT positive cells in the pharyngeal arch region, we further attempted to eliminate 5-HT within those cells through para-chlorophenylalanine (pCPA), a drug that interferes with 5-HT synthesis

by acting as a selective and irreversible inhibitor of Tph. However, pCPA doses that did not cause gross morphological defects also failed to eliminate 5-HT in skin NECs completely (Fig. S3.5).

To further examine the role of 5-HT within NECs in the control of ventilation, the ventilatory responses to hypoxia were monitored in the four genotypes from 4 – 15 dpf as well as 4 dpf *tph1b* morphants. During hypoxia, WT larvae at all stages increased and maintained f_V. However, despite both detectable serotonergic skin NEC density and detectable serotonergic cell density in the pharyngeal arches showing similar trends in *tph1a*$^{-/-}$ and *tph1b*$^{-/-}$ mutants, their responses to hypoxia were markedly different. These differences were especially evident in 7 dpf larvae, when detectable skin NEC density was similar in WTs and mutants and detectable serotonergic cell density in the pharyngeal arches region was the same between WTs and *tph1b*$^{-/-}$ mutants. Although all three genotypes increased ventilation in response to hypoxia, *tph1a*$^{-/-}$ mutants increased f_V to a greater extent than WTs whereas *tph1b*$^{-/-}$ mutants exhibited a lower f_V compared to WTs. These results suggest that although 5-HT may indeed regulate ventilation as previously indicated (Shakarchi et al., 2013), the site of action is likely not in the peripheral skin NECs or serotonergic cells in the pharyngeal arches. The relationship between detectable skin NEC density and the ventilatory response to hypoxia in *tph1b* morphants further supports this notion because although *tph1b* knockdown resulted in similar decreases of detectable skin NEC density as in the *tph1b*$^{-/-}$ mutants, their f_V in hypoxia was not different than WTs. The different response to hypoxia in the *tph1b*$^{-/-}$ mutants and *tph1b* morphants is noteworthy. In *tph1b*$^{-/-}$ mutants, a complete elimination of functional Tph1b protein is expected, yet in the *tph1b* morphants, it is likely that some functional Tph1b protein remains (Zimmer et al., 2019). However, detectable skin NEC density was the same in *tph1b*$^{-/-}$ mutants and *tph1b* morphants,

and further injection of *tph1b* morpholino into *tph1b*$^{-/-}$ mutants did not further decrease skin NEC density, suggesting that the small proportion of functioning Tph1b protein in the *tph1b* morphants is functioning elsewhere such as the CNS. Thus, one possible explanation for the discrepancy in the response to hypoxia between the *tph1b*$^{-/-}$ mutants and *tph1b* morphants is that the remaining Tph1b protein is producing sufficient 5-HT to regulate the response to hypoxia, and in turn, further supports the view that 5-HT, at least within skin NECs, is not the predominant factor for regulating ventilation during hypoxia.

Although the results of the current study clearly reveal a significant role of 5-HT in the acute hypoxic ventilatory response (HVR), its mode and site of action are unknown. However, the present data set suggests that there may be a central location of 5-HT acting independently and/or in addition to potential peripheral mechanisms. In mammals, medullary serotonergic neurons can act as central respiratory chemoreceptors, with intrinsic chemosensitivity to physiologically relevant changes in CO_2/pH, which is the main driver of ventilation in mammals, and able to induce appropriate effects on respiratory output (Corcoran et al., 2009; Hodges and Richerson, 2010). 5-HT itself also plays an important role in the hypercapnic ventilatory response (HCVR), with 5-HT being able to completely rescue the blunted HCVR in mice lacking central serotonergic neurons (Hodges et al., 2008). In addition, distinct subtypes of serotonergic neurons are present in mouse, with some specialized to drive increased ventilation in response to CO_2 elevation and acidosis (Brust et al., 2014). Thus, it is not farfetched to hypothesize that in larval zebrafish, central 5-HT production via Tph1a and Tph1b occurs at distinctly different sites where opposing effects on ventilation are exerted. In the *tph1b* knockouts, the HVR was markedly reduced at all the developmental ages studied whereas the *tph1a* knockouts exhibited an enhanced HVR at least until 7 dpf, suggesting that centrally, a subset of neurons in which 5-

HT is produced by Tph1a inhibit ventilation while another subset of neurons in which 5-HT is produced by Tph1b stimulate ventilation.

Excitatory and inhibitory effects of 5-HT acting at different sites within the CNS may also contribute to the biphasic nature of the HVR whereby in mammals an initial acute response (AR) phase consisting of a rapid increase in f_V followed by a short term depression (STD) phase where f_V decreases progressively during hypoxia to correct for the overshoot in f_V during AR, after which f_V remains stable although at a higher level than baseline (Dick and Coles, 2000; Powell et al., 1998). A similar biphasic response to hypoxia was reported for zebrafish larvae (Mandic et al., 2019; Pan et al., 2019) although it was not particularly evident in the WT larvae of this study. Thus, one can speculate that the differences in f_V between *tph1a*$^{-/-}$ and *tph1b*$^{-/-}$ mutants during hypoxia reflects the presence of Tph1a expressing neurons in the CNS that are responsible for inhibiting f_V during AR and STD and Tph1b expressing neurons that serve to maintain the elevated f_V during hypoxia. With the lack of Tph1a in the *tph1a*$^{-/-}$ mutants, the overshoot of f_V cannot be inhibited, resulting in a higher f_V in hypoxia compared to WTs. Conversely, with the lack of Tph1b in the *tph1b*$^{-/-}$ mutants, f_V during hypoxia cannot be maintained resulting in a lower f_V compared to WTs. The response to hypoxia in the *tph1a*$^{-/-}$*b*$^{-/-}$ double mutants is especially interesting because it combines the phenotype of the two single mutants. When first exposed to hypoxia, f_V of *tph1a*$^{-/-}$*b*$^{-/-}$ mutants overshoot to a much greater extent compared to WTs, suggesting a lack of inhibitory input during AR and STD owing to the loss of Tph1a neurons. As hypoxia progresses, f_V in the *tph1a*$^{-/-}$*b*$^{-/-}$ mutants drops back down to a level similar to *tph1b*$^{-/-}$ mutants, both much lower than WTs, suggesting that the absence of Tph1b neurons prevents the usual maintenance of elevated f_V.

In conclusion, even though 5-HT is expressed within skin NECs, pharyngeal arch NECs and MLCs, the discrepancy in detectable serotonergic NEC density and the ventilatory response to hypoxia in the *tph1* knockouts suggest that 5-HT located in locations other than NECs may play a more important role in regulating the ventilatory response. In addition, based on the location that 5-HT is acting upon, most likely within the CNS, 5-HT could have markedly different effects on the HVR. Certainly, future studies examining the role of CNS 5-HT in the control of breathing are needed.

3.6 Supplementary Tables and Figures

Table S3.1. List of real-time PCR primers used assess the expression of *tph* genes in 4 days post fertilization WT, *tph1a*$^{-/-}$, *tph1b*$^{-/-}$ and *tph1a*$^{-/-}$*b*$^{-/-}$ zebrafish. All sequences listed 5′ to 3′ with the reverse primer sequences listed as the reverse compliment of the gene sequence.

Gene	Orientation	Sequence
eef1α1l1	F	TACCTACCCTCCTCTTGGTCG
	R	TTGGAACGGTGTGATTGAGGG
actβ1	F	GATCAAGATCATTGCTCCCCCT
	R	GGCCATTTAAGGTGGCAACAG
tph1a	F	TCCATGAACCTCGGAATGACT
	R	TTGACTAGCCCACCGACTTC
tph1b	F	TGCGCAAGCAAACAAGCATA
	R	GAATCCCGGATGATCTGCGT
tph2	F	TCCTCCATGGACATCCTTTAATCG
	R	TCTCCGAGACTCAATGTGCG

Figure S3.1. Colocalization of Calretinin (red) and 5-HT (magenta) in 7 dpf larval zebrafish. (A) Lateral view of the head of whole mount 7 dpf larval zebrafish co-stained for Calretinin and 5-HT using 1:500 dilution mouse anti-calretinin (Swant Inc. Cat#: 6B3PUR) and 1:1000 dilution rabbit anti-5HT (Sigma Aldrich Inc., Cat#: S5545). See manuscript section 2.7 for further details on methods. (B) Higher magnification view of the pharyngeal arch region shown in (A). Merkel-like cells (MLCs) are shown with arrowheads, while pharyngeal arch neuroepithelial cells (NECs) are shown with arrows. MLCs can be identified by association with calretinin positive taste bud cells, and unlike NECs, MLCs align with the curvature of individual pharyngeal arches. NECs on the other hand are not associated with calretinin positive taste bud cells and are mainly found on budding filaments (bf) emerging from the pharyngeal arch (pa).

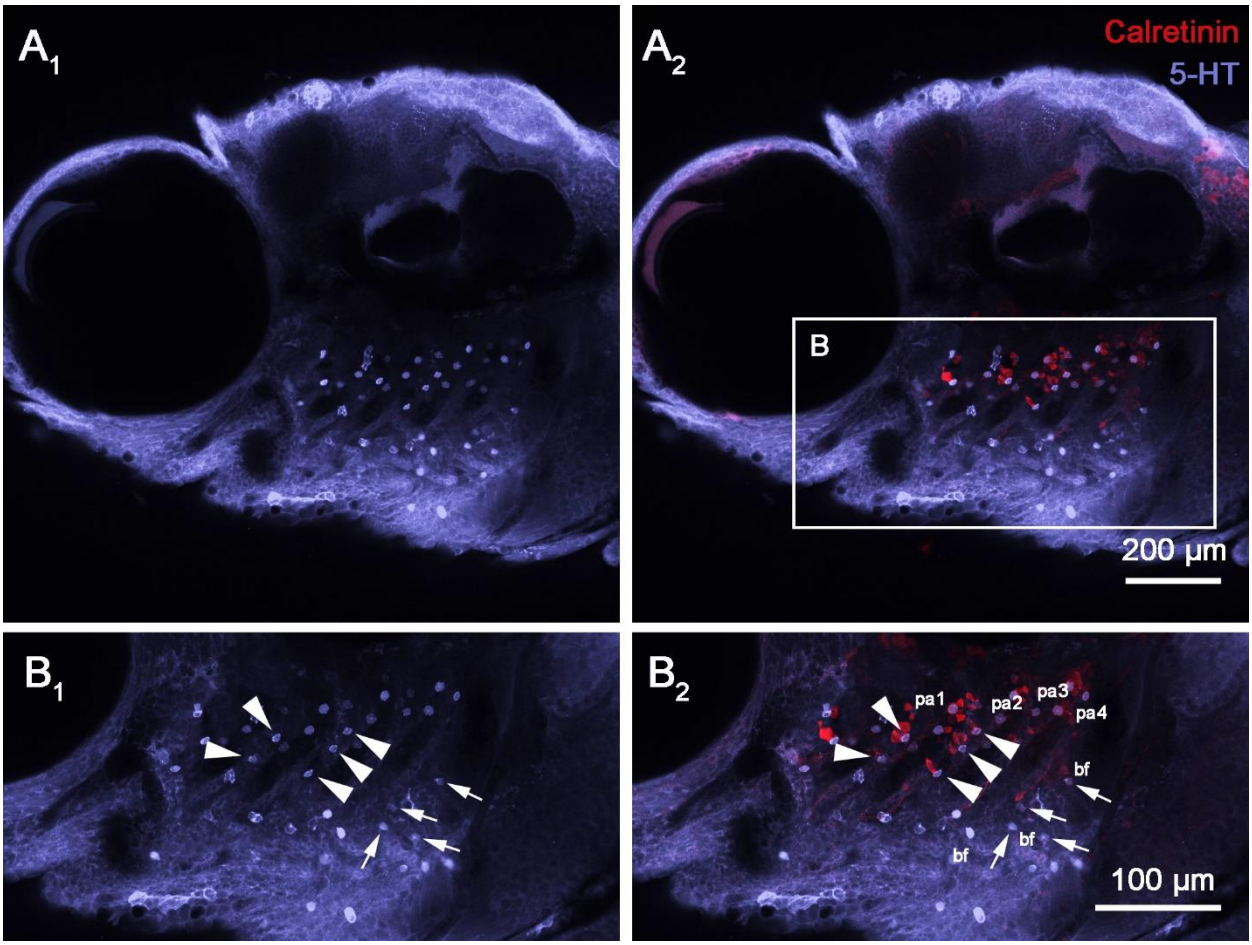
A1
A2
Calretinin
5-HT
B
200 µm
B1
B2
pa1
pa2
pa3
pa4
bf
bf
bf
100 µm

Fig. S3.1

Figure S3.2. The average differences in f_V (delta f_V) between normoxia and hypoxia, and normoxia and recovery in wild-type (WT), *tph1a*$^{-/-}$, *tph1b*$^{-/-}$ and *tph1 a*$^{-/-}$*b*$^{-/-}$ larval zebrafish (data based on Figure 5A-C). Panels A-D are larvae at 4 days post fertilization (dpf), panels E-H are larvae at 7 dpf, and panels I-L are larvae at 15 dpf. Panels A, E, I are WT larvae, panels B, F, J are tph1a$^{-/-}$ larvae, panels C, G, K are *tph1b*$^{-/-}$ larvae, and panels D, H, L are *tph1 a*$^{-/-}$*b*$^{-/-}$ larvae. Estimates are presented with 95% credible intervals (CI) based on Bayesian analysis. Data are significant if the 95% CI do not intersect zero (dashed horizontal line).

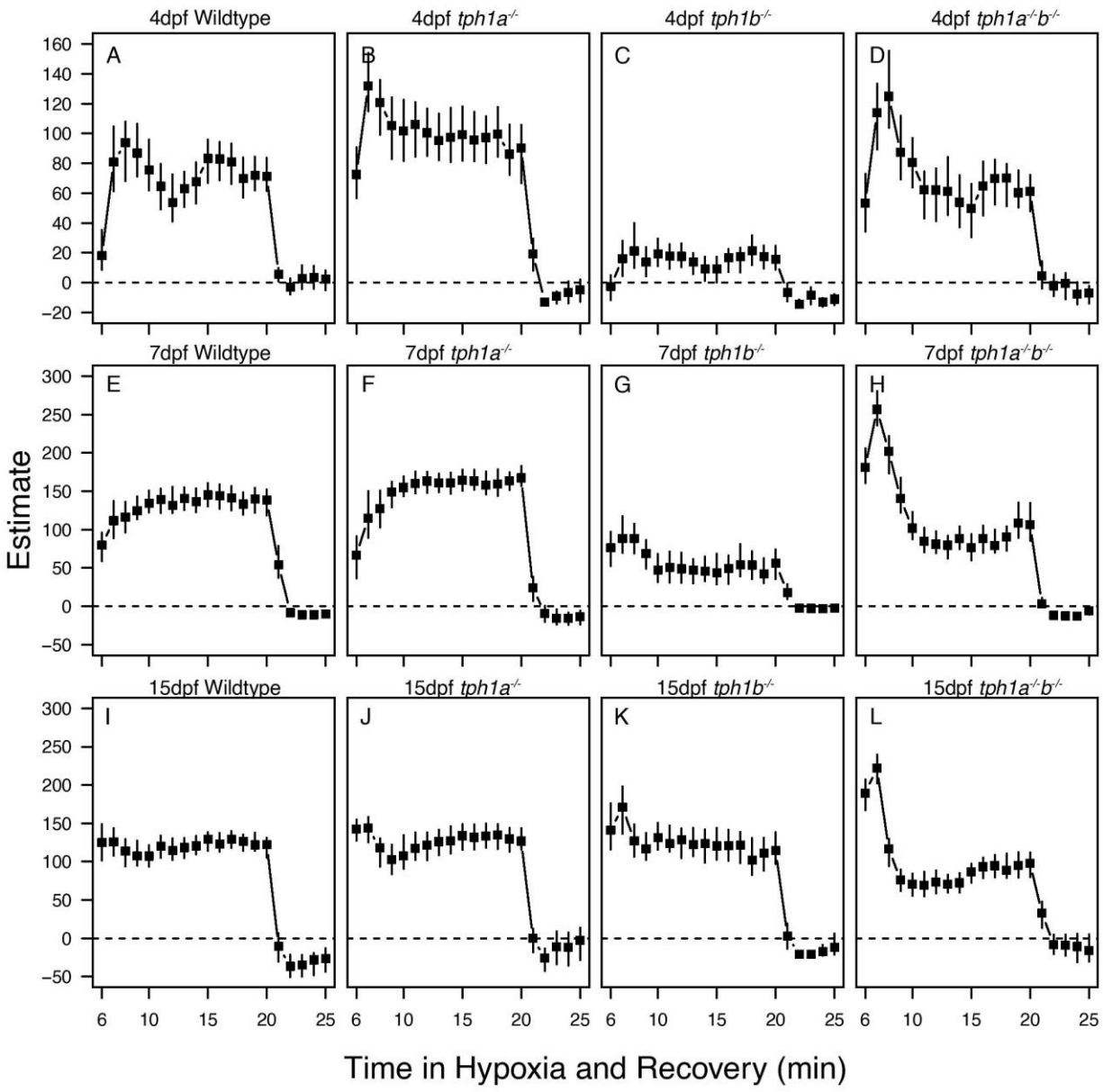
4dpf Wildtype
4dpf tph1a-/-
4dpf tph1b-/-
4dpf tph1a-/-b-/-
A
B
C
D
7dpf Wildtype
7dpf tph1a-/-
7dpf tph1b-/-
7dpf tph1a-/-b-/-
E
F
G
H
15dpf Wildtype
15dpf tph1a-/-
15dpf tph1b-/-
15dpf tph1a-/-b-/-
I
J
K
L
Estimate
Time in Hypoxia and Recovery (min)

Fig. S3.2

Figure S3.3. The average differences in f_V (delta f_V) between *tph1* knockout and WT larval zebrafish (data based on Figure 5A-C). Panels A-C are larvae at 4 dpf, panels D-F are larvae at 7 dpf, and panels G-I are larvae at 15 dpf. Panels A, D, G are *tph1a*$^{-/-}$ larvae compared to WT larvae, panels B, E, H are *tph1b*$^{-/-}$ larvae compared to WT larvae, and panels C, F, I are *tph1 a*$^{-/-}$*b*$^{-/-}$ larvae compared to WT larvae. Estimates are presented with 95% credible intervals (CI) based on Bayesian analysis. Data are significant if the 95% CI do not intersect zero (dashed horizontal line).

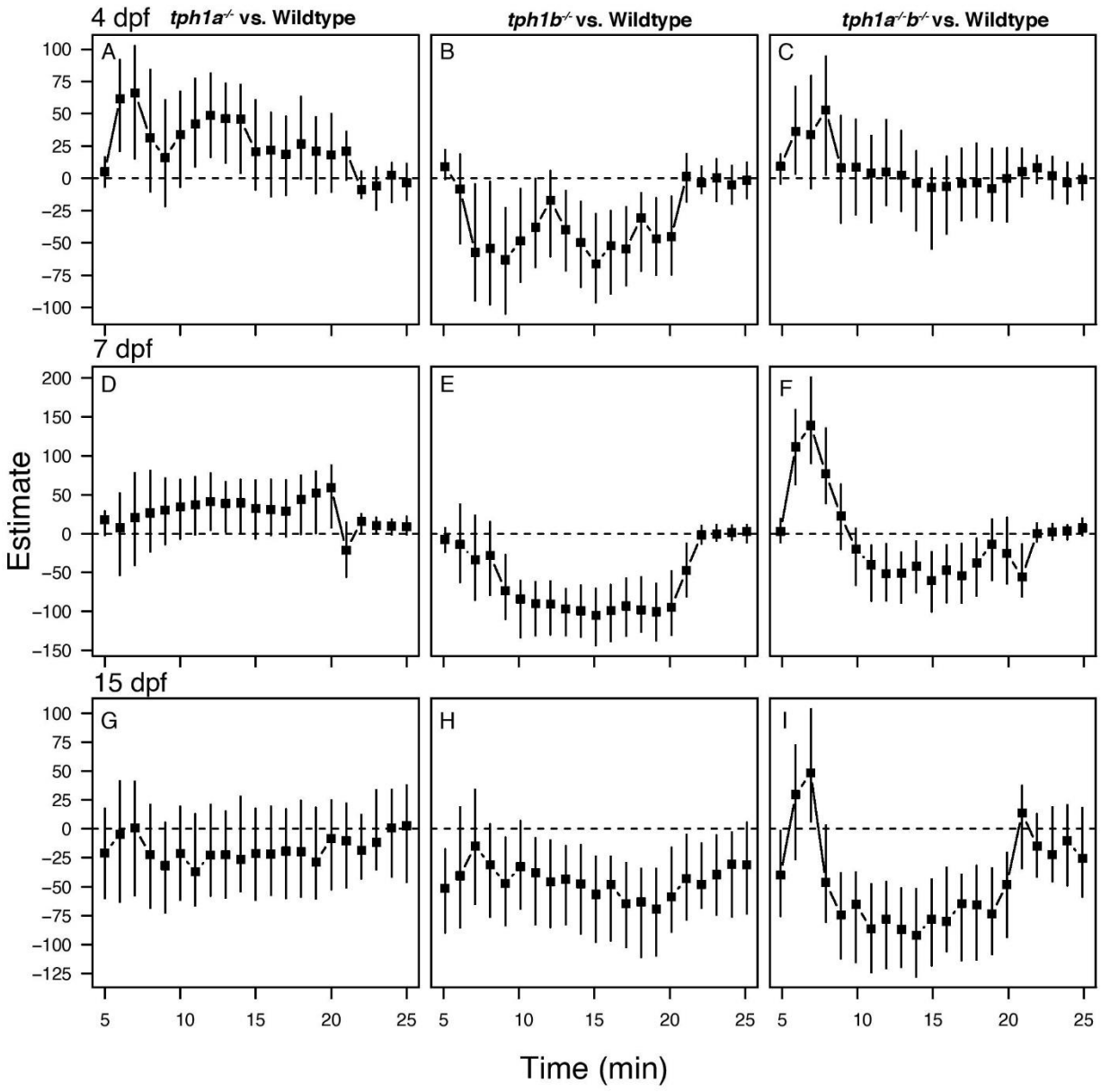
4 dpf
tph1a-/- vs. Wildtype
tph1b-/- vs. Wildtype
tph1a-/-b-/- vs. Wildtype
A
B
C
7 dpf
D
E
F
15 dpf
G
H
I
Estimate
Time (min)

Fig. S3.3

Figure S3.4. The average differences in f_V (delta f_V) between normoxia and hypoxia, and normoxia and recovery in control morpholino injected WTs (A) and *tph1b* morpholino injected WTs (B), and the average differences in f_V (delta f_V) between *tph1b* morpholino injected and control morpholino injected larvae (C). Data based on Figure 5D. Estimates are presented with 95% credible intervals (CI) based on Bayesian analysis. Data are significant if the 95% CI do not intersect zero (dashed horizontal line).

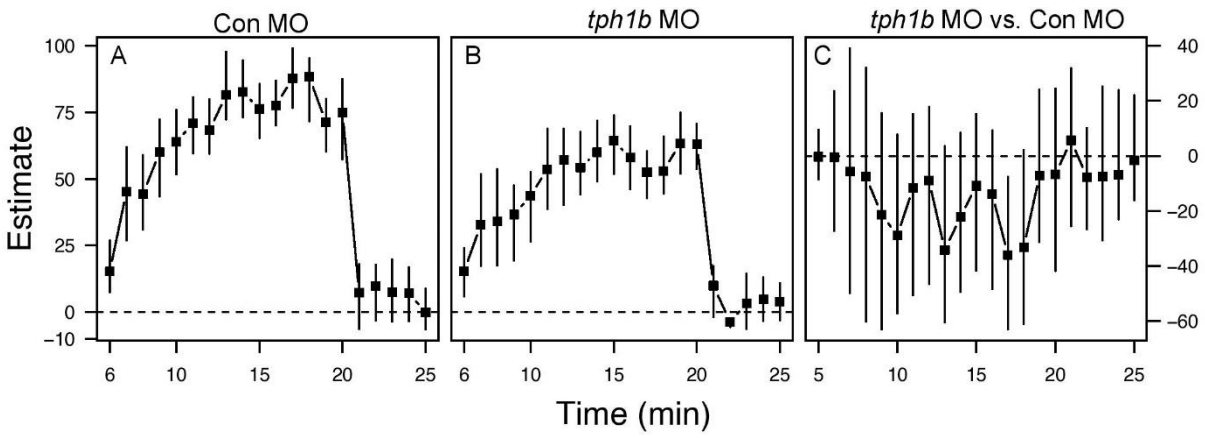
Con MO
tph1b MO
tph1b MO vs. Con MO
A
B
C
Estimate
Time (min)
100
75
50
25
0
−10
40
20
0
−20
−40
−60
6
10
15
20
25
5

Fig. S3.4

Figure S3.5. (A) Representative images of 4 days post fertilization (dpf) larvae treated with para-chlorophenylalanine (pCPA) from 24-48 h post fertilization (hpf). (B-D) Representative image of detectable 5-HT positive cells on the skin of 4 dpf larvae treated with 0 µM (B), 10 µM (C), and 20 µM (D) pCPA from 24-48 hpf. (E) Detectable 5-HT positive cell density on the skin of 4 dpf larvae treated with 0, 10 or 20 µM pCPA from 24-48 hpf. N=8-11 for each group. Data are presented as means ± s.e.m. Statistical analysis was conducted using one-way ANOVA (Holm-Sidak post-hoc multiple comparison test at $P < 0.05$). Asterisks represent significance. (F) The interactive effects of 20 µM pCPA treatment from 24-48 hpf and 50 µM 5-HT during hypoxia on ventilation frequency (f_V) in 4 dpf larval zebrafish. Larvae (N=7-8 for each group) were exposed to hypoxia only (solid symbols) or hypoxia with 50 µM 5-HT (open symbols) and subsequently returned to system water. Vertical dashed lines represent delineations among baseline, treatment and recovery. Data are presented as means ± s.e.m. (G-J) The average differences in f_V (delta f_V) between baseline and treatment (hypoxia only (G, I) or hypoxia + 50 µM 5-HT (H, J)), and baseline and recovery in 4 dpf no pCPA (G, H) or 20 µM pCPA treated (I, J) larval zebrafish. (K-M) The average differences in f_V (delta f_V) compared to control treated larvae exposed to hypoxia only. Estimates are presented with 95% credible intervals (CI) based on Bayesian analysis. Data are significant if the 95% CI do not intersect zero (dashed horizontal line). Control larvae increased f_V to a similar extent during hypoxia with or without 5-HT. Larvae exposed to pCPA did not increase f_V during hypoxia except in the presence of exogenous 5-HT. However, the apparent rescue of the hyperventilatory response by 5-HT may have reflected elevated baseline f_V of pCPA treated larvae; f_V in hypoxia or hypoxia with 5-HT was identical to the f_V of non-pCPA treated larvae during hypoxia.

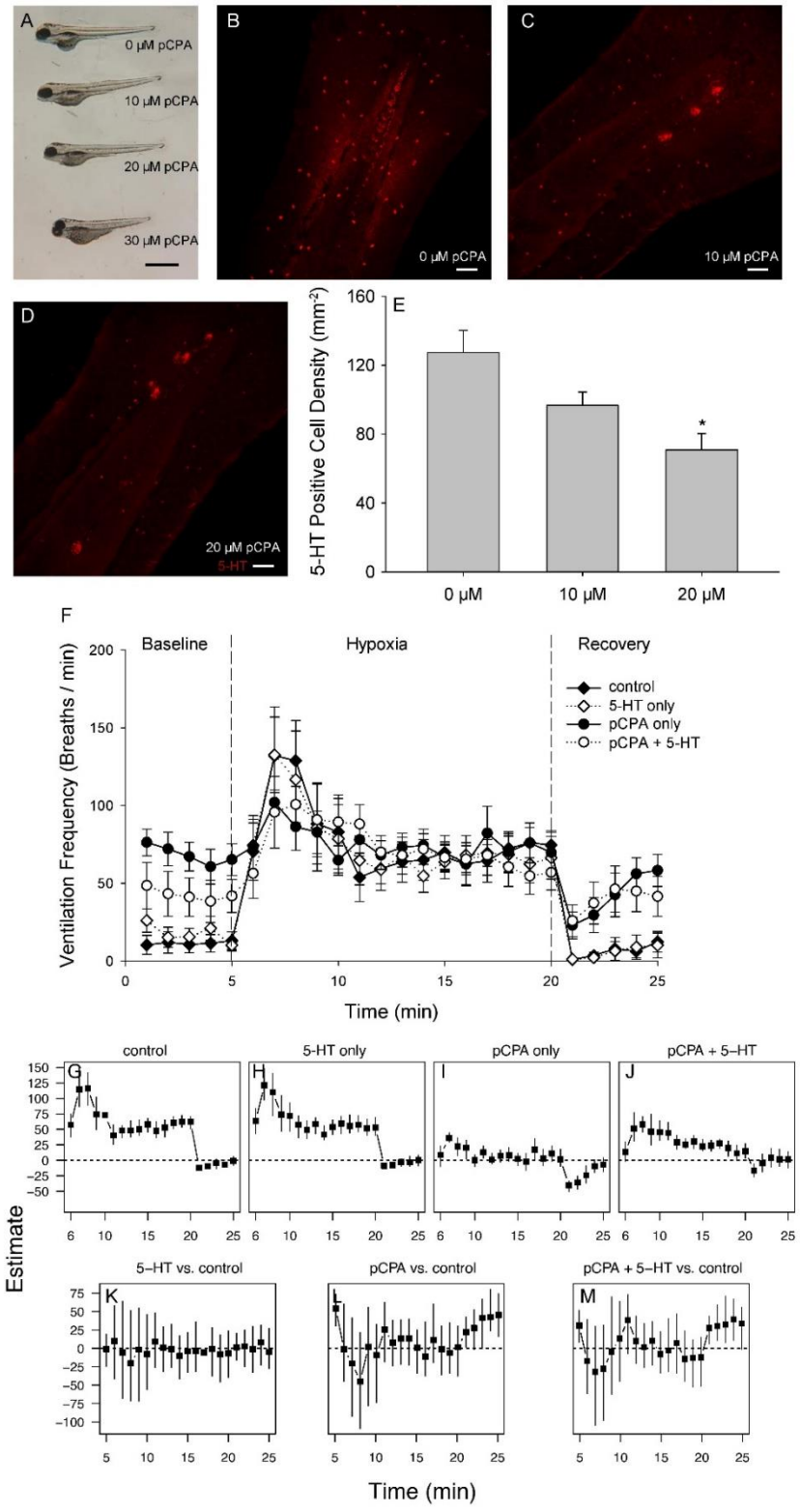
A
0 µM pCPA
10 µM pCPA
20 µM pCPA
30 µM pCPA
B
0 µM pCPA
C
10 µM pCPA
D
20 µM pCPA
5-HT
E
5-HT Positive Cell Density (mm-2)
0 µM
10 µM
20 µM
F
Baseline
Hypoxia
Recovery
control
5-HT only
pCPA only
pCPA + 5-HT
Ventilation Frequency (Breaths / min)
Time (min)
G
H
I
J
Estimate
5–HT vs. control
pCPA vs. control
pCPA + 5–HT vs. control
K
L
M
Time (min)

Fig. S3.5

CHAPTER 4. Merkel-like cells (MLCs) are putative O_2 chemoreceptors in larval zebrafish

Abstract

In adult fish, it is generally assumed that neuroepithelial cells (NECs) located on gill filaments function as peripheral chemoreceptors. However, some fish experiencing total gill denervation can still sense hypoxia, with this response abolished only after further denervation of the orobranchial cavity. These results suggest that not all O_2 chemoreceptors are confined to the gills but could also be located in the orobranchial cavity. One population of cells located within the orobranchial cavity that share similar characteristics to NECs are Merkel-like cells (MLCs). MLCs are neurosecretory, receive innervation from hypoxia-responsive cranial nerves IX and X and contain serotonin (5-HT)-filled synaptic vesicles, suggesting that they are involved in environmental sensing. In the current study, *in vivo* confocal imaging in concert with genetically encoded Ca^{2+} indicators was used to demonstrate that MLCs and peripheral sensory neurons (PSNs) with nerve endings impinging on MLCs exhibited increased Ca^{2+} events during acute hypoxia. Additionally, it was observed that peripheral sensory ganglia (PSGs) displayed an increase in mean $[Ca^{2+}]_i$ levels when exposed to hypoxia. In *ascl1a*$^{-/-}$ mutants that lack MLCs, the initial increase in ventilation frequency (f_V) during hypoxia was absent. Using nitroreductase-mediated ablation of PSNs and PSGs, it was shown that larvae with MLCs lacking innervation exhibited a heightened f_V in the later stages of hypoxia. Taken together, these data suggest that MLCs are responsive to hypoxia and thus are considered a novel class of O_2 chemoreceptors. It is proposed that their stimulation contributes to the initiation of hyperventilation during hypoxia, whereas PSNs/PSGs transmit an inhibitory signal to the central nervous system during the later phases of hypoxia to lower f_V to a steady level above normoxic baseline values.

4.1 Introduction

The aqueous environment is prone to O_2 fluctuations (Mandic and Regan, 2018). Thus, the ability of fish to sense changes in water O_2 tensions (PO_2) and to elicit appropriate responses to low environmental PO_2 levels (hypoxia) is crucial for their survival. Arguably, one of the most important physiological reflex response to hypoxia in fish is hyperventilation, termed the hypoxic ventilatory response (HVR). In mammals, the Type I cells of the carotid body serve as the peripheral O_2 chemoreceptor (De Castro, 1926; Duchen et al., 1988; Heymans and Heymans, 1927; Lopez-Barneo et al., 1988; Lopez-Lopez et al., 1989; Pietruschka, 1985; Pietruschka and Acker, 1985; Urena et al., 1989; von Euler et al., 1940). Although the molecular underpinnings of the O_2 sensitivity of the carotid body Type I cells are debated, there is general consensus that once hypoxia is sensed, K^+ flux thorough K^+ channels is reduced, leading to membrane depolarization and the opening of voltage-gated Ca^{2+} channels (Cummins et al., 2020; Kumar and Prabhakar, 2011; Lopez-Barneo et al., 2016; Lopez-Barneo et al., 1988; Peers et al., 2010; Prabhakar and Semenza, 2015). In turn, depolarization leads to an influx of Ca^{2+}, an increase in intracellular Ca^{2+} levels and Ca^{2+}-mediated neurotransmitter release, of which ATP and acetylcholine (ACh) are stimulatory and dopamine (DA) is inhibitory (Kumar and Prabhakar, 2011; Leonard et al., 2018; Nurse, 2010). These neurotransmitters activate cognate receptors on the afferent fibres of the glossopharyngeal nerve (cranial nerve IX) leading to signal propagation to the central respiratory center to elicit the appropriate reflex physiological responses (Cummins et al., 2020; Kumar and Prabhakar, 2011). In fish, the identity of the peripheral O_2 chemoreceptor and its signal transduction processes are less clear.

In fish, the peripheral O_2 chemoreceptors are believed to be neuroepithelial cells (NECs), first identified in rainbow trout (*Oncorhynchus mykiss*) by Dunel-Erb et al. (1982) by analogy to

the morphology of pulmonary NECs found in the respiratory tract of mammals. The NECs are located in highest numbers at the tip of gill filaments and are further characterized by the presence of dense-cored vesicles containing serotonin [5-HT, (Dunel-Erb et al., 1982)]. In rainbow trout, exposure to hypoxia results in the "degranulation" of NECs, suggesting the release of neurotransmitter (5-HT) onto afferent nerves (Dunel-Erb et al., 1982). Based on their morphology, location, innervation patterns and "degranulation" response to hypoxia, the NECs of trout were suggested to serve as peripheral O_2 chemoreceptors. In zebrafish (*Danio rerio*), gill filament NECs are innervated by both intrinsic and extrinsic nerve fibres (Jonz and Nurse, 2003).

Direct and convincing evidence that gill NECs are O_2 sensors (and thus may potentially act as peripheral O_2 chemoreceptors *in vivo*) was first provided using cells isolated from adult gill filaments and tested *in vitro* under primary cell culture conditions. With exposure to hypoxia, isolated gill NECs from zebrafish and channel catfish (*Ictalurus punctatus*) exhibited an inhibition of K^+ currents (Burleson et al., 2006; Jonz et al., 2004) leading to membrane depolarization (Jonz et al., 2004; Qin et al., 2010). Membrane depolarization during hypoxia also was reported for NECs isolated from adult goldfish (*Carassius auratus*) gill (Zachar and Jonz, 2012c). Though not specific to O_2 chemoreception, isolated gill NECs from zebrafish or rainbow trout displayed an increase of intracellular Ca^{2+} concentration ($[Ca^{2+}]_i$) when exposed to conditions of hypercapnia or high environmental ammonia (Abdallah et al., 2015a; Zhang et al., 2011), both of which are ventilatory stimulants in fish. Additionally, isolated gill NECs from goldfish responded to hypoxia with increased $[Ca^{2+}]_i$ and synaptic vesicle activity (Zachar et al., 2017), suggesting that NECs are neurosecretory. Thus, there is ample evidence that at least *in vitro*, gill NECs are responsive to hypoxia and therefore have the potential to serve as O_2 chemoreceptors. Although the NECs of the adult zebrafish gill exhibit characteristics expected of

functional O_2 chemoreceptors such as hypertrophy during exposure to hypoxia (Jonz et al., 2004), there is no direct evidence as yet that NECs act as chemoreceptors *in vivo* and a direct link between the activation of NECs and the downstream physiological responses to hypoxia has not been established. The lack of direct evidence stems, in part, from technical limitations and in particular, the difficulty of identifying gill NECs and measuring cellular activity within NECs such as membrane potential or $[Ca^{2+}]_i$ *in vivo*. Only recently has progress been made in identifying NECs *in vivo* with the use of green fluorescent protein (GFP) under the control of the vmat2 promoter (Pan et al., 2021).

In addition to gill NECs, it is possible that other cell types may function as peripheral chemoreceptors. In larval zebrafish, a behavioural response to hypoxia develops as early as 2 days post fertilization (dpf), yet gill NECs are not innervated until 7 dpf (Jonz and Nurse, 2005). Coccimiglio and Jonz (2012) proposed that serotonergic cells on the skin of larval zebrafish that resemble gill NECs, termed skin NECs, could play a role in initiating responses to hypoxia in the developing zebrafish because they respond morphologically to changes in environmental PO_2 and receive innervation between 26-28 h post fertilization (Coccimiglio and Jonz, 2012). However, unlike for the gill NECs, there are no data demonstrating direct O_2 sensitivity of the cutaneous NECs. There is also conflicting evidence regarding skin NECs being morphologically sensitive to changes in PO_2 – in larval mangrove rivulus (*Kryptolebias marmoratus*), skin NEC development is largely unaffected by environmental PO_2 levels (Cochrane et al., 2021). In support of an alternate site of peripheral O_2 chemoreception, a study using genetically encoded Ca^{2+} indicators showed that upon hypoxic stimulation, peripheral sensory ganglionic neurons (cranial nerves IX and X) from 5-6 dpf larval zebrafish exhibited an increase in their activity (Yeh et al., 2019). This finding is particularly interesting because cranial nerves IX and X appear

to initiate most cardiorespiratory responses to hypoxia including the HVR [reviewed by Milsom (2012)] and that rhythmic stimulation of the cranial nerve X ganglion can entrain the ventilation response (De Graaf and Roberts, 1991). These peripheral sensory neurons (PSNs) extend into the pharyngeal arch region and wrap around 5-HT positive cells (Yeh et al., 2019), which based on their position and morphology are Merkel-like cells (MLCs) previously described to be present at the base of the taste bud complex (Zachar and Jonz, 2012a). These MLCs receive innervation as early as 3 dpf and are also neurosecretory as indicated by the styryl dye, FM1-43 and the synaptic vesicle marker, SV2 (Zachar and Jonz, 2012a). Considering that PSNs express P2X3 receptors (Yeh et al., 2019) and that ATP is a well know neurotransmitter involved in taste (Finger and Kinnamon, 2021), it would suggest that MLCs might also signal through purinergic pathways. In adult zebrafish , MLCs are also located on the gill rakers (Zachar and Jonz, 2012a), the first point of contact for inspired water flowing over the gills. Overall, these characteristics implicate MLCs as potential O_2 chemoreceptors. In addition, some MLCs are located extra-branchially (Kapsimali et al., 2011), addressing the issue of the persistence of ventilatory responses to hypoxia in some species experiencing total gill denervation, which was attributed to the presence of putative extra-branchial receptors (Milsom, 2012).

Significant research has focused on identifying the neurotransmitter(s) involved in promoting the reflex HVR (Rahbar et al., 2016; Shakarchi et al., 2013). These studies used pharmalogical methods, i.e. treatment of fish with agonists/antagonists of various neurotransmitter receptors. Based on the results of these studies it would appear that in zebrafish 5-HT, ACh, ATP and adrenaline stimulate ventilation while DA is inhibitory (Pan and Perry, 2020). Although these neurotransmitters are potentially involved in the HVR, there is no evidence that they are present within NECs other than 5-HT (Porteus et al., 2012), and that any

of these putative neurotransmitters are actually secreted by NECs during hypoxia. An unavoidable limitation of the experimental design used in these previous studies is that the drugs added to the water not only activate receptors on the afferent nerve fibres of NECs, but also all accessible receptors in the entire fish including the NECs themselves and receptors within the CNS.

With this background, the goal of this study was to test the hypothesis that MLCs serve as O_2 chemoreceptors in larval zebrafish. To do so, transgenic zebrafish with genetically encoded Ca^{2+} indicators specifically expressed within MLCs and the PSNs were generated, allowing *in vivo* real time measurements of $[Ca^{2+}]_i$ of MLCs and the PSNs upon exposure to hypoxia. In addition, the HVR was assessed in larval zebrafish lacking MLCs or PSNs; MLCs were prevented from developing by creating an *ascl1a* knockout line (Kapsimali et al., 2011) and PSNs and peripheral sensory ganglia (PSGs) were ablated using the nitroreductase mediated tissue ablation method (Curado et al., 2008). To further examine the potential neurotransmitter(s) involved in the signal transduction process, we exposed larval zebrafish to various putative neurotransmitters under normoxic or hypoxic conditions and examined the changes in $[Ca^{2+}]_i$ of PSGs under these conditions.

4.2 Materials and Methods

4.2.1 Experimental Animals

Adult zebrafish, *Danio rerio* (F. Hamilton 1822), were housed in 10 l polycarbonate tanks in a recirculating aquatic system (Aquatic Habitats, Apopka, FL, USA). Fish were maintained at 28°C under a 14 h:10 h light:dark cycle in dechloraminated city of Ottawa tap

water and fed to satiation twice a day. Wild-type (WT) zebrafish were obtained from in-house stock at the University of Ottawa aquatic care facility. The *Tg(tph1b:mCherry)* line was obtained courtesy of Dr. Marika Kapsimali of L'Institut de Biologie de l'École Normale Supérieure (IBENS), France (Soulika et al., 2016). The *Tg(tph1b:jRCaMP1a), Tg(p2rx3b:eGFP), Tg(p2rx3b:GCaMP6s), Tg(p2rx3b:NTR-mCherry)* transgenic lines and *ascl1a*$^{-/-}$ mutant line were generated in house as described below. The *Tg(tph1b:jRCaMP1a, p2rx3b:GCaMP6s)* line was generated by cross breeding the *Tg(tph1b:jRCaMP1a)* and *Tg(p2rx3b:GCaMP6s)* fish. Embryos from all genotypes were obtained using standard protocols (Westerfield, 2000). Embryos were collected and reared in 50 ml Petri dishes containing E3 medium (in mM: 5 NaCl, 0.17 KCl, 0.33 $MgSO_4$, 0.33 $CaCl_2$, and 0.1% methylene blue) in an incubator maintained at 28.5°C. Water was changed daily in the Petri dishes and every alternate day in the static tanks. All procedures for animal use and experimentation were carried out in compliance with the University of Ottawa Animal Care and Veterinary Service guidelines under protocols BL-226 and BL-1700 and adhered to the recommendations for animal use provided by the Canadian Council for Animal Care.

4.2.2 Generation of transgenic zebrafish

Promoter and reporter gene sequences were PCR amplified using Q5 high-fidelity DNA polymerase (NEB, Cat#: M0491S) and cloned into a Tol2 expression vector containing the *myl7:egfp* heart-specific transgenesis marker in the reverse orientation using restriction cloning. All restriction enzymes used were purchased from New England Biolabs. The promoter regions were amplified from WT zebrafish larval DNA extracted using PureLink™ genomic DNA mini kit (Invitrogen, Cat#: K182002) following the manual's procedures. Reporter gene sequences were amplified from plasmids courtesy of Misha Ahrens (Addgene plasmid # 59531 ;

http://n2t.net/addgene:59531 ; RRID:Addgene_59531), Douglas Kim & GENIE Project (Addgene plasmid # 100848 ; http://n2t.net/addgene:100848 ; RRID:Addgene_100848) and Luke Lavis (Addgene plasmid # 113760 ; http://n2t.net/addgene:113760 ; RRID:Addgene_113760). Primers for amplifying the promoter and reporter gene sequences are provided in Table S4.1. Transposase mRNA was synthesized from linearized transposase plasmid using mMESSAGE mMACHINE SP6 kit (Invitrogen, Cat#: AM1340). Both the Tol2 expression vector and the transposase plasmid were courtesy of Dr. Marc Ekker (University of Ottawa). To generate founder transgenic fish, one-cell-stage WT embryos were injected with ~1 nl of 100 ng/µl synthesized plasmid and 200 ng/µl transposase mRNA, and screened for cardiac green fluorescent protein (GFP) expression at 2 dpf. Founders with cardiac GFP expression were raised to adults and crossed with WTs to screen for embryos expressing the corresponding reporter gene to establish the line.

4.2.3 Generation of *ascl1a*$^{-/-}$ mutant zebrafish

Expression of *ascl1a* was knocked out using CRISPR/Cas9. The sequence of the sgRNA was designed using CHOPCHOP (https://chopchop.cbu.uib.no/) and was specific to the starting region of the only exon of *ascl1a* (GAGGCGAAAAAGCAAGCAGG). The sgRNA was synthesized using a cloning-free method described previously (Talbot and Amacher, 2014). Cas9 mRNA was synthesized from zebrafish codon-optimized Cas9 (Jao et al., 2013) using mMESSAGE mMACHINE SP6 kit (Invitrogen, Cat#: AM1340). One-cell-stage WT embryos were injected with ~1 nl of injection solution containing 150 pg Cas9 mRNA, 50 pg of sgRNA, and 0.01% phenol red suspended in Danieau buffer (in mM: 58 NaCl, 0.7 KCl, 0.4 $MgSO_4$, 0.6 $Ca(NO_3)_2$, and 5.0 Hepes; pH 7.6). Embryos were reared to sexual maturity (60-90 dpf) and mutants in this adult F0 population were identified through DNA extraction of fin clips and

Sanger Sequencing (Genome Quebec, McGill University, Montreal, Canada). The final mutant line that was established carried a 7-bp deletion 49 bps after the start codon in the *ascl1a* gene, resulting in a premature stop codon. The resulting protein was 9.5 kDa rather than the normal 22 kDa.

4.2.4 Immunohistochemistry

Zebrafish larvae were fixed overnight at 4 °C in 4% paraformaldehyde (PFA) prepared in phosphate buffered saline (PBS). The following day, larvae were rinsed 5X in PBS containing 0.1% tween-20 (PBST). For samples that required sectioning, the larvae were transferred to a 30% sucrose solution in PBS for 12 – 18 h at 4 °C, embedded in OCT embedding matrix (Fisher Scientific, Cat#: 23-730-571) on powdered dry ice and sectioned to 30 µm thickness using a Leica CM3050 S cryostat (Leica Biosystems). Specimens (zebrafish larvae or sections) were then placed in a blocking solution containing 0.8% Triton-X 100, 3% bovine serum albumin (BSA), and 2% normal goat serum (Sigma Aldrich Inc., Cat#: NS02L-1ML) dissolved in PBST for 1 h at room temperature or overnight at 4 °C. Primary antibodies (anti-5-HT, anti-calretinin, anti-zn-12, anti-SV2, anti-GFP or anti-mCherry) were added in blocking solution and specimens were placed on a shaker overnight at 4°C in darkness. After 5 x 5 min washes in PBST, secondary antibodies were added at a dilution of 1:500 in 0.8% Triton-X 100 dissolved in PBST. A complete list of primary and secondary antibodies used is provided in Table S4.2. Specimens were then incubated with the secondary antibody in the dark at room temperature for 1 h or at 4 °C overnight, washed 5 X 5 min in PBST and mounted using Vectasheild^{TM} antifade mounting medium (Vector Laboratories, Cat#: H-1000-10) in a concave depression glass slide for imaging. Specimens were imaged using an A1R MP^{+} confocal microscope (Nikon Instruments Inc. USA) with 25X/1.10 W, 20X/0.75 MImm or 10X/0.50 W objectives.

4.2.5 Quantification of MLCs and NECs through development

To quantify morphological changes of MLCs and NECs through development under normoxic and hypoxic conditions, *Tg(tph1b:mCherry)* larvae were raised under normoxic (153 mmHg) or hypoxic (45 mmHg) flow through conditions beginning from 10 h post fertilization until 4, 7 or 14 dpf. Larvae raised to 7 and 14 dpf were fed daily. At the end of the exposure, larvae were euthanized on ice and stained with 5-HT and mCherry antibodies as described above and the pharyngeal arch region was imaged with the ventral region facing towards the objective. Cells positive for both 5-HT and mCherry were identified as MLCs while cells positive only for 5-HT were identified as NECs. Analysis of MLC and NEC number and size was carried out using ImageJ (https://imagej.nih.gov/ij/). Briefly, the image was first converted to 8 bits and threshold set just above background. The "analyze particles" plugin was used to count cells greater than 20 μm^2 in area with a circularity of at least 0.3. The number of cells and the average area were extracted from the analysis. The cells were then identified as MLCs or NECs, and the total number and cell size of each cell type were tabulated. During the analysis, images were relabelled and analyzed "blindly" without knowing the treatments of the fish in the image.

4.2.6 *In vivo* Ca^{2+} imaging

All experiments were performed on 4 dpf larvae in system water. Imaging of larvae was performed with an A1R MP+ confocal microscope (Nikon Instruments Inc. USA) with 20X water-immersion objective (0.75 NA, time-lapse imaging). The microscope was further equipped with a custom-made water perfusion system enabling switching of perfusion solutions into the imaging chamber. The imaging chamber was made of glass with an O_2 sensor spot attached (Loligo Systems, Denmark) to allow for O_2 measurement within the chamber using the Witrox 4 O_2 meter and the AutoResp software (Loligo Systems, Denmark). An individual larva was

mounted with its side facing upwards in 1.5% low melting-point agarose (BioShop, Cat#: AGA101.25) onto a coverslip. The coverslip was then placed on top of the imaging chamber with the larva facing downwards into the chamber (See Fig. S4.1). This setup allowed for the chamber to be sealed once water flow was started and the larva to be imaged through the coverslip. To image the sensor expression pattern, images were acquired with a field of view of 512 × 512 or 512 × 256 pixels with spatial resolution of 322 × 322 or 322 × 161 µm (x × y) at a rate of 30 frames per second.

4.2.6.1 Series I. NaCN exposure

Tg(tph1b:jRCaMP1a) larvae were used to examine MLCs response to 100 µM NaCN exposure and resultant chemical hypoxia (Hamel, 2011). Each larva was exposed to 5 min of system water (baseline) followed by 10 min of either system water or 100 µM NaCN (Sigma-Aldrich, Cat#: 380970) dissolved in system water. For larvae exposed to NaCN, MLCs were classified as either responsive or non-responsive based on whether Ca^{2+} event (a single spike of $[Ca^{2+}]_i$) frequency under NaCN exposure exceeded that in the 5 min baseline conditions. As long as a single time point during NaCN exposure had a higher Ca^{2+} event that that of baseline, it was deemed a responsive cell.

4.2.6.2 Series II. Hypoxia exposure

Tg(tph1b:jRCaMP1a, p2rx3b:GCaMP6s) larvae were used to examine the response of MLCs and PSN/PSGs to hypoxia exposure (30 mmHg). Each larva was first exposed to 5 min of normoxic system water (baseline). After baseline exposure, the imaging chamber was perfused with hypoxic water, resulting in a decrease of PO_2 from 153 to 30 mmHg over the course of approximately 5 min. The fish were then held in hypoxic water for an additional 10 min thus

yielding an overall period of 15 min for hypoxia exposure (5 min of rapid decline of PO_2 followed by 10 min of stable hypoxia). After the hypoxia exposure, normoxic water again was perfused into the imaging chamber (recovery), resulting in an increase of PO_2 to 153 mmHg over the course of approximately 5 min. The larva was then held under normoxic conditions for an additional 5 min resulting in a total of 10 min for the recovery phase. In this set of experiments, Ca^{2+} responses were recorded for individual MLCs, individual PSN-endings innervating MLCs, and all cells within the PSGs when viewed in totality (i.e. the entire PSG was viewed as a region of interest (ROI) rather than individual cells within the PSGs) due to technical challenges of identifying individual cells within the PSGs when co-imaged with MLCs.

4.2.6.3 Series III. Neurotransmitter exposure

Tg(p2rx3b:GCaMP6s) larvae were used to examine the response of individual cells within the PSG to either hypoxia or neurotransmitter exposure. Two sets of experiments were conducted. In the first set, each larva was exposed to 5 min of normoxic system water (baseline) followed by 15 min of hypoxia exposure as described above or 15 min of neurotransmitter exposure, and lastly returned to normoxic system water for 10 min (recovery). The putative neurotransmitters used were 5-HT (50 µM serotonin hydrochloride, Sigma-Aldrich, Cat#: H9523), ACh (50 µM acetylcholine chloride, Sigma-Aldrich, Cat#: A6625), ATP (100 µM adenosine 5′-triphosphate disodium salt hydrate, Sigma-Aldrich, Cat#: A1852), adrenaline [100 µM (−)-epinephrine (+)-bitartrate salt, Sigma-Aldrich, Cat#: E4375] and DA (50 µM dopamine hydrochloride, Sigma-Aldrich, Cat#: H8502). Each larva was exposed only to a single neurotransmitter. Concentrations were chosen based on previous studies showing that ventilation in larval zebrafish was altered when exposed to these concentrations of putative neurotransmitters (Pan and Perry, 2020; Rahbar et al., 2016; Shakarchi et al., 2013). In the

second set of experiments, each larva was first exposed to 5 min of normoxic system water followed by 7.5 min of hypoxia exposure. The larva was then exposed to an additional 7.5 min of hypoxia with the same putative neurotransmitters as in the first set of experiments added to the hypoxic water. Each larva was exposed simultaneously to only a single neurotransmitter and hypoxia. Finally, the larva was retuned to normoxic system water for 10 min.

4.2.6.4 Image data analysis

Image data were motion corrected before exporting raw traces for ROIs using CaImAn under the Mesmerize platform (Giovannucci et al., 2019; Kolar et al., 2021). Baseline corrections for raw traces were performed in R using the baseline package (Liland et al., 2010). Ca^{2+} events were then detected using the peakPick package, and Ca^{2+} event frequency and mean $[Ca^{2+}]_i$ were calculated using a custom-written R script. A representative R-script is provided in the supplementary material. For series II hypoxia exposure, synchronized peaks were defined as Ca^{2+} peaks that occurred within 1 sec of each other in MLCs, PSN endings and PSGs.

4.2.7 Ventilation experiments

The HVR was assessed in larvae with ablated MLCs or PSNs. Ablation of MLCs was achieved in *ascl1a*$^{-/-}$ mutants as confirmed by immunohistochemistry as described above. Peripheral sensory neuron ablation was achieved by exposing *Tg(p2rx3b:NTR-mCherry)* larvae to 5 mM metronidazole (mtz; Sigma-Aldrich, Cat#: M1547) in 0.2% DMSO (Sigma-Aldrich, Cat#: D8418) beginning from 2 dpf. Confirmation of ablation was achieved using immunohistochemistry as described above in 4 dpf larvae. The HVR was assessed by monitoring f_V as described previously (Pan et al., 2019). Briefly, after light anesthesia (0.05 mg ml^{-1} Tris-buffered MS-222 (ethyl-3-aminobenzoate methanesulfonate salt, Sigma Aldrich Cat#: E10521),

an individual larva was placed in a microcapillary tube with an inner diameter of 1 mm. Zebrafish water containing MS-222 at room temperature was delivered to the microcapillary tube by gravity at a rate of 1.6 – 1.8 ml min^{-1}. Previous studies demonstrated that at the anesthesia concentration used, the response of larvae to hypoxia is not significantly reduced (Coe et al., 2017; Jonz and Nurse, 2005). Each larva was allowed to adjust to the chamber for 10 min in normoxic water (PO_2 = 153 mmHg) prior to the start of the trial. During each trial, f_V was recorded for 5 min under normoxic conditions (baseline), followed by 15 min of hypoxia (treatment) and an additional 5 min after returning to normoxia (recovery) using an iPhone mounted onto a dissecting microscope [stereo trinocular microscope (AmScope)]. Breathing frequency was determined for each minute by counting either buccal or opercular movements depending on the orientation of the fish in the chamber and the visibility of the mouth and/or operculum.

4.2.8 Statistical analysis

Calcium event frequency in MLCs and the PSNs, and ventilation frequency in zebrafish larvae were analyzed using Markov chain Monte Carlo sampler for multivariate generalized linear models using MCMCglmm package (Hadfield, 2010) in R (https://www.R-project.org/). To compare Ca^{2+} event frequencies and f_V between different treatments, all Ca^{2+} event frequency and f_V measurements were fitted as dependent variables and the treatment group that the data are to be compared against were fitted as a fixed effect. To compare f_V between normoxic baseline and the hypoxic treatment period, f_V measurements in hypoxia were fitted as dependent variables and the last minute of the 5 min normoxia treatment was fitted as a fixed effect. The model included an unstructured (co)variance matrix at the residual level, using weakly informative inverse-Wishart priors with the scale parameter defined as a diagonal matrix containing values of one and

distribution parameters set to 0.001 for the degrees of freedom. Posterior distributions were estimated from 13,000 MCMC iterations sampled at 10 iteration intervals following an initial burn-in period of 3000 iterations. This yielded effective samples sizes of 1000 for the parameters of interest. We inspected the 95% highest posterior density (HPD) associated with each fixed effect estimate to check whether they overlapped with zero. A 95% HPD interval contains most of the posterior distribution and is analogous to a confidence interval (CI) in the frequentist approach; a 95% HPD that overlaps 0 indicates that the effect does not differ significantly from zero. Thus, for each estimate associated with the fixed effect we determined whether the 95% HPDs included or excluded zero.

All other statistical analyses were carried out in Sigmaplot (Systat Software). To compare group means against zero, a one sample t-test was conducted. To compare means of two groups, a Student's t-test was conducted. Single factor comparisons among multiple means were conducted using a one-way ANOVA, while two-factor comparisons among multiple means were conducted using a two-way ANOVA. When data did not pass a normality test (Shapiro–Wilk test), data were either log transformed or the Kruskal-Wallis ANOVA on ranks was used. Holm–Šidák *post hoc* test was used if a significant interaction was detected. Significance was set at $P<0.05$.

4.3 Results

4.3.1 Characterization of MLCs and PSNs/PSGs by immunohistochemistry

Merkel-like cells were identified in 4 dpf *Tg(tph1b:mCherry)* transgenic larvae as cells expressing tryptophan hydroxylase 1b (TPH1b) and 5-HT; these cells were located at the base of the taste bud cells positive for calretinin (Fig. 4.1A) forming the taste bud complex. Further

characterization of MLCs in 4 dpf larvae revealed that they expressed synaptic vesicle protein 2 [SV2, (Fig. 4.1B)] and were associated with zn-12 positive nerve fibres (Fig. 4.1C & D, Fig. 4.2C). The pattern of MLC staining and their innervation were different from the pharyngeal arch NECs, which were positive for only 5-HT and did not exhibit close association with zn-12 positive nerve fibres (Fig. 4.1C & E, Fig. 4.2D). Characterization of MLC innervation patterns at 3, 7, 14 and 21 dpf revealed that MLCs receive innervation from zn-12 positive nerve fibres as early as 3 dpf (Fig. 4.1F-I).

Characterization of 4 dpf *Tg(p2rx3b:eGFP)* transgenic larvae revealed that P2RX3b is expressed within the PSNs and PSGs, specifically the cranial nerves V, VII, IX and X (Fig. 4.2A). Nerves positive for zn-12 emanating from cranial ganglia IX and X projected into the pharyngeal arch region and associated with MLCs on one end and the central nervous system (CNS) on the other end (Fig. 4.2).

4.3.2 Morphological changes of MLCs and NECs during hypoxia

At all developmental stages examined, MLCs were more abundant than NECs and were larger in size (Fig. 4.3). MLC numbers significantly decreased after 4 days of hypoxia acclimation but were unchanged after 7 and 14 days of exposure (Fig. 4.3). The number of NECs was unaltered after 4 days but was increased after 7 and 14 days of hypoxia acclimation (Fig. 4.3B). The size of both MLCs and NECs was increased during hypoxia exposure (Fig. 4.3C).

4.3.3 *In vivo* calcium imaging of MLCs, PSNs and PSGs

To test the hypothesis that MLCs are O_2 chemoreceptors, we first examined Ca^{2+} signalling in MLCs when exposed to 100 µM NaCN, a reagent that induces chemical hypoxia (Fig. 4.4). MLCs from which Ca^{2+} measurements were taken were divided into two groups. One

group termed non-responsive cells were MLCs that did not increase Ca^{2+} event frequency compared to the baseline at any time during NaCN exposure. A second group termed responsive cells were MLCs that increased Ca^{2+} event frequency in at least one of the NaCN exposure time points. Ca^{2+} event frequency in non-responsive cells was identical to control cells that were not exposed to NaCN, but responsive cells significantly increased Ca^{2+} event frequency (Fig. 4.4C, Fig. S4.2). Of all the cells measured from 8 larvae, 52 were responsive while 26 were non-responsive. Thus, when exposed to NaCN, 66% of MLCs increased Ca^{2+} event frequency.

Calcium event frequencies of individual MLCs, PSN-endings, and the whole PSGs were examined when exposed to hypoxia (Fig. 4.5). Both MLCs and nerve-endings exhibited a significant increase in Ca^{2+} event frequencies as PO_2 levels declined from 60 to 30 mmHg (Fig. 4.5C & D). Of the 40 MLCs examined, 38 of them had higher Ca^{2+} event frequencies during this PO_2 decline phase compared to the normoxic baseline. A significant difference was not observed when examining the PSGs as a whole, and this could be due to the dilution of signals by cells that did not respond. When examining the Ca^{2+} events within the PSGs, the signal amplitude was smaller compared to that in the MLCs or PSN-endings presumably because only a sub-population of cells within the PSGs (with projections innervating MLCs) responded in synchrony with the MLCs they innervate. Thus, at a specific time point, only a small population of cells within the PSGs might be responding and their signals would be diluted by the other cells that are not responding. However, all three locations examined displayed higher maximum Ca^{2+} event frequencies during the hypoxia exposure compared to the normoxia baseline (Fig. 4.5C-E). Even though the PSG did not increase Ca^{2+} event frequency at a specific time point, mean $[Ca^{2+}]_i$ when examining all cells within the PSG ROI was elevated during the hypoxia exposure (Fig. 4.5F). To assess whether there was synchrony in Ca^{2+} events between MLCs, PSNs and PSGs,

the timing of the peak responses was compared at the three measurement sites. There was a ~200 ms delay in the Ca^{2+} peaks of PSGs compared to the peaks of MLCs; this time difference between the Ca^{2+} peaks of PSGs and MLCs was significantly greater than zero (p=0.001; one sample t-test).

4.3.4 The HVR in zebrafish experiencing MLC or PSN/PSG ablation

Ventilation experiments were performed on 4 dpf *ascl1a* knockout mutants that lacked MLCs, as well as skin NECs (Fig. 4.6). When exposed to hypoxia, *ascl1a*$^{+/+}$, *ascl1a*$^{+/-}$, and *ascl1a*$^{-/-}$ all exhibited an increase in f_V (Fig. 4.6C, Fig. S4.4A-C). However, in *ascl1a*$^{+/+}$and *ascl1a*$^{+/-}$ larvae that retained MLCs, the ventilatory response was multiphasic, with an initial large increase of f_V during the first 5 min of hypoxia that gradually declined to a stable level but remaining higher than in normoxic control fish (Fig. 4.6C). In the *ascl1a*$^{-/-}$ mutants that lacked MLCs, the initial large increase in f_V was abolished, as indicated by the significantly lower f_V compared to *ascl1a*$^{+/+}$and *ascl1a*$^{+/-}$ during the initial 5 min of hypoxia (Fig. 4.6C, Fig. S4.4D & E).

Ventilation experiments were also performed on 4 dpf larvae that lacked PSNs/PSGs (Fig. 4.7). Ablation of PSNs/PSGs was achieved by exposing *Tg(p2rx3b:NTR-mCherry)* larvae to mtz. To rule out the potential effects of mtz on ventilation, WT larvae were treated with mtz; these fish did not show a difference in f_V when compared to *Tg(p2rx3b:NTR-mCherry)* larvae that did not receive the mtz treatment (Fig. 4.7E, Fig. S4.5A & B). All larvae exposed to hypoxia showed a multiphasic response and larvae lacking PSNs/PSGs displayed a significantly higher f_V compared to the controls regardless of the water PO_2 (Fig. 4.7E, Fig. S4.5C). Because of the upward shift in baseline f_V in the ablated fish, it was important to compare the absolute changes

in f_V during hypoxia in larvae lacking PSNs/PSGs with control fish. Thus, the maximum Δf_V and the Δf_V during the final 5 min of hypoxia (representing the stabilized f_V during hypoxia) were compared between larvae with or without PSNs/PSGs. No difference between maximum Δf_V was observed, but larvae lacking PSNs/PSGs exhibited a significantly higher Δf_V in the final 5 min of hypoxia (Fig. 4.7F).

4.3.5 *In vivo* Ca^{2+} imaging of PSGs exposed to putative neurotransmitters

When exposed to hypoxia, Ca^{2+} event frequency in individual cells of the PSG at two of the time points in hypoxia was higher than that of the control cells, but dropped below control cells during the recovery phase (Fig. 4.8A, Fig. S4.6A). Similarly, mean $[Ca^{2+}]_i$ during hypoxia increased above baseline and was significantly higher than mean $[Ca^{2+}]_i$ in control cells, but returned to the same level as the control cells during the recovery phase, though slightly lower than baseline levels (Fig. 4.8G). During sustained normoxia, 5-HT, ACh and ATP did not affect either Ca^{2+} event frequency or mean $[Ca^{2+}]_i$ (Fig. 4.8B-D & H-J, Fig. S4.6B-D). However, the addition of adrenaline increased Ca^{2+} event frequency initially but the effect was not sustained (Fig 8E). Interestingly, after adrenaline was removed (recovery), an elevated Ca^{2+} event frequency again was observed (Fig. 4.8E, Fig. S4.6E). Conversely, DA supressed Ca^{2+} event frequency but the effect again was not sustained throughout the exposure (Fig. 4.8F, Fig. S4.6F). Mean $[Ca^{2+}]_i$ was unaffected by AD or DA exposure, alone (Fig. 4.8K & L). During co-exposure to hypoxia and putative neurotransmitters, ACh and ATP again did affect either Ca^{2+} event frequency or mean $[Ca^{2+}]_i$ (Fig. 4.9C-D & G-H, Fig. S4.7C-D). On the other hand, 5-HT and AD suppressed the increase of Ca^{2+} event frequency during hypoxia (Fig. 4.9A & D, Fig. S4.7 A & D), and AD also suppressed the increase of mean $[Ca^{2+}]_i$ (Fig. 4.9I). Interestingly, an elevated Ca^{2+} event frequency was observed after co-exposure of hypoxia and DA, once the exposures

were terminated (Fig. 4.9E, Fig. S4.7E). Representative raw traces from these two sets of experiments are shown in Fig. S4.8 & Fig. S4.9.

4.4 Tables and Figures

Figure 4.1. Immunohistochemical -characterization of Merkel-like cells (MLCs) in larval zebrafish. (A) Co-localization of TPH1b (red), 5-HT (green) and calretinin (magenta) in a *Tg(tph1b:mCherry)* larva at 4 days post fertilization (dpf). Image shows a sagittal section of the larva's head with the anterior pointing towards the left (same orientation for all images below). Inserts show enlarged images of the boxed regions. Arrowheads point to calretinin positive taste bud cells while arrows indicate MLCs positive for both 5-HT and TPH1b. Endogenous mCherry expression in the heart is the result of an insertion of a heart specific screening marker in the transgenic line. (B) Co-localization of TPH1b (red), 5-HT (green) and synaptic vesicle protein [SV2, (magenta)] in a *Tg(tph1b:mCherry)* larva at 4 dpf. Inserts show enlarged images of the boxed regions. The arrow points to a MLC that is positive for TPH1b, 5-HT and SV2. The arrowhead indicates a neuroepithelial cell (NEC) that is positive for 5-HT and SV2 but not TPH1b. (C) Co-localization of TPH1b (red), 5-HT (green) and zn-12 (magenta) in a *Tg(tph1b:mCherry)* larva at 4 dpf. Boxed areas show regions of MLCs that are positive for both TPH1b and 5-HT (D) and NECs that are positive only for 5-HT (E). (F-I) Co-localization of TPH1b (red), 5-HT (green) and zn-12 (magenta) in 3 (F), 7 (G), 14 (H), and 21 (I) dpf *Tg(tph1b:mCherry)* larvae. Inserts show enlarged images of the boxed regions.

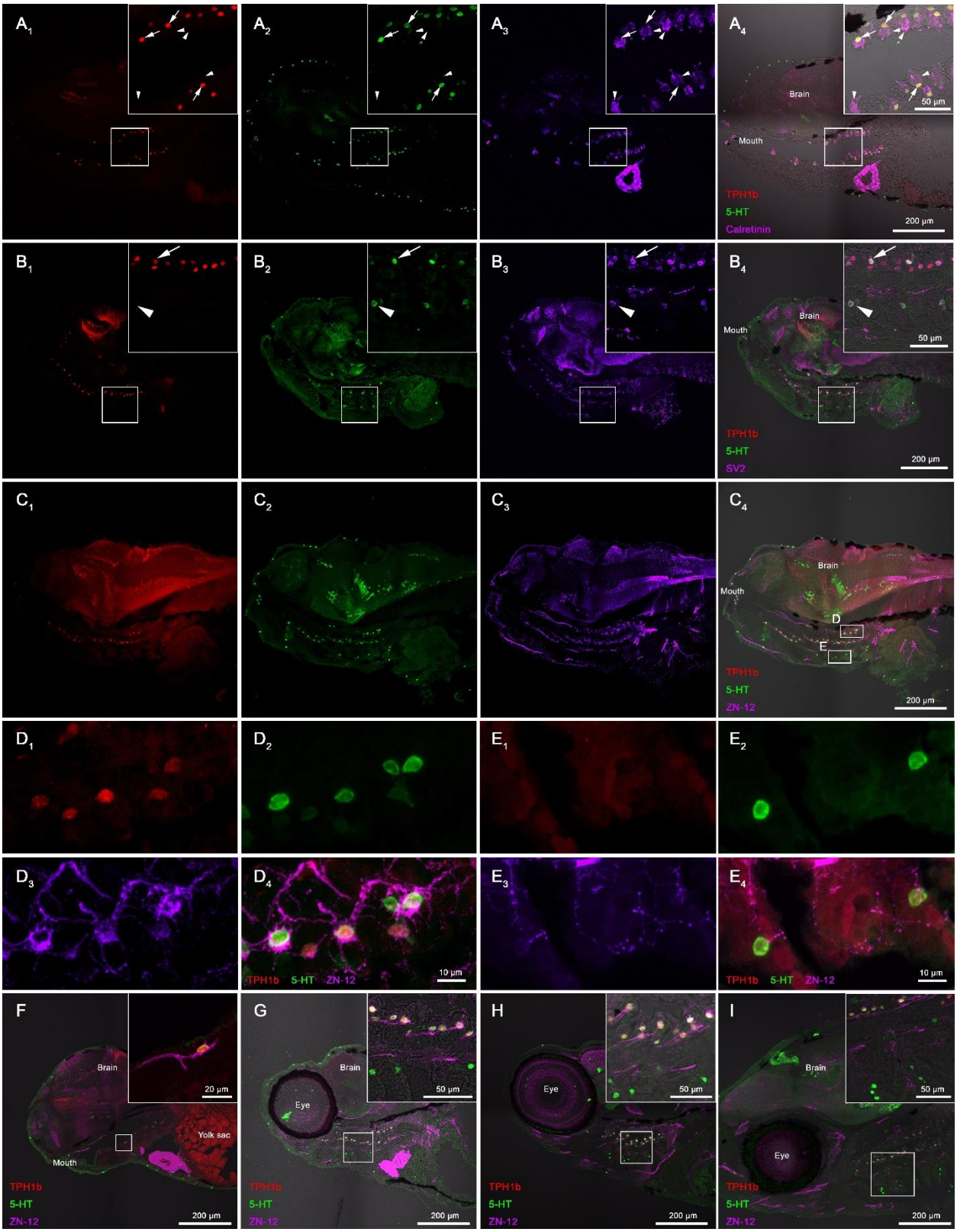
A1
A2
A3
A4
Brain
Mouth
50 μm
TPH1b
5-HT
Calretinin
200 μm
B1
B2
B3
B4
Brain
Mouth
50 μm
TPH1b
5-HT
SV2
200 μm
C1
C2
C3
C4
Brain
Mouth
D
E
TPH1b
5-HT
ZN-12
200 μm
D1
D2
E1
E2
D3
D4
TPH1b 5-HT ZN-12
10 μm
E3
E4
TPH1b 5-HT ZN-12
10 μm
F
Brain
20 μm
Yolk sac
Mouth
TPH1b
5-HT
ZN-12
200 μm
G
Brain
50 μm
Eye
TPH1b
5-HT
ZN-12
200 μm
H
Eye
50 μm
TPH1b
5-HT
ZN-12
200 μm
I
Brain
50 μm
Eye
TPH1b
5-HT
ZN-12
200 μm

Fig. 4.1

Figure 4.2. Immunohistochemical characterization of the peripheral sensory neurons (PSNs) and peripheral sensory ganglia (PSGs) in larval zebrafish at 4 days post fertilization (dpf). (A) Lateral view of a *Tg(p2rx3b:eGFP, tph1b:mCherry)* transgenic larva with the V/VII, IX, and X PSG expressing GFP and Merkel-like cells (MLCs) expressing mCherry. The arrow indicates a nerve bundle from the PSG projecting into the brain region traced out with white dashed lines. Arrowheads point to nerve bundles projecting into the pharyngeal arch region and associating with MLCs. (B-C) Co-localization of p2rx3b (red), 5-HT (green) and zn-12 (blue) in the pharyngeal arch region of a *Tg(p2rx3b:mCherry)* transgenic larva. Arrowheads point to 5-HT positive MLCs that are associated with nerve bundles positive for both p2rx3b and zn-12, while arrows indicate 5-HT positive NECs that are not associated with nerve bundles. Identification of MLCs and NECs were based on the position of the different cell types. MLCs were located on the pharyngeal arch while NECs were positioned at the tip of the gill arch.

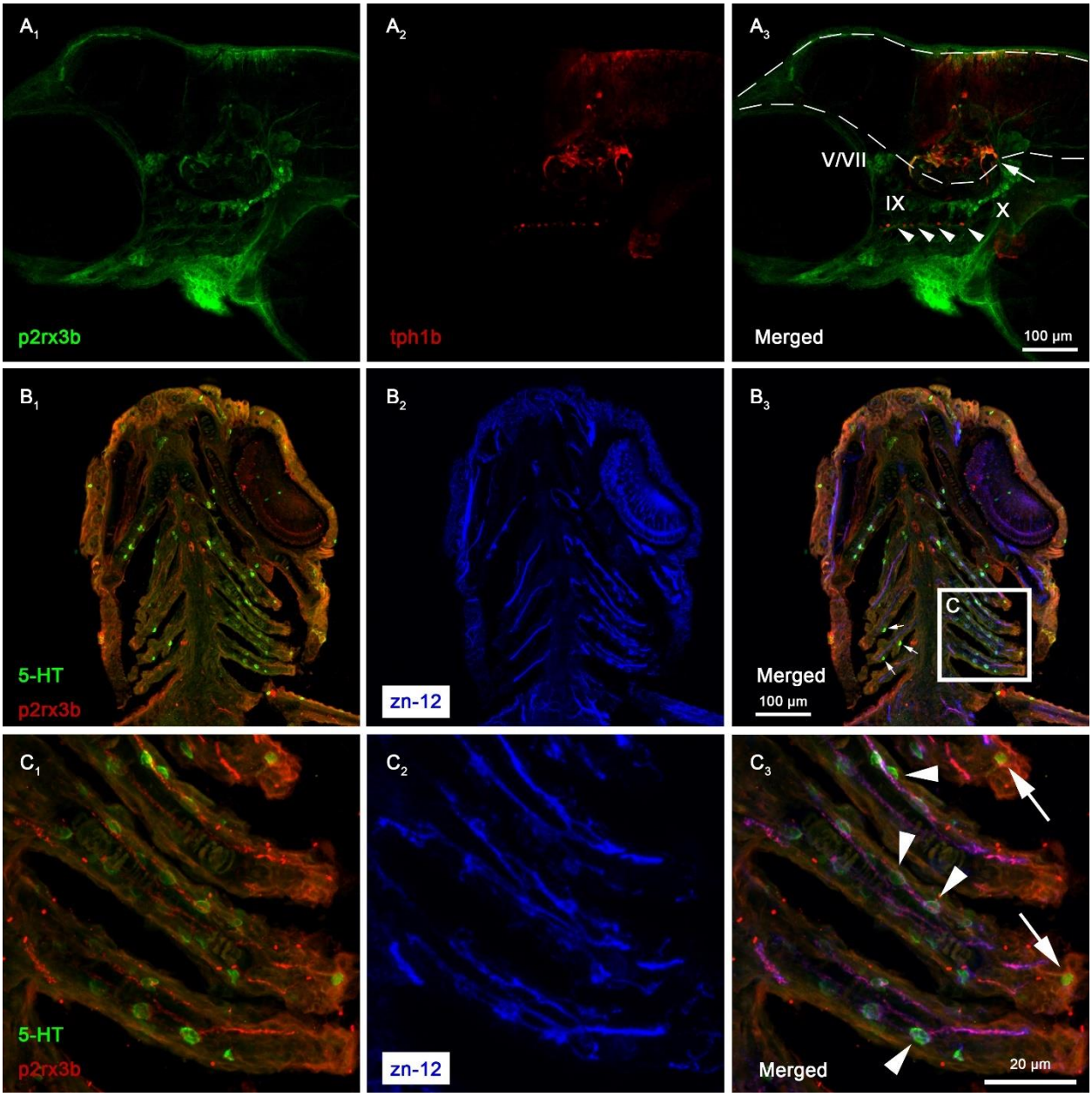
A1
p2rx3b
A2
tph1b
A3
V/VII
IX
X
Merged
100 µm
B1
5-HT
p2rx3b
B2
zn-12
B3
C
Merged
100 µm
C1
5-HT
p2rx3b
C2
zn-12
C3
Merged
20 µm

Fig. 4.2

Figure 4.3. Morphological characterization of Merkel-like cells (MLCs) and neuroepithelial cells (NECs) during acclimation to hypoxia. (A) Representative image of a *Tg(tph1b:mCherry)* larva at 7 days post fertilization (dpf) stained for TPH1b (mCherry) in red and 5-HT in green. Arrows point to MLCs that are positive for both TPH1b and 5-HT and arrowheads indicate NECs that are positive only for 5-HT. (B-C) MLC and NEC number (B) and size (C) in the pharyngeal arch region of *Tg(tph1b:mCherry)* larvae at 4, 7 and 14 dpf during normoxia or acclimation to hypoxia (45 mmHg) beginning at 10 h post fertilization. Data are presented as means ± s.e.m. Statistical analysis was conducted using two-way ANOVA (Holm–Šidák post-hoc multiple comparison test at $P < 0.05$). Asterisks (*) represent significance between normoxia and hypoxia treatment for MLCs, while daggers (†) represent significance between normoxia and hypoxia treatment for NECs. Within the same normoxia or hypoxia acclimation treatment, different upper-case letters indicate significances between the different developmental time points in the normoxia acclimation group, while different lower-case letters indicate significant differences between the different developmental time points in the hypoxia acclimation group.

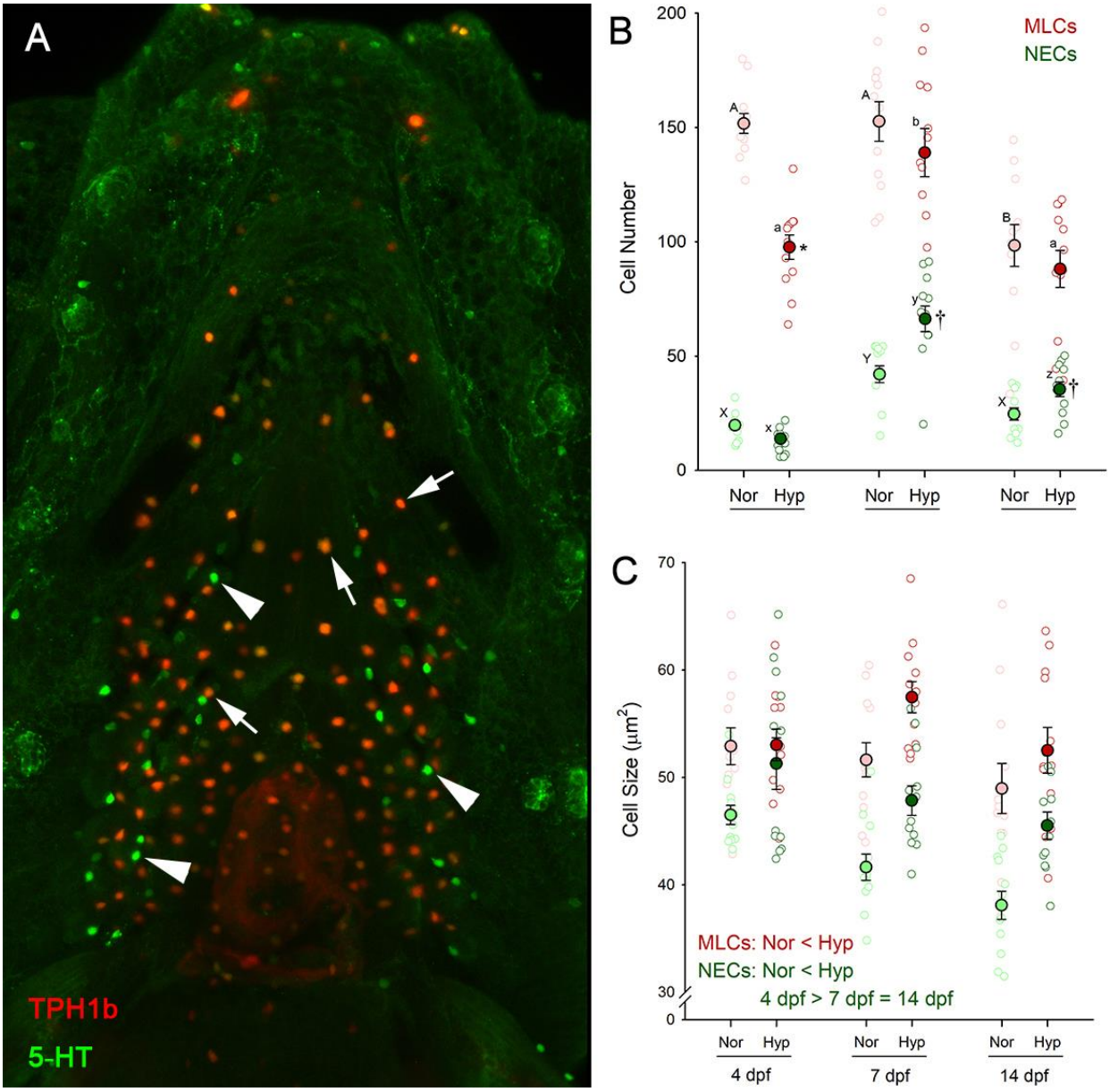
A
TPH1b
5-HT
B
MLCs
NECs
Cell Number
200
150
100
50
0
Nor
Hyp
C
Cell Size (µm²)
70
60
50
40
30
0
MLCs: Nor < Hyp
NECs: Nor < Hyp
4 dpf > 7 dpf = 14 dpf
4 dpf
7 dpf
14 dpf

Fig. 4.3

Figure 4.4. *In vivo* Ca^{2+} imaging of Merkel-like cells (MLCs) exposed to NaCN. (A) Representative image of a *Tg(tph1b:jRCaMP1a)* larva at 4 days post fertilization (dpf) with MLCs expressing the red-colored *in vivo* Ca^{2+} indicator (arrowhead). (B) Representative Ca^{2+} traces for larvae exposed to 5 min of normoxic system water followed by 10 min of 100 μM NaCN. Control traces were obtained from MLCs of larvae exposed to 15 min of normoxic system water. A calcium event is characterized as a single spike of $[Ca^{2+}]_i$ and calcium event frequency is presented as peaks per minute (ppm). Two categories of MLCs were observed; non-responsive cells were MLCs that did not increase Ca^{2+} event frequency when exposed to NaCN whereas responsive cells were MLCs that increased Ca^{2+} event frequency when exposed to NaCN. (C) Mean Ca^{2+} event frequencies of control, non-responsive and responsive cells. Data are presented as means ± s.e.m. Asterisks (*) represent significant differences compared to control cells. See Fig. S4.2 for statistical analysis.

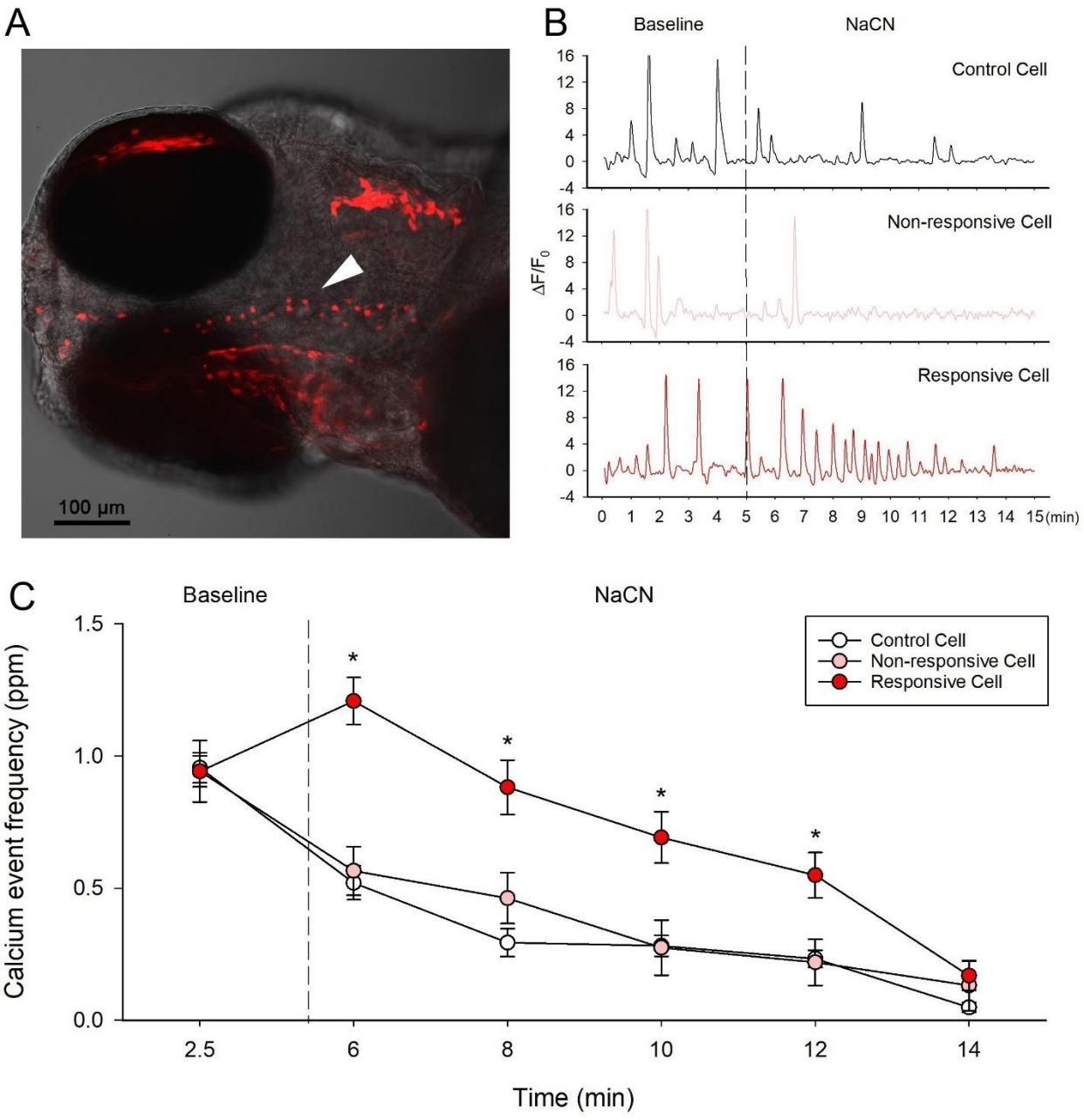
A
100 µm
B
Baseline
NaCN
Control Cell
Non-responsive Cell
Responsive Cell
ΔF/F0
16
12
8
4
0
-4
0 1 2 3 4 5 6 7 8 9 10 11 12 13 14 15(min)
C
Baseline
NaCN
Control Cell
Non-responsive Cell
Responsive Cell
Calcium event frequency (ppm)
1.5
1.0
0.5
0.0
2.5
6
8
10
12
14
Time (min)
*

Fig. 4.4

Figure 4.5. *In vivo* Ca^{2+} imaging of Merkel-like cells (MLCs), peripheral sensory neurons (PSNs), and peripheral sensory ganglia (PSGs) in larval zebrafish exposed to hypoxia. (A) Representative O_2 exposure scheme of a *Tg(tph1b:jRCaMP1a, p2rx3b:GCaMP6s)* larva at 4 days post fertilization (dpf). Each larva was first exposed to 5 min of normoxia (1). Oxygen levels were then gradually lowered to 30 mmHg over the course of approximately 5 min (2-4, each number represents a drop of 30 mmHg), and held at 30 mmHg for an additional 10 min (5-8). After hypoxia exposure, PO_2 was raised back to normoxic levels over the course of approximately 5 min (9-12, each number represents a rise of 30 mmHg) and further held at normoxic levels for an additional 5 min (13). (B) Representative Ca^{2+} traces from MLCs, PSNs, and PSGs of a larva exposed to hypoxia. Arrows point to a synchronized peak between the three locations. Inserts show an enlarged view of the synchronized peaks, showing the time delay present between the peaks from different locations. (C-E) Ca^{2+} event frequencies of MLCs (C, n=40 cells), PSNs (D, n=15 nerve endings) and PSGs (E, n=10 ganglia). Data are presented as means ± s.e.m. Asterisks (*) indicate significant increases compared to time point 1. See Fig. S4.3 for statistical analysis. (F) Mean $[Ca^{2+}]_i$ of PSGs exposed to hypoxia. Data are presented as means ± s.e.m. Statistical analysis was conducted using one-way ANOVA. Asterisks (*) represent significant differences compared to baseline. Statistical significance was set at $P < 0.05$. (G) Time difference of synchronized peaks between peripheral sensory nerve-ending and MLC, and PSG and MLC. Data are presented as means ± s.e.m. Asterisks (*) represent significant difference of mean from zero (one sample t-test; $P < 0.05$).

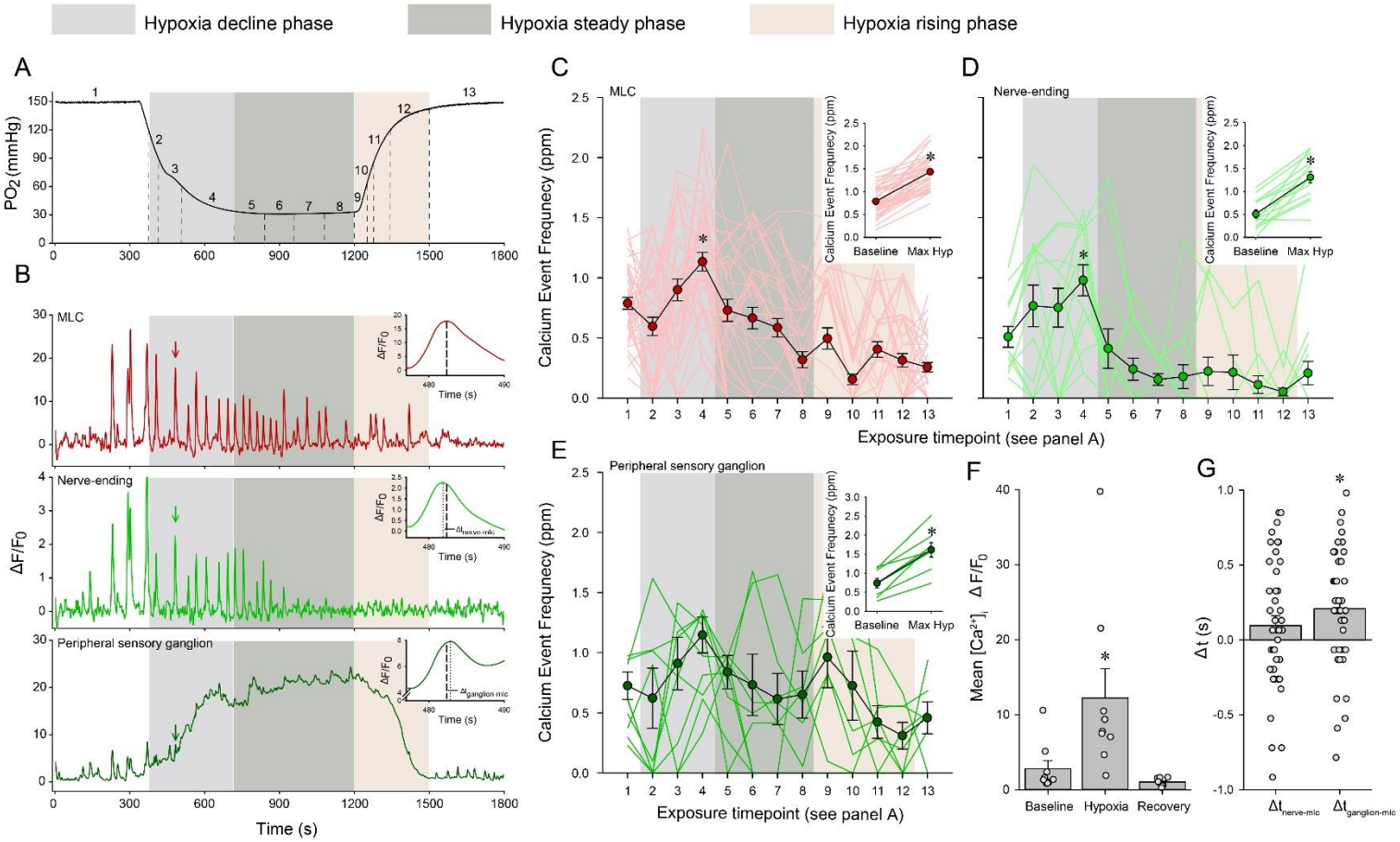
Hypoxia decline phase
Hypoxia steady phase
Hypoxia rising phase
A
B
C
D
E
F
G
MLC
Nerve-ending
Peripheral sensory ganglion
Time (s)
Calcium Event Frequency (ppm)
Exposure timepoint (see panel A)
Baseline
Max Hyp
Hypoxia
Recovery

Fig. 4.5

Figure 4.6. The effects of hypoxia on ventilation frequency (f_V) in larval zebrafish lacking Merkel-like cells (MLCs) at 4 days post fertilization. (A-B) Representative ventral and lateral views of *ascl1a*$^{+/+}$ or *ascl1a*$^{+/-}$ larval zebrafish. Arrowheads point to MLCs in the pharyngeal arch region and arrows indicate skin neuroepithelial cells (NECs). (C-D) Representative ventral and lateral views of *ascl1a*$^{-/-}$ larval zebrafish; MLCs in the pharyngeal arch region and skin NECs were not observed. (E) Ventilation frequency of *ascl1a*$^{+/+}$ (n=6), *ascl1a*$^{+/-}$ (n=7), and *ascl1a*$^{-/-}$ (n=11) larval zebrafish exposed to hypoxia (35 mmHg) and subsequently returned to normoxia (153 mmHg). Data are presented as means ± s.e.m. Asterisks (*) represent significant differences between *ascl1a*$^{+/-}$ and *ascl1a*$^{+/+}$, while daggers (†) represent significant differences between *ascl1a*$^{-/-}$ and *ascl1a*$^{+/+}$. For *ascl1a*$^{+/+}$ and *ascl1a*$^{+/-}$, all data points during hypoxia were significantly greater than during the last minute of normoxia. For *ascl1a*$^{-/-}$, except for the 6th and 18th-20th min, all data points in hypoxia are significantly greater than the last minute of normoxia. See Fig. S4.4 for statistical analysis.

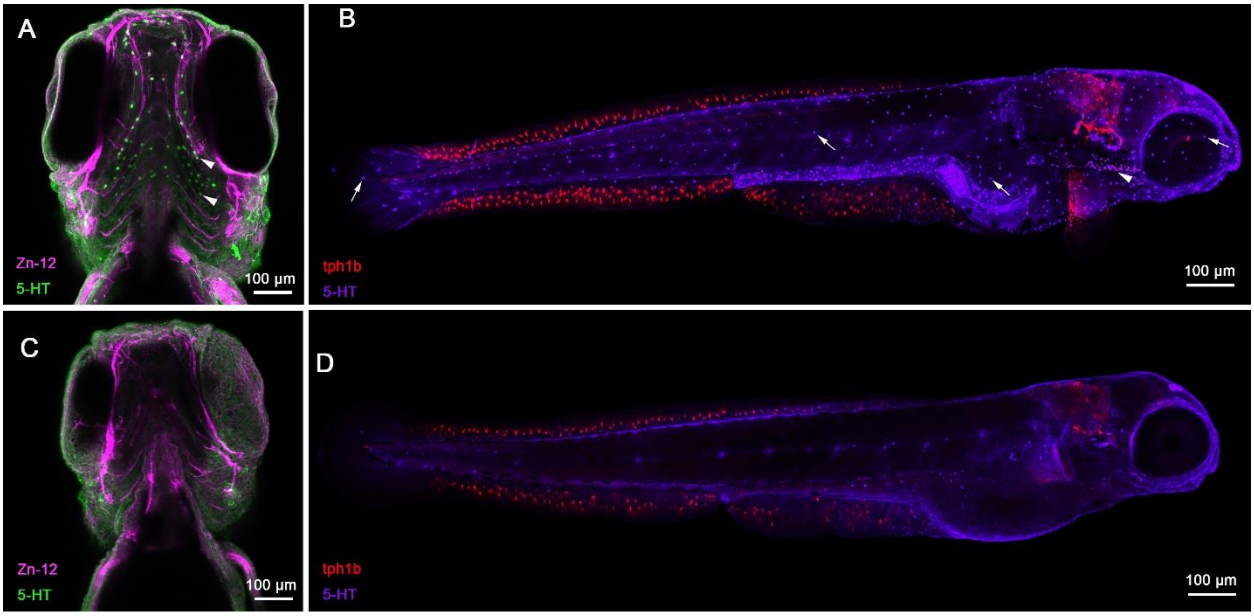
A
Zn-12
5-HT
100 µm
B
tph1b
5-HT
100 µm
C
Zn-12
5-HT
100 µm
D
tph1b
5-HT
100 µm

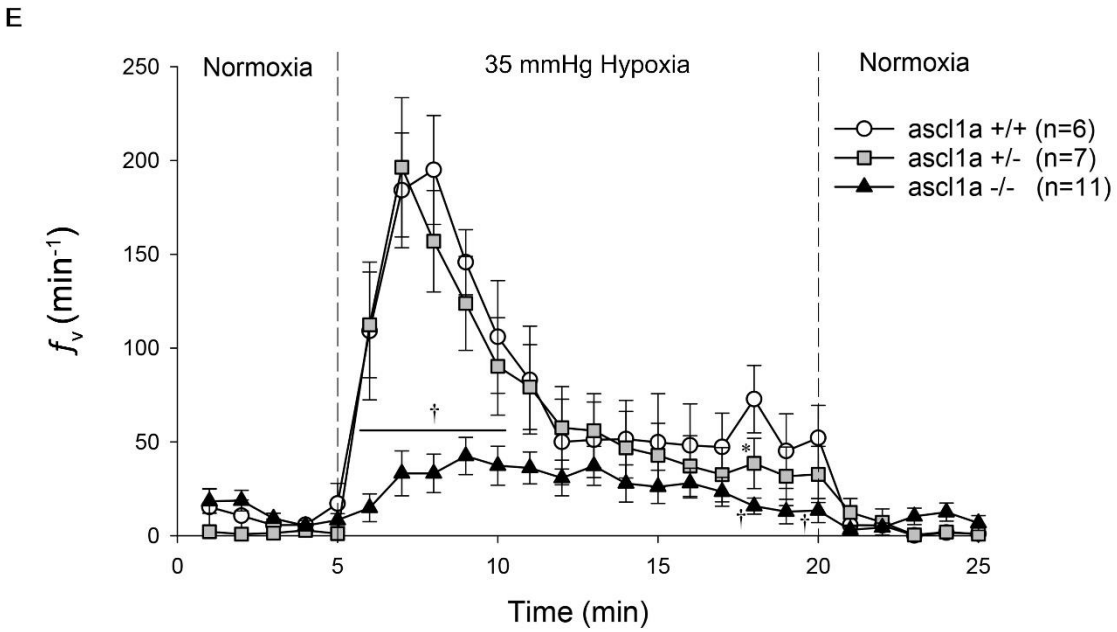
E
Normoxia
35 mmHg Hypoxia
Normoxia
ascl1a +/+ (n=6)
ascl1a +/- (n=7)
ascl1a -/- (n=11)
f_v (min^{-1})
Time (min)
0
50
100
150
200
250
0
5
10
15
20
25
†
*
†
†

Fig. 4.6

Figure 4.7. The effects of hypoxia on ventilation frequency (f_V) in 4 days post fertilization (dpf) larval zebrafish lacking peripheral sensory neurons (PSNs)/peripheral sensory ganglia (PSGs). (A-B) Representative lateral views of *Tg(p2rx3b:NTR-mCherry)* larval zebrafish at 4 dpf treated with DMSO control (A) or DMSO and metronidazole [mtz, (B)]. (C-D) Ventral views of the pharyngeal arch regions of 4 dpf *Tg(p2rx3b:NTR-mCherry)* larval zebrafish treated with DMSO control (C) or DMSO and mtz (D). (E) Ventilation frequency of WT control, WT treated with mtz, *Tg(p2rx3b:NTR-mCherry)* control and *Tg(p2rx3b:NTR-mCherry)* treated with mtz larval zebrafish (n=8 for each group) exposed to hypoxia (35 mmHg) and subsequently returned to normoxia (153 mmHg). Data are presented as means ± s.e.m. Asterisks (*) represent significant differences from the *Tg(p2rx3b:NTR-mCherry)* control group. See Fig. S4.5 for statistical analysis. (F) Comparison of maximum Δf_V, mean Δf_V in the last 5 min of hypoxia, and mean Δf_V during the recovery phase in control and mtz treated *Tg(p2rx3b:NTR-mCherry)* larvae. Data are presented as means ± s.e.m. Statistical analysis was conducted using Student's t-test to compare between the control and mtz treated groups. Asterisks (*) represent significance compared to the control. Statistical significance was set at $P < 0.05$.

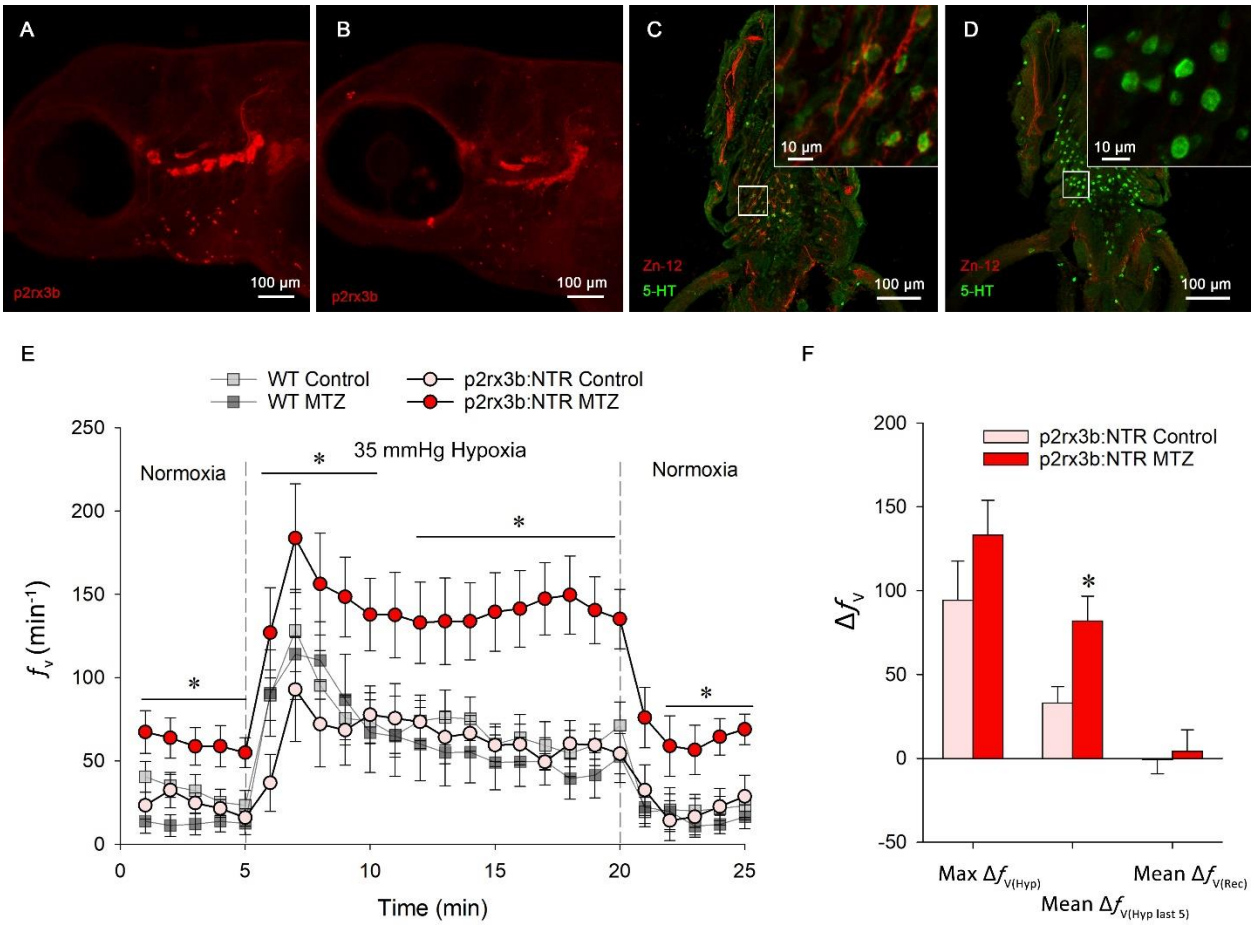
A
p2rx3b
100 µm
B
p2rx3b
100 µm
C
10 µm
Zn-12
5-HT
100 µm
D
10 µm
Zn-12
5-HT
100 µm
E
WT Control
WT MTZ
p2rx3b:NTR Control
p2rx3b:NTR MTZ
Normoxia
35 mmHg Hypoxia
Normoxia
f_v (min^{-1})
Time (min)
F
p2rx3b:NTR Control
p2rx3b:NTR MTZ
Δf_v
Max $\Delta f_{V(Hyp)}$
Mean $\Delta f_{V(Rec)}$
Mean $\Delta f_{V(Hyp\ last\ 5)}$

Fig. 4.7

Figure 4.8. *In vivo* Ca^{2+} imaging of individual cells within the peripheral sensory ganglia (PSGs) in 4 days post fertilization larval zebrafish exposed to various putative neurotransmitters. (A-F) Ca^{2+} event frequency fold changes of individual cells within the PSGs exposed to hypoxia [30 mmHg, (A), n=58 cells], 50 µM serotonin [5-HT, (B), n=50 cells], 50 µM acetylcholine [ACh, (C), n=46 cells], 100 µM ATP [(D), n=41 cells], 100 µM adrenaline [AD, (E), n=38 cells], or 50 µM dopamine [DA, (F), n=45 cells]. Data are presented as means ± s.e.m. Grey shaded areas represent time points under hypoxia or putative neurotransmitter treatment. Asterisks (*) represent significant differences from the controls (normoxic system water during the treatment phase). See Fig. S4.6 for statistical analysis. (G-H) Mean $[Ca^{2+}]_i$ fold change of individual cells within the PSGs exposed to hypoxia [30 mmHg, (G)], 50 µM 5-HT (H), 50 µM ACh (I), 100 µM ATP (J), 100 µM AD (K), or 50 µM DA (L). Data are presented as means ± s.e.m. Grey shaded areas represent time points under hypoxia or putative neurotransmitter treatment. Asterisks (*) represent significant differences between a specific time point and the corresponding control value. Daggers (†) represent a significant difference between a specific time point and baseline; two-way ANOVA (Holm–Šidák post-hoc multiple comparison test. Statistical significance was set at $P < 0.05$.

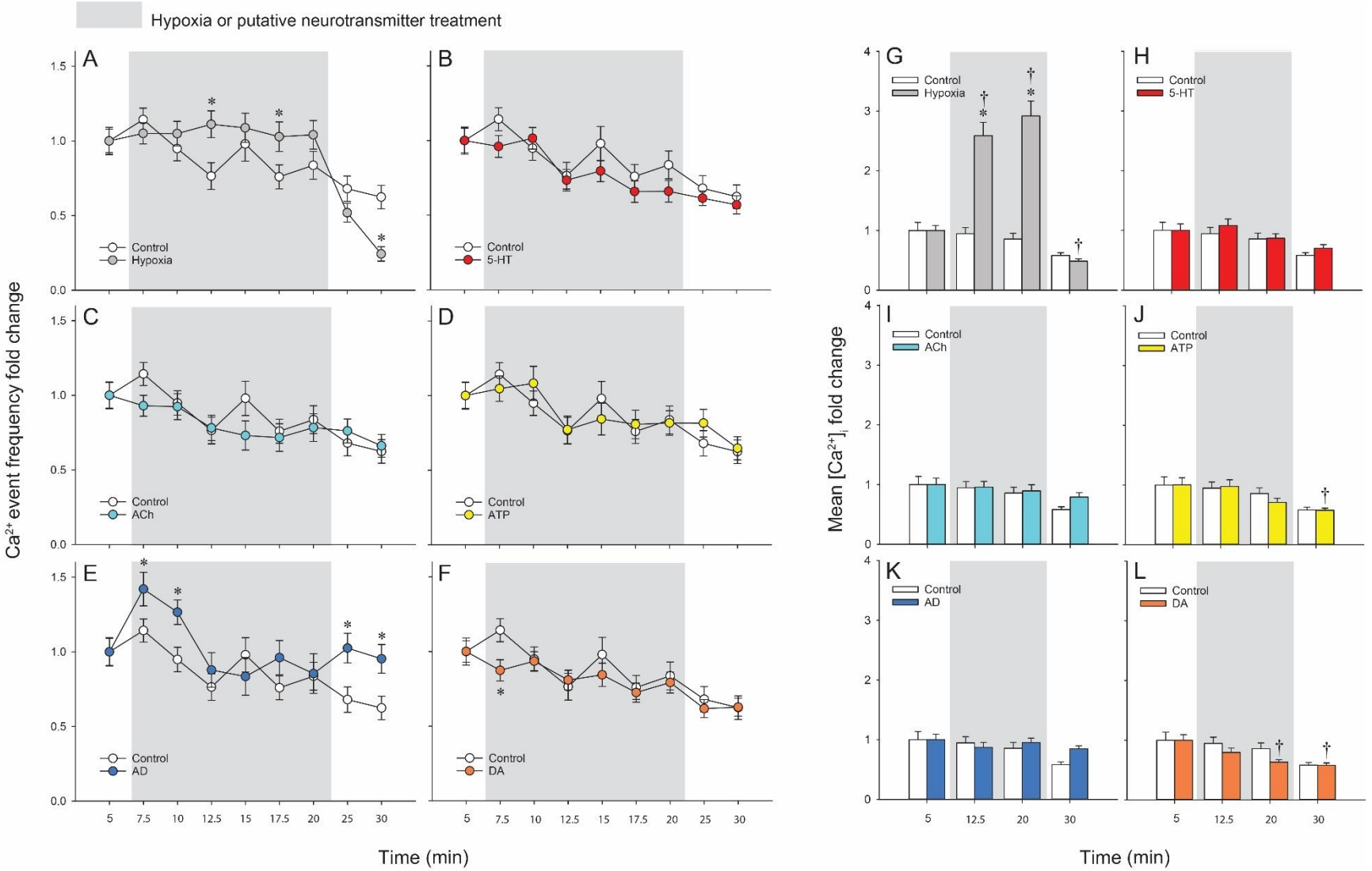
Hypoxia or putative neurotransmitter treatment
A
B
C
D
E
F
G
H
I
J
K
L
Control
Hypoxia
5-HT
ACh
ATP
AD
DA
Ca2+ event frequency fold change
Mean [Ca2+]i fold change
Time (min)
Time (min)

Fig. 4.8

Figure 4.9. *In vivo* Ca^{2+} imaging of individual cells within the peripheral sensory ganglia (PSGs) in 4 days post fertilization larval zebrafish co-exposed to hypoxia and various putative neurotransmitters. (A-F) Ca^{2+} event frequency fold changes of individual cells within the PSGs first exposed to hypoxia (30 mmHg) followed by co-exposure of hypoxia and 50 µM serotonin [5-HT, (A), n=45 cells], 50 µM acetylcholine [ACh, (B), n=60 cells], 100 µM [ATP (C), n=46 cells], 100 µM adrenaline [AD, (D), n=48 cells], or 50 µM dopamine [DA, (E), n=53 cells]. Data are presented as means ± s.e.m. Light grey shaded areas represent time points under hypoxia treatment, dark grey shaded areas represent time points under hypoxia and putative neurotransmitter co-treatment. Asterisks (*) represent significant differences from the hypoxia treatment value. See Fig. S4.7 for statistical analysis. (G-H) Mean $[Ca^{2+}]_i$ fold change of individual cells within the PSGs first exposed to hypoxia (30 mmHg) followed by co-exposure of hypoxia and 50 µM 5-HT (F), 50 µM ACh (G), 100 µM ATP (H), 100 µM AD (I), or 50 µM DA (J). Data are presented as means ± s.e.m. Light grey shaded areas represent time points under hypoxia treatment, dark grey shaded areas represent time points under hypoxia and putative neurotransmitter co-treatment. Asterisks (*) represent significant difference between a specific time point compared to the hypoxia treatment value. Daggers (†) represent a significant difference between a specific time point and baseline; two-way ANOVA (Holm–Šidák post-hoc multiple comparison test. Statistical significance was set at $P < 0.05$.

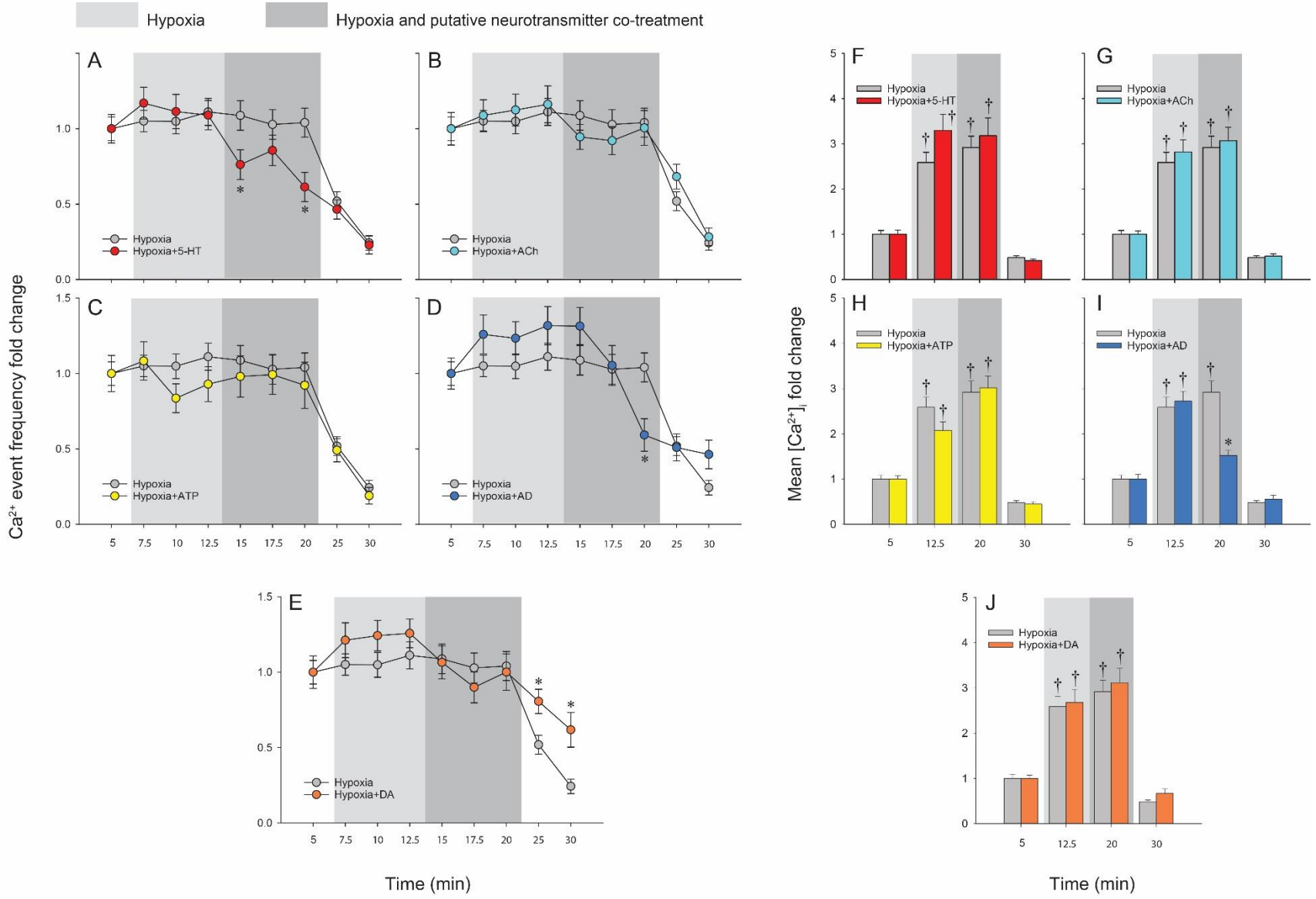
Hypoxia
Hypoxia and putative neurotransmitter co-treatment
A
B
C
D
E
F
G
H
I
J
Hypoxia
Hypoxia+5-HT
Hypoxia+ACh
Hypoxia+ATP
Hypoxia+AD
Hypoxia+DA
Ca2+ event frequency fold change
Mean [Ca2+]i fold change
Time (min)
Time (min)

Fig. 4.9

Figure 4.10. A proposed model for O_2 chemoreception in larval zebrafish. The model was adapted from Fig. 4.4 of Zachar and Jonz (2012b). Dashed lines represent components not confirmed in this study, while solid lines represent oathways demonstrated in this study. (1) A decrease in PO_2 is detected by an uncharacterized O_2 sensor within the Merkel-like cells (MLCs). (2) Detection of hypoxia leads to inhibition of K^+ current. (3) Membrane depolarization. (4) Influx of Ca^{2+} resulting in an increase of $[Ca^{2+}]_i$. (5) Neurotransmitters [potentially serotonin (5-HT), adrenaline (AD) and dopamine (DA)] are released. (6) Signals from MLCs are carried by peripheral sensory neurons (PSNs)/peripheral sensory ganglia (PSGs) to the central nervous system (CNS). (7) Stimulates the first phase of ventilation in the multiphasic hypoxic ventilatory response (HVR). (8) As hypoxia progresses, $[Ca^{2+}]_i$ rise in the PSGs. (9) An inhibitory signal is transduced to the CNS and integrated with an excitatory signal from an unknown source, potentially the CNS. (10) The integrated signal results in the second and third phase of ventilation in the multiphasic HVR. See discussion 4.4.4 for additional details.

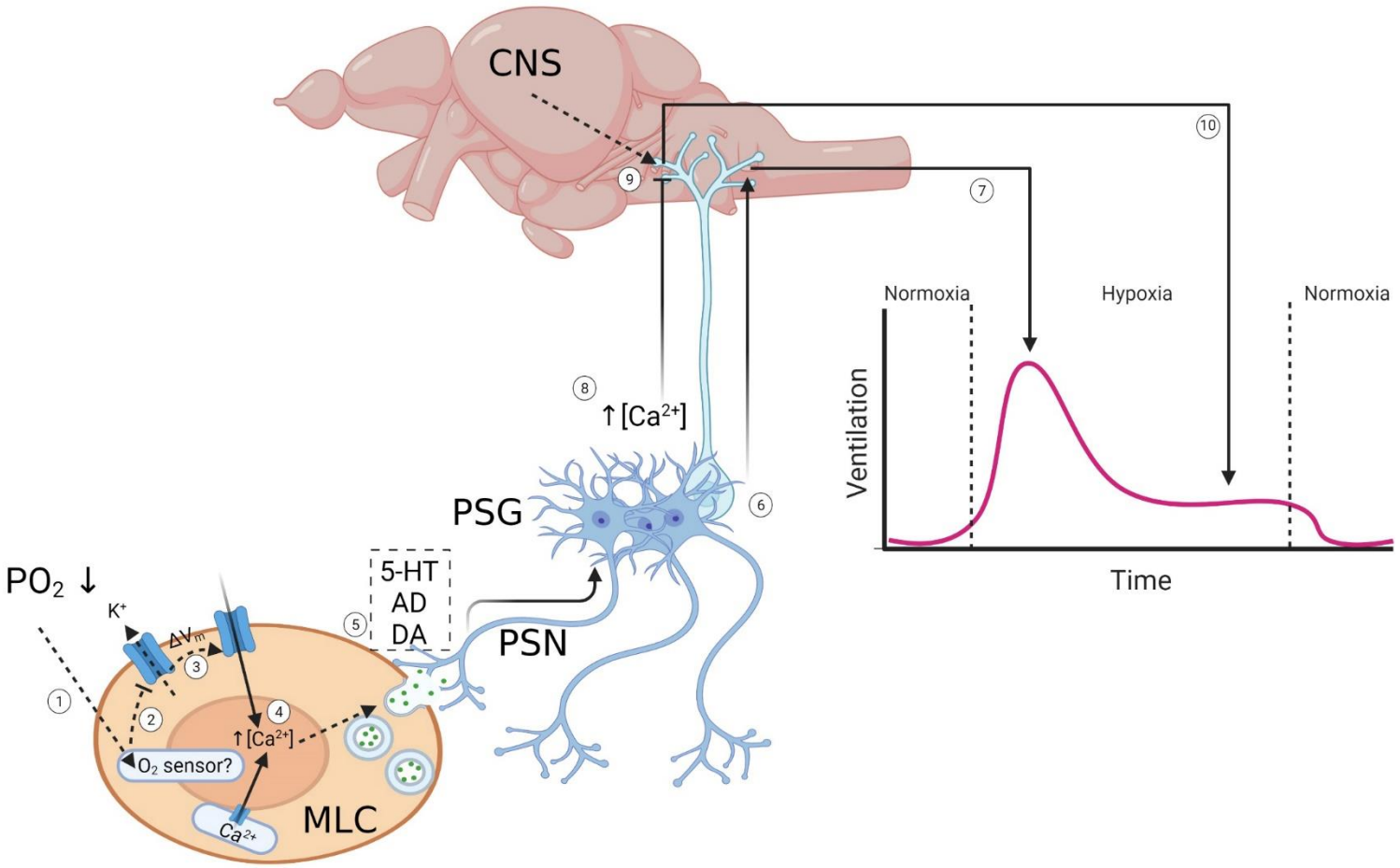
CNS
9
10
7
Normoxia
Hypoxia
Normoxia
Ventilation
Time
8
↑ [Ca2+]
PSG
6
PO2 ↓
K+
ΔVm
3
5-HT
AD
DA
5
PSN
1
2
4
↑ [Ca2+]
O2 sensor?
MLC
Ca2+

Fig. 4.10

4.5 Discussion

The purpose of this study was to test the hypothesis that MLCs are potential O_2 chemoreceptors in zebrafish by showing that they exhibit hypoxia responsiveness *in vivo* and that their ablation can directly alter the HVR. The results clearly demonstrated that 1) MLCs exhibit hypertrophy under hypoxic conditions, 2) MLCs respond to hypoxia *in vivo* through an increase in Ca^{2+} event frequency and 3) ablation of MLCs results in a supressed HVR.

4.5.1 Morphological characterization of MLCs

MLCs associated with the pharyngeal arches and orobranchial cavity express the 5-HT synthesis rate-limiting enzyme TPH1b whereas NECs within the pharyngeal arch region express 5-HT but not TPH1b. Thus, the *tph1b* promoter is suitable for driving the expression of *in vivo* Ca^{2+} indicators within MLCs in transgenic zebrafish lines. Moreover, TPH1b expression alone is sufficient to identify MLCs whereas NECs can be distinguished as TPH1b negative cells that contain 5-HT. MLCs were identified *in vivo* based on specific cellular fluorescence using *Tg(tph1b:mCherry)* larvae as described previously by Kapsimali et al. (2011). Further characterization of MLCs using immunohistochemistry confirmed that similar to NECs, MLCs express SV2, a protein within synaptic vesicles in nerve terminals and endocrine cells (Buckley and Kelly, 1985; Zachar and Jonz, 2012a), suggesting that MLCs also are neurosecretory. Importantly, MLCs were confirmed to be innervated as early as 3 dpf. In younger larvae, mCherry expression in *Tg(tph1b:mCherry)* was not observed, but this does not exclude the possibility of MLCs being present at this stage because mCherry might not have accumulated to detectable levels. Alternatively, TPH1b might not yet be expressed in MLCs at this early stage of development. Regardless, innervation of MLCs occurs at an earlier age than in the pharyngeal

arch NECs, which are not fully innervated until 7 dpf (Jonz and Nurse, 2005). Thus, at least at the morphological level, MLCs are potential candidates for regulating ventilatory/behavioural responses to hypoxia that appear as early as 2 dpf (Jonz and Nurse, 2005). Tracing the nerves innervating MLCs using the *Tg(p2rx3b: eGFP)* and *Tg(p2rx3b: NTR-mcherry)* lines (Kucenas et al., 2006) showed that at 4 dpf, MLCs are innervated by PSNs, specifically originating from cranial nerves IX (glossopharyngeal nerve) and X (vagus nerve), projecting into the pharyngeal arch region. This is an important observation because cranial nerves IX and X are thought to be responsible for the innervation of O_2-sensitive chemoreceptors involved in ventilatory responses (Milsom, 2012). Nerves projecting from the cranial nerve ganglia also reach the CNS, thus forming a potential signal transduction pathway from putative O_2 chemoreceptors through to the CNS, a pathway that has not yet been demonstrated for NECs.

Chemoreceptor hypertrophy and/or proliferation are characteristics of chemoreceptors under prolonged hypoxia exposure (Jonz et al., 2004; Mills and Nurse, 1993; Nurse and Vollmer, 1997; Stea et al., 1992; Wang and Bisgard, 2002). Thus, to examine whether MLCs experience hypertrophy or proliferation, cell number and size were quantified for NECs and MLCs in larvae exposed to hypoxia for 4, 7 or 14 dpf. In agreement with a previous study (Jonz et al., 2004), NECs increased in both cell number and size during chronic hypoxia. Although proliferation of MLCs was not observed, MLC hypertrophy was apparent. Thus, MLCs do respond to hypoxia morphologically as would be expected of an O_2 chemoreceptor.

4.5.2 MLCs as putative O_2 chemoreceptors

Direct evidence that MLCs are responsive to hypoxia and thus could function in O_2 chemoreception was demonstrated using *in vivo* Ca^{2+} imaging. When exposed to NaCN, which results in intracellular chemical hypoxia, a population of MLCs increased Ca^{2+} event

frequencies. In addition, during progressive hypoxia exposure, as PO_2 levels decreased from 60 to 30 mmHg, both MLCs and PSN-endings innervating MLCs increased Ca^{2+} event frequencies. It is during these severe levels of hypoxia when f_V is maximal in 4 dpf zebrafish larvae (Mandic et al., 2020). As hypoxia progresses, this increase in Ca^{2+} event frequency was no longer observed, suggesting MLCs either acclimatized to hypoxia, or experienced receptor failure owing to hypoxia as previously observed in Merkel cells and slowly adapting mechanoreceptors (Findlater et al., 1987). Together, these results suggest that MLCs may play an important role in contributing to the initial increase of f_V during the HVR. It is also possible that the entire taste bud complex might be involved in O_2 chemoreception, whereby the taste receptor cells sense a change in PO_2 and transmit an excitatory signal to the MLCs where it is integrated, similar to the process of taste perception (Finger and Kinnamon, 2021). Regardless, this does not undermine the fact that MLCs play an important role in the O_2 signal transduction process. Ablation of MLCs in the *ascl1a*$^{-/-}$ mutants also prevented the initial large increase in the multiphasic HVR. However, in the *ascl1a*$^{-/-}$ mutants, skin NECs also were absent and thus it is possible that skin NECs also are contributing to the initial large increase of f_V during the HVR.

Upon aligning the Ca^{2+} event signals from the MLCs, PSN-endings and PSGs, a delay in the Ca^{2+} peak of approximately 200 ms was observed between the MLC and PSG. It is unlikely that this difference reflected the different *in vivo* calcium indicators used because both jRCaMP1a and GCaMP6s exhibit mean rise times of around 75-100 ms (Chen et al., 2013; Dana et al., 2016). Although the delay in the Ca^{2+} event response is much longer than the time required for signals to transduce across a chemical synapse (Lodish et al., 2000), it nevertheless suggests that the signal is moving in the direction of MLCs to the PSGs.

Within the PSGs, the gradual rise of mean $[Ca^{2+}]_i$ is of particular interest. Considering that the HVR is multiphasic and that f_V is stable during the later stages of hypoxia exposure, it was thought initially that the rise in mean $[Ca^{2+}]_i$ in PSGs was responsible for the stable increase in f_V above baseline normoxic conditions. However, in larvae experiencing PSG ablation, the opposite was observed; larvae lacking PSGs displayed an elevated f_V under both normoxia and hypoxia, suggesting that PSGs have a tonic inhibitory effect on f_V under normoxic conditions and further inhibit f_V under hypoxia. Upon careful examination of the various stages of the HVR, it is clear that the maximum change in f_V (Δf_V) was unaltered by the loss of PSGs. Thus, the initial large increase in f_V may not be mediated through the PSGs, raising the question as to whether the hypoxia-responsive MLCs, which are innervated by nerves originating from these PSGs do indeed play a role in initiating the rapid rise in f_V during the early stage of the HVR. It is possible that these MLCs convey an inhibitory signal to the PSG to lower f_V in the later phase of the HVR. This possibility is discussed and further expanded upon in Chapter 5. Thus, in addition to MLCs, there are likely other cell types that participate in the initiation of the HVR, such as the skin NECs. Without PSGs, signals from the MLCs may not be transmitted to the CNS such that skin NECs play the more important role in initiating the HVR. To date, however, there are no direct data implicating the skin NECs as O_2 chemoreceptors and the route whereby excitatory signals are propagated from the skin NECs to the CNS is unknown. Alternatively, PSGs might not have been fully ablated in the current study with any remaining functional units being sufficient to transduce the initiation of ventilation signal from MLCs to the CNS. Lastly, there could be other signal transduction pathways from the MLCs to the CNS that were unobserved in this study. Even though PSGs might not be important for the initiation of he HVR, PSGs clearly play a role once ventilation has been stabilized. Without PSGs, f_V was stabilized at a much higher

level than in larvae with PSGs, suggesting that PSGs exert an inhibitory effect on ventilation potentially due to the rise of mean $[Ca^{2+}]_i$. Because the stabilized f_V is above normoxic baseline values, the final stabilized f_V likely reflects an interplay between the inhibitory signal from PSGs and an excitatory signal originating elsewhere. This excitatory signal during the stabilized f_V phase is not likely to be from skin NECs, because *ascl1a*$^{-/-}$ mutants that lack skin NECs are still able to increase f_V under hypoxic conditions. One potential site of the excitatory signal could be the CNS, itself. In fish, there is considerable debate surrounding the existence of a central O_2 chemoreceptor capable of stimulating breathing, and to some extent this is also true for the mammalian literature (Funk and Gourine, 2018a; Funk and Gourine, 2018b; Gourine and Funk, 2017; SheikhBahaei, 2020; Teppema, 2018). Evidence for the presence of central O_2 chemoreceptors in fish is mixed. In some species, infusion of hypoxic blood into the dorsal aorta of normoxic fish or exposing *in vitro* brain stem preparations resulted in an increase of ventilation or ventilatory drive (Bamford, 1974; Côté et al., 2014; Saunders and Sutterlin, 1971) yet in other species, direct perfusion of the brain with hypoxic saline did not alter breathing (Hedrick et al., 1991; Milsom et al., 2002). Certainly, the presence of central O_2 chemoreceptors is an interesting concept that merits further investigation.

4.5.3 Neurotransmitters involved in O_2 chemoreception/afferent signalling

This study focused on the Ca^{2+} responses in individual cells of the PSGs to putative neurotransmitters, resulting in the measurements not being influenced by potential off-target effects of the drugs on the CNS. The drugs chosen were reported previously to alter ventilation in larval zebrafish. Specifically, 5-HT, ACh, ATP and AD are known to increase f_V, while DA decreases f_V (Coe et al., 2017; Rahbar et al., 2016; Shakarchi et al., 2013). When exposed to hypoxia, individual cells within the PSG responded similarly to the PSG as a whole. Ca^{2+} event

frequencies were sustained during hypoxia and mean $[Ca^{2+}]_i$ was elevated, potentially contributing to the decline in f_V during the second phase of the multiphasic HVR.

Of the five putative neurotransmitters tested, ACh and ATP had no effect on the Ca^{2+} profiles in PSGs, whether they were administered under normoxic conditions or co-administered with hypoxia. This result was somewhat unexpected considering that ACh and ATP are the two excitatory neurotransmitters secreted by the mammalian carotid body when activated (Nurse, 2010), and that ACh has been shown to increase f_V in larval zebrafish (Shakarchi et al., 2013). The same is also true for 5-HT where administration of 5-HT alone can elicit ventilatory responses (Shakarchi et al., 2013) yet failed to elicit Ca^{2+} responses in the PSGs. 5-HT only supressed Ca^{2+} event frequency in the cells of PSG when co-administered with hypoxia. Assuming that all peripheral signals are transduced to the CNS by the PSNs/PSGs, these results suggest that ACh and 5-HT, when administered during normoxia, are directly affecting the CNS to modulate ventilation at 4 dpf. This potential central action at 4 dpf however, does not rule out the possibility that ACh and 5-HT might be acting peripherally at later stages when the gill NECs are innervated. The other two putative neurotransmitters AD and DA had varying effects on the Ca^{2+} profiles of cells in the PSG. Under normoxic conditions, administration of AD stimulated Ca^{2+} event frequency while addition of DA resulted in a suppression of Ca^{2+} event frequency. The reverse was observed when AD or DA were co-administrated with hypoxia – AD caused a suppression of Ca^{2+} event frequency and DA, while not affecting Ca^{2+} event frequency during the drug administration phase, resulted in an increase in Ca^{2+} event frequency once the neurotransmitter and hypoxia treatment were removed.

Considering that the HVR is multiphasic, it is possible that the increase in Ca^{2+} event frequency could encode different signals during different phases of the HVR. During the first

phase of the HVR when a large increase in f_V was observed, an increase in Ca^{2+} event frequency might transduce an excitatory ventilation signal to the CNS. This would explain the increase of Ca^{2+} event frequency in AD treated larvae and the decrease of Ca^{2+} event frequency in DA treated larvae under normoxic conditions. The second phase of the HVR consists of a decline in f_V to a stable state above baseline normoxic levels. Thus, at this stage, an increase of Ca^{2+} event frequency would code for an inhibitory signal, much like the increase in mean $[Ca^{2+}]_i$, so that even though 5-HT and AD stimulate ventilation (Pan and Perry, 2020; Shakarchi et al., 2013), they cause a decrease in Ca^{2+} event frequency when administered under hypoxic conditions. Thus, it is possible that they are inhibiting an inhibitory ventilation signal being transmitted to the CNS, resulting in a stimulation of ventilation. A similar explanation would also explain DA's lingering effect on Ca^{2+} event frequency. Because DA inhibits ventilation, it would result in an increase in Ca^{2+} event frequency when administered under hypoxia. Further evidence to support Ca^{2+} event frequency encoding different signals under different phases of the HVR is that when administered under normoxic conditions, AD (Pan and Perry, 2020) results in an elevated f_V that is monophasic – f_V increases to a stable level and there is no secondary decline of f_V. Thus, without a period of hypoxia exposure, the increase in Ca^{2+} event frequency will only be transducing a signal to increase f_V, resulting in a monophasic elevation of f_V. Further evidence for AD stimulating ventilation also comes from co-administration of AD and hypoxia. Under hypoxic conditions, AD inhibits the rise of mean $[Ca^{2+}]_i$ caused by hypoxia. Because the rise of mean $[Ca^{2+}]_i$ potentially inhibits ventilation, AD is inhibiting an inhibitory ventilation signal and thus stimulating ventilation. Despite showing that 5-HT, AD and DA have an effect on the Ca^{2+} profile of cells in the PSGs, it remains unknown whether these putative neurotransmitters are directly released from MLCs or other presumptive O_2 chemoreceptors during hypoxia.

4.5.4 A proposed model for O_2 chemoreception in larval zebrafish and future directions

Consolidating the results from this study and integrating previously known literature on O_2 chemoreception (Jonz et al., 2015; Zachar and Jonz, 2012b), a proposed model for O_2 chemoreceptor in larval zebrafish is presented (Fig. 4.10). Upon hypoxic exposure, a yet unidentified O_2 sensor within the MLCs detects the change in PO_2, which results in the inhibition of background K^+ channels and membrane depolarization. Membrane depolarization activates voltage dependent Ca^{2+} channels allowing for the influx of extracellular Ca^{2+} or release from intracellular stores. The rise in $[Ca^{2+}]_i$ triggers the release of neurotransmitters, possibly 5-HT or ACh, onto the PSN-endings thereby transmitting the signal via the PSGs to the respiratory centers of the CNS, resulting in the large increase of f_V during the first phase of the multiphasic HVR. As the hypoxia exposure progresses, MLCs no longer send an excitatory signal to the CNS via the PSNs and PSGs, while the rise in mean $[Ca^{2+}]_i$ within the PSGs confers an inhibitory signal to the respiratory centers of the CNS resulting in a gradual decrease of ventilation (the second phase of the multiphasic HVR). A potential excitatory signal from the CNS then interplays with the inhibitory signals from the PSGs, resulting in the sustained ventilation above normoxic baseline in the last phase of the multiphasic HVR. Several steps within the signal transduction process still require further examination, such as the potential role of skin NECs in initiating the initial ventilatory response in the first phase of the HVR, the specific neurotransmitters released by MLCs, and whether or not there is a central O_2 chemoreceptor that can provide an excitatory stimulus to sustain ventilation during the HVR.

4.6 Supplementary Tables and Figures

Table S4.1. List of PCR primers used to amplify promoter and reporter gene regions. All sequences listed 5′ to 3′ with the reverse primer sequences listed as the reverse compliment of the gene sequence. Sequence in bold indicates the restriction site.

	Orientation	Sequence	Template	Restriction Site
Promoters				
tph1b	F	TAAGCA **GAATTC** TCTAAGGTGAATCTGTCACATTC	WT DNA	EcoRI
	R	TGCTTA **GTCGAC** GGATGGATGCTCTTGTTTTATAG		SalI
p2rx3b	F	TAAGCA **GAATTC** AGCCAGCGTCTAAGGACAAC	WT DNA	EcoRI
	R	TGCTTA **GTCGAC** GGTGGCGAATCCGTCTAGTT		SalI
Reporter Genes				
GCaMP6s	F	TAAGCA **CCTGCAGG** ATGGGTTCTCATCATCATCATCATC	Addgene #59531	SbfI
	R	TGCTTA **GCGGCCGC** TCACTTCGCTGTCATCATTTGTAC		NotI
jRCaMP1a	F	TAAGCA **ACCGGT** CATCATCATCATCATCATGGTATGGC	Addgene #100848	AgeI
	R	TGCTTA **GCGGCCGC** TCACTTCGCTGTCATCATTTGTACAA		NotI
NTR-mCherry	F	TAAGCA **GTCGAC** GAGTCGTGTCGTGCCTGAGA	Addgene #113760	SalI
	R	TGCTTA **GCGGCCGC** AGCAGCGTATCCACATAGCG		NotI

Table S4.2. List of primary and secondary antibodies used.

Antibody	Antigen	Host	Dilution	Source	Catalog No.
Primary					
5-HT	serotonin	rabbit	1:1000	Sigma-Aldrich	S5545
zn-12	neuron, surface	mouse	1:250	DSHB	zn-12-s
SV2	SV2	mouse	1:500	DSHB	zn-12-s
Calretinin	Calretinin	mouse	1:500	Swant	6B3
mCherry	mCherry	mouse	1:500	Sigma-Aldrich	SAB2702291
mCherry	mCherry	chicken	1:500	Sigma-Aldrich	AB356481
GFP	GFP	rabbit	1:500	Sigma-Aldrich	SAB4301138
Secondary					
Alexa Fluor Plus 488	rabbit	goat	1:500	Invitrogen	A32731
Alexa Fluor Plus 647	rabbit	goat	1:500	Invitrogen	A32732
Alexa Fluor Plus 594	mouse	donkey	1:500	Invitrogen	A32744
Alexa Fluor Plus 647	mouse	goat	1:500	Invitrogen	A32728
Alexa Fluor Plus 555	chicken	goat	1:500	Invitrogen	A32932

Figure S4.1. Image of the calcium imaging chamber.

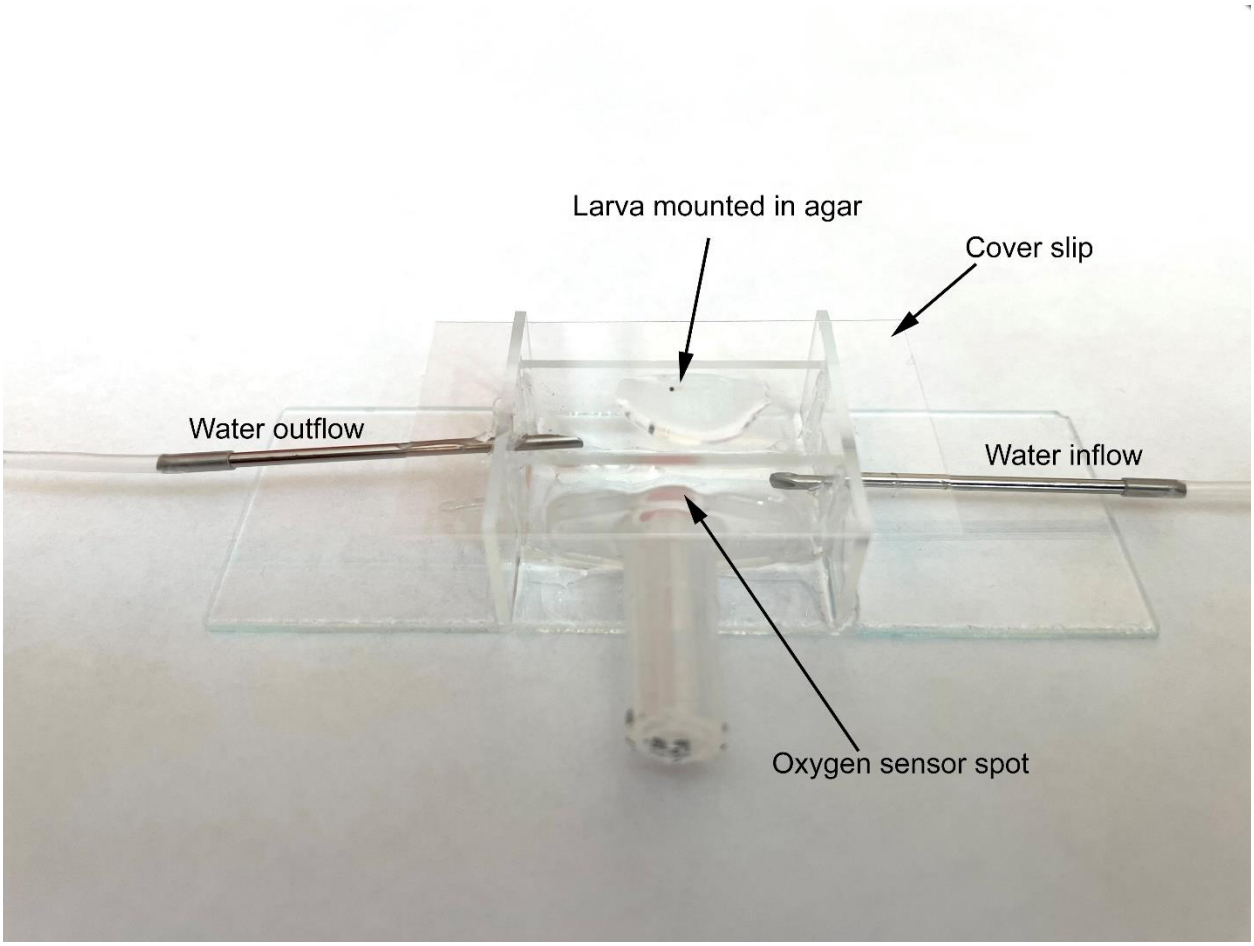
Larva mounted in agar
Cover slip
Water outflow
Water inflow
Oxygen sensor spot

Fig. S4.2

Figure S4.2. The average differences in calcium event frequency (delta f_{Ca}^{2+}) in MLCs between non-responsive cell and control cell (A), and responsive cell and control cell (B), with data based on Figure 4C. Estimates are presented with 95% credible intervals (CI) based on Bayesian analysis. Data are significant if the 95% CI do not intersect zero (dashed horizontal line).

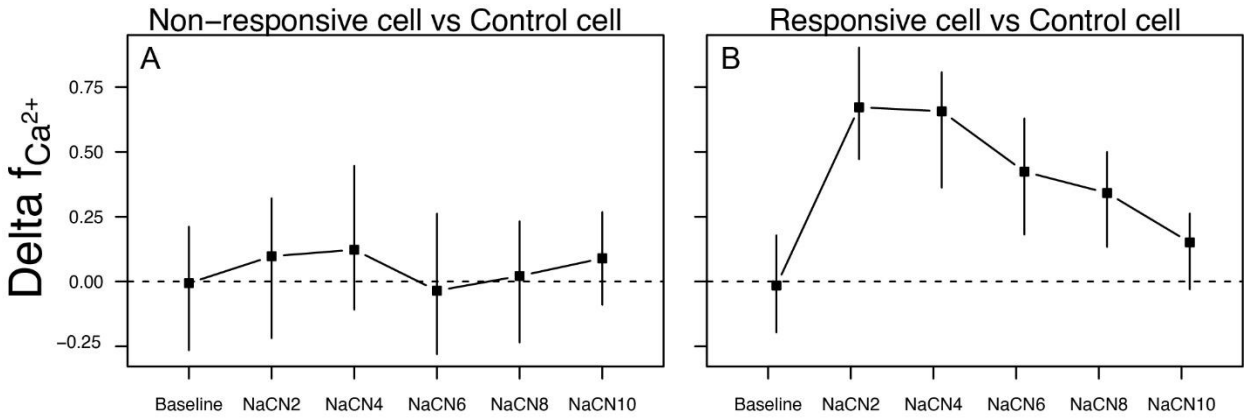
Non−responsive cell vs Control cell
Responsive cell vs Control cell
A
B
Delta $f_{Ca^{2+}}$
0.75
0.50
0.25
0.00
−0.25
Baseline
NaCN2
NaCN4
NaCN6
NaCN8
NaCN10

Fig. S4.2

Figure S4.3. The average differences in calcium event frequency (delta f_{Ca}^{2+}) between normoxia and hypoxia, and normoxia and recovery in MLCs (A), peripheral sensory nerve-endings (B) and PSGs (C). Data based on Figure 5C-E. Estimates are presented with 95% credible intervals (CI) based on Bayesian analysis. Data are significant if the 95% CI do not intersect zero (dashed horizontal line).

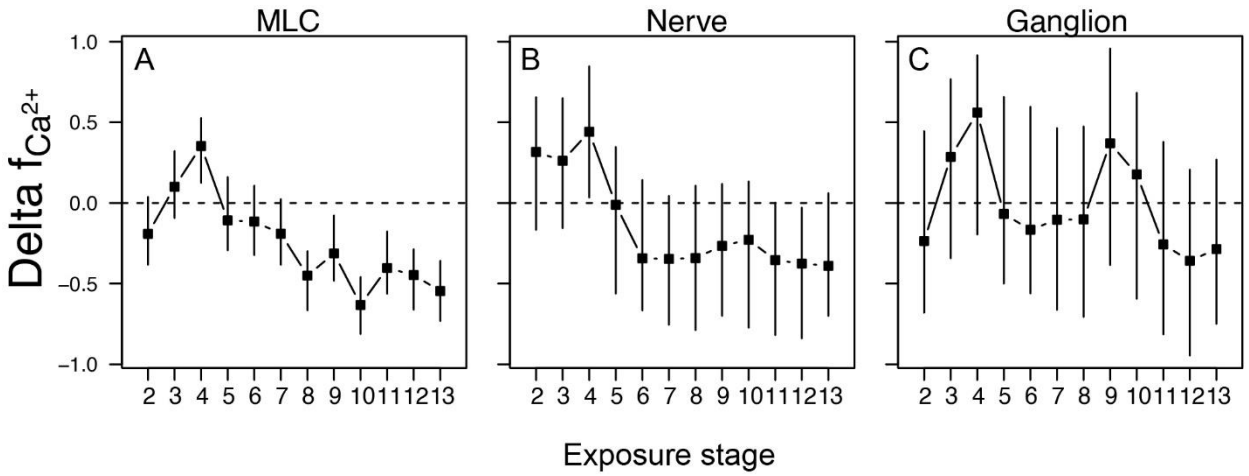
MLC
Nerve
Ganglion
A
B
C
Delta $f_{Ca^{2+}}$
1.0
0.5
0.0
−0.5
−1.0
2 3 4 5 6 7 8 9 10 11 12 13
Exposure stage

Fig. S4.3

Figure S4.4. The average differences in f_V (delta f_V) between normoxia and hypoxia, and normoxia and recovery in *ascl1a*$^{+/+}$ (A), *ascl1a*$^{+/-}$ (B), and *ascl1a*$^{-/-}$ (C) larvae, and the average differences in f_V (delta f_V) between *ascl1a*$^{+/-}$ and *ascl1a*$^{+/+}$ (D), and *ascl1a*$^{-/-}$ and *ascl1a*$^{+/+}$ larvae (E). Data based on Figure 6E. Estimates are presented with 95% credible intervals (CI) based on Bayesian analysis. Data are significant if the 95% CI do not intersect zero (dashed horizontal line).

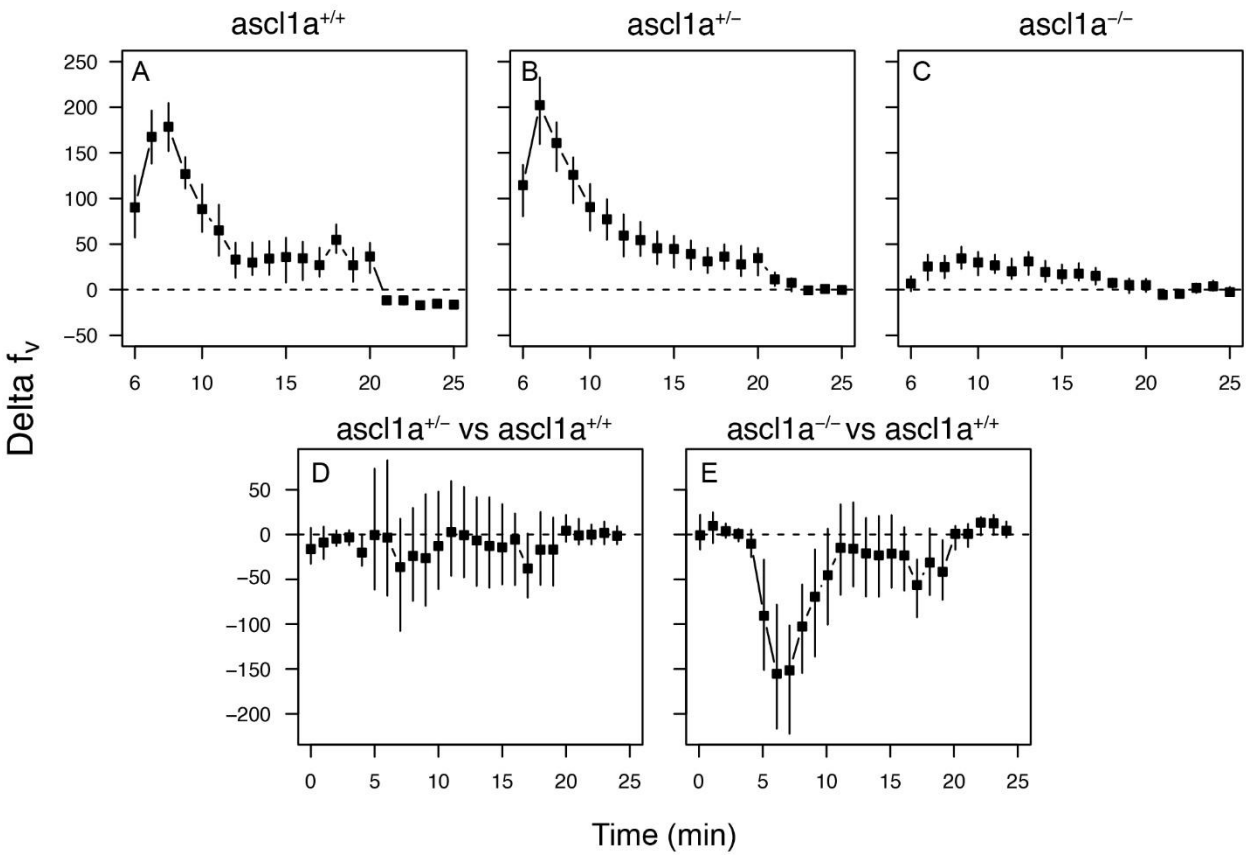
ascl1a+/+
ascl1a+/−
ascl1a−/−
A
B
C
D
E
Delta fv
ascl1a+/− vs ascl1a+/+
ascl1a−/− vs ascl1a+/+
Time (min)

Fig. S4.4

Figure S4.5. The average differences in f_V (delta f_V) between WT control treatment and *Tg(p2rx3b:NTR-mCherry)* control treatment (A), between WT metronidazole (mtz) treatment and *Tg(p2rx3b:NTR-mCherry)* control treatment (B), and between *Tg(p2rx3b:NTR-mCherry)* mtz treatment and *Tg(p2rx3b:NTR-mCherry)* control treatment (C). Data based on Figure 7E. Estimates are presented with 95% credible intervals (CI) based on Bayesian analysis. Data are significant if the 95% CI do not intersect zero (dashed horizontal line).

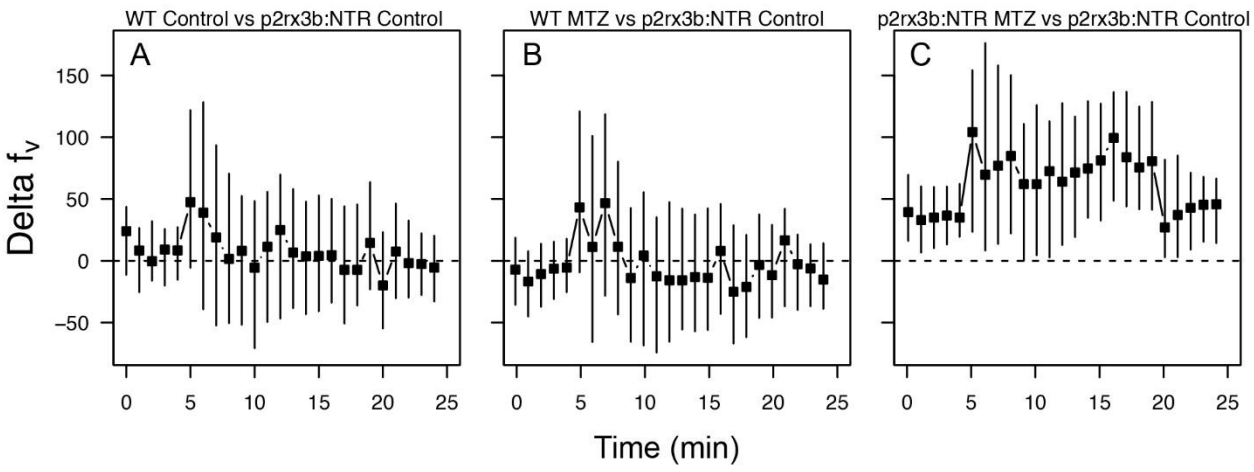
WT Control vs p2rx3b:NTR Control
WT MTZ vs p2rx3b:NTR Control
p2rx3b:NTR MTZ vs p2rx3b:NTR Control
A
B
C
Delta f_v
150
100
50
0
−50
0
5
10
15
20
25
Time (min)

Fig. S4.5

Figure S4.6. The average differences in calcium event frequency (delta f_{Ca}^{2+}) in individual PSG cells between hypoxia and control treatment (A), 5-HT and control treatment (B), ACh and control treatment (C), ATP and control treatment (D), AD and control treatment (E), and DA and control treatment (F). Data based on Figure 8A-F. Estimates are presented with 95% credible intervals (CI) based on Bayesian analysis. Data are significant if the 95% CI do not intersect zero (dashed horizontal line).

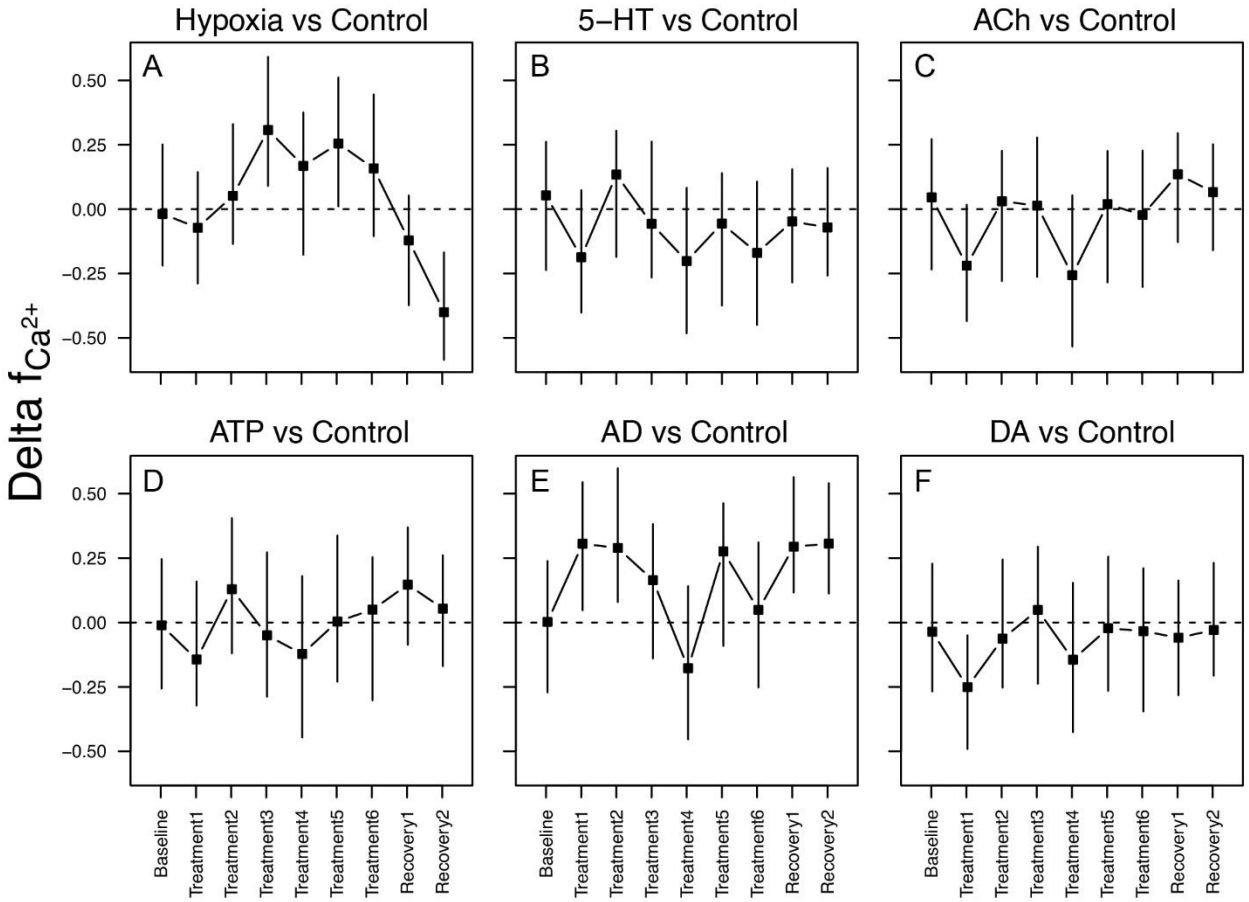
Hypoxia vs Control
5–HT vs Control
ACh vs Control
ATP vs Control
AD vs Control
DA vs Control
A
B
C
D
E
F
Delta $f_{Ca^{2+}}$
0.50
0.25
0.00
−0.25
−0.50
Baseline
Treatment1
Treatment2
Treatment3
Treatment4
Treatment5
Treatment6
Recovery1
Recovery2

Fig. S4.6

Figure S4.7. The average differences in calcium event frequency (delta f_{Ca}^{2+}) in individual PSG cells between 5-HT and hypoxia treatment (A), ACh and hypoxia treatment (B), ATP and hypoxia treatment (C), AD and hypoxia treatment (D), and DA and hypoxia treatment (E). Data based on Figure 9A-E. Estimates are presented with 95% credible intervals (CI) based on Bayesian analysis. Data are significant if the 95% CI do not intersect zero (dashed horizontal line).

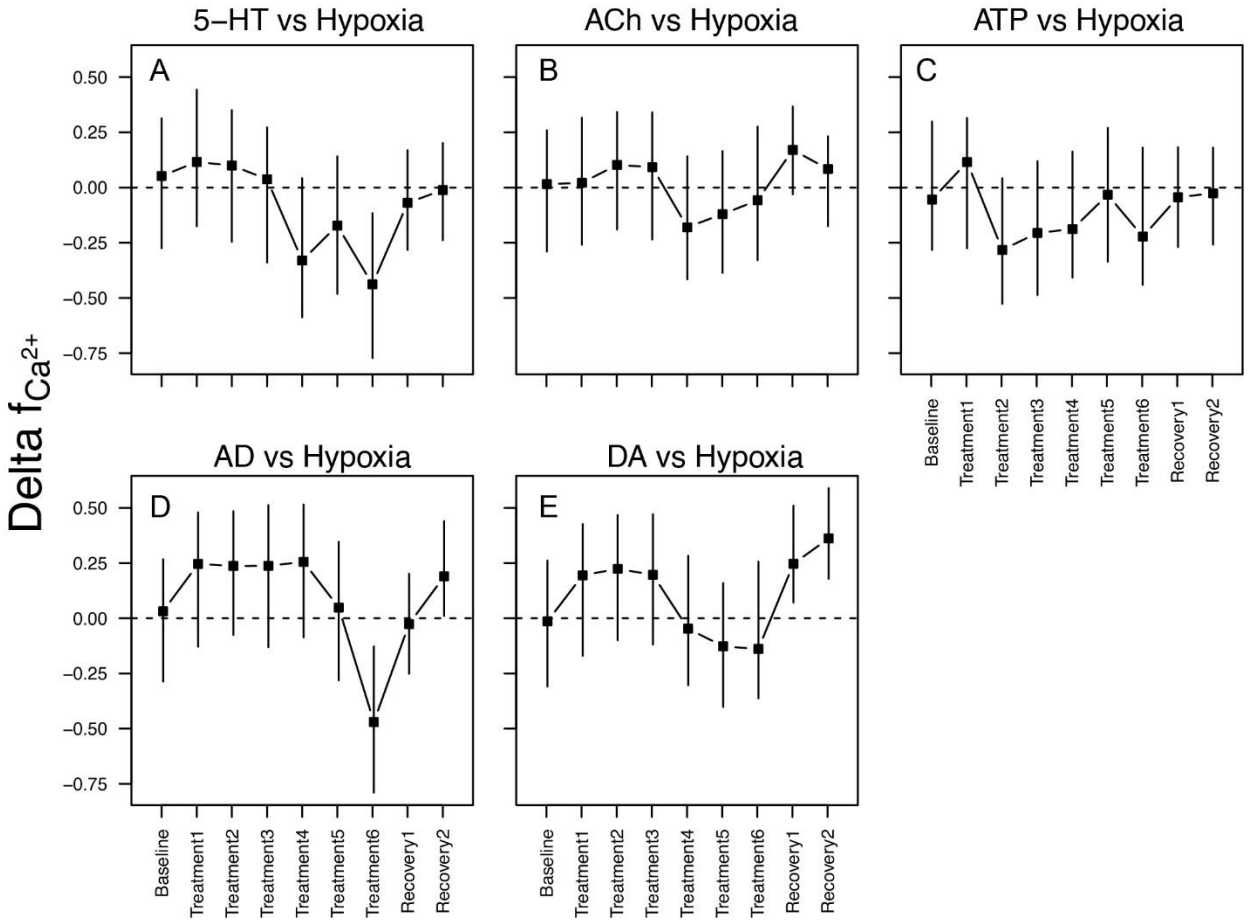
5–HT vs Hypoxia
ACh vs Hypoxia
ATP vs Hypoxia
AD vs Hypoxia
DA vs Hypoxia
A
B
C
D
E
Delta $f_{Ca^{2+}}$
0.50
0.25
0.00
−0.25
−0.50
−0.75
Baseline
Treatment1
Treatment2
Treatment3
Treatment4
Treatment5
Treatment6
Recovery1
Recovery2

Fig. S4.7

Figure S4.8. Representative raw traces of $[Ca^{2+}]_i$ in individual cells of the PSN when exposed to either hypoxia or the various neurotransmitters (grey shaded area).

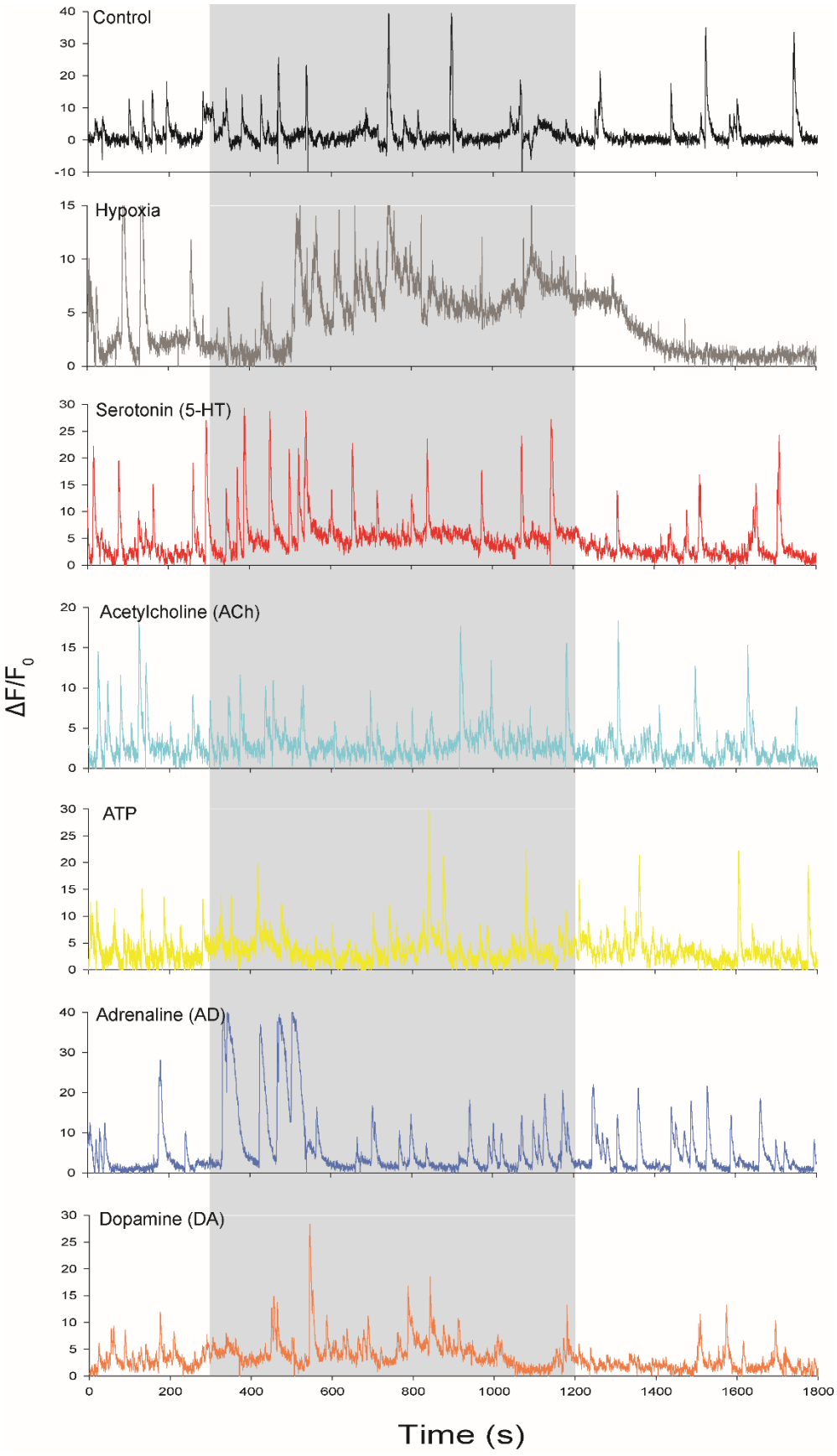
Control
Hypoxia
Serotonin (5-HT)
Acetylcholine (ACh)
ATP
Adrenaline (AD)
Dopamine (DA)
ΔF/F0
Time (s)

Fig. S4.8

Figure S4.9. Representative raw traces of $[Ca^{2+}]_i$ in individual cells of the PSN when exposed to hypoxia (light gray shaded area) or co-exposed to hypoxia and one of the various neurotransmitters (dark gray shaded area).

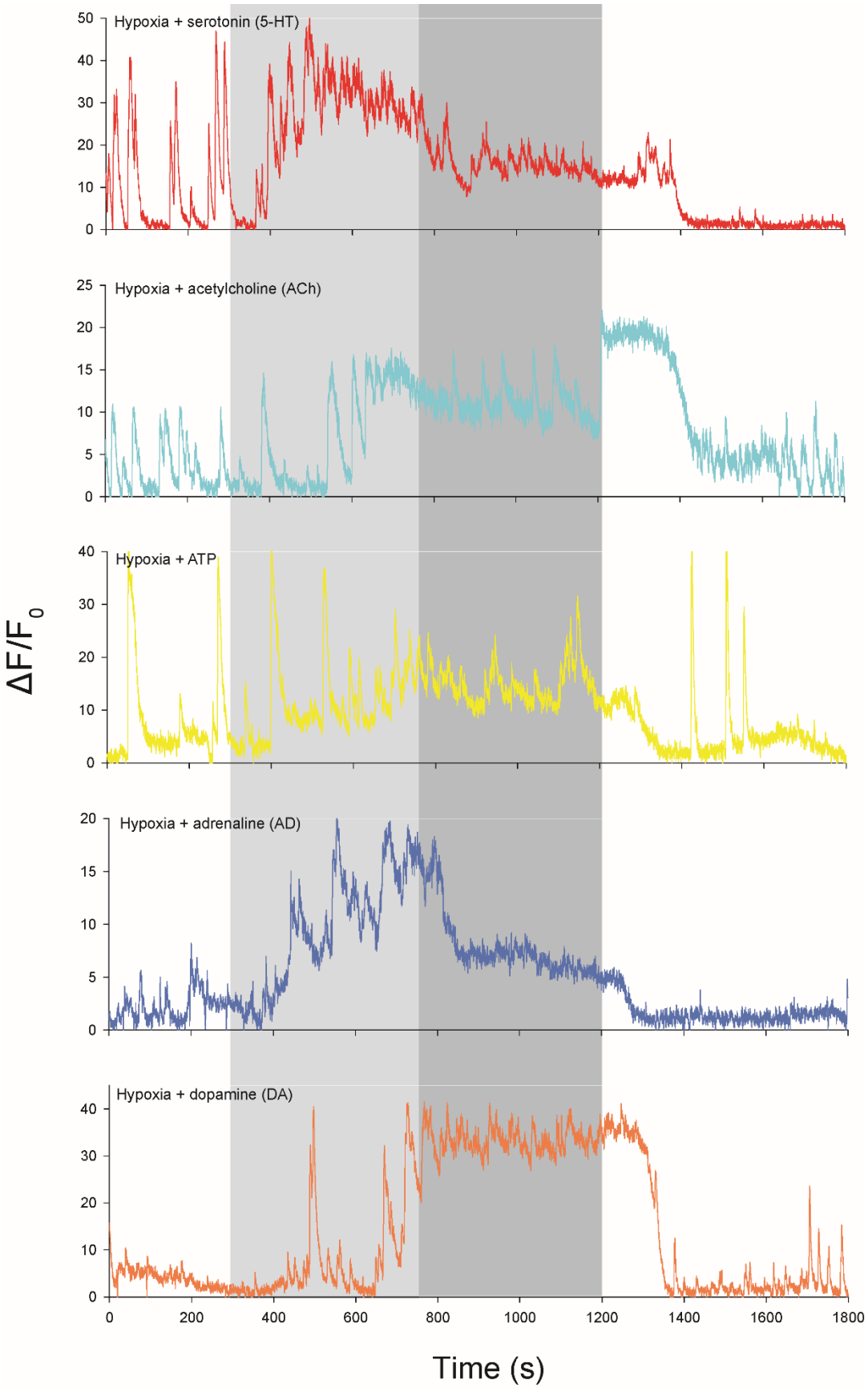
Hypoxia + serotonin (5-HT)
Hypoxia + acetylcholine (ACh)
Hypoxia + ATP
Hypoxia + adrenaline (AD)
Hypoxia + dopamine (DA)
ΔF/F0
Time (s)

Fig. S4.9

CHAPTER 5. General Discussion

5.1 Thesis summary

The overall objective of this thesis was to examine the O_2 chemoreception pathway in larval zebrafish and the associated downstream physiological responses. Chapter 2 evaluated the physiological significance of the HVR in larvae with the main finding being that branchial/buccal gas transfer plays a significant role in O_2 uptake during hypoxic conditions, supporting a physiological benefit of the HVR as early as 7 dpf. Chapter 3 examined the role of 5-HT in regulating the HVR using *tph1* loss-of-function zebrafish (knockouts). The major finding was that while 5-HT modulated the HVR, 5-HT within the skin NECs does not appear to be a major contributor. Finally, Chapter 4 provided *in vivo* evidence for O_2 chemoreception in MLCs, a newly proposed branchial O_2 chemoreceptor. The following discussion serves to synthesize information obtained from the three data chapters and concludes by providing a new working model for O_2 chemoreception in zebrafish larvae.

5.2 The multiphasic HVR

The first novel finding from this thesis was that the HVR is tightly regulated in larval zebrafish as early as 4 dpf and by 7 dpf, the HVR aids in O_2 uptake under hypoxic conditions. An equally interesting observation was that similar to the HVR in mammals (Powell et al., 1998), the HVR in larval zebrafish is multiphasic, with a large initial increase (initiation phase) gradually declining (decline phase) to reach a new steady-state above that of normoxia values (steady phase). This dynamic response was a previously overlooked phenomenon because prior studies did not analyze or report the full time course of the HVR and often only documented a few time points (e.g. the maximal response) within hypoxia (Rahbar et al., 2016; Tzaneva and Perry, 2014).

Because most of the experiments in Chapter 3 and all of the experiments in Chapter 4 were conducted on 4 dpf larvae, at which time they exhibit a fine-tuned HVR, it would suggest that all of the pathways required to regulate the different phases of the HVR are present at this stage. However, based on Chapter 2, the HVR does not appear to have any physiological benefit at 4 dpf. Thus, it remains unclear as to why larval zebrafish hyperventilate at this stage. One possibility is that the HVR is an innate response in 4 dpf larvae, acting to ensure that O_2-sensing pathways are functional by the time the larvae become dependent on branchial respiration (Jonz and Nurse, 2005). Regardless, Chapter 2 clearly showed that by 7 dpf, the HVR is playing a physiological role under hypoxic conditions because buccal O_2 uptake is occurring at ths time and preventing the HVR resulted in a diminished ability to maintain O_2 uptake under hypoxic conditions as reflected by an increase in P_{crit}. This is a significant result because the benefit of branchial ventilation clearly is occurring much earlier than 14 dpf, the time at which branchial respiration begins to play the dominant role in O_2 uptake (Rombough, 2002).

5.3 Initiation phase of the HVR

Because the HVR is multiphasic, it is possible that the different phases of the response are mediated by separate mechanisms. In chapter 4, it was shown that MLCs, the putative O_2 chemoreceptors, only exhibited an increase in Ca^{2+} event frequency during the PO_2 decline phase of hypoxia and that the ablation of MLCs and NECs resulted in the loss of the initiation phase of the HVR but not the steady phase. Thus, the initiation phase of the HVR may be mediated by the activation of MLCs. It is also possible that the MLCs may play a more important role in signal transmission and integration, and that the taste receptor cells forming the taste bud complex with MLCs are the actual O_2 chemoreceptors which sense changes in PO_2 and pass on that signal to the MLCs. Regardless, MLCs play an important role in the signal transduction process of the

initiation phase of the HVR. Alternatively, although clearly responsive to hypoxia, the MLCs may not play a role in the initiation phase but are more important during the decline and steady phases given that PSN/PSG transmit inhibitory signals to the CNS (see discussion below). In the latter scenario, the traditionally labelled O_2 chemoreceptors – gill and skin NECs (Coccimiglio and Jonz, 2012; Jonz et al., 2004) – could mediate the initiation phase of the HVR. Data from Chapter 4 support this idea because ablating the PSN/PSG innervating the MLCs did not prevent the initiation phase of the HVR. The most likely explanation is that skin NECs or another extra-branchial O_2 chemoreceptor are mediating the initiation phase of the HVR at such times. At 4 dpf when experiments in Chapter 4 were conducted, skin NECs are present and fully innervated. Coccimiglio and Jonz (2012) demonstrated that partial chemical denervation of skin NECs at this stage eliminated the HVR and the data in Chapter 4 showed that the initiation phase of the HVR was prevented in *ascl1a*$^{-/-}$ mutants lacking MLCs and skin NECs. However, the pathways whereby signals are transduced from the skin NECs to the CNS remain uncharacterized. It would seem that identifying a neural pathway connecting cutaneous NECs to the CNS is a crucial step in establishing the skin NECs as O_2 chemoreceptors *in vivo*.

It must be emphasised that gill NECs also cannot be ruled out as O_2 chemoreceptors in larvae. Although at 4 dpf, gill NECs are not fully innervated (Jonz and Nurse, 2005), there could be other unidentified pathways that transduce the signal from gill NECs to the CNS, making them suitable to initiate the HVR. It is also possible that O_2 is sensed directly within the CNS although evidence for the presence of central O_2 chemoreceptors is inconclusive (Bamford, 1974; Burleson and Smatresk, 1990a; Côté et al., 2014; Hedrick et al., 1991; Milsom et al., 2002; Saunders and Sutterlin, 1971). However, studies were conducted in adult fish that rely predominantly on the gills for O_2 uptake. In larval zebrafish, cutaneous O_2 uptake is more

important in the early stages (Pan et al., 2019; Rombough, 2002) and thus it is not unreasonable to hypothesize that at least in larvae, O_2 could directly diffuse into the CNS and be sensed within the CNS.

Once O_2 chemoreceptors are activated, the next step in O_2 signal transduction involves the release of neurotransmitters onto afferent nerves. However, all direct evidence of neurotransmitters (e.g. ATP and ACh) being released from peripheral O_2 chemoreceptors are derived from studies on the mammalian carotid body (Buttigieg and Nurse, 2004; Conde et al., 2012; Fitzgerald et al., 1999; Kåhlin et al., 2014). In fish, pharmacological studies have pointed to neuroendocrine factors including 5-HT, ACh, ATP, AD, DA and gaseous neurotransmitters being important in mediating ventilatory responses (Burleson and Milsom, 1995a; Burleson and Milsom, 1995b; Jonz et al., 2015; Perry et al., 2016; Rahbar et al., 2016; Randall and Taylor, 1991; Shakarchi et al., 2013). However, their site(s) and modes of action, and whether they are actually secreted by NECs are unknown. Even though the $[Ca^{2+}]_i$ measurement method employed in Chapter 4 was unable to provide direct evidence of the release of neurotransmitters by peripheral O_2 chemoreceptors, it was possible to examine the potential role of these neuroendocrine factors in a pathway shown to be relevant to O_2 signal transduction. Unexpectedly, ACh and ATP, which are the stimulatory neurotransmitters released by the carotid body in response to hypoxia (Leonard et al., 2018; Nurse, 2010) did not affect $[Ca^{2+}]_i$ within the PSG. Serotonin also did not induce a $[Ca^{2+}]_i$ response except when administered during hypoxia, suggesting that it is not responsible for the initiation phase of the HVR even though it is found in abundance within NECs and MLCs, and potentially can be released in response to hypoxia (Dunel-Erb et al., 1982). These findings are consistent with the data from Chapter 3 showing that 5-HT, at least within NECs or MLCs, does not mediate the HVR. Interestingly, of the five

neuroendocrine factors tested, AD and DA were the only two that affected $[Ca^{2+}]_i$ within cells of the PSG when delivered during normoxia, with AD stimulating and DA inhibiting Ca^{2+} frequency, suggesting their roles in the initiation phase of the HVR. However, there is little evidence that catecholamines are expressed within gill O_2 chemoreceptors. In gill NECs of trout, goldfish (Porteus et al., 2013) or Indian catfish [*Heteropneustes fossilis*, (Zaccone et al., 2003)], tyrosine hydroxylase (TH), the rate limiting enzyme of catecholamine synthesis, is not present. In barramundi (*Lates calcarifer*), TH was undetectable in the gills based on western blot analysis (Candy and Collet, 2005). The only evidence for the presence of TH arose from experiments using cultured gill NECs of the channel catfish where 5-HT and TH were co-localized to cells dissociated from the gills (Burleson et al., 2006). No studies have examined the expression of TH within MLCs. Even in the case where TH is not expressed in NECs or MLCs, the presence of catecholamines within these cells cannot be excluded. Similar to 5-HT being synthesized directly from 5-HTP without the need for the 5-HT synthesis rate-limiting enzyme TPH (Pan et al., 2018), a similar process could be hypothesized for catecholamine synthesis.

Neurotransmitters released by activated O_2 chemoreceptors will then activate the afferent nerves in contact with the peripheral O_2 chemoreceptors and convey the signal to the CNS. Even though data from Chapter 4 showed that when examining the PSG as a whole, hypoxia exposure did not increase Ca^{2+} event frequency, the maximum Ca^{2+} event frequency was still higher during hypoxia when compared to the normoxic baseline values. In addition, when looking at individual cells within the PSG, Ca^{2+} event frequency was higher in hypoxia exposed fish compared to the normoxic control fish. One caveat, however, is that the ablation of PSN/PSG did not abolish the initiation phase of the HVR, which may have been a consequence of incomplete ablation or the presence of other O_2 chemoreceptors/signal transduction pathways also able to

evoke the initiation phase (see previous discussion). Regardless, it is likely that the PSN and PSG play an important role in transducing signals between the O_2 chemoreceptors and the CNS, especially when considering that previous work has shown that cranial nerves IX and X are responsible for transducing ventilation signals between the gills and the CNS (Milsom, 2012). Once the signal reaches the CNS, an integration of signals likely occurs before the final ventilation output exits the CNS. Data from Chapter 3 suggest that 5-HT, especially 5-HT synthesized by the TPH1a paralog, may play an important role in modulating this response within the CNS. In *tph1a*$^{-/-}$ and *tph1a*$^{-/-}$*1b*$^{-/-}$ mutants, f_V during the initiation phase was significantly higher than that of the WTs, suggesting that 5-HT synthesized by TPH1a provides an inhibitory signal to ventilation. Thus, the activation of peripheral O_2 chemoreceptors could be sending a signal via the PSN/PSG to the CNS to inhibit this inhibitory signal, resulting in a rapid increase of ventilation when first exposed to hypoxia. In support of this idea, nerve fibers emanating from the PSG into the CNS terminate in close association with 5-HT positive cells, though whether these 5-HT positive cells express TPH1a is unclear (Fig. 5.1). Stimulating a response by lifting a tonic inhibitory signal is not uncommon in sensory systems. For example, in the human visual system, light induced stimulation of photoreceptors results in hyperpolarization of the photoreceptors to reduce the inhibition of retinal nerves, leading to excitation of these nerves (Yau, 1994).

5.4 Decline phase of the HVR

After the initiation phase of the HVR, f_V gradually declines and reaches a steady phase that remains above the normoxic baseline conditions. The mechanisms leading to this decline and steady phase of the HVR are likely very different from those of the initiation phase. One potential mechanism responsible for the decline phase is the increase in mean $[Ca^{2+}]_i$ within the

PSG as shown in Chapter 4. Thus, ablating the PSN/PSG not only resulted in an increase of f_V under normoxic conditions, but also an increase in Δf_V during the steady phase of hypoxia, suggesting that the PSN/PSG produce a tonic inhibitory signal that is sent to the ventilatory control centers in the CNS under normoxic conditions, and further send an inhibitory signal to the CNS during hypoxia that is likely conveyed by an increase in mean $[Ca^{2+}]_i$ within the PSG. The mechanisms underlying the rise in mean $[Ca^{2+}]_i$ remain unclear although one possibility is that O_2 could directly stimulate the PSN/PSG to elicit a rise of mean $[Ca^{2+}]_i$. Alternatively, it is conceivable that MLCs, instead of being stimulatory and initiating the HVR as discussed above, could be sending a signal to increase mean $[Ca^{2+}]_i$ in PSG under hypoxic conditions to reduce ventilation. The latter mechanism could explain the elevated Δf_V during the decline and steady phases of hypoxia when PSN/PSG are ablated because the inhibitory signals from the MLCs would no longer be transduced to the CNS.

5.5 Steady phase of the HVR

An inhibitory signal from the PSG however cannot explain the steady phase of the HVR because the final f_V during the steady phase is above f_V under normoxic conditions, suggesting that there must be an additional excitatory signal originating elsewhere. This excitatory signal is unlikely to originate from MLCs or skin NECs, because *ascl1a*$^{-/-}$ mutants that lack MLCs or skin NECs are still able to hyperventilate during the steady phase of the HVR. One potential candidate is the gill NEC although the transduction pathway of signals from these cells to the CNS is not obvious given that the gill NECs are not yet fully innervated at 4 dpf (Jonz and Nurse, 2005). Another potential explanation is that the excitatory signal originates directly within the CNS, and again data from Chapter 3 provide hints of evidence for this claim. In both *tph1b*$^{-/-}$

and *tph1a*$^{-/-}$*1b*$^{-/-}$ mutants, f_V during the steady phase was significantly lower than that of the WTs, suggesting that 5-HT synthesized by TPH1b is providing an excitatory influence on ventilation. Although the specific site of action of 5-HT was not determined, it is unlikely to be the MLCs or NECs as the *tph1a*$^{-/-}$, *tph1b*$^{-/-}$ and *tph1a*$^{-/-}$*1b*$^{-/-}$ mutants all had similar densities of detectable serotonergic cells in the pharyngeal arch region yet responded differently to hypoxia. Thus, the most likely location is within the CNS, where in mammals it has been shown that *Egr2-Pet1* subgroup of 5-HT neurons is specialized to drive increased ventilation in response to CO_2 elevation and acidosis and that these neurons selectively project to the respiratory chemosensory center within the CNS (Brust et al., 2014). In addition, using the *Tg(tph1b:mCherry)* transgenic zebrafish, TPH1b expression was also demonstrated within the CNS as shown in Chapter 3.

5.6 Proposed models for O_2 signal transduction in larval zebrafish

In summary, this thesis provides *in vivo* evidence for O_2 chemoreception in larval zebrafish and presents potential mechanisms whereby the O_2 signal transduction pathway ultimately determines the HVR. Two separate models for O_2 sensing and the triggering of the HVR are summarized in Fig. 5.2. In the first model, MLCs are activated upon hypoxia exposure and release neurotransmitters such as AD and DA onto afferent PSNs (Fig. 5.2A①), which then transduce an inhibitory signal via the PSN/PSG to the ventilatory control centers of the CNS (Fig. 5.2A②-③). Within the CNS, the inhibitory signal originating from MLCs serves to inhibit pre-existing inhibitory output to respiratory control centres that is dependent upon 5-HT synthesized from TPH1a positive cells (Fig. 5.2A③). The net effect is a lifting of tonic ventilatory suppression leading to the initiation phase of the HVR (Fig. 5.2A④). As hypoxia progresses, mean $[Ca^{2+}]_i$ within the PSG rises owing to a direct stimulation of hypoxia (Fig. 5.2A⑤-⑥), leading to an inhibitory signal being sent to the CNS (Fig. 5.2A⑦) and a resultant

decline of ventilation from the maximum point during the initiation phase. This inhibitory signal then integrates with excitatory signals likely originating from the CNS and modulated by 5-HT synthesized from TPH1b positive cells to stabilize ventilation during the steady phase of HVR to a level above normoxic values (Fig. 5.2A⑦-⑧). In the second model, skin NECs, O_2 chemoreceptors in the CNS and potentially gill NECs are activated upon hypoxia exposure to initiate the HVR (Fig. 5.2B①-③). MLCs on the other hand are activated only when hypoxia progresses to below 60 mmHg (Fig. 5.2A④) at which point they transmit a signal to the PSN/PSG resulting in a rise of mean $[Ca^{2+}]_i$ within the PSG to lower f_V to the steady phase (Fig. 5.2B⑤-⑧). It is also entirely possible that a combination of the two models could be what is actually happening within a larval zebrafish, ultimately leading to the HVR during hypoxia exposure.

5.7 Directions for further research

This thesis provided experimental evidence to advance our understanding of piscine O_2 chemoreception and generated preliminary models as to how peripheral O_2 chemoreceptors elicit physiological responses in zebrafish larvae facing hypoxia. However, there remain several critical unanswered questions that merit further investigation. The first and foremost need is to provide *in vivo* evidence for O_2 sensitivity in both gill and skin NECs and to establish the transduction pathways to the CNS. All existing direct evidence for gill NECs as O_2 chemoreceptors was derived from dissociated cells *in vitro* (Burleson et al., 2006; Jonz et al., 2004) and the only indirect evidence for O_2 sensitivity of skin NECs arose from predictable morphological responses of zebrafish skin NECs to fluctuations in ambient PO_2 (Coccimiglio and Jonz, 2012). Even though chemical denervation of skin NECs did result in a diminished HVR (Coccimiglio and Jonz, 2012), with new insight from this thesis on MLCs being potential

O_2 chemoreceptors, the diminished HVR could also be attributed to the denervation of skin NECs and MLCs. The biggest hurdle previously was the inability to identify gill or skin NECs *in vivo*. Recently, however, it was demonstrated that the promoter of *vmat2* can be used to control reporter gene expression within skin and gill NECs (Pan et al., 2021). Thus, it may now be possible to express *in vivo* calcium indicators within skin and gill NECs to provide evidence for their O_2 sensitivity *in vivo*. In addition, it would also be interesting to test the hypothesis that taste receptor cells within the taste bud complex may be responding to changes in environmental PO_2. To do so, the promoter region of *sall4* could be used for introducing calcium indicators into these cells (Jackson et al., 2013). Another key issue that needs to be addressed further concerns the specific neurotransmitters being released by O_2 chemoreceptors when activated. Currently, there is no direct evidence demonstrating the release of neurotransmitters from any putative O_2 chemoreceptor in fish. An interesting tool that was developed in the past decade is the use of *in vivo* neurotransmitter sensors (Jing et al., 2019). Similar to *in vivo* genetically encoded calcium indicators, these sensors are able to respond to neurotransmitter binding, and by expressing them within PSNs innervating peripheral sensory ganglia, direct evidence of neurotransmitter release could be provided if this process is indeed being triggered by hypoxia. Finally, signal integration within the CNS is an interesting, albeit complex topic, worthy of further investigation, particularly because there might be signals related to O_2 chemoreception and the control of ventilation originating within the CNS. In mammals, the pre-Bötzinger complex within the CNS is essential for the generation of the respiratory rhythm and integration of sensory information from changes in the environment (Smith et al., 1991). A similar structure is likely to be present in fish as well, though few studies have attempted to identify this structure. Thus, in summary, future research in the field of piscine O_2 chemoreception should be focused on providing *in vivo*

evidence for O_2 sensitivity of skin and gill NECs, providing direct evidence of neurotransmitter release by O_2 chemoreceptors and identifying the respiratory rhythm generation and integration sites within the CNS.

5.8 Tables and Figures

Figure 5.1 Immunohistochemistry of p2rx3b positive nerves in the central nervous system. (A) Whole mount of 4 days post fertilization (dpf) *Tg(p2rx3b:mCherry)* larvae stained with mCherry antibody. White line represents plane of section in (B). (B) Horizontal section of the brain region of 4 dpf *Tg(p2rx3b:mCherry)* stained with mCherry and 5-HT antibody. (C) Zoomed in region of (B) stained with DAPI, mCherry and 5-HT antibody. Arrowheads point to 5-HT positive cells in close association with p2rx3b positive nerves.

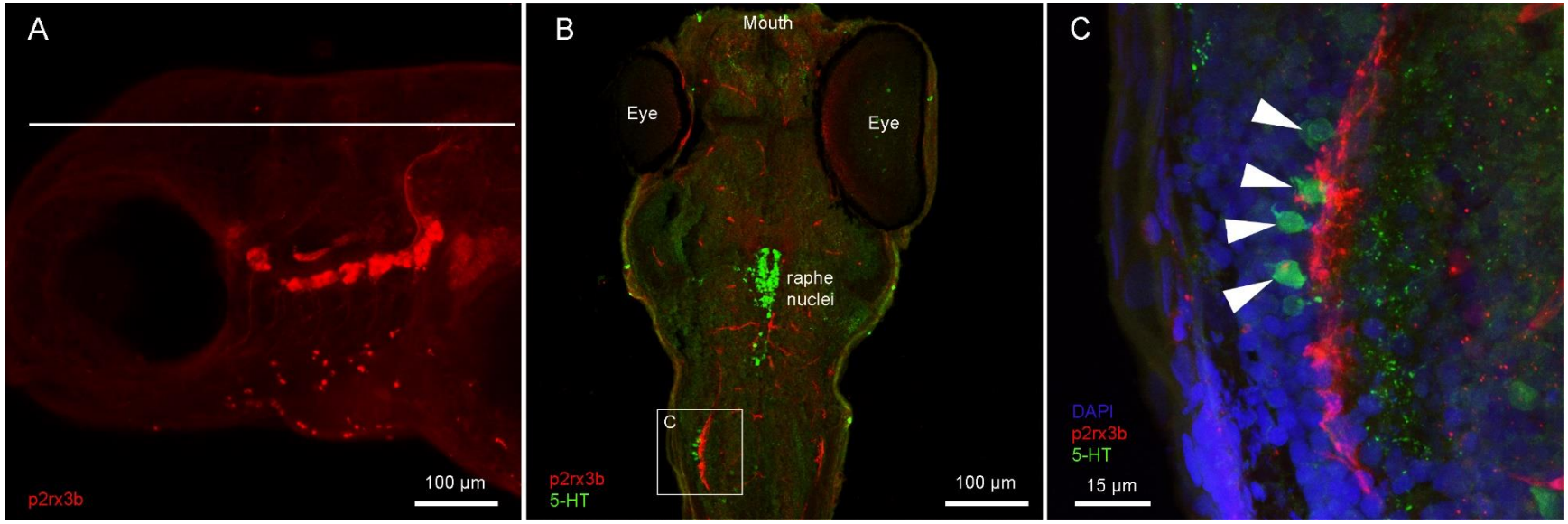
A
p2rx3b
100 µm
B
Mouth
Eye
Eye
raphe
nuclei
C
p2rx3b
5-HT
100 µm
C
DAPI
p2rx3b
5-HT
15 µm

Fig. 5.1

Figure 5.2 Proposed models for O_2 chemoreception in larval zebrafish. (A) ① Hypoxia activates Merkel-like cells (MLCs). ② MLCs activate peripheral sensory neurons (PSNs)/peripheral sensory ganglia (PSGs). ③ PSGs inhibits the inhibitory signal from TPH1a positive cells in the central nervous system (CNS). ④ Initiation of hypoxic ventilatory response (HVR). ⑤ Progression of hypoxia stimulates PSGs. ⑥ $[Ca^{2+}]_i$ within PSGs rises. ⑦ PSGs inhibits HVR and inhibits excitatory signal from TPH1b positive cells in the CNS. ⑧ HVR declines to a steady state above normoxic baseline. (B) ① Hypoxia activates skin neuroepithelial cells (NECs) or central O_2 chemoreceptors. ② An unknown pathway results in the inhibitory signal from TPH1a positive cells in the CNS. ③ Initiation of HVR. ④ Progression of hypoxia stimulates MLCs. ⑤ MLCs activate PSNs/PSGs. ⑥ $[Ca^{2+}]_i$ within PSG rises. ⑦ PSGs inhibits HVR and inhibits excitatory signal from TPH1b positive cells in the CNS. ⑧ HVR declines to a steady state above normoxic baseline.

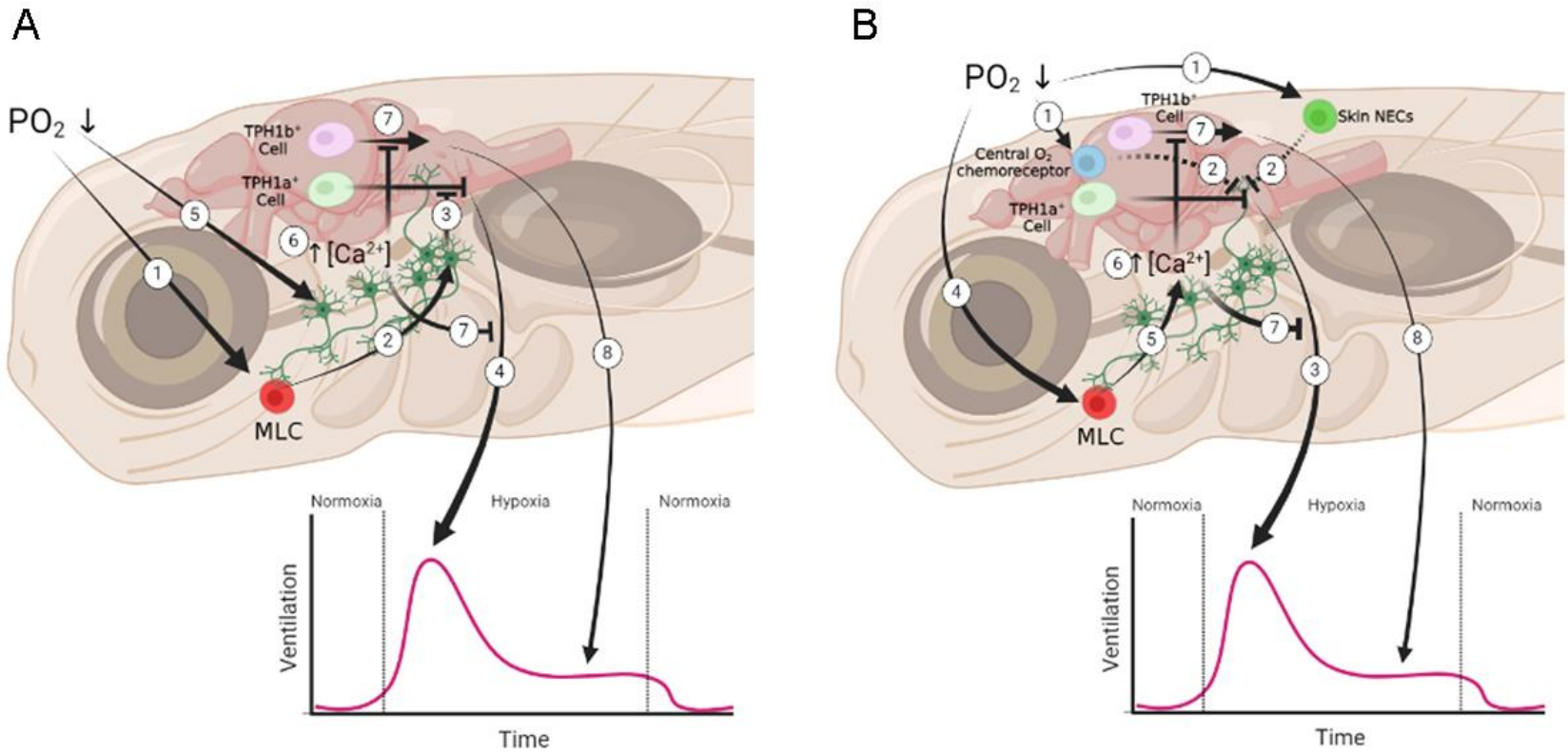
A
PO2 ↓
TPH1b+ Cell
TPH1a+ Cell
↑ [Ca2+]
MLC
Normoxia
Hypoxia
Normoxia
Ventilation
Time
B
PO2 ↓
TPH1b+ Cell
Skin NECs
Central O2 chemoreceptor
TPH1a+ Cell
↑ [Ca2+]
MLC
Normoxia
Hypoxia
Normoxia
Ventilation
Time

Fig. 5.2

References

Abdallah, S. J., Jonz, M. G. and Perry, S. F. (2015a). Extracellular H^+ induces Ca^{2+} signals in respiratory chemoreceptors of zebrafish. *Pflugers Arch - Eur J Physiol* **467**, 399-413.

Abdallah, S. J., Thomas, B. S. and Jonz, M. G. (2015b). Aquatic surface respiration and swimming behaviour in adult and developing zebrafish exposed to hypoxia. *J. Exp. Biol.* **218**, 1777-86.

Anderson, J. L., Mulligan, T. S., Shen, M.-C., Wang, H., Scahill, C. M., Tan, F. J., Du, S. J., Busch-Nentwich, E. M. and Farber, S. A. (2017). mRNA processing in mutant zebrafish lines generated by chemical and CRISPR-mediated mutagenesis produces unexpected transcripts that escape nonsense-mediated decay. *PLoS Genet.* **13**, e1007105.

Bailly, Y. (2009). Serotonergic neuroepithelial cells in fish gills: cytology and innervation.

Bailly, Y., Dunel-Erb, S., Geffard, M. and Laurent, P. (1989). The vascular and epithelial serotonergic innervation of the actinopterygian gill filament with special reference to the trout, *Salmo gairdneri*. *Cell Tissue Res.* **258**, 349-363.

Bailly, Y., Dunel-Erb, S. and Laurent, P. (1992). The neuroepithelial cells of the fish gill filament: indolamine-immunocytochemistry and innervation. *Anat. Rec.* **233**, 143-61.

Bamford, O. (1974). Oxygen recption in the rainbow trout (*Salmo Gairdneri*). *Comp. Biochem. Physiol. A Mol. Integr. Physiol.* **48**, 69-76.

Bissonnette, J. M. (2000). Mechanisms regulating hypoxic respiratory depression during fetal and postnatal life. *Am. J. Physiol. Regul. Integr. Comp. Physiol.* **278**, R1391-R1400.

Boutilier, R., Dobson, G., Hoeger, U. and Randall, D. (1988). Acute exposure to graded levels of hypoxia in rainbow trout (*Salmo gairdneri*): metabolic and respiratory adaptations. *Respir. Physiol.* **71**, 69-82.

Boutilier, R. G., Heming, T. A. and Iwama, G. K. (1984). Physicochemical parameters for use in fish respiratory physiology. In *Fish Physiol.*, vol. 10, pp. 403-430: Elsevier.

Brust, R. D., Corcoran, A. E., Richerson, G. B., Nattie, E. and Dymecki, S. M. (2014). Functional and developmental identification of a molecular subtype of brain serotonergic neuron specialized to regulate breathing dynamics. *Cell Rep.* **9**, 2152-2165.

Buckley, K. and Kelly, R. B. (1985). Identification of a transmembrane glycoprotein specific for secretory vesicles of neural and endocrine cells. *J. Cell Biol.* **100**, 1284-1294.

Burggren, W. W., Bautista, G. M., Coop, S. C., Couturier, G. M., Delgadillo, S. P., García, R. M. and González, C. A. A. (2016). Developmental cardiorespiratory physiology of the air-breathing tropical gar, *Atractosteus tropicus*. *Am. J. Physiol. Regul. Integr. Comp. Physiol.* **311**, R689-R701.

Burleson, M. L., Mercer, S. E. and Wilk-Blaszczak, M. A. (2006). Isolation and characterization of putative O_2 chemoreceptor cells from the gills of channel catfish (*Ictalurus punctatus*). *Brain. Res.* **1092**, 100-7.

Burleson, M. L. and Milsom, W. K. (1990). Propranolol inhibits O_2-sensitive chemoreceptor activity in trout gills. *Am. J. Physiol. Regul. Integr. Comp. Physiol.* **258**, R1089-R1091.

Burleson, M. L. and Milsom, W. K. (1995a). Cardio-ventilatory control in rainbow trout: I. Pharmacology of branchial, oxygen-sensitive chemoreceptors. *Respir. Physiol.* **100**, 231-238.

Burleson, M. L. and Milsom, W. K. (1995b). Cardio-ventilatory control in rainbow trout: II. Reflex effects of exogenous neurochemicals. *Respir. Physiol.* **101**, 289-99.

Burleson, M. L. and Smatresk, N. J. (1990a). Effects of sectioning cranial nerves IX and X on cardiovascular and ventilatory reflex responses to hypoxia and NaCN in channel catfish. *J. Exp. Biol.* **154**, 407-420.

Burleson, M. L. and Smatresk, N. J. (1990b). Evidence for two oxygen-sensitive chemoreceptor loci in channel catfish, *Ictalurus punctatus*. *Physiol. Zool.* **63**, 208-221.

Butler, P., Taylor, E., Capra, M. and Davison, W. (1978). The effect of hypoxia on the levels of circulating catecholamines in the dogfish *Scyliorhinus canicula*. *J. Comp. Physiol.* **127**, 325-330.

Buttigieg, J. and Nurse, C. A. (2004). Detection of hypoxia-evoked ATP release from chemoreceptor cells of the rat carotid body. *Biochem. Biophys. Res. Commun.* **322**, 82-87.

Candy, J. and Collet, C. (2005). Two tyrosine hydroxylase genes in teleosts. *Biochim. Biophys. Acta.* **1727**, 35-44.

Cerezo, J. and García García, B. (2004). The effects of oxygen levels on oxygen consumption, survival and ventilatory frequency of sharpsnout sea bream (*Diplodus puntazzo* Gmelin, 1789) at different conditions of temperature and fish weight. *J. Appl. Ichthyol.* **20**, 488-492.

Chang, N., Sun, C., Gao, L., Zhu, D., Xu, X., Zhu, X., Xiong, J. W. and Xi, J. J. (2013). Genome editing with RNA-guided Cas9 nuclease in zebrafish embryos. *Cell. Res.* **23**, 465-72.

Chang, Y.-F., Imam, J. S. and Wilkinson, M. F. (2007). The nonsense-mediated decay RNA surveillance pathway. *Annu. Rev. Biochem.* **76**, 51-74.

Chen, T.-W., Wardill, T. J., Sun, Y., Pulver, S. R., Renninger, S. L., Baohan, A., Schreiter, E. R., Kerr, R. A., Orger, M. B. and Jayaraman, V. (2013). Ultrasensitive fluorescent proteins for imaging neuronal activity. *Nature* **499**, 295-300.

Cinelli, E., Iovino, L. and Mutolo, D. (2017). ATP and astrocytes play a prominent role in the control of the respiratory pattern generator in the lamprey. *J. Physiol.* **595**, 7063-7079.

Coccimiglio, M. L. and Jonz, M. G. (2012). Serotonergic neuroepithelial cells of the skin in developing zebrafish: morphology, innervation and oxygen-sensitive properties. *J. Exp. Biol.* **215**, 3881-94.

Cochrane, P. V., Jonz, M. G. and Wright, P. A. (2021). The development of the O_2-sensing system in an amphibious fish: consequences of variation in environmental O_2 levels. *J. Comp. Physiol. B*, 1-19.

Coe, A. J., Picard, A. J. and Jonz, M. G. (2017). Purinergic and adenosine receptors contribute to hypoxic hyperventilation in zebrafish (*Danio rerio*). *Comp. Biochem. Physiol. A Mol. Integr. Physiol.* **214**, 50-57.

Conde, S. V., Monteiro, E. C., Rigual, R., Obeso, A. and Gonzalez, C. (2012). Hypoxic intensity: a determinant for the contribution of ATP and adenosine to the genesis of carotid body chemosensory activity. *J. Appl. Physiol.* **112**, 2002-2010.

Corcoran, A. E., Hodges, M. R., Wu, Y., Wang, W., Wylie, C. J., Deneris, E. S. and Richerson, G. B. (2009). Medullary serotonin neurons and central CO_2 chemoreception. *Respir. Physiol. Neurobiol.* **168**, 49-58.

Côté, É., Rousseau, J.-P., Fournier, S. and Kinkead, R. (2014). Control of breathing in in vitro brain stem preparation from goldfish (*Carassius auratus;* Linnaeus). *Physiol. Biochem. Zool.* **87**, 464-474.

Côté, F., Thévenot, E., Fligny, C., Fromes, Y., Darmon, M., Ripoche, M.-A., Bayard, E., Hanoun, N., Saurini, F. and Lechat, P. (2003). Disruption of the nonneuronal *tph1* gene demonstrates the importance of peripheral serotonin in cardiac function. *PNAS* **100**, 13525-13530.

Cummins, E. P., Strowitzki, M. J. and Taylor, C. T. (2020). Mechanisms and consequences of oxygen and carbon dioxide sensing in mammals. *Physiol. Rev.* **100**, 463-488.

Curado, S., Stainier, D. Y. and Anderson, R. M. (2008). Nitroreductase-mediated cell/tissue ablation in zebrafish: a spatially and temporally controlled ablation method with applications in developmental and regeneration studies. *Nat. Protoc.* **3**, 948.

Curran, A. K., Rodman, J. R., Eastwood, P. R., Henderson, K. S., Dempsey, J. A. and Smith, C. A. (2000). Ventilatory responses to specific CNS hypoxia in sleeping dogs. *J. Appl. Physiol.* **88**, 1840-1852.

Dana, H., Mohar, B., Sun, Y., Narayan, S., Gordus, A., Hasseman, J. P., Tsegaye, G., Holt, G. T., Hu, A. and Walpita, D. (2016). Sensitive red protein calcium indicators for imaging neural activity. *Elife* **5**, e12727.

Daristotle, L., Engwall, M. J., Niu, W. and Bisgard, G. E. (1991). Ventilatory effects and interactions with change in PaO_2 in awake goats. *J. Appl. Physiol.* **71**, 1254-1260.

De Castro, F. (1926). Sur la structure et l'innervation de la glande intercarotidienne (*glomus caroticum*) de l'homme et des mammifères, et sur un nouveau système d'innervation autonome du nerf glossopharyngien. *Trab. Lab. Invest. Biol. Univ. Madrid* **24**, 13.

De Graaf, P. and Roberts, B. (1991). Effects of vagal sensory input on the breathing rhythm of the carp. *J. Exp. Biol.* **155**, 77-91.

Dick, T. E. and Coles, S. K. (2000). Ventrolateral pons mediates short-term depression of respiratory frequency after brief hypoxia. *Respir. Physiol.* **121**, 87-100.

Duchen, M., Caddy, K., Kirby, G., Patterson, D., Ponte, J. and Biscoe, T. (1988). Biophysical studies of the cellular elements of the rabbit carotid body. *Neuroscience* **26**, 291-311.

Dunel-Erb, S., Bailly, Y. and Laurent, P. (1982). Neuroepithelial cells in fish gill primary lamellae. *J. Appl. Physiol. Respir. Environ. Exerc. Physiol.* **53**, 1342-53.

Düring, M. v. and Andres, K. H. (1976). The ultrastructure of taste and touch receptors of the frog's taste organ. *Cell Tissue Res.* **165**, 185-198.

Findlater, G., Cooksey, E., Anand, A., Paintal, A. and Iggo, A. (1987). The effects of hypoxia on slowly adapting type I (SAI) cutaneous mechanoreceptors in the cat and rat. *Somatosens. Res.* **5**, 01-17.

Finger, T. and Kinnamon, S. (2021). Purinergic neurotransmission in the gustatory system. *Auton. Neurosci.*, 102874.

Fitzgerald, R. S., Shirahata, M. and Wang, H.-Y. J. (1999). Acetylcholine release from cat carotid bodies. *Brain Res.* **841**, 53-61.

Forgue, J., Burtin, B. and MASSABUAU, J.-C. (1989). Maintenance of oxygen consumption in resting *Silurus glanis* at different levels of ambient oxygenation. *J. Exp. Biol.* **143**, 305-319.

Fritsche, R., Reid, S. G., Thomas, S. and Perry, S. F. (1993). Serotonin-mediated release of catecholamines in the rainbow trout *Oncorhynchus mykiss*. *J. Exp. Biol.* **178**, 191-204.

Fritsche, R., Thomas, S. and Perry, S. F. (1992). Effects of serotonin on circulation and respiration in the rainbow trout *Oncorhynchus mykiss*. *J. Exp. Biol.* **173**, 59-73.

Fu, C., Wilson, J. M., Rombough, P. J. and Brauner, C. J. (2010). Ions first: Na^+ uptake shifts from the skin to the gills before O_2 uptake in developing rainbow trout, *Oncorhynchus mykiss*. *Proceedings of the Royal Society B: Biological Sciences* **277**, 1553-1560.

Funk, G. D. and Gourine, A. V. (2018a). CrossTalk proposal: a central hypoxia sensor contributes to the excitatory hypoxic ventilatory response. *J. Physiol.* **596**, 2935.

Funk, G. D. and Gourine, A. V. (2018b). Rebuttal from Gregory D. Funk and Alexander V. Gourine. *J. Physiol.* **596**, 2943.

Giovannucci, A., Friedrich, J., Gunn, P., Kalfon, J., Brown, B. L., Koay, S. A., Taxidis, J., Najafi, F., Gauthier, J. L. and Zhou, P. (2019). CaImAn an open source tool for scalable calcium imaging data analysis. *Elife* **8**, e38173.

Glass, M., Andersen, N., Kruhøffer, M., Williams, E. and Heisler, N. (1990). Combined effects of environmental PO_2 and temperature on ventilation and blood gases in the carp *Cyprinus carpio* L. *J. Exp. Biol.* **148**, 1-17.

Gonzalez, C., Almaraz, L., Obeso, A. and Rigual, R. (1994). Carotid body chemoreceptors: from natural stimuli to sensory discharges. *Physiol. Rev.* **74**, 829-898.

Gonzalez, M., Blanquez, M. and Rojo, C. (1996). Early gill development in the rainbow trout, *Oncorhynchus mykiss*. *J. Morphol.* **229**, 201-217.

Gourine, A. V. and Funk, G. D. (2017). On the existence of a central respiratory oxygen sensor. *J. Appl. Physiol.* **123**, 1344-1349.

Grillitsch, S., Medgyesy, N., Schwerte, T. and Pelster, B. (2005). The influence of environmental PO_2 on hemoglobin oxygen saturation in developing zebrafish *Danio rerio*. *J. Exp. Biol.* **208**, 309-316.

Hadfield, J. D. (2010). MCMC methods for multi-response generalized linear mixed models: the MCMCglmm R package. *J. Stat. Softw* **33**, 1-22.

Hamel, J. (2011). A review of acute cyanide poisoning with a treatment update. *Crit. Care Nurse* **31**, 72-82.

Hansen, A., Reutter, K. and Zeiske, E. (2002). Taste bud development in the zebrafish, *Danio rerio*. *Dev. Dyn.* **223**, 483-496.

Hayashi, F., Coles, S., Bach, K., Mitchell, G. and McCrimmon, D. R. (1993). Time-dependent phrenic nerve responses to carotid afferent activation: intact vs. decerebellate rats. *Am. J. Physiol. Regul. Integr. Comp. Physiol.* **265**, R811-R819.

Hedrick, M., Burleson, M., Jones, D. and Milsom, W. (1991). An examination of central chemosensitivity in an air-breathing fish (*Amia calva*). *J. Exp. Biol.* **155**, 165-174.

Heymans, J. and Heymans, C. (1927). Sur les modifications directes et sur la régulation réflexe de l'activité du centre respiratoire de la tête isolée du chien. *Arch. Int. Pharmacodyn. Ther.* **33**, 273-372.

Hodges, M. R. and Richerson, G. B. (2010). Medullary serotonin neurons and their roles in central respiratory chemoreception. *Respir. Physiol. Neurobiol.* **173**, 256-263.

Hodges, M. R., Tattersall, G. J., Harris, M. B., McEvoy, S. D., Richerson, D. N., Deneris, E. S., Johnson, R. L., Chen, Z.-F. and Richerson, G. B. (2008). Defects in breathing and thermoregulation in mice with near-complete absence of central serotonin neurons. *J. Neurosci.* **28**, 2495-2505.

Holeton, G. (1971). Respiratory and circulatory responses of rainbow trout larvae to carbon monoxide and to hypoxia. *J. Exp. Biol.* **55**, 683-694.

Holmqvist, B., Ellingsen, B., Alm, P., Forsell, J., Øyan, A.-M., Goksøyr, A., Fjose, A. and Seo, H.-C. (2000). Identification and distribution of nitric oxide synthase in the brain of adult zebrafish. *Neurosci. Lett.* **292**, 119-122.

Holmqvist, B., Ellingsen, B., Forsell, J., Zhdanova, I. and Alm, P. (2004). The early ontogeny of neuronal nitric oxide synthase systems in the zebrafish. *J. Exp. Biol.* **207**, 923-935.

Hu, Y., Xie, S. and Yao, J. (2016). Identification of novel reference genes suitable for qRT-PCR normalization with respect to the zebrafish developmental stage. *PLoS ONE* **11**, e0149277.

Hughes, M. C., Zimmer, A. M. and Perry, S. F. (2019). The role of internal convection in respiratory gas transfer and aerobic metabolism in larval zebrafish (*Danio rerio*). *Am. J. Physiol. Regul. Integr. Comp. Physiol.*

Hwang, W. Y., Fu, Y., Reyon, D., Maeder, M. L., Tsai, S. Q., Sander, J. D., Peterson, R. T., Yeh, J. J. and Joung, J. K. (2013). Efficient genome editing in zebrafish using a CRISPR-Cas system. *Nat. Biotechnol.* **31**, 227.

Itazawa, Y. and Takeda, T. (1978). Gas exchange in the carp gills in normoxic and hypoxic conditions. *Respir. Physiol.* **35**, 263-269.

Jackson, R., Braubach, O. R., Bilkey, J., Zhang, J., Akimenko, M. A., Fine, A., Croll, R. P. and Jonz, M. G. (2013). Expression of *sall4* in taste buds of zebrafish. *Dev. Neurobiol.* **73**, 543-558.

Janvier, J. J., Peyraud-Waitzenegger, M. and Soulier, P. (1996). Mediation of serotonin-induced hyperventilation via 5-HT_3-receptor in European eel *Anguilla anguilla*. *J. Comp. Physiol. B* **165**, 640-6.

Jao, L.-E., Wente, S. R. and Chen, W. (2013). Efficient multiplex biallelic zebrafish genome editing using a CRISPR nuclease system. *PNAS* **110**, 13904-13909.

Jing, M., Zhang, Y., Wang, H. and Li, Y. (2019). GPCR-based sensors for imaging neurochemicals with high sensitivity and specificity. *J. Neurochem.*

Joels, N. and White, H. (1968). The contribution of the arterial chemoreceptors to the stimulation of respiration by adrenaline and noradrenaline in the cat. *J. Physiol.* **197**, 1-23.

Johansen, K. and Lenfant, C. (1968). Respiration in the African lungfish *Protopterus aethiopicus*: II. Control of breathing. *J. Exp. Biol.* **49**, 453-468.

Jones, D. R. and Schwarzfeld, T. (1974). The oxygen cost to the metabolism and efficiency of breathing in trout (*Salmo gairdneri*). *Respir. Physiol.* **21**, 241-254.

Jonz, M. G., Fearon, I. M. and Nurse, C. A. (2004). Neuroepithelial oxygen chemoreceptors of the zebrafish gill. *J. Physiol.* **560**, 737-752.

Jonz, M. G. and Nurse, C. A. (2003). Neuroepithelial cells and associated innervation of the zebrafish gill: a confocal immunofluorescence study. *J. Comp. Neurol.* **461**, 1-17.

Jonz, M. G. and Nurse, C. A. (2005). Development of oxygen sensing in the gills of zebrafish. *J. Exp. Biol.* **208**, 1537-49.

Jonz, M. G. and Nurse, C. A. (2006). Ontogenesis of oxygen chemoreception in aquatic vertebrates. *Respir. Physiol. Neurobiol.* **154**, 139-152.

Jonz, M. G. and Nurse, C. A. (2009). Oxygen-sensitive neuroepithelial cells in the gills of aquatic vertebrates: Science Publishers.

Jonz, M. G., Zachar, P. C., Da Fonte, D. F. and Mierzwa, A. S. (2015). Peripheral chemoreceptors in fish: A brief history and a look ahead. *Comp Biochem Physiol A Mol Integr Physiol* **186**, 27-38.

Kåhlin, J., Mkrtchian, S., Ebberyd, A., Hammarstedt-Nordenvall, L., Nordlander, B., Yoshitake, T., Kehr, J., Prabhakar, N., Poellinger, L. and Fagerlund, M. J. (2014). The human carotid body releases acetylcholine, ATP and cytokines during hypoxia. *Exp. Physiol.* **99**, 1089-1098.

Kapsimali, M., Kaushik, A.-L., Gibon, G., Dirian, L., Ernest, S. and Rosa, F. M. (2011). Fgf signaling controls pharyngeal taste bud formation through miR-200 and Delta-Notch activity. *Development* **138**, 3473-3484.

Kermorgant, M., Lancien, F., Mimassi, N. and Le Mevel, J. C. (2014a). Central ventilatory and cardiovascular actions of serotonin in trout. *Respir. Physiol. Neurobiol.* **192**, 55-65.

Kermorgant, M., Lancien, F., Mimassi, N., Tyler, C. R. and Le Mével, J.-C. (2014b). Effects of intracerebroventricular administered fluoxetine on cardio-ventilatory functions in rainbow trout (*Oncorhynchus mykiss*). *Gen. Comp. Endocrinol.* **205**, 176-184.

Kimmel, C. B., Ballard, W. W., Kimmel, S. R., Ullmann, B. and Schilling, T. F. (1995). Stages of embryonic development of the zebrafish. *Dev. Dyn.* **203**, 253-310.

Kinkead, R., Fritsche, R., Perry, S. F. and Nilsson, S. (1991). The role of circulating catecholamines in the ventilatory and hypertensive responses to hypoxia in the Atlantic cod (*Gadus morhua*). *Physiol. Zool.* **64**, 1087-1109.

Kinkead, R. and Perry, S. F. (1991). The effects of catecholamines on ventilation in rainbow trout during hypoxia or hypercapnia. *Respir. Physiol.* **84**, 77-92.

Kolar, K., Dondorp, D., Zwiggelaar, J. C., Høyer, J. and Chatzigeorgiou, M. (2021). Mesmerize: a dynamically adaptable user-friendly analysis platform for 2D & 3D calcium imaging data. *bioRxiv*, 840488.

Kucenas, S., Soto, F., Cox, J. and Voigt, M. (2006). Selective labeling of central and peripheral sensory neurons in the developing zebrafish using P2X3 receptor subunit transgenes. *Neuroscience* **138**, 641-652.

Kumar, P. and Prabhakar, N. R. (2011). Peripheral chemoreceptors: function and plasticity of the carotid body. *Compr. Physiol.* **2**, 141-219.

Leonard, E. M., Salman, S. and Nurse, C. A. (2018). Sensory processing and integration at the carotid body tripartite synapse: neurotransmitter functions and effects of chronic hypoxia. *Front. physiol.* **9**, 225.

Liland, K. H., Almøy, T. and Mevik, B.-H. (2010). Optimal choice of baseline correction for multivariate calibration of spectra. *Appl. Spectrosc.* **64**, 1007-1016.

Lillesaar, C. (2011). The serotonergic system in fish. *J. Chem. Neuroanat.* **41**, 294-308.

Lodish, H., Berk, A., Zipursky, S. L., Matsudaira, P., Baltimore, D. and Darnell, J. (2000). Neurotransmitters, synapses, and impulse transmission. In *Molecular Cell Biology. 4th edition*: WH Freeman.

Lopez-Barneo, J., Gonzalez-Rodriguez, P., Gao, L., Fernandez-Aguera, M. C., Pardal, R. and Ortega-Saenz, P. (2016). Oxygen sensing by the carotid body: mechanisms and role in adaptation to hypoxia. *Am. J. Physiol. Cell Physiol.* **310**, C629-42.

Lopez-Barneo, J., Lopez-Lopez, J. R., Urena, J. and Gonzalez, C. (1988). Chemotransduction in the carotid body: K^+ current modulated by PO_2 in type I chemoreceptor cells. *Science* **241**, 580-582.

Lopez-Lopez, J., González, C., Urena, J. and López-Barneo, J. (1989). Low pO_2 selectively inhibits K^+ channel activity in chemoreceptor cells of the mammalian carotid body. *J. Gen. Physiol.* **93**, 1001-1015.

Lumpkin, E. A. and Caterina, M. J. (2007). Mechanisms of sensory transduction in the skin. *Nature* **445**, 858-865.

Ma, Q. (2014). Merkel cells are a touchy subject. *Cell* **157**, 531-533.

Makarenko, V. V., Nanduri, J., Raghuraman, G., Fox, A. P., Gadalla, M. M., Kumar, G. K., Snyder, S. H. and Prabhakar, N. R. (2012). Endogenous H_2S is required for hypoxic sensing by carotid body glomus cells. *American Journal of Physiology-Cell Physiology* **303**, C916-C923.

Maksimovic, S., Baba, Y. and Lumpkin, E. A. (2013). Neurotransmitters and synaptic components in the Merkel cell-neurite complex, a gentle touch receptor. *Ann. N. Y. Acad. Sci* **1279**, 13.

Mandic, M., Pan, Y. K., Gilmour, K. M. and Perry, S. F. (2020). Relationships between the peak hypoxic ventilatory response and critical O_2 tension in larval and adult zebrafish (*Danio rerio*). *J. Exp. Biol.* **223**.

Mandic, M. and Regan, M. D. (2018). Can variation among hypoxic environments explain why different fish species use different hypoxic survival strategies? *J. Exp. Biol* **221**, jeb161349.

Mandic, M., Tzaneva, V., Careau, V. and Perry, S. F. (2019). Hif-1α paralogs play a role in the hypoxic ventilatory response of larval and adult zebrafish (*Danio rerio*). *J. Exp. Biol* **222**, jeb195198.

Maricich, S. M., Wellnitz, S. A., Nelson, A. M., Lesniak, D. R., Gerling, G. J., Lumpkin, E. A. and Zoghbi, H. Y. (2009). Merkel cells are essential for light-touch responses. *Science* **324**, 1580-1582.

Mauceri, A., Fasulo, S., Ainis, L., Licata, A., Martfnez, A., Mayer, B. and Zaccone, G. (1999). Neuronal nitric oxide synthase (nNOS) expression in the epithelial neuroendocrine cell system and nerve fibers in the gill of the catfish, *Heteropneustes fossilis*. *Acta Histochem.* **101**, 437-448.

Maxime, V., Nonnotte, G., Peyraud, C., Williot, P. and Truchot, J. (1995). Circulatory and respiratory effects of an hypoxic stress in the Siberian sturgeon. *Respir. Physiol.* **100**, 203-212.

McDonald, D. and McMahon, B. (1977). Respiratory development in Arctic char *Salvelinus alpinus* under conditions of normoxia and chronic hypoxia. *Can. J. Zool.* **55**, 1461-1467.

McDonald, M. D., Gilmour, K. M., Walsh, P. J. and Perry, S. F. (2010). Cardiovascular and respiratory reflexes of the gulf toadfish (*Opsanus beta*) during acute hypoxia. *Respir. Physiol. Neurobiol.* **170**, 59-66.

McKenzie, D. J., Taylor, E. W., Bronzi, P. and Bolis, C. L. (1995). Aspects of cardioventilatory control in the adriatic sturgeon (*Acipenser naccarii*). *Respir. Physiol.* **100**, 45-53.

McKinney, J., Knappskog, P. M. and Haavik, J. (2005). Different properties of the central and peripheral forms of human tryptophan hydroxylase. *J. Neurochem.* **92**, 311-320.

Merkel, F. S. (1880). Über die Endigungen der sensiblen Nerven in der Haut der Wirbelthiere: Stiller.

Mills, L. and Nurse, C. (1993). Chronic hypoxia in vitro increases volume of dissociated carotid body chemoreceptors. *Neuroreport* **4**, 619-622.

Milsom, W. K. (2012). New insights into gill chemoreception: receptor distribution and roles in water and air breathing fish. *Respir. Physiol. Neurobiol.* **184**, 326-339.

Milsom, W. K. and Burleson, M. L. (2007). Peripheral arterial chemoreceptors and the evolution of the carotid body. *Respir. Physiol. Neurobiol.* **157**, 4-11.

Milsom, W. K., Reid, S. G., Rantin, F. T. and Sundin, L. (2002). Extrabranchial chemoreceptors involved in respiratory reflexes in the neotropical fish *Colossoma macropomum* (the tambaqui). *J. Exp. Biol.* **205**, 1765-74.

Miura, H., Kusakabe, Y., Sugiyama, C., Kawamatsu, M., Ninomiya, Y., Motoyama, J. and Hino, A. (2001). Shh and Ptc are associated with taste bud maintenance in the adult mouse. *Mech. Dev.* **106**, 143-145.

Morgan, M. (1974). The development of gill arches and gill blood vessels of the rainbow trout, *Salmo gairdneri*. *J. Morphol.* **142**, 351-363.

Moss, I. R. (2000). Respiratory responses to single and episodic hypoxia during development: mechanisms of adaptation. *Respir. Physiol.* **121**, 185-197.

Nekvasil, N. P. and Olson, K. R. (1986). Plasma clearance, metabolism, and tissue accumulation of 3H-labeled catecholamines in trout. *Am. J. Physiol. Regul. Integr. Comp. Physiol.* **250**, R519-R525.

Nurse, C. A. (2010). Neurotransmitter and neuromodulatory mechanisms at peripheral arterial chemoreceptors. *Exp. Physiol.* **95**, 657-667.

Nurse, C. A. and Vollmer, C. (1997). Role of basic FGF and oxygen in control of proliferation, survival, and neuronal differentiation in carotid body chromaffin cells. *Dev. Biol.* **184**, 197-206.

Ogawa, K., Marui, T. and Caprio, J. (1997). Bimodal (taste/tactile) fibers innervate the maxillary barbel in the channel catfish. *Chem. Senses* **22**, 477-482.

Olson, K. R., Donald, J. A., Dombkowski, R. A. and Perry, S. F. (2012). Evolutionary and comparative aspects of nitric oxide, carbon monoxide and hydrogen sulfide. *Respir Physiol Neurobiol* **184**, 117-29.

Olson, K. R., Healy, M. J., Qin, Z., Skovgaard, N., Vulesevic, B., Duff, D. W., Whitfield, N. L., Yang, G., Wang, R. and Perry, S. F. (2008). Hydrogen sulfide as an oxygen sensor in trout gill chemoreceptors. *American Journal of Physiology-Regulatory, Integrative and Comparative Physiology* **295**, R669-R680.

Pan, H.-R., Tian, M., Xue, J.-B., Li, S.-M., Luo, X.-C., Huang, X., Chen, Z.-H. and Huang, L. (2018). Mammalian taste bud bells utilize extragemmal 5-hydroxy-L-tryptophan to biosynthesize the neurotransmitter serotonin. *Front. Cell. Neurosci.* **12**, 461.

Pan, W., Scott, A. L., Nurse, C. A. and Jonz, M. G. (2021). Identification of oxygen-sensitive neuroepithelial cells through an endogenous reporter gene in larval and adult transgenic zebrafish. *Cell Tissue Res.* **384**, 35-47.

Pan, Y. K., Mandic, M., Zimmer, A. M. and Perry, S. F. (2019). Evaluating the physiological significance of hypoxic hyperventilation in larval zebrafish (*Danio rerio*). *J. Exp. Biol* **222**, jeb204800.

Pan, Y. K. and Perry, S. F. (2020). Neuroendocrine control of breathing in fish. *Mol. Cell. Endocrinol.*, 110800.

Panlilio, J. M., Marin, S., Lobl, M. B. and McDonald, M. D. (2016). Treatment with the selective serotonin reuptake inhibitor, fluoxetine, attenuates the fish hypoxia response. *Sci. Rep.* **6**, 31148.

Peers, C., Wyatt, C. N. and Evans, A. M. (2010). Mechanisms for acute oxygen sensing in the carotid body. *Respir Physiol Neurobiol* **174**, 292-8.

Peng, Y.-J., Nanduri, J., Raghuraman, G., Souvannakitti, D., Gadalla, M. M., Kumar, G. K., Snyder, S. H. and Prabhakar, N. R. (2010). H_2S mediates O_2 sensing in the carotid body. *Proceedings of the National Academy of Sciences* **107**, 10719-10724.

Perry, S. and Gilmour, K. (1996). Consequences of catecholamine release on ventilation and blood oxygen transport during hypoxia and hypercapnia in an elasmobranch *Squalus acanthias* and a teleost *Oncorhynchus mykiss*. *J. Exp. Biol.* **199**, 2105-2118.

Perry, S., Jonz, M. and Gilmour, K. (2009). Oxygen sensing and the hypoxic ventilatory response. *Fish Physiol.* **27**, 193-253.

Perry, S., Kinkead, R. and Fritsche, R. (1992). Are circulating catecholamines involved in the control of breathing by fishes? *Rev. Fish Biol. Fish.* **2**, 65-83.

Perry, S., Kumai, Y., Porteus, C. S., Tzaneva, V. and Kwong, R. W. M. (2016). An emerging role for gasotransmitters in the control of breathing and ionic regulation in fish. *J. Comp. Physiol. B* **186**, 145-159.

Perry, S. F., Fritsche, R., Kinkead, R. and Nilsson, S. (1991). Control of catecholamine release in vivo and in situ in the Atlantic cod (*Gadus morhua*) during hypoxia. *J. Exp. Biol.* **155**, 549-566.

Perry, S. F. and Gilmour, K. M. (2002). Sensing and transfer of respiratory gases at the fish gill. *J. Exp. Zool. A Ecol. Genet. Physiol.* **293**, 249-263.

Perry, S. F. and Reid, S. D. (1992). Relationship between blood O_2 content and catecholamine levels during hypoxia in rainbow trout and American eel. *Am. J. Physiol. Regul. Integr. Comp. Physiol.* **263**, R240-9.

Perry, S. F., Reid, S. G., Gilmour, K. M., Boijink, C. L., Lopes, J. M., Milsom, W. K. and Rantin, F. T. (2004). A comparison of adrenergic stress responses in three tropical teleosts exposed to acute hypoxia. *Am. J. Physiol. Regul. Integr. Comp. Physiol.* **287**, R188-97.

Perry, S. F. and Thomas, S. (1991). The effects of endogenous or exogenous catecholamines on blood respiratory status during acute hypoxia in rainbow trout (*Oncorhynchus mykiss*). *J. Comp. Physiol. B* **161**, 489-97.

Perry, S. F. and Wood, C. M. (1989). Control and coordination of gas transfer in fishes. *Can. J. Zool.* **67**, 2961-2970.

Peterson, R. H. (1975). Pectoral fin and opercular movements of atlantic salmon (*Salmo salar*) alevins. *JFRBC* **32**, 643-647.

Peyraud-Waitzenegger, M. (1979). Simultaneous modifications of ventilation and arterial PO_2 by catecholamines in the eel, A*nguilla anguilla* L.: Participation of α and β effects. *J. Comp. Physiol.* **129**, 343-354.

Peyraud-Waitzenegger, M., Barthelemy, L. and Peyraud, C. (1980). Cardiovascular and ventilatory effects of catecholamines in unrestrained eels (*Anguilla anguilla* L.). *J. Comp. Physiol.* **138**, 367-375.

Pietruschka, F. (1985). Calcium influx in cultured carotid body cells is stimulated by acetylcholine and hypoxia. *Brain Res.* **347**, 140-143.

Pietruschka, F. and Acker, A. (1985). Membrane potential and Ca^{2+} influx in hypoxic and normoxic carotid body type-I cells.

Poole, C. and Satchell, G. (1979). Nociceptors in the gills of the dogfish *Squalus acanthias*. *J. Comp. Physiol.* **130**, 1-7.

Porteus, C., Hedrick, M. S., Hicks, J. W., Wang, T. and Milsom, W. K. (2011). Time domains of the hypoxic ventilatory response in ectothermic vertebrates. *J. Comp. Physiol. B* **181**, 311-333.

Porteus, C., Kumai, Y., Abdallah, S. J., Yew, H. M., Kwong, R. W., Pan, Y., Milsom, W. K. and Perry, S. F. (2021). Respiratory responses to external ammonia in zebrafish (*Danio rerio*). *Comp. Biochem. Physiol. A Mol. Integr. Physiol.* **251**, 110822.

Porteus, C. S., Abdallah, S. J., Pollack, J., Kumai, Y., Kwong, R. W., Yew, H. M., Milsom, W. K. and Perry, S. F. (2014a). The role of hydrogen sulphide in the control of breathing in hypoxic zebrafish (*Danio rerio*). *The Journal of physiology* **592**, 3075-3088.

Porteus, C. S., Brink, D. L., Coolidge, E. H., Fong, A. Y. and Milsom, W. K. (2013). Distribution of acetylcholine and catecholamines in fish gills and their potential roles in the hypoxic ventilatory response. *Acta Histochem.* **115**, 158-169.

Porteus, C. S., Brink, D. L. and Milsom, W. K. (2012). Neurotransmitter profiles in fish gills: putative gill oxygen chemoreceptors. *Respir Physiol Neurobiol* **184**, 316-25.

Porteus, C. S., Pollack, J., Tzaneva, V., Kwong, R. W., Kumai, Y., Abdallah, S. J., Zaccone, G., Lauriano, E. R., Milsom, W. K. and Perry, S. F. (2015). A role for nitric oxide in the control of breathing in zebrafish (*Danio rerio*). *J Exp Biol* **218**, 3746-3753.

Porteus, C. S., Wright, P. A. and Milsom, W. K. (2014b). Characterisation of putative oxygen chemoreceptors in bowfin (*Amia calva*). *J. Exp. Biol.* **217**, 1269-1277.

Powell, F., Milsom, W. and Mitchell, G. (1998). Time domains of the hypoxic ventilatory response. *Respir. Physiol.* **112**, 123-134.

Prabhakar, N. R. (2012). Carbon monoxide (CO) and hydrogen sulfide (H_2S) in hypoxic sensing by the carotid body. *Respiratory Physiology & Neurobiology* **184**, 165-169.

Prabhakar, N. R. and Semenza, G. L. (2015). Oxygen sensing and homeostasis. *Physiology* **30**, 340-348.

Prado, M. A., Reis, R. A., Prado, V., de Mello, M. C., Gomez, M. V. and de Mello, F. G. (2002). Regulation of acetylcholine synthesis and storage. *Neurochem. Int.* **41**, 291-299.

Qin, Z., Lewis, J. E. and Perry, S. F. (2010). Zebrafish (*Danio rerio*) gill neuroepithelial cells are sensitive chemoreceptors for environmental CO_2. *J. Physiol.* **588**, 861-72.

Rahbar, S., Pan, W. and Jonz, M. G. (2016). Purinergic and cholinergic drugs mediate hyperventilation in zebrafish: evidence from a novel chemical screen. *PLoS ONE* **11**, e0154261.

Randall, D. J. and Taylor, E. W. (1991). Evidence of a role for catecholamines in the control of breathing in fish. *Rev. Fish Biol. Fish.* **1**, 139-157.

Regan, K. S., Jonz, M. G. and Wright, P. A. (2011). Neuroepithelial cells and the hypoxia emersion response in the amphibious fish *Kryptolebias marmoratus*. *J. Exp. Biol.* **214**, 2560-2568.

Reid, S. G. and Perry, S. F. (2003). Peripheral O_2 chemoreceptors mediate humoral catecholamine secretion from fish chromaffin cells. *Am. J. Physiol. Regul. Integr. Comp. Physiol.* **284**, R990-9.

Rombough, P. (1999). The gill of fish larvae. Is it primarily a respiratory or an ionoregulatory structure? *J. Fish Biol.* **55**, 186-204.

Rombough, P. (2002). Gills are needed for ionoregulation before they are needed for O_2 uptake in developing zebrafish, *Danio rerio*. *J. Exp. Biol.* **205**, 1787-1794.

Rombough, P. (2007). The functional ontogeny of the teleost gill: which comes first, gas or ion exchange? *Comp. Biochem. Physiol. A Mol. Integr. Physiol.* **148**, 732-742.

Rombough, P. and Drader, H. (2009). Hemoglobin enhances oxygen uptake in larval zebrafish (*Danio rerio*) but only under conditions of extreme hypoxia. *J. Exp. Biol.* **212**, 778-784.

Rombough, P. J. (1988). Respiratory gas exchange, aerobic metabolism, and effects of hypoxia during early life. In *Fish Physiol.*, vol. 11, pp. 59-161: Elsevier.

Rombough, P. J. (1992). Intravascular oxygen tensions in cutaneously respiring rainbow trout (*Oncorhynchus mykiss*) larvae. *Comp. Biochem. Physiol. A Mol. Integr. Physiol.* **101**, 23-27.

Rombough, P. J. (1998). Partitioning of oxygen uptake between the gills and skin in fish larvae: a novel method for estimating cutaneous oxygen uptake. *J. Exp. Biol.* **201**, 1763-1769.

Rombough, P. J. and Ure, D. (1991). Partitioning of oxygen uptake between cutaneous and branchial surfaces in larval and young juvenile chinook salmon *Oncorhynchus tshawytscha*. *Physiol. Zool.* **64**, 717-727.

Rossi, G. S., Cochrane, P. V. and Wright, P. A. (2020). Fluctuating environments during early development can limit adult phenotypic flexibility: insights from an amphibious fish. *J. Exp. Biol.* **223**.

Saunders, R. and Sutterlin, A. (1971). Cardiac and respiratory responses to hypoxia in the sea raven, *Hemitripterus americanus*, and an investigation of possible control mechanisms. *JFRBC* **28**, 491-503.

Scott, G. R., Wood, C. M., Sloman, K. A., Iftikar, F. I., De Boeck, G., Almeida-Val, V. M. and Val, A. L. (2008). Respiratory responses to progressive hypoxia in the Amazonian oscar, *Astronotus ocellatus*. *Respiratory Physiology & Neurobiology* **162**, 109-116.

Shakarchi, K., Zachar, P. C. and Jonz, M. G. (2013). Serotonergic and cholinergic elements of the hypoxic ventilatory response in developing zebrafish. *J. Exp. Biol.* **216**, 869-80.

SheikhBahaei, S. (2020). Physiology: New insights into central oxygen sensing. *Curr. Biol.* **30**, R1004-R1006.

Smith, J. C., Ellenberger, H. H., Ballanyi, K., Richter, D. W. and Feldman, J. L. (1991). Pre-Botzinger complex: a brainstem region that may generate respiratory rhythm in mammals. *Science* **254**, 726-729.

Soulika, M., Kaushik, A.-L., Mathieu, B., Lourenço, R., Komisarczuk, A. Z., Romano, S. A., Jouary, A., Lardennois, A., Tissot, N. and Okada, S. (2016). Diversity in cell motility reveals the dynamic nature of the formation of zebrafish taste sensory organs. *Development* **143**, 2012-2024.

Stea, A., Jackson, A. and Nurse, C. (1992). Hypoxia and N6, O2'-dibutyryladenosine 3', 5'-cyclic monophosphate, but not nerve growth factor, induce Na^+ channels and hypertrophy in chromaffin-like arterial chemoreceptors. *PNAS* **89**, 9469-9473.

Stecyk, J. A. and Farrell, A. P. (2006). Regulation of the cardiorespiratory system of common carp (*Cyprinus carpio*) during severe hypoxia at three seasonal acclimation temperatures. *Physiol Biochem Zool* **79**, 614-27.

Steffensen, J. F. (1985). The transition between branchial pumping and ram ventilation in fishes: energetic consequences and dependence on water oxygen tension. *J. Exp. Biol.* **114**, 141-150.

Talbot, J. C. and Amacher, S. L. (2014). A streamlined CRISPR pipeline to reliably generate zebrafish frameshifting alleles. *Zebrafish* **11**, 583-585.

Teppema, L. J. (2018). CrossTalk opposing view: the hypoxic ventilatory response does not include a central, excitatory hypoxia sensing component. *J. Physiol.* **596**, 2939.

Teppema, L. J. and Dahan, A. (2010). The ventilatory response to hypoxia in mammals: mechanisms, measurement, and analysis. *Physiol. Rev.*

Thomas, S., Belaud, A. and Peyraud, C. (1979). Arguments for serotonergic adjustments in gill blood circulation in fish. *IRCS Med. Sci. Cardiovasc. Syst.*

Tornini, V. A., Puliafito, A., Slota, L. A., Thompson, J. D., Nachtrab, G., Kaushik, A.-L., Kapsimali, M., Primo, L., Di Talia, S. and Poss, K. D. (2016). Live monitoring of blastemal cell contributions during appendage regeneration. *Curr. Biol.* **26**, 2981-2991.

Tzaneva, V. and Perry, S. F. (2014). Heme oxygenase-1 (HO-1) mediated respiratory responses to hypoxia in the goldfish, *Carassius auratus*. *Respir Physiol Neurobiol* **199**, 1-8.

Tzaneva, V. and Perry, S. F. (2016). Role of endogenous carbon monoxide in the control of breathing in zebrafish (*Danio rerio*). *American Journal of Physiology-Regulatory, Integrative and Comparative Physiology* **311**, R1262-R1270.

Ultsch, G. R., Boschung, H. and Ross, M. J. (1978). Metabolism, critical oxygen tension, and habitat selection in darters (*Etheostoma*). *Ecology* **59**, 99-107.

Urena, J., López-López, J., González, C. and López-Barneo, J. (1989). Ionic currents in dispersed chemoreceptor cells of the mammalian carotid body. *J. Gen. Physiol.* **93**, 979-999.

von Euler, U. S., Liljestrand, G. and Zotterman, Y. (1940). The excitation mechanism of the chemoreceptors of the carotid body. *Skand. Arch. Physiol.* **83**, 132-152.

Vulesevic, B., McNeill, B. and Perry, S. (2006). Chemoreceptor plasticity and respiratory acclimation in the zebrafish *Danio rerio*. *J. Exp. Biol.* **209**, 1261-1273.

Vulesevic, B. and Perry, S. (2006). Developmental plasticity of ventilatory control in zebrafish, *Danio rerio*. *Respiratory Physiology & Neurobiology* **154**, 396-405.

Wake, M. H. and Schwenk, K. (1986). A preliminary report on the morphology and distribution of taste buds in gymnophiones, with comparison to other amphibians. *J. Herpetol.* **20**, 254-256.

Walther, D. J. and Bader, M. (2003). A unique central tryptophan hydroxylase isoform. *Biochem. Pharmacol.* **66**, 1673-1680.

Wang, R. (2002). Two's company, three's a crowd: Can H_2S be the third endogenous gaseous transmitter? *FASEB J.* **16**, 1792-1798.

Wang, Z. Y. and Bisgard, G. E. (2002). Chronic hypoxia-induced morphological and neurochemical changes in the carotid body. *Microsc. Res. Tech.* **59**, 168-177.

Wells, P. and Pinder, A. (1996). The respiratory development of Atlantic salmon. II. Partitioning of oxygen uptake among gills, yolk sac and body surfaces. *J. Exp. Biol.* **199**, 2737-2744.

Westerfield, M. (2000). The zebrafish book: a guide for the laboratory use of zebrafish.

Whitear, M. (1989). Merkel cells in lower vertebrates. *Archives of histology and cytology* **52**, 415-422.

Yau, K.-W. (1994). Phototransduction mechanism in retinal rods and cones. The Friedenwald Lecture. *Invest. Ophthalmol. Vis. Sci.* **35**, 9-32.

Yeager, D. P. and Ultsch, G. R. (1989). Physiological regulation and conformation: a BASIC program for the determination of critical points. *Physiol. Zool.* **62**, 888-907.

Yeh, C.-M., Pao, G. M., Villa-Real, R., Rosales, K., DePasquale, E., Groisman, A. and Chalasani, S. H. (2019). A many-to-one sensory circuit encodes oxygen levels and drives respiratory behaviour in *Danio rerio*. *bioRxiv*, 655084.

Yokogawa, T., Hannan, M. C. and Burgess, H. A. (2012). The dorsal raphe modulates sensory responsiveness during arousal in zebrafish. *J. Neurosci.* **32**, 15205-15215.

Zaccone, G., Ainis, L., Mauceri, A., Cascio, P. L., Francesco, L. G. and Fasulo, S. (2003). NANC nerves in the respiratory air sac and branchial vasculature of the Indian catfish, Heteropneustes fossilis. *Acta Histochem.* **105**, 151-163.

Zaccone, G., Lauriano, E. R., Kuciel, M., Capillo, G., Pergolizzi, S., Alesci, A., Ishimatsu, A., Ip, Y. K. and Icardo, J. M. (2017). Identification and distribution of neuronal nitric oxide synthase and neurochemical markers in the neuroepithelial cells of the gill and the skin in the giant mudskipper, *Periophthalmodon schlosseri*. *Zoology* **125**, 41-52.

Zachar, P. C. and Jonz, M. G. (2012a). Confocal imaging of Merkel-like basal cells in the taste buds of zebrafish. *Acta Histochemica* **114**, 101-115.

Zachar, P. C. and Jonz, M. G. (2012b). Neuroepithelial cells of the gill and their role in oxygen sensing. *Respir. Physiol. Neurobiol.* **184**, 301-308.

Zachar, P. C. and Jonz, M. G. (2012c). Oxygen sensitivity of gill neuroepithelial cells in the anoxia-tolerant goldfish. In *Arterial Chemoreception*, pp. 167-172: Springer.

Zachar, P. C., Pan, W. and Jonz, M. G. (2017). Characterization of ion channels and O_2 sensitivity in gill neuroepithelial cells of the anoxia-tolerant goldfish (*Carassius auratus*). *J. Neurophysiol.* **118**, 3014-3023.

Zhang, L., Nurse, C. A., Jonz, M. G. and Wood, C. M. (2011). Ammonia sensing by neuroepithelial cells and ventilatory responses to ammonia in rainbow trout. *J Exp Biol* **214**, 2678-89.

Zhang, X., Beaulieu, J.-M., Gainetdinov, R. and Caron, M. (2006). Functional polymorphisms of the brain serotonin synthesizing enzyme tryptophan hydroxylase-2. *Cell. Mol. Life Sci.* **63**, 6.

Zimmer, A. M., Mandic, M., Rourke, K. M. and Perry, S. F. (2020). Breathing with fins: do the pectoral fins of larval fishes play a respiratory role? *Am. J. Physiol. Regul. Integr. Comp. Physiol.* **318**, R89-R97.

Zimmer, A. M., Pan, Y. K., Chandrapalan, T., Kwong, R. W. and Perry, S. F. (2019). Loss-of-function approaches in comparative physiology: is there a future for knockdown experiments in the era of genome editing? *J. Exp. Biol* **222**, jeb175737.

Zimmer, A. M. and Perry, S. F. (2020). The Rhesus glycoprotein Rhcgb is expendable for ammonia excretion and Na^+ uptake in zebrafish (*Danio rerio*). *Comp. Biochem. Physiol. A Mol. Integr. Physiol.*, 110722.

Zimmer, A. M., Wright, P. A. and Wood, C. M. (2014). What is the primary function of the early teleost gill? Evidence for Na^+/NH_4^+ exchange in developing rainbow trout (*Oncorhynchus mykiss*). *Proc. R. Soc. B* **281**, 20141422.